Tesis Doctoral
Ingeniería de Telecomunicación

MEMS-based Lab-on-chip platform with integrated 3D and planar microelectrodes for organotypic and cell cultures

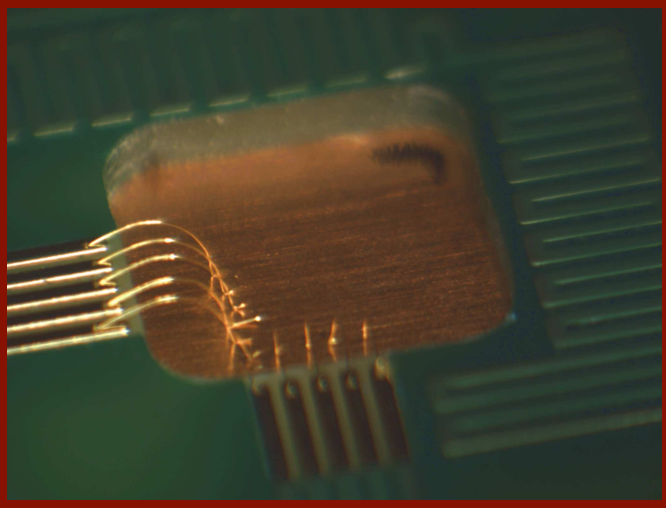

Autor: Miguel Cabello Valverde
Directores: José Manuel Quero Reboul
Carmen Aracil Fernández

Dept. Ingeniería Electrónica
Escuela Técnica Superior de Ingeniería
Universidad de Sevilla

Sevilla, 2020

Tesis Doctoral
Ingeniería de Telecomunicación

MEMS-based Lab-on-chip platform with integrated 3D and planar microelectrodes for organotypic and cell cultures

Autor:

Miguel Cabello Valverde

Directores:

José Manuel Quero Reboul
Carmen Aracil Fernández

Dept. Ingeniería Electrónica
Escuela Técnica Superior de Ingeniería
Universidad de Sevilla

2020

A Montse y mis padres. Gracias por vuestro apoyo incondicional.

Index

Figures index

Table index

Agradecimientos

A punto de terminar la que probablemente sea la prueba más difícil a la que he tenido que enfretarme en mi corta carrera profesional, no puedo evitar echar la vista atrás y comprobar que, a pesar de las dificultades y obstáculos encontrados y superados durante esta tesis doctoral, siempre ha habido detrás de mí muchas personas sin las que nada de esto habría sido posible. Tras cinco años muy intensos, durante los que se han hecho sacrificios personales y profesionales, no solo por mi parte, sino también por la de aquellos que me rodean, no querría dejar pasar la oportunidad de agradecer a todas esas personas que, directa o indirectamente, me han ayudado en esta odisea. Por eso, este apartado especial de mi tesis va dirigido a todos ellos, así que espero no olvidarme de nadie.

En primer lugar, como no podía ser de otra manera, quiero darles las gracias a mis padres, sin los que nada de esto habría podido ni tan siquiera comenzar. Sin ellos no habría podido estudiar en Sevilla Ingeniería de Telecomunicaciones. Sin su apoyo, tanto moral como económico, no podría haber sobrevivido a esa primera prueba antes del doctorado. Mención especial para mi madre, que sé bien que se ha sentido más identificada que nadie, ya que ella también realizó un doctorado en Biología que finalizó con tan solo 25 años. Ahora soy capaz de valorar, incluso más de lo que ya lo hacía, lo que significa su hazaña. A punto estuve de acceder a sus peticiones, en las que me pedía venir aunque sólo fuera a limpiar los tubos que usábamos en el laboratorio.

En segundo lugar, pero no menos importante, quiero darle las gracias mil y una veces a Montse. Llegó cuando ya estaba inmerso en esta aventura y desde el primer día supo como llevarla conmigo para que no me viera aplastado por su peso. Ha compartido conmigo los buenos momentos y, especialmente, me ha aguantado en los malos y muy malos. Sabiendo lo que implicaban para mí estos últimos meses, fue capaz de organizar casi en exclusiva uno de los días más importantes en la vida de alguien, como es el día de su boda, y convertirlo en algo inolvidable sin disminuir un ápice su apoyo constante. Gracias, gracias y gracias.

Y por supuesto a toda mi familia, que siempre estuvieron apoyándome e interesándose por mi trabajo, aún cuando ni yo mismo era capaz de explicar lo que estaba haciendo. Igualmente me gustaría dar las gracias a mi nueva familia, la que he encontrado gracias a Montse, que han sido y son parte imprescindible de esta tesis y de mi vida en general.

No puedo dejar de agradecer también el apoyo de mis amigos. Siempre entendían que faltara, incluso a algunos eventos importantes, por tener que trabajar en el laboratorio, y que después de 20 veces de decir que no, seguían contando conmigo.

Como no podía ser de otra manera, tengo que dar las gracias a mis directores de tesis José Manuel Quero Reboul y Carmen Aracil Fernández. A José Manuel, por haberme dado la primera oportunidad allá por junio de 2014 de empezar a trabajar con ellos, así como por su guía y consejos durante toda la tesis y por apostar siempre por mí. A Carmen, por estar ahí cada vez que hizo falta. He perdido la cuenta de las veces que he tocado en la puerta de su despacho y me ha ayudado, aguantado, oído, fuera por algo relacionado con la tesis o con cualquier otra cosa, pero allí estaba con su sonrisa contagiosa y su predisposición a echar una mano en lo que hiciera falta. Y claro, luego tenemos al tercer director en la sombra, Francisco Perdigones. Se ha involucrado como si fuera un director más, pero sin figurar como tal. Muchas gracias Fran, porque te has tomado esta tesis doctoral como si realmente fuera tu responsabilidad, sin que así fuera. Han sido muchas horas de laboratorio, pruebas, artículos y contribuciones para que este doctorado fuera posible.

No me olvido de los demás compañeros del grupo de Microsistemas. Gracias a Antonio y a Juan que siempre estuvieron ahí para cualquier duda que tuviera. También a los que ya no forman parte del grupo, Guada y Blas. El compañerismo de este grupo es envidiable y hace que tantas horas de laboratorio sean más llevaderas. No puedo dejar de acordarme igualmente de esa tercera pata que sustenta esta tesis doctoral, los biólogos. Tengo que reconocer que tratar con ingenieros no es tarea fácil, pero vosotros lo habéis sabido llevar muy bien. Así que, gracias a Berta de la Cerda y todo su equipo de Cabimer, no exagero si digo que sin vosotros nada se habría hecho, ya que pusisteis vuestros medios y conocimientos a disposición de este trabajo desde el primer día. También agradecer su tiempo y dedicación a Clara Macías y a la profesora Inmaculada Domínguez, que de forma desinteresada nos han introducido y han colaborado con nosotros en los cultivos celulares.

Finalmente, quiero agradecer al doctor Paulo Rocha los cuatro meses de estancia que pasé en la Universidad de Bath. No dudó ni un segundo en aceptarme, en guiarme y enseñarme todo lo que fuera necesario para hacer que esa estancia fuera realmente fructífera. También a la doctora Despina Moschou, quien me presentó al Dr. Rocha y fue nuestro nexo de unión para poder comenzar una colaboración entre la Universidad de Sevilla y la de Bath. Muchas gracias a ellos y su grupo de investigación (C3Bio).

Miguel Cabello Valverde

Sevilla, 2020

+

Resumen

La presente tesis doctoral se centra en el desarrollo y la validación de plataformas **lab on chip (LOC)** para su aplicación en el campo de la Biología, la Medicina y la Biomedicina, particularmente relacionados con el cultivo de células y tejidos, así como su tratamiento mediante electroestimulación y su actividad eléctrica.

Actualmente, las investigaciones centradas en el desarrollo de LOCs han experimentado un crecimiento considerable, gracias, en gran medida, a la versatilidad que ofrecen. Dicha versatilidad se traduce en numerosas aplicaciones, de las cuales, aquellas relacionadas con la Biología y la Medicina, están alcanzando especial relevancia. La **integración** de sensores, actuadores, circuitos microfluídicos y circuitos electrónicos en la misma plataforma, permite fabricar sistemas con múltiples aplicaciones. Esta tesis se centra fundamentalmente en el desarrollo de plataformas para el **cultivo *in vitro*** de tejidos y células, así como para la monitorización y la interacción con dicho cultivo. Los cultivos *in vitro* resultan de vital importancia para realizar estudios en células o tejidos, experimentar con medicamentos o estudiar su proliferación y morfología. De esta manera, se cubriría la creciente necesidad de encontrar una alternativa para replicar modelos humanos de enfermedades *in vitro* para poder desarrollar nuevos fármacos y avanzar en la medicina personalizada. Por tanto, la posibilidad de realizar cultivos de media o larga duración en plataformas que no precisen de un equipamiento costoso como las incubadoras de CO_2 y que puedan ser monitorizadas mediante aplicaciones ópticas, supone un salto cualitativo en el desarrollo de los cultivos *in vitro*.

En este contexto, se presenta el trabajo relacionado con esta tesis que ha sido desarrollada dentro del grupo de Microsistemas de la Escuela Superior de Ingeniería de la Universidad de Sevilla. La tesis está estructurada de manera que a lo largo de este escrito se da respuesta a los distintos aspectos anteriormente descritos.

En primer lugar, se hace una breve introducción a la tecnología MEMS y a los principios

básicos de la microfluídica. Dado que este trabajo se ha desarrollado en un ambiente multidisciplinar, esta sección resulta necesaria para dar una visión general a aquellos no familiarizados con esta disciplina. Tras esa introducción se realiza una descripción del estado del arte en el que se encuadra este trabajo, incluyendo los sistemas LoCs, y sus principales aplicaciones en el campo de la Biología, Medicina y Biomedicina, prestando especial atención a las aplicaciones de los LoCs relacionadas con cultivos organotípicos y de células.

Tras la introducción y el estado del arte en el que se enmarca la tesis, se explican los resultados obtenidos durante este trabajo. Durante la primera parte, se describe el desarrollo, fabricación y caracterización de un sistema autónomo para el **cultivo y electroestimulación** de tejidos que integra un lab on PCB (LOP) formado por un **array de microelectrodos en 3D** (MEA) formado por hilos de oro de 25 μm en **sustrato transparente**, sensores y actuadores, junto con una plataforma microfluídica fabricada en metacrilato (PMMA) y polidimetilsiloxano (PDMS). El LOP permite mantener las condiciones de temperatura idóneas para llevar a cabo cultivos de media-larga duración sin necesidad de usar incubadoras de CO_2, así como su seguimiento de forma continua a través de un microscopio, gracias al uso de materiales transparentes. Este sistema también incluye una electrónica suplementaria y un programa que permite la monitorización del sistema y la electrostimulación de la muestra biológica. Tras explicar detalladamente el diseño y el novedoso proceso de fabricación del LOP, se presentan los resultados experimentales. En primer lugar, se ha demostrado que es posible desarrollar **cultivos organotípicos** de retinas de ratón durante **más de 7 días**, obteniendo resultados muy similares a los conseguidos para las mismas muestras biológicas, pero mediante métodos de cultivo tradicionales. Además, se ha logrado la **neuro-protección** mediante la electroestimulación de retinas de ratón con la enfermedad de la **retinosis pigmentaria**, logrando de esta manera ralentizar la degeneración de la muestra debido a la enfermedad.

Otra de las aplicaciones que se quiere conseguir con el desarrollo del LOP anteriormente descrito se centra en la adquisición de señales eléctricas procedentes de las muestras biológicas cultivadas en el dispositivo, así como extrapolar su uso a **cultivos celulares**. Para la adquisición de señales procedentes del cultivo, la impedancia de los electrodos fabricados con hilos de oro de 25 μm ha resultado ser demasiado alta como para discernir entre el ruido base y la actividad eléctrica del cultivo. Por ello, la segunda parte de esta tesis doctoral se centra en la mejora de la MEA para la adquisición de actividad eléctrica.

Dado el objetivo marcado en esta segunda parte, durante esta tesis se ha realizado una estancia en la Universidad de Bath. En dicha estancia, se ha caracterizado la **actividad eléctrica de células del cáncer de próstata** (PC-3), que fueron cultivadas en chips de silicio con electrodos de oro.

La experiencia obtenida durante la estancia ha permitido avanzar en el desarrollo y la fabricación de nuevas MEAs para la adquisición de señales eléctricas de cultivos celulares. La primera aproximación para mejorar la MEA se ha realizado sobre PCB. Se trata de un dispositivo compuesto por **pilares de oro en 3D** fabricados mediante la técnica de

electroplating. Estos electrodos tienen 100 μm de diámetro y una altura de 25 μm que aseguran el contacto en el caso de cultivos de tejidos. Se ha demostrado una mejora significativa, traducida tanto en una impedancia más baja, como en una línea base de ruido menor con respecto a la MEA con hilos de oro. Asimismo, se han obtenido patrones de actividad eléctrica en las células PC-3 muy similares a los obtenidos con el chip de silicio y oro empleado en la estancia. Como mejora de la MEA 3D se ha cambiado el sustrato por otro transparente, como **vidrio o PMMA**, para permitir su uso en aplicaciones ópticas. Dichas MEAs integran electrodos planares fabricados mediante la técnica de **sputtering de oro** sobre su superficie. Estas MEAs están en una fase preliminar de desarrollo, y se está probando en primer lugar su biocompatibilidad y viabilidad para el desarrollo de cultivos celulares.

Para finalizar, se exponen las conclusiones de esta tesis doctoral, entre las que destacan: el proceso de fabricación del LOP con electrodos de oro y la aplicación del sistema completo para desarrollar cultivos organotípicos, monitorizarlos y aplicar electroestimulación, logrando la neuro-protección de retinas de ratón con la retinosis pigmentaria; la transición hacia el desarrollo de una plataforma para cultivos celulares mejorando la MEA y su fabricación usando diferentes sustratos; la caracterización de la actividad eléctrica de las células PC-3. También se incluyen las líneas de investigación abiertas para continuar lo que se ha empezado en esta tesis doctoral.

Para facilitar la comprensión del lector, se adjuntan los apéndices complementarios a esta tesis doctoral.

Abstract

The presented thesis is focused on the development and validation of **lab on chip (LOC)** platforms for their application on Biology, Medicine and Biomedicine, particularly those related with cells and tissues cultures, as well as their treatment through electrostimulation and their electrical behavior.

Nowadays, research works focused on the development of LOCs have significantly increased, mostly thanks to its high versatility, which involves countless applications. Among all this applications, those related with Biology and Medicine are becoming more and more important. The **integration** of sensors, actuators, microfluidic circuits and electronic circuits in the same platform allows the fabrication of systems with lots of applications. This thesis is focused on the development of platforms for *in vitro* cultures of cells and tissues, to monitor their behavior and interact with the biological samples. The importance of *in vitro* cultures lies on the study of cells and tissues proliferation and morphology or performing drug delivery experiments. In this respect, through LOC technologies, it would be possible to model human diseases *in vitro*, in order to improve the development of new drugs and advance personalized medicine. Thus, the possibility of carrying out medium-long term cultures on platforms without the need of any expensive equipment, such as CO_2 incubators, with software and monitoring, implies a qualitative step forward in the development of *in vitro* cultures.

Within this framework, the work related to this thesis is presented. This PhD has been undertaken in the Microsystem group of the High School Engineering of the University of Seville. The structure of this thesis is organized in such a way that, all along the text, the different aspects previously described are explained in detail.

Firstly, a brief introduction about MEMS technology and the basic principles of Microfluidics is presented. Due to this work has been developed in a multidisciplinary environment, this section becomes necessary in order to give a wide view to those non

directly familiarized with these fields. Subsequently, a description of the state of the art is presented, including LOC systems and their applications in Biology, Medicine and Biomedicine, taking special attention to those applications related to organotypic and cell cultures.

After the introduction and the state of the art of the framework of this thesis, the results obtained are presented. In the first part of this PhD, the development, fabrication and characterization of the autonomous system for **culture and electrostimulation** of tissues is described. This system includes a lab on PCB (LOP) composed of a **3D microelectrode array** (MEA), with gold wires of 25 μm on **transparent substrate**, sensors and actuators, together with a microfluidic platform made of PMMA and PDMS. This LOP allows to maintain the appropriate temperature conditions to carry out medium-long term cultures without using a CO_2 incubator, as well as its continuous monitoring through an inverted microscope, thanks to the transparent materials used for its fabrication. This system is connected to an external electronic circuit and a software to control the whole system, including the electrostimulation of the biological sample. After explaining the design and the innovative fabrication process of the LOP, the experimental results are presented. Firstly, it has been demonstrated the suitability of this system to perform **organotypic cultures** of mice retinas for **longer than 7 days**, obtaining similar results to the same samples, but cultured through traditional methods. In addition, it has been provided **neuroprotection** to mice retinal explants with the **retinitis pigmentosa (RP)** disease through the electrostimulation of the samples, being able to slowdown the degeneration of the retinas caused by RP.

Another application of the presented system is focused on the acquisition of electrical signals from the biological samples cultured inside the LOP, as well as its use with cells culture. The impedance of the electrodes made of gold wires of 25 μm of diameter results too high to distinguish between the baseline noise and the electrical activity. For that reason, the second part of this thesis work consists on improving the MEA for the acquisition of electrical signals.

To achieve this goal, a stay at the University of Bath has been carried out. In this stay, the **electrical activity of prostate cancer cells** (PC-3) has been characterized by using silicon/silicon dioxide chips with gold electrodes to culture the cells.

The experiencie acquired during this stay has resulted really useful for the development and fabrication of new MEAs for electrical recordings of cells cultures. The first approach to improve the MEA has been made on PCB. It is based on growing gold by using the **electroplating technique** to create **3D gold pillars** as microelectrodes. These 3D pillars have 100 μm of diameter and 25 μm of height, to assure the contact in case of organotypic cultures. It has been demonstrated that the 3D MEA presents a lower impdenace and baseline noise with respect to the WB MEA. In addition, the experiment with PC-3 cells have been replicated inside this 3D MEA, obtaining similar electrical patterns than those achieved with the silicon chip with gold used during the stay. To improve the 3D MEA, we have decided to fabricate it on a transparent substrate, such as **glass or PMMA**, to

allow its used on optical applications. These transparent MEAs integrate planar electode fabricated through the **gold sputtering** technique over its surface. These MEAs are in a preliminary stage, and we are currently working on its biocompatibility and suitability for cell culture applications.

Finally, the conclusions of this thesis are presented, among which highlight: the fabrication process of the LOP with gold electrodes and the application of the whole system to perform organotypic cultures, including the monitoring and electrostimulation to provide neuro-protection of RP mice retinas; the transition toward the development of cell culture platforms by improving the MEA and its fabrication process in different substrates; the characterization of the electrical activity of PC-3 cells. The open lines to continue this research work are also included.

To help the reader to understand this thesis, the complementary appendices of this PhD work are attached at the end of the document.

1 Objetives and Framework

In this chapter the motivation of this thesis work is described, together with the objectives pursued during this research. Then, the structure of the document is outlined. Finally, the framework in which this PhD has been developed, and that have made it possible, is detailed.

1.1 Motivation

During the last decades, the development of numerous miniaturized devices, such as sensors, actuators, microstructures, etc. has demonstrated the capabilities of MEMS technologies, improving the functionality of their macroscale equivalents and lowering the manufacturing prices. Among all the possible platforms that could be fabricated by using MEMS technologies, those related with the microfluidic field and lab on chip (LOC) devices have seen a steady growth in different areas of application, such as Chemistry, Biology or Medicine. LOCs integrate in the same platform both microfluidic and electronic components, comprising in a small device the functionality of large scale systems, but with higher resolution, shorter time analysis and lower fabrication and maintenance costs, besides the use of smaller quantities of samples and reagents. The potential of this LOC devices make this research field very attractive, specially the possibility of decreasing prices to not depend on expensive facilities to carried out complex biological experiments, such as substances analysis or cells and tissue cultures. Related to the culture of cells and tissues, the microincubators facilitates the development of cultures without the needing of an external CO_2 incubator. Moreover, in cell and organotypic cultures, the use of microelectrode arrays (MEAs) for developing the culture allows the acquirement of electrical signal, as well as the electrostimulation of the culture, making possible a real time monitoring and an interaction directly with the biological material. The developed devices so far does not integrate these structures in an "all-in-one" system to permit an

autonomous microfluidic culture platform, which works as a microincubator, together with a MEA device to stimulate or acquire signals from the culture. In this framework, the development of an inexpensive autonomous LOC for cell and tissue cultures by using PCB-MEMS technologies and microfluidic structures will make this research line more accessible.

The Microsystem Group of University of Seville is making important progresses in the microfluidic field and the development of LOC devices. Several PhD works focused on the fabrication of microfluidic platforms have been written, laying down the first brick of this research line inside the Microsystem Group, including micropumps, microvalves, or LOC systems. The aim of this PhD thesis is to integrate in the same platform a MEA device, with sensors, actuators, and a microfluidic structure to perform an autonomous system for cells and tissue culture, with the possibility of stimulating the biological material or acquiring its electrical activity, by using both microfluidic basis and PCB-MEMS technologies.

Regarding this background, it is indispensable to settle the requirements and make a correct hypothesis of this LOC device to analyze the likely restrictions that could appear during this work, as well as to be able to contribute to this research field with new and useful approaches.

1.2 Objectives

The aim of this PhD work is the development and validation of lab on chip (LOC) platforms for its application on organotypic and cell cultures. Our hypothesis is that, by using MEMS and microfluidic technologies, we can develop an autonomous culture system, integrating a MEA device, a microfluidic structure, actuators and sensors, such as heaters and temperature sensors, an external electronic circuit and a software, to monitor the whole system and stimulate or acquire electrical signals of the biological material. On this basis, the main objectives of this thesis are outlined below:

Reliability. This is a mandatory goal no matter the device it is intended to develop. The system must be able to work in the way it has been design to. In this respect, the proposed LOP must allow a medium-long term culture, assuring the appropriate medium distribution and conditions to perform the culture, which implies temperature, CO_2 and oxygen control, as well as the functionality of the microelectrode array, whether it is for electrostimulating or recording electrical activity. Moreover, it is indispensable to guarantee the complete absence of contamination and the watertightness of the whole microfluidic structure, as well as its suitability with sterilization methods.

Integrability. The developed LOP have been designed in such a way that microfluidics, electronics, actuators, sensors, microelectrodes, etc. have been clustered in the same platform, which is connected with external electronic circuits and software. The integration of

each part of the system improve its functionality, increasing its applicability for performing continuous organotypic or cell cultures.

Self-contained. The designed LOP for organotypic cultures works as a microincubator. This means that the culture could be developed without the need of any CO_2 incubator, due to the oxygen or CO_2 levels needed are controlled through the perfusion of medium, as well as the temperature and its control are assured.

User-friendly. The presented system is intended to be used for biologists or physicians which are not familiar with it. Thus, this system is user-friendly thanks to the integration of microfluidic structures for an easy insertion and extraction of the biological material, as well as thanks to the development of a program that facilitates the monitoring of the whole system, not only of the culture environment, but also of the electrostimulation and signal recording, through an intuitive interface.

Cost effective. Finally, the last, but not least important, goal to achieve is an inexpensive fabrication method of the presented system. This implies the use of cost effective biocompatible materials with a simple fabrication process. Our culture system aims to provide the same culture conditions than traditional methods without the need of high expensive facilities, including electrical stimulation and acquisition functions.

1.3 Structure

The presented PhD thesis is composed of six chapters and four appendices along which the developed work, results and conclusions are explained, as well as a state of the art in which this line of research is framed. Finally, the most important references are included in the bibliography section.

Objectives and framework

This is the first section of this PhD work. It includes the motivation, objectives, structure and framework of the presented thesis.

Introduction to MEMS and Microfluidics

In this section, a comprehensive approach of MEMS, including microfluidic basis and materials, is presented. This section is included to facilitate the understanding of those that are not familiar with this field.

State of the art

In this section, a review of the state of the art is carried out. It is divided in two different

parts: firstly, an overview of LOC devices and its applications in Biology and Biomedicine; secondly, a detailed summary of the LOC applications on organotypic and cell cultures.

Autonomous lab on PCB for retinal culture and electrostimulation

The design and fabrication process of an autonomous LOP for organotypic culture and electrostimulation is presented in this section, as well as the different parts which compose the whole system are explained in detail. Finally, some experimental results to test the functionality of this platform as a culture LOP are presented, demonstrating its suitability for medium-long term mice retinas cultures and the electrostimulation of them to provide neuroprotection to those mice retinas with the retinitis pigmentosa disease.

Cell culture and electrical recordings application

In this section, the work carried out during the stay of the PhD student in the University of Bath, where a culture and electrophysiology of prostate cancer cells were successfully performed, is presented. The good results obtained during this stay leads this thesis work to the development of transparent MEAs in different substrates, with gold microelectrodes for recording electrical activity of cells.

Conclusions

The last section clusters the main conclusions drawn from this PhD thesis and the future lines that could continue and improve this research work.

Appendix A: Publications

The different contributions on high impact factor journals and conferences directly related with this thesis work are included in this appendix.

Appendix B: Other contributions

In this appendix, other contributions not directly related with this thesis are included.

Appendix C: Media impact

The media impact resulted from this thesis work is described on this appendix.

1.4 Framework

The presented PhD thesis has been developed in the Microsystem group of the Higher Technical School of Engineering of the University of Seville. This research work has been

supported by the Spanish Ministry of Economy, Industry and Competitiveness under grant TEC2014-54449-C3-2-R, BIOLOP, entitled "Desarrollo y Validación de una Plataforma Lab on Chip para Aplicaciones Biomédicas sobre Sustrato Pcb". Moreover, the PhD student which is the author of this thesis, Miguel Cabello Valverde, was funded by the Ministry of Economy and Competitivity under a FPI (Formación de Personal Investigador) grant, BES-2015-072059.

2 Introduction to MEMS and Microfluidics

In this chapter, the basis, principles, materials, fabrication processes and applications of MEMS, microfluidic are presented. Firstly, MEMS are described, explaining the necessity of transition from the macroscale to the microscale, the materials used for manufacturing MEMS devices and their main applications. Then, a detailed review of literature about microfluidics is presented, including basis of fluids at the microscale, materials and applications. Regarding the multidisciplinary work needed to complete the presented thesis work, including biologist or physician, this chapter can be used as a guidance for non expert on these fields.

2.1 Micro-electro-mechanical Systems (MEMS)

The acronym "MEMS", for micro-electro-mechanical systems, is original from United States, but all along the world MEMS are also known as Mycrosystem Technology (MST) in Europe, or Micromachines in Japan. MEMS comprise the integration of mechanical and electro-mechanical elements (sensors and actuators) on a substrate, for instance silicon or ceramic, at the microscale, through the use of microfabrication techniques. Dimensions of MEMS can vary from several microns to a few millimeter. Figure 2.1 is a very representative image of the dimensions of a MEMS device, in this case comparing its size with a human finger. The chance of combining many different elements implies that MEMS can be as complex as we want to, depending on if moving elements, actuators or sensors elements, among many other possibilities, are included. This type of devices allow the miniaturization of a macroscale system, permitting the sensing, actuation and control of the whole system [1].

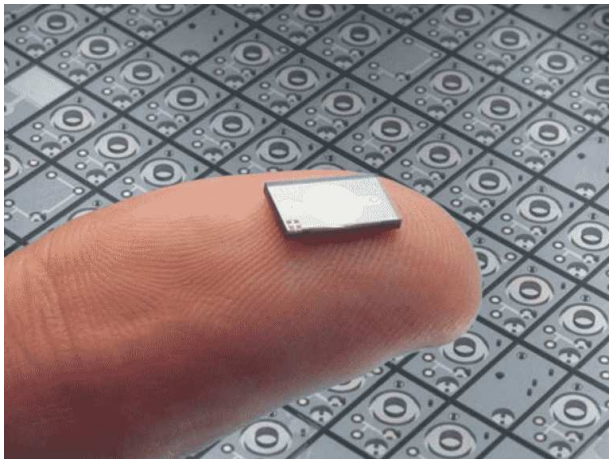

Figure 2.1 Dimensions of a MEMS device.

MEMS are presented in our daily lives more than many people believe, almost in every single electronic device that we use since we wake up in the morning. For instance, the gyroscopes or accelerometers integrated in the smartphones; the armband to measure the heart rate or monitor the activity also has MEMS sensors; the cars include MEMS in many elements, such as the air bag, which needs inertial sensors to work appropriately. Nevertheless, it is in life sciences, medicine and engineering where the applications of MEMS become more important. All the advantages and improvements that MEMS bring to the consumer explain their initial emergence during the 80's and 90's [2], as well as their growth since the beginning of the XXI century [3] until the present time [4]. Figure 2.2 shows the electronic trends of MEMS in the market, in which the smart automotive and mobile applications stand out above the rest [5].

2.1.1 From the macroscale to the microscale

As it has been previously commented, MEMS are miniaturized devices which, in the most general form, consist on clustering mechanical microstructures, microsensors, microactuators and microelectronics in the same chip (figure 2.3). Despite the progression of microelectronics are directly related to Moore's law, it is also true that, as most of the important advances in many other fields, the economic considerations play an important role.

The main reasons why MEMS have been growing exponentially in the last decades can be summarized as follow:

- It is possible to fabricate large number of MEMS devices with a low cost.

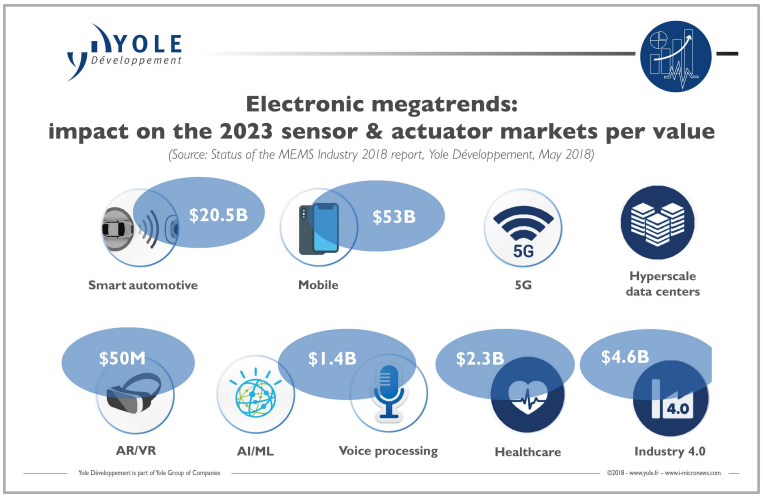

Figure 2.2 Electronic megatrends: impact on the 2023 sensor and actuator markets per value. Copyright (2018) Yole Development.

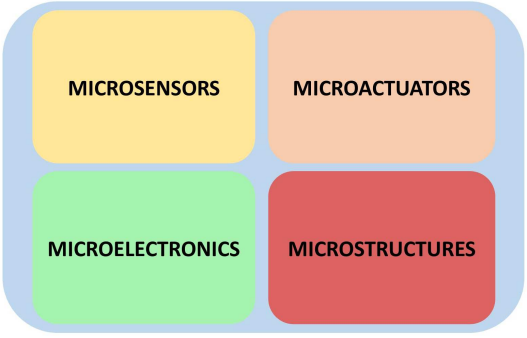

Figure 2.3 Schematic of MEMS components.

- The consumption is significantly lower than the same processes at the macroscale.

- The use of high sensitive components increase the accuracy.

- Scaling laws result favorable in MEMS. For instance, gravitational and inertial strengths are attenuated.

- Their potential is beyond question, as well as their applications and integrability with many other elements, which opens up many possibilities in the future.

The beginning of MEMS technologies date back to the early 1950s when Bell Laboratories start the development of silicon sensors [6]. In this manuscript, Smith discussed

the piezoresistance effect in germanium and silicon, demonstrating how the resistivity of both materials changed depending on the uniaxial tension. It is probably that Smith did not imagine how this research work would be as important as it is nowadays, laying the foundations of MEMS industry. Based on Smith's research, Kilby, working for National Instrument, and Noice, working for Fairchild Semiconductor, create the first integrated circuit, Kilby by using germanium as a substrate, and Noice silicon. At the end of that decade, the physicist Richard Feynman give one of his most famous talk entitled "There's plenty of Room at the Bottom", in which he gave a first approach about the miniaturization of machines and their processes [7]. Further on, in 1965 Gordon Moore made an empirical observation in which the "Moore's law" is based. This observation was that component density and performance of integrated circuits double every year [8]. Feynman and Moore are only two examples, but probably the most relevant, of scientists predicting the huge potential of what nowadays we know as MEMS.

After these first predictions, studies and approaches, many more would come, which set the basis that underpin MEMS technologies. For instance, in the 1960s Nathanson developed the first batch fabricated MEMS device, which was called "Resonant Gate Transistor (RGT)" [9]. The RGT is considered to be the first micro-electrostatic actuator. In the early 1970s, Intel presented the first single chip microprocessor, which was named Intel 4004 [10]. During the 1970 decade, HP developed the Thermal Inkjet Technology (TIJ), resulting in the first micromachined inkjet nozzles, which set the direction that must be followed in the future: reduce the size of the nozzles and increase their density [11]. At the beginning of the 1980s, Petersen published an articled entitled: "Silicon as a mechanical material", demonstrating the potential of this material for fabricating MEMS devices [12]. The development of the LIGA process allowed the manufacturing of high aspect ratio microstructures [13]. All along the 80s many companies entirely dedicated to MEMS fabrication appeared, demonstrating that this new technology had a huge potential that was still for exploiting. The products commercialized during this decade were mostly silicon pressure sensors. However, many other MEMS devices were developed during the 80s, such as accelerometers, yaw sensors or air flow sensors [14, 15, 16].

During the 90s, the growth of MEMS technology was evident. New methods of micromachining were developed, increasing the accuracy of the fabricated devices [17]. The Microelectronic Center of North Carolina (MCNC) created what was called MUMPs (multiuser MEMS processes), which consisted on three layer polysilicon surface micromachining process, and made microsystems fabrication more accessible for many users, mostly by decreasing its cost. Regarding the MEMS market, in 1993 the company Analog Devices manufactured the first surface micromachined accelerometer in high volume, which meant a huge advance in automotive security, benefitting the development of this accelerometer for its use a car airbags. At the end of the 90s and the beginning of the 21st century, optical MEMS and Bio-MEMS made their appearance, not only in research, but also in the market. Since the 2000s, MEMS devices are part of our daily lives, and they are part of our lives in a way that we cannot imagine. Their applications and integration in many things we use every day are colossal and almost unmanageable. This have created an emerging market around BioMEMS whose forecast is shown in figure 2.4. Their main

applications in the recent times are explained in detail in section 2.1.3.

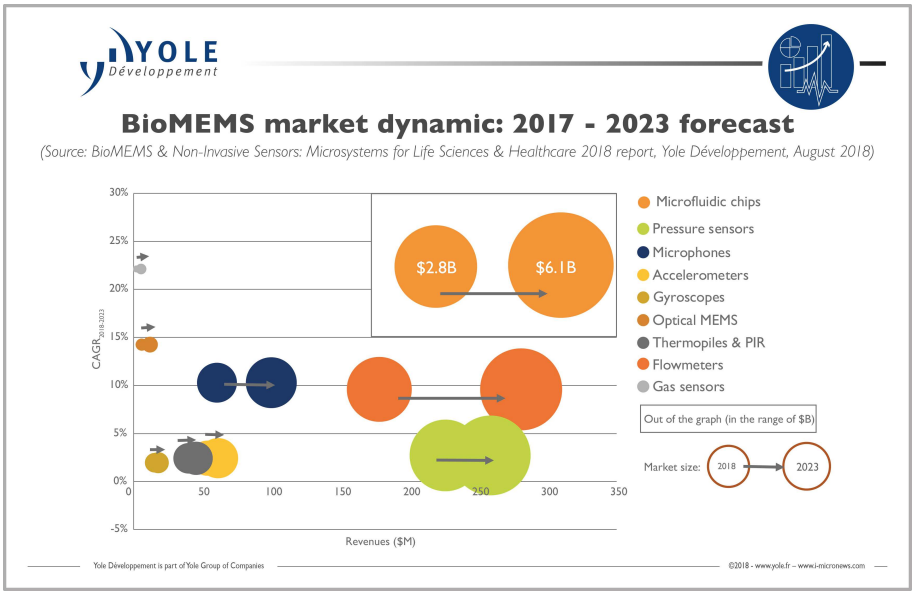

Figure 2.4 BioMEMS market dynamic. Copyright (2017) Yole Development.

2.1.2 Fabrication processes

There are many different techniques for MEMS fabrication. Normally, this fabrication implies the use of more than one of those techniques. In this section, the most widely used methods for manufacture MEMS are described.

IC fabrication techniques

Some of the processes carried out in the development of MEMS are the same than those use for integrated circuit (IC). Several steps are necessary to complete the fabrication of IC devices, and usually it is needed to repeat them several times during the manufacturing. Normally, the substrate used is silicon, but it could also be a FR4 or glass. The different steps of the process are described outline below:

- **Thin film growth**. The deposition of a thin film layer of a conductive material allow the building of passive and active components. In the case of a PCB of FR4, copper is widely used as this thin film.

- **Doping.** By thermal deposition or ion implantation, a low level of impurities are deposited to control the conductivity.

- **Lithography and etching.** A photosensitive layer (photoresist) deposited on the substrate allows the use of a mask with a designed pattern that is transferred to the this layer by using UV light. This process is called photolithography. Then, through the etching it is possible to selectively remove those parts of the conductive layer or even the substrate designed in the mask. This part of the process could be by dry or wet etching [18, 19]. Depending on the type of resist used (negative or positive), it remains what it is exposed to the UV light (negative) or it is removed what it is exposed, as it is shown in figure 2.5.

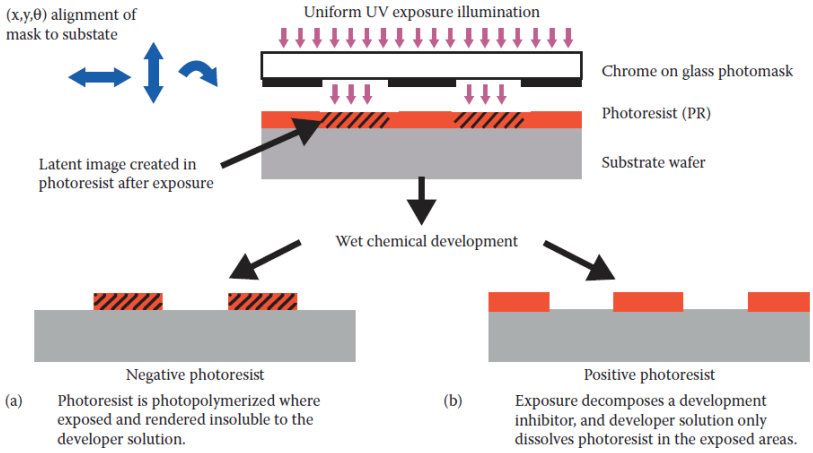

Figure 2.5 Positive and negative resist: exposure, development, and pattern transfer. (a) Negative resists remain in the exposed region. (b) Positive resists develop in the exposed region. Copyright (2011) CRC Press.

On the basis of the processes and combining them with micromachining processes, it is possible to obtain the final MEMS device. These micromachining processes are: bulk micromachining, surface micromachining and high-aspect-ratio micromachining (HARM) [20, 21]. Despite there are more different micromachining processes, in the following paragrapahs only the most representative and interesting ones for this thesis work are described.

Bulk micromachining

Bulk micromachining was the first technique developed, that is to say, it is the oldest one. Essentially, this technique consists on removing a layer to integrate mechanical parts. The two ways to perform the removal are by physical (dry etching) or chemical means (wet

etching) [22].

The wet etching process consists on immersing the substrate into a chemical solution to etch that regions of the substrate that are wanted to be removed. The etch rate and selectivity can be easily modified in the wet etching process. Its high-aspect resolution, together with its simplicity, of wet etching has converted this technique in the most widely used [23]. There are two types of chemical etching in bulk micromachining: isotropic and anisotropic wet etching. The main difference between both is that in the isotropic wet etching, the etch rate is independent of the crystallographic orientation of the substrate, so the etching occurs in all directions and at equal rates. This provoques an under etching with the same rate than the etch rate, and the etching is not completely rectangular but with a circular shape. The anisotropic wet etching is commonly used for silicon micromachining. This process is similar to the isotropic one as the substrate needs to be immersed in a chemical solution, but in this case, the etch rate depends on the crystallographic orientation of the substrate [24, 25]. The shape of the etching part is not rectangular but trapezoidal.

There are three separate classes for dry etching process: reactive ion etching (RIE), sputter etching, and vapor phase etching. RIE technique consists on producing a bombardment of ions which removes the desired parts of the substrate. There is a variant of the RIE process, called DRIE, which permits an etching depth of hundreds of microns with almost vertical sidewalls. Sputter etching is similar to RIE but without reactive ions. Vapor phase etching dissolves the material to be etched at the surface of the substrate by chemical reaction of gas molecules [26, 27]. Despite its very high resolution and precission, its high cost makes this method less popular than wet etching in MEMS industry. Figure 2.6 shows the scanning electron micrographs of nanopillars fabricated on a silicon substrate.

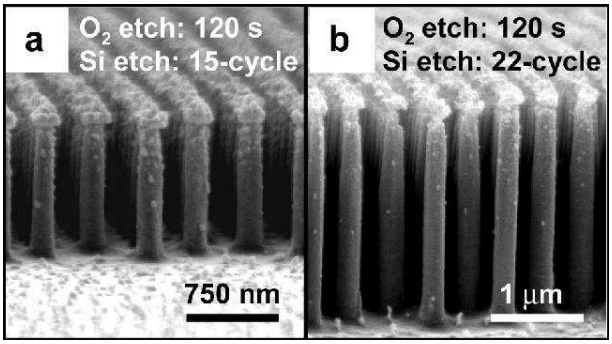

Figure 2.6 Scanning electron micrographs of nanopillars fabricated from a polystyrene bead patterned silicon surface pre-etched with a 120 seconds oxygen RIE etch period, followed by (a) 15 or (b) 22 cycles of the silicon etch process. Copyright (2006) Institute of Physics Publishing.

Surface micromachinging

Surface micromachining is another widely used technique for MEMS manufacturing [28]. Among all the different methods to carry out the surface micromachining, those based on the use of sacrificial layers are the most common. The steps followed in the process start with the deposition of the thin film, which act as a temporary mechanical layer, over the substrate. After the deposition of this thin film, another layer, which is called structural layer, is deposited and patterned. Then, the temporary layer is removed, leaving the substrate with the structural layer, but not the sacrificial one. One of the main reasons why this micromachining process is commonly used is that it allows a very accurate control in the vertical direction through the control of the thickness of the sacrificial layer. Thus, many different structures can be defined by using this technique. Nevertheless, this method shows also some disadvantages such as the need of knowing the mechanical properties of the thin film deposited as a sacrificial layer, which is not always specified in the material data-sheet. Another inconvenient that it is important to take into account is the stress that occurs to the structural layer when the sacrificial layer is released. Not only residual stress, but also stiction effect can appear. Polysilicon is one of the most typical material used as a structural layer, and silicon dioxide as a sacrificial layer.

High aspect ratio micromachining (HARM)

The high aspect ratio micromachining (HARM) technique provides a relation between depth and width (what is called "aspect ratio") with a very high precision. This method allows to obtain structures of a few microns width, with a very controlled depth [29, 30]. There are several process related to this technique, but two of them are the most important: DRIE and LIGA processes. Deep Reactive Ion Etchin (DRIE) was briefly described in the "Bulk micromachining" section, but here it is going to be detailed. DRIE process permits the fabrication of microstructures with almost vertical walls on the etched parts, and a depth of several hundreds or even thousands microns. This method requires the use of dry plasma etching, in such a way that the substrate is placed inside the plasma reactor and then bombarded by heavy ions to remove the desired part of the substrate [31]. Figure 2.7 shows a high aspect ratio microstructures fabricated by using the DRIE method on silicon.

The other popular method related with the HARM techniques is the LIGA process, which is the German acronym for "LIthographie Galvanoformung Adformung". This process is characterized for being devised as a non-silicon based technology and for requiring synchrotron generated x-ray radiation. The fabrication involves the exposition of a PMMA substrate to the x-ray radiation using a lithographic mask. After the x-ray exposition, the structure is developed following the pattern of the mask, obtaining a very high resolution and almost vertical walls. Then, this developed piece of PMMA is used as a mold, inserted inside an electroplating bath solution to deposit metal in the open areas. The final step of the process consists on demolding the metal part from the PMMA [32, 33, 34]. There is another method with is closely related with the HARM techniques which is called hot embossing that consists on creating structures by molding [35, 36]. To carry out this

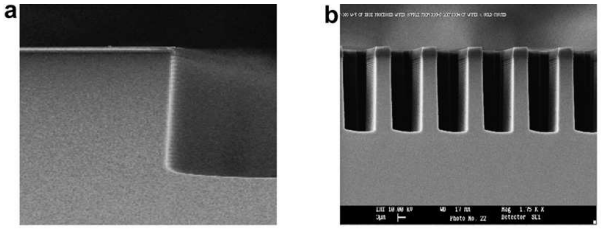

Structure Having Negative Tapering (SF_6 = 150 SCCM, C_4F_8 = 100 SCCM) (Passivation Time : Etch Time :: 5 Sec : 14 Sec)

Structure Having No Tapering at all (SF_6 = 150 SCCM, C_4F_8 = 100 SCCM) (Passivation Time : Etch Time :: 8 Sec : 14 Sec)

Figure 2.7 SEM images for two different etch cycles (a) more tapered (b) no tapering in side wall profile. Copyright (2010) Elsevier Ltd.

process, it is only need a mold, that could be similar to those used on the LIGA process and a polymer substrate (thermoplastics are very common). The mold and the substrate are placed between two hot plates and then by the application of pressure and a temperature close to the glass transition temperature of the substrate the mold design is transferred to the substrate, resulting in a micromachining structure with a high resolution and almost vertical walls. This hot embossing method could be considered a LIGA low cost method, because it is not needed the use of x-ray radiation.

Wafer bonding

The wafer bonding technique consists on joining several (at least two) wafers together to create a multiwafer stack [37, 38]. There are basically three main types of wafer bonding, which are: direct bonding, anodic bonding, and bonding using an intermediate layer. It is crucial for a correct performance of this technique to have a very flat substrate and carry it out in a extremely clean environment to have a successful result free of voids [39]. Direct bonding is normally used to join two silicon wafers together but without an intermediate layer [40, 41]. This technique is also useful to fabricate Silicon-On-Insulators (SOI) wafers with layers of several microns thick [42]. The anodic bonding is another popular method in which a silicon wafer is bonded to a glass wafer by using electric fields and high temperature [43]. This technique allow the pre-processing and alignment of the two wafers before the bonding. Over the years, several improvements of anodic bonding has demonstrated that the procedure can be performed at low temperature [44]. As it occurred in the direct bonding method, anodic bonding also requires an extremely flat and clean substrate to obtain a good result. Other processes that are important to highlight related to the wafer bonding are those that utilize an intermediate layer and a high temperature to bond both wafers [45]. Different materials can be used as intermediate layers, such as epoxy resins, photoresists, polyamides, silicones, etc.

Table 2.1 MEMS applications.

Electronics	Defense	Communications	Medical	Automotive
Disk drive heads	Surveillance	RF relays switches filters	Miniature analytical instruments	Intelligent tires
Projection screen TV accelerometers	Data storage	Tuneable lasers	Drug delivery systems	Airbag sensors
Inkjet printer heads	Munitions guidance	Voltage control oscillators	Blood pressure sensors	Brake force sensors suspension control
Avionic pressure sensors	Aircraft control	Fiber optic network component	Pacemakers	Air conditioning compressor sensors
Mass data storage systems	Embedded sensors	Projection displays in portable communication devices	Prosthetics	Fuel level and vapor pressure sensors
Earthquake sensors	Arming systems	Splitters and couplers	Implanted pressure sensors	Internal navigation systems

2.1.3 MEMS applications

The huge number of MEMS applications make almost impossible to include all of them in this subsection. Those related with the medical and biological field are explained with more details in the following sections. However, table 2.1 summarizes some of the most important applications of MEMS [46].

2.2 Microfluidic platforms

In this section, the state of the art of microfluidic platforms is described. Hence, in the following paragraphs are included: a brief explanation about the microfluidic principles; the most widely used materials for fabricating microfluidic structures, taking special attention on those used in this thesis work; the most representative microfluidic applications.

The development of microstructures with biological applications demands the use of fluids at the microscale. This miniaturization has led to an increasing development of

microfluidic devices, which provide highly versatile platforms in which it is possible to perform a huge variety of biological processes. In essence, microfluidics study the behavior, manipulation and control of fluids at the microscale, namely volumes of fluid even lower than μL within micrometer-sized structures between 1 to 500 μm. Microfluidics involve a multidisciplinar field including engineering, physics, chemistry or biotechnology, among many others.

Despite the term "microfluidic" was applied for the first time in 1940 [47], it was not before the late 1970s, with the development of the silicon-based microfabrication techniques, when the principles of this concept were set and the first devices were developed, through the introduction of gas chromatography systems [48]. Even so, the field of microfluidics start to gain a real impact around the 1990s [49]. Over the last three decades, the development of new microfabrication techniques, as well as the advances related to the materials used to create microfluidic structures, such as polymers or thermoplastics, have led this research field to establish it as one of the most popular approach and with the highest possibilities between MEMS platforms. One of the main reasons why microfluidics have undergone this increase is due to its countless applications in biology, biochemistry or medicine [50, 51, 52], specially through the development of lab on chip devices [53]. The potential of the microfluidic field is so huge that many commercial systems have been developed and brought to the market from big companies such as Abbot, Agilent or Dolomite, among many others. Moreover, there are a huge range of possibilities that this research field offers, so the future of microfluidics is still bright.

2.2.1 Microfluidic principles

Before explaining the principles that rule microfluidics, it is necessary to understand why do we need the microscale and what kind of benefits does it have. Carrying out fluidic processes at the microscale have lot of advantages in comparison with the same processes but performed through "traditional methods", including low volumes, high speed of analysis, low cost, transparency, portability, biocompatibility and mass production. These advantages are described below.

1. **Low volumes.** A microfluidic platform contains channels with small dimensions, inside which only a small volume of sample or reagent is required. Normally, the volume needed to perform this kind of processes at the microscale are lower than 1μL, which is clearly much smaller than the volume utilized in the same process at the macroscale.

2. **High speed of analysis.** The processes performed through bulk solution chemistry have an inherent problem: diffusion is slow. Thus, the smaller distance between sample and reagent, the faster the interaction occurs. Moreover, at the microscale, flows are normally laminar and the mixing of fluids normally happens by diffusion. In adition, high surface-to-volume ratio makes the microfluidic devices more sensitive and faster.

3. **Low cost.** The amount of material needed to fabricate microfluidic devices is considerably lower in the microscale, resulting in a reduction in the production cost. Furthermore, the use of very low volumes of samples and reagents implies a significant cost saving compared to the macroscale methods.

4. **Transparency.** The fabrication of most of the microfluidic devices requires materials with a high transparency, such as thermoplastic or polymers. This fact, is a great advantage for the microfluidic platforms, permitting their use for optical sensing applications, being possible the visualization of the liquids movement all along the microchannels.

5. **Portability.** Miniaturize the processes by using microfluidic structures makes them easily portable, approaching the utilization of this type of devices in on-site testing, provided the appropriate portable hardware together with the microfluidic part.

6. **Integration of multiple processes.** The possibility of integrating many different processes in the same platform, such as mixing, heating, labeling, detection, etc, makes this type of devices suitable for many applications, specially in the biological and medical fields, but also in many others.

7. **Biocompatibility.** As it has been explained before, microfluidic devices have found some of their most important applications in the life sciences field, specially in biology, medicine or chemistry. Thus, the biocompatibility requirement becomes indispensable, resulting in the use of biocompaible materials, such as polymers or thermoplastics. In addition, many of the fabrication processes for microfluidic platforms are carried out in clean rooms, where the aseptic environment is assured, making them suitable for biological or biomedical applications.

8. **Parallelization.** The recent improvements in the microfabrication techniques have made possible the massive production of microfluidic devices with the same characteristics. Moreover, the miniaturization allows the fabrication of high density microstructures. As it was explained in point 6, not only the fabrication, but also the operation, of this kind of platforms should be able to be worked in a high-throughput way.

Once the advantages of microfluidics have been exposed and settled, it is time to explain the theoretical principles of microfluidics. It is necessary to highlight that, despite there are some common principles to both macroscale fluidics and microfluidics, there are some important differences that needs to be explained. This principles are detailed in the following paragraphs.

Fluid dynamics exhibits such inherent complexity that requires to be exactly modeled. In the case of microfluidics, its physical behavior is based on the Navier-Stokes (NS) equations [54]. These equations are also known as the Newton's second law for fluid

particles.

$$\rho(\frac{\partial \mathbf{u}}{\partial t} + (\mathbf{u}\cdot\nabla)\mathbf{u} - f) + \nabla p - \mu\nabla^2\mathbf{u} = 0 \tag{2.1}$$

$$\nabla \cdot u = 0 \tag{2.2}$$

Equations 2.1 and 2.2 shown the Navier-Stokes equations, in which ρ is the fluid density, u is the flow velocity, ∇ is the vector differential operator, f represents the mass forces, p is the pressure and μ is the fluid dynamic viscosity.

NS equations derived from different mathematics calculations carried out during the first half of the XIX century by Navier, Poisson, Saint-Venant and Stokes. These equations correspond to the extensions of Euler equations, but including the effect of viscosity on the flow of liquid. The complexity to solve NS equations analytically has derived in approximations to simplify the calculations. These simplifications are characterized by different dimensionless numbers, being the most important: Reynolds number, Weber number, Capillary number and Péclet number.

Reynolds number.

Reynolds number measures the ratio between inertial forces to viscous forces [55]. The Reynolds number is calculated as follow 2.3:

$$Re = \frac{\rho v L}{\nu} \tag{2.3}$$

Being ρ the density of the fluid, v the velocity of the fluid, L the characteristic length and ν the viscosity of the fluid. The Reynolds number is derived from the NS equations when it is not necessary to considerate the compressibility of the fluid. Moreover, for fluids flowing inside a tube, the parameter L is normally substituted by the hydraulic diameter, which depends on the area and the perimeter.

Reynolds number main application is to determine whether the fluid flow is laminar or turbulent. Thus, for a $Re < 2300$ the flow is considered to be laminar, whereas for a $Re > 2900$ the flow is considered to be turbulent [56]. It is important to highlight that in microfluidics, most of the situations occur for a laminar flow, mainly due to the very small dimensions of the microchannels [57].

Weber number.

The Weber number defines the ratio between the inertial forces and the surface tension

forces, indicating whether the kinetic force or the surface tension is the dominating one. The equation for the Weber number is described as follow 2.4:

$$We = \frac{\rho v^2 L}{\sigma} \tag{2.4}$$

Being ρ the density of the fluid, v the velocity of the fluid, L the characteristic length and σ the surface tension [58]. The surface tension will be dominant when the Weber number is low, otherwise the kinetic force will be dominant. In microfluidic, high values for Weber number tend to favour the formation of bubbles [59].

Capillary number.

The Capillary number represents the ratio between the viscous forces and the surface tension across an interface between a liquid and a gas [60], determining whether the capillary forces or the viscous forces are dominant. Equation 2.5 represents the capillary number:

$$Ca = \frac{v\mu}{\sigma} \tag{2.5}$$

Being v the velocity of the fluid, μ the viscosity of the fluid and σ the surface tension between the two gas and the liquid. For values of Ca lower than 10^{-5} capillary forces are dominant, while for values of Ca higher than 10^{-5} viscous forces dominate, making capillary forces negligible [61]. Capillary number is usually small in microfluidics, thus the capillary forces tend to be dominant [62].

Péclet number.

The Péclet number represents the ratio between the thermal energy convected to the fluid and the thermal energy conducted within the fluid [63], indicating whether the diffusion or convection affects more to mass transfer of the fluid. Equation 2.6 shows the Péclet number formula:

$$Pe = \frac{vL}{D} \tag{2.6}$$

Being v the velocity of the fluid, L the characteristic length and D the diffusion coefficient. The lower the Péclet number is, the higher the influence of diffusion to mass transfer is, while the higher the Péclet number is the higher the influence of convection becomes. This dimensionless number is lower than 1 in the microscale, thus in microfluidics diffusion dominates the mass transfer.

Inherent to small-scales devices, microfluidics present some advantages that simplify considerably the calculations of the equations previously described. Firstly, and probably the most important one, is the low Reynolds number in the micro-scale. A low Reynold number implies a laminar flow inside the microchannels, making the fluid flow more predictive in microfluidic than at the macro-scale. The fact that diffusion dominates at the micro-scale, as it has been previously explained, has an influence specially in the mixing of different liquids inside the microfluidic device, being the basis over which the passive micromixer are supported [64]. Péclet number is close related with this last claim, because this parameter is normally lower than 1 in the microscale, which facilitate the mixing by diffusion. Moreover, capillary number is normally small in microfluidics, which is reflected in a dominance of the capillary forces. Finally, it is important to take into account the Weber number at the microscale to avoid or provoke the formation of bubbles.

2.2.2 Building materials and its fabrications processes for microfluidic devices

Once the principles and basis of microfluidics has been properly described, the understanding of this field makes indispensable an overview of the building materials and the fabrication processes of microfluidic devices. When a microfluidic device is intended to be developed, the main question that needs to be answered is: "what function is trying to be accomplished with this device?" Depending on the answer, the material chosen must have some characteristics such as optical transparency, biocompatibility, flexibility, air permeability, etc.

Since the early 1990s, the technology of microfluidics has experimented an unstoppable growth, including important improvements related to the different materials used to fabricate the microfluidic devices [65, 66]. The first microfluidic chips were fabricated on silicon, glass or ceramic substrates, which are usually named *inorganic materials*, mainly because these materials were the commonly used for the fabrication of microelectronic components. Later on, the breakthrough of polymers as fabrication materials for microfluidic structures marked a turning point, specially due to its impact in the medical and biological fields, thanks to the biocompatibility of these materials. In the last decade, a new technology based on the fabrication of microfluidic devices using paper is emerging. In this section, the different materials used for the fabrication of microfluidic devices are described, highlighting those related with this thesis work, which are PDMS and thermoplastics.

Inorganic materials

Silicon.

Silicon was the first material used for the fabrication of microfluidic devices, particularly for gas chromatography and capillary electrophoresis. [67, 68]. As it has been described in section 2.1.2, silicon is widely use for the fabrication of integrated circuits (IC), and

nowadays is still the most used material for this purpose, even with the appearance of many others materials suitable for IC. Silicon fabrication processes are previously included in section 2.1.2. Related to microfluidics, silicon can be the correct choice in case a high temperature resilience is demanded, or a high aspect ratio structures are required. Silicon is also a good option if the integration of electrodes or other electronic components is needed, or if an uniform temperature distribution has to be ensured [69, 70]. Elastic modulus of silicon is high (130-180 GPa), and its surface chemistry is based on the silanol group, being possible its modification through silanes.

However, silicon cost is probably the main disadvantage of this material, but not the only one to fabricate microfluidics. Despite silicon is transparent to infrared, it is not to the visible spectrum, making this material not suitable for optical applications, unless combined together with transparent structures made of glass or plastic. If combining silicon with other materials, the bonding method becomes crucial. Wafer bonding methods, which was firstly explained in subsection 2.1.2, are also used for microfluidic applications and can be divided on three types: direct bonding, anodic bonding and adhesive bonding. For instance, anodic bonding is used for sealing a glass cover to a patterned silicon wafer [71]. Silicon has been used to fabricate active components such as pumps or valves [72, 73], and more complex structures such as nebulizers chips or cell growth chambers [74, 75]. Figure 2.8 shows an integrable silicon microfluidic valve with pneumatic actuation developed by Luque et al. [76].

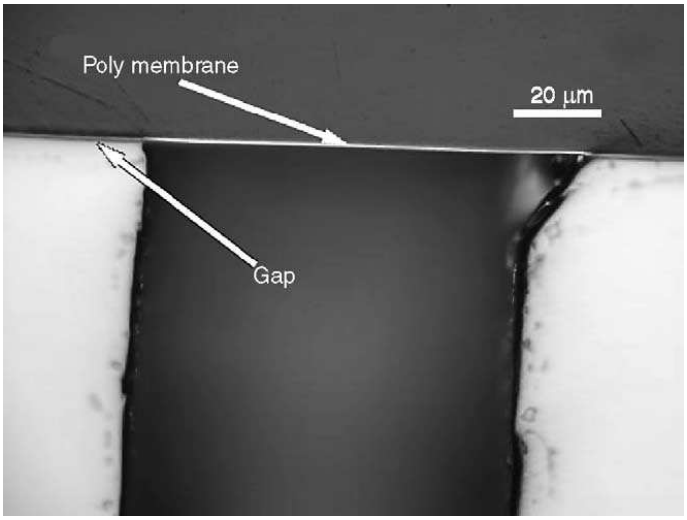

Figure 2.8 Detailed view of polysilicon membrane and fluid orifice, obtained by cutting a finished device. The gap through which working fluid flows is also shown. Copyright (2005) Elsevier Ltd.

Glass.

Glass is another widely used material for fabricating microfluidic devices. Despite at the beginning glass was mainly used in combination with silicon, microfluidic structures started to be created only with glass [77]. These microstructures are usually fabricated by dry or wet etching methods on glass [78]. Regarding the borosilicate glass, which is the most commonly used, it is possible to create microfluidic channels by using bonding methods or hybrid layer attachment. Its surface chemistry is based on silanol, just like silicon. One important advantage of glass is its compatibility with biological material, as well as its transparency for optical applications. Moreover, glass has a low non specific absorption and it is not gas permeable. Glass applications are diverse, from capillary electrophoresis to gas chromatography, including polymerase chain reactions (PCR) devices [79, 80, 81]. The microfluidic device fabricated on glass for DNA amplification is shown in figure 2.9.

Polymers

Over the past 25 years, polymers have experimented an important growth as the main material to fabricate microfluidic devices. Despite the advantages that silicon and glass have, their high cost and limitations have made the efforts to be focused in developing new materials and fabrication techniques to implement non-expensive microfluidic structures with new applications and possibilities. In this context is where polymers makes their appearance in the field of microfluidics.

Polymers are organic-based, long-chain materials. Based on their definition, polymers materials are formed by polymerization, which is *the process of converting a mixture of monomers into a polymer* [82]. Their main advantages are their low cost, their fast fabrication process and suitability for mass production, for instance through hot embossing or injection moulding techniques, and their flexibility to changes and modifications.

Nowadays, the emergence of polymeric materials as the most widely used material for microfluidic applications implies the appearance of new microfabrication techniques which are directly related to polymers, some of them were described in section 2.1.2. In addition, polymeric materials can be integrated with other materials which are normally used as substrates, such as glass, silicon or PCB [83, 84, 85].

Polymers advantages that have increased their use over other materials, such as silicon or glass, for the fabrication of microfluidic devices are their easy manufacturing processes, such as lithography, molding, hot embossing, etc, and their biocompatibility, which make them suitable for multiple biological and biomedical applications [86].

In this section, among the different synthetic polymers usually utilized for microfluidic applications, SU-8, polydimethylsiloxane and thermoplastics are described.

SU-8.

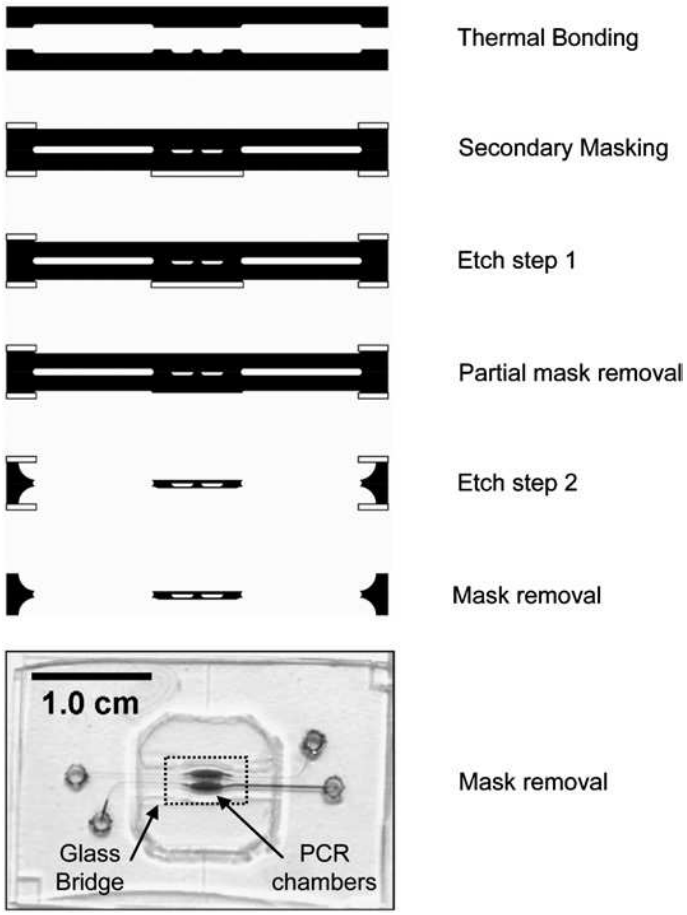

Figure 2.9 Illustration of the thermal mass removal procedure using a cross-sectional view through the center of the reaction chambers. A five-step process follows thermal bonding, consistent with typical fabrication techniques. Glass layers are shown in blacknand masking tape in white (outlined in black). Digital image of the completed device (filled with ink), with reaction chambers in the bridge configuration. The dotted rectangular region outlines the primary focus of the tungsten lamp (4mm×7mm), corresponding to the region for which heat transfer analysis was performed. Copyright (2007) IOP publishing.

"SU-8 is a high contrast, epoxy-based photoresist designed for micromachining and other microelectronic applications where a thick chemically and thermally stable image is desired. The exposed and subsequently cross-linked portions of the film are rendered insoluble to liquid developers. SU-8 has very high optical transparency above 360 nm, which makes it ideally suited for imaging near vertical sidewalls in very thick films. SU-8 is best suited for permanent applications where it is imaged, cured and left in place." [87].

This definition of the SU-8 is given by MicroChem, which is the most important distributor of SU-8, in their website.

SU-8 was developed and, subsequently, patented by IBM [88]. SU-8 is one of the most widely used materials for microfluidic applications, due to, basically, its optical transparency, high resolution, high aspect ratio, excellent sensitivity, and good mechanical, thermal and chemical stability [89]. Moreover, the SU-8 is hydrophobic, avoiding the liquids to adhere to the walls of the microchannels, which benefit the fluidic flow at the microscale, and biocompatible, making it suitable for its use in biological and biomedical applications [90, 91]. However, SU-8 presents some disadvantages during its fabrication, being the most important the adhesion selectivity depending on the substrate, the stress and resist stripping [92]. In figure 2.10 a group of gold electrodes in SU-8 are shown.

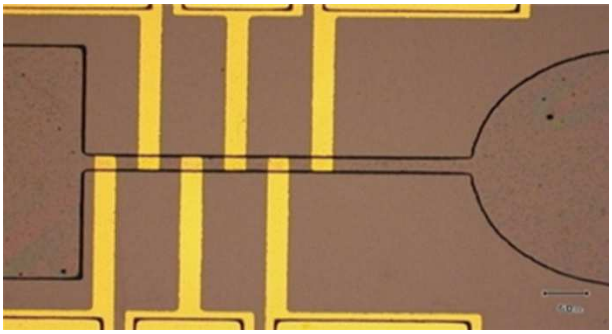

Figure 2.10 Gold electrodes in SU-8 2010. Copyright (2012) Hindawi Publishing Corporation.

Normally, SU-8 is used for fabricating microfluidic structures with a height ranging between a few microns and a few millimeters. The high aspect ratio of this polymer, which is 10:1, allow the fabrication of narrow microchannels with a considerable height and vertical walls. Their fabrication process is a standard procedure with several steps, and the coating speed, temperature and time needed for a correct deposition and growth of SU-8 layers over a substrate are perfectly described in the SU-8 data sheet provided by the manufacturer.

The first step of the fabrication process of SU-8 is the pretreatment and cleaning of the substrate, which could be, for instance, a silicon wafer or a PCB of FR4 and a copper layer. This cleaning can be done by rinsing the wafer on different aqueous solutions, together with ultrasonic sound, to eliminate the particles and contamination of the substrate. The next step is the coating of the SU-8 layers that are going to be deposited on the substrate. Depending on the viscosity of the SU-8 and the speed (r.p.m) of the spin coater, the height of the deposited layer varies. This relation is given by the manufacturer [87]. The third step is called soft bake and consist on heating the wafer with the deposited SU-8 at a certain

temperature to eliminate the solvent of the polymer. The heating is normally carried out on a hot plate, and temperature and time required are given in the data sheet. Then, the wafer with the deposited SU-8 is exposed to UV light through a mask with a certain design, to remain or eliminate the desired parts of the SU-8. The data sheet also includes the different exposure energy needed depending on the thickness of the SU-8 layer. The next step is called post-exposure bake (PEB), and consist on heating the wafer with the exposed SU-8 to a certain temperature to crosslink the polymer. After the PEB step, the wafer with the crosslinked SU-8 should be cool down slowly to avoid any stress in the layers. The next step is the development by rinsing the wafer with SU-8 on a specific solution to remove the SU-8 which was not exposed to UV light and remain those parts which were exposed to UV light. Finally, the wafer with SU-8 is rinsed in Isopropyl alcohol (IPA) to clean the possible remains of non cured polymer.

PDMS.

An elastomer is a cross-linked polymer that can compress or stretch by an external force, returning to the original shape once that force withdrawn [66]. Among the different elastomers that can be suitable for microfluidic applications, polydimethylsiloxane (PDMS) is clearly the most widely used. It is not before the end of the XX century when the advantages of PDMS as a microfluidic material start to be demonstrated, considering the most important the reproducibility of the microscale features through the molding technique, its suitability for its use with biological samples and its optical transparency, as well as its low cost fabrication [93].

PDMS physical and chemical properties were accurately described by Mcdonald and Whitesides, including optical, mechanical or thermal ones [94]. These properties make this elastomer suitable for fabricating microfluidic structures with biological applications. There are some advantages related to these properties, such as the high reproducibility through pattern transfer by using the molding technique which is very important in microfludic applications, being able to replicate structures in the micro and even in the nano scale [95]. In accordance with the high reproducibility, being an elastomer deposited in liquid state permit the adaptation of PDMS to non planar surfaces and its releasing from them without breaks, even in the case of microstructures. Their optical transparency to a huge range of the light spectrum (from 240 to 1100 nm) permit its use with many optical detection techniques, such as fluorescence, making this characteristic vital for biological applications.

PDMS is commonly used in liquid state and then cured at different temperatures, needing a higher curing time for lower temperatures, and vice versa, depending on the manufacturer datasheet. Typically, PDMS is composed of two components mixing in a proportion of 10:1 and then deposited inside a mold with the designed structure. These molds, which are used to obtain microfluidic structures in PDMS, are normally fabricated via micromachining or photolithography processes [96, 97, 98]. PDMS is deposited and cured on these molds, resulting in microfluidic structures with the same shape of those molds, obtaining a high reproducibility of them. Figure 2.11 shows a mold made of SU-8 and the microchannels

fabricated in PDMS after molding and peeling from the mold. It is also possible to fabricate multilayer devices and closed structures by bonding different layers of PDMS before its complete curing [99, 100].

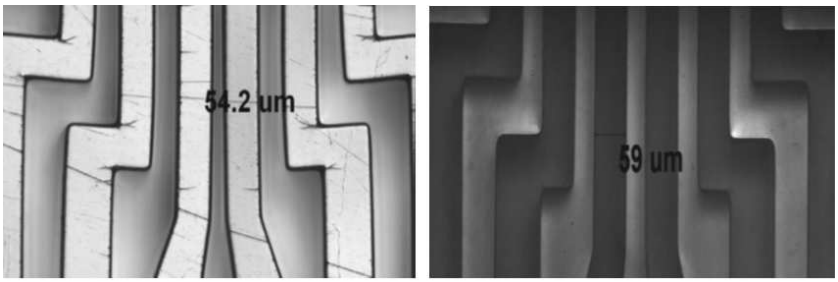

Figure 2.11 (a) Features in the SU-8 mold and (b) microchannels created in PDMS after molding and peeling from SU-8. The channels arefilled with a dye. Copyright (2008) IOP Publishing.

In addition, PDMS shows good sealing with itself and with many other materials, such as plastics, glass or silicon. One of the most used techniques to bond PDMS with PDMS, glass or silicon, is by exposition to plasma oxygen to form covalent bonds [101]. Despite PDMS is a hydrophobic material, this elastomer can be turned to hydrophilic by oxidation treatments or by the previously mentioned plasma oxygen exposition [102]. PDMS presents a permeability to gases, making this materials specially interesting for cell applications [103, 104]. Together with its gas permeability, the biocompatibility of PDMS are two indispensable characteristics in biological applications. As it has been mentioned before, this material is widely used for the development of lab on chip devices, allowing the living of cells which are directly in contact with the PDMS [104, 105].

Nevertheless, not all the properties of PDMS can be considered an advantage, but a disadvantage or a limitation [106]. For instance, the possibility of deformation of the structure or the hydrophobic recovery can be difficult problems to solve when developing microfluidic structures with biological applications with PDMS. Related with one of the main characteristic that allow the use of PDMS for cell culturing, this permeability to gases has also some problems, such as the incompatibility of PDMS with organic solvents, or the absorption of hydrophobic molecules or even water in gaseous state due to the evaporation of water inside the microchannels. For cell and organotypic culture applications, this problems should be taken into account, specially in those cases in which evaporation of molecules could occur, for instance when high temperatures and liquid handling are required [107].

Thermoplastics

Thermoplastics are an alternative to both SU-8 and PDMS for the fabrication of microfluidic structures. Their widely use in industry provides a huge experience and characterization of these materials. Thermoplastics are densely crosslinked polymers which become moldable when heated over their glass transition temperature (T_g), but maintain their shape when cool. At the glass transition temperature, the viscosity changes and thermoplastics become soft and, consequently, moldable. Over T_g, at the melt temperature, thermoplastics change from solid to liquid state, and depending on the material, this temperature could be very high. The volume of thermoplastics changes with temperature, being the thermal expansion coefficient the relation between both variables [108]. Moreover, these materials can be reshaped and remolded many times by reheating, making them suitable for thermal bonding.

The most widely used thermoplastics for microfluidic applications and LOC devices fabrication are: polystyrene (PS), polymethylmethacrylate (PMMA), polycarbonate (PC), Cycloolefine copolymer (COC) and polyethylene terephthalate (PET) [109]. Thermoplastics are generally lasting, suitable for micromachining, almost impermeable to small molecule and optically clear. Their impermeability to gases make these materials suitable for sealing chambers, but not for long term cell cultures in closed devices. Apart from the impermeability, other important differences between thermoplastics and PDMS are the higher rigidity of the first ones and their better solvent compatibility. The microfluidic suitability of the most used thermoplastics is described below:

Polystyrene (PS)

Polystyrene is a vinyl polymer, made from the polymerization of styrene, which is obtained by reacting ethylene with benzene. PS has a relatively low melting point (between 200 and 250 °C) and a glass transition temperature of about 100 °C [110]. It is a hard material which can be naturally transparent, but can also be colored. Among the disadvantages of PS, its flammability and its low resistance to breaks are the most important ones. Its low cost makes it very common in many everyday life items, such as disposable eating elements or foamed cups and plates. PS surface is hidrophobic, requiring specific treatments, such as plasma oxygen or chemical modification, to make it hydrophilic. PS is widely used as a microfluidic material for many biological and chemical applications [111], as it is shown in figure 2.12, demonstrating a particular feasibility for cell culture applications [112]. PS allows thermal bonding with other thermoplastics, such as PS or PMMA, to create closed microfluidic systems [113].

Polymethylmethacrylate (PMMA)

PMMA results from the polymerization of methyl methacrylate. Its melting point is around 160 °C, lower than PS, and its T_g is about 100 °C, but it can vary considerably depending on the commercial type of PMMA. This thermoplastic is rigid and transparent to the visible spectrum and the UV light [114], being the perfect substitute for glass due to its lightweight and its low cost. Morover, PMMA is biocompatible, gas impermeable and easily machinable. Some disadvantages that should take into account are its limited heat

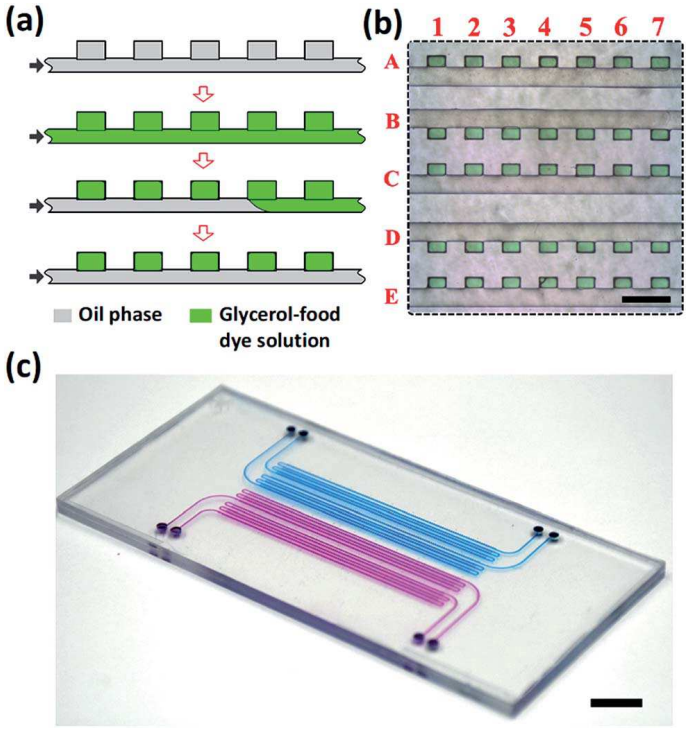

Figure 2.12 Polystyrene well plate device hosting a dense 2D array of droplets. (a) Schematic of aqueous droplet generation. (b) Optical microscopy image of the fragment of indexed 2D droplet array (the droplets are labeled with a green food dye). Scale bar is 500 mm. (c) Photograph of a PS device containing 2000 wells filled with a blue and red food dyes, with each row of 500 wells connected to an individual supplying channel. Scale bar is 1 cm. Copyright (2017) The Royal Society of Chemistry.

resistance (not recommended over 80 °C) and its limited chemical resistance to organic solvent. PMMA is commonly known by its commercial name Plexiglas. In daily life items, instead of glass, PMMA can be found in outdoors constructions or in the automotive industry, as car windows or motorcycle windshields. The applicability of PMMA for mass production makes this thermoplastic very useful for microfluidics applications, making possible the fabrication of low cost disposable devices. Moreover, PMMA is the least hydrophobic plastics of common use [115], besides being compatible to electrophoresis [116, 117], as can be seen in figure 2.13. In the biological field, PMMA has been used, for instance, for drug release applications [118] or for cell culture applications, used in combination with other materials such as PDMS [119] or paper [120].

Polycarbonate (PC)

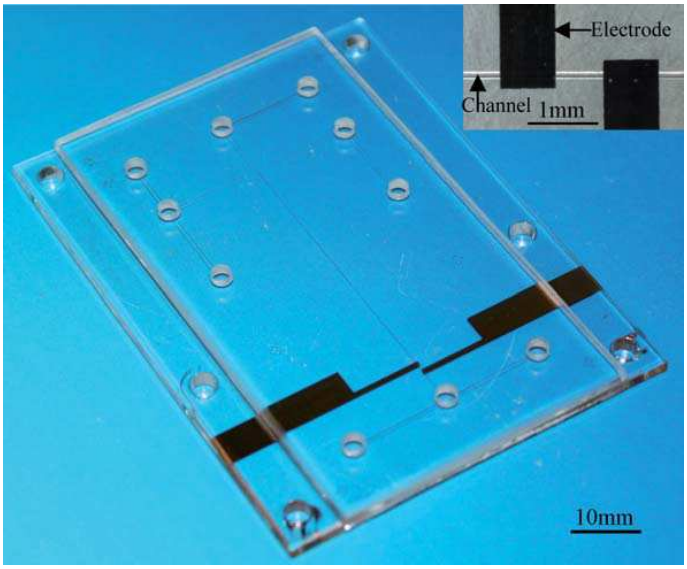

Figure 2.13 The three-layer PMMA electrophoresis microchip integrated with Pt microelectrodes. The enlarged view of the microelectrode and the microchannel region is shown in the inset. Copyright (2011) The Royal Society of Chemistry.

Polycarbonate is a thermoplastic created by polymerization of bisphenol and phosgene, containing repeated carbonate groups in its structure. Its melting point is around 155 °C, similar to PMMA and lower than PS, and its glass transition temperature is around 147 °C. PC is durable, rigid and transparent material with a high impact resistance. As it occurs with PMMA, PC is also a good substitute for glass, but with the difference of being a natural UV filter. Some disadvantages in comparison with other plastics is that polycarbonate is normally more expensive than other alternatives, and PC has a poor scratch resistance and a limited resistance to organic solvents. PC can be found in many daily life items, such as eyewears, or in the construction of greenhouses, to name a few examples. In electronics, PC has been used to develop printed electronics on flexible susbtrate [121]. In microfluidics, polycarbonate is used to create microfluidic structures by bonding two pieces of this thermoplastic [122]. Another important application of PC in microfluidics is to create porous membranes integrated within microfluidic structures made of PDMS [123] or glass [124], as it is presented in figure 2.14. in the biological and biomedical fields, PC is used for many applications. Besides being widely used to fabricate surgical instruments replacing metal [125], PC is also used to develop microfluidic systems with biosensor electrodes [126] or for cell culture applications [127].

Cycloolefine copolymer (COC)

Cycloolefine copolymer is manufactured by the copolymerization of two cyclic olefins, particularly ethylene and norbonene. COC is in solid state at room temperature, its melting

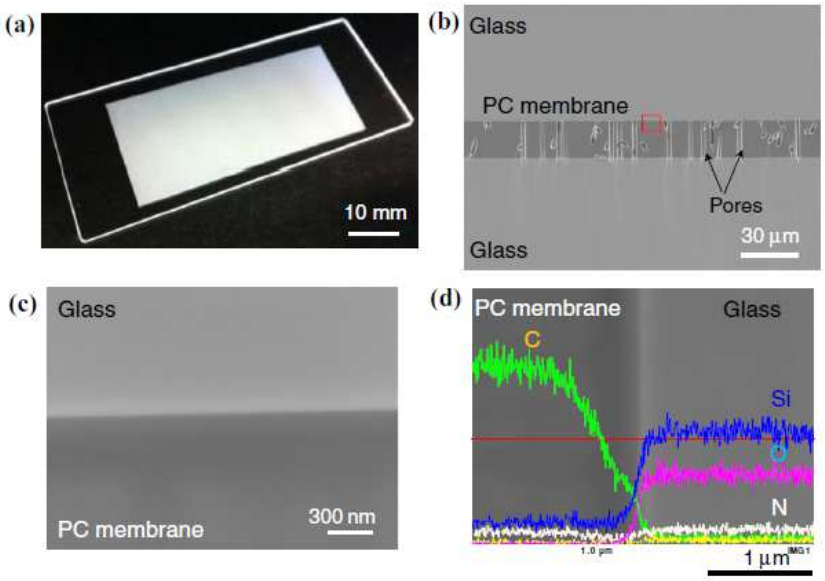

Figure 2.14 Evaluation of the bonding quality. (a) A picture of the bonded sandwich structure of the glass substrates and the PC membrane; (b) Scanning electron microscopy (SEM) image of the bonding interface without clogging in the pores; (c) a magnified image at the red rectangular region in (b); and (d) elemental analysis across the bonding interface with energy dispersive X-ray spectroscopy (EDS). Copyright (2017) The Electrochemical Society.

point is really high compared to other thermoplastics, that is between 350 and 400 °C [128], and its glass transition temperature varies from 20 to 260 °C, by modifying the cyclic olefin comonomer content [129]. COC is optically transparent and have a good resistance to many organic solvents and aqueous solutions [130, 131]. In addition, COC presents a good moldability and biocompatibility. Some disadvantages that must be taken into account are their huge range of glass transition temperature and their sensitiveness to stress cracking. In daily life applications, COC can be found in many food packaging, including films, bottle or jars. Its biocompatibility makes this material perfect for the fabrication of many medical items, such as tubes, vials, needle injector, etc. In microfluidics, COC is used for rapid prototyping of microfluidic chips [132, 133]. Nevertheless, sealing channels made of COC with other materials normally required external adhesives [134] or surface treatments [135]. For biological and biomedical applications COC is used for recapitulating cellular functions [136], for cell cultures [137] or as a biochip for blood typing [138]. Particularly relevant is the fabrication of the microfluidic chip made of COC shown in figure 2.15.

Polyethylene terephthalate (PET)

Polyethylene terephthalate is a thermoplastic polymer resin of the polyester family, and

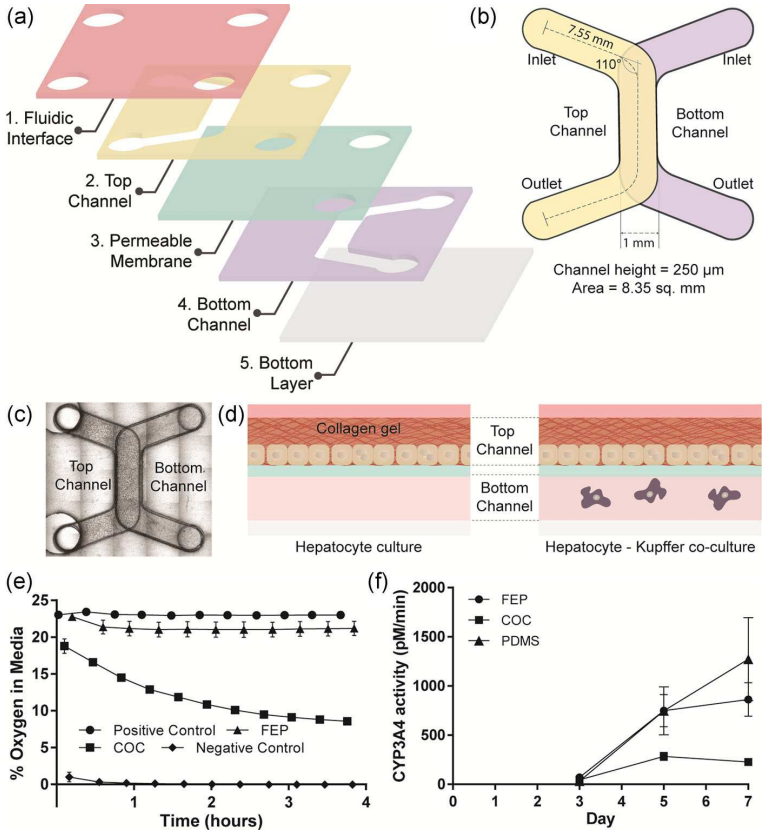

Figure 2.15 Microfluidic MPS design and PHH culture. (a) Multilayered stack of thermoplastic materials used in the generation of microfluidic MPS. Bottom layer is tailored to accommodate oxygen transport for hepatic culture, (b) Schematic showing microfluidic MPS channels and dimensions, (c) Top-view of assembled microfluidic MPS. Channels are separated by a 3.0 μm tissue-culture PCTE track etched membrane. (d) schematic showing PHH and PHH-PKC cell cultures in microfluidic MPS(cross-section view), (e) oxygen concentrations measured in the microfluidic MPS with PHH in COC and FEP (50 μm) in the bottom layer and (f) metabolic (CYP3A4) activity of hepatocytes in microfluidic MPS. COC, cyclic olefin copolymer; CYP3A4, cytochrome P450 3A4; FEP, fluorinated ethylene propylene; MPS, microphysiological system; PCTE, polycarbonate tissue culture; PHH, primary human hepatocyte; PKC, primary Kupffer cell. Copyright (2019) Wiley Periodicals, Inc.

the most common one. PET has a melting point of about 260 °C and a glass transition temperature around relatively low, around 75 °C. This thermoplastic is highly flexible and semi-crystalline, and depending on the processing it can be rigid or semi-rigid, offering a good impact resistance, as well as a high resistance to many solvents. PET is also

biocompatible. Its low cost makes PET to be one of the most used thermoplastics in the world. Among the disadvantages of this material, two of them must be highlighted: its susceptibility to heat degradation and its limitation for optical application, despite of being transparent it is not the best option for this kind of applications. In daily life, PET is very easy to be found, for instance in food packaging, in the fabrication of plastic bottles, or in the form of synthetic fibers PET is common used for manufacturing clothes [139]. In microfluidics, PET can be used to fabricate microfluidic structures [140, 141] and to create porous membranes [142]. Figure 2.16 shows the schematic diagram of an arrayed flexible screen-printed glucose biosensor, reported on [141]. In the biological and biomedical fields, PET is commonly used for cell proliferation [143] or for the fabrication of implantable medical devices [144].

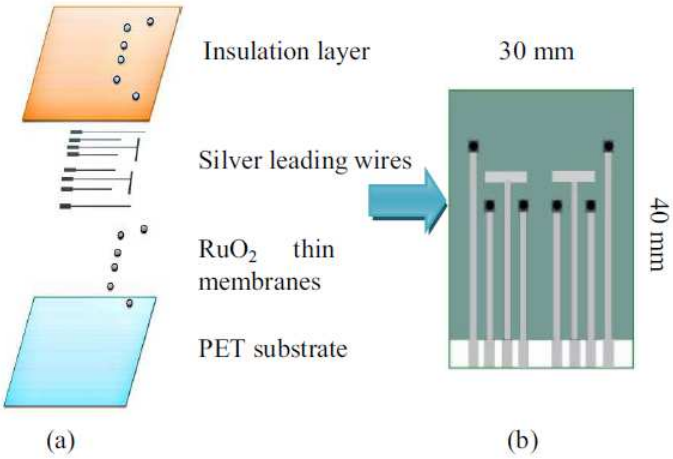

Figure 2.16 (a) Schematic diagram of arrayed flexible pH biosensor. (b) Finished product of arrayed flexible pH biosensor. Copyright (2014) IEEE.

Thermoplastics fabrication processes are so important in this thesis that they deserve a detailed explanation, as it is done in the following paragraphs. There are different fabrication processes for microfluidic devices made with thermoplastics. Each technique is more appropriate depending on the material chosen and the application. Despite there are several methods to manipulate thermoplastics and obtain microfluidic structures, there are two of them that have reached a higher development and commercial acceptance over the other techniques, which are injection molding and hot embossing. However, another methods such as laser ablation or mechanical micromachining are also used for prototyping. These fabrication processes are outlined below:

Injection molding

The use of injection molding for microfluidic structures was firstly presented and

developed during the decade of 1980 [145, 146]. Nevertheless, this method started to be reliable during the next decade, when the development of microfluidic structures made of thermoplastics became a feasible possibility [147]. To perform the injection molding process is indispensable to have the thermoplastic in liquid state, which means a high temperature, equal or over the melted temperature of the material. The liquid thermoplastic is deposited into a mold, which must be able to withstand a temperature considerably higher than the temperature of the thermoplastic. That is the reason why these molds are usually made of metal or silicon. After the deposition, the injected thermoplastic and the mold are cooled down under T_g. The last step consists on demolding the resulting piece.

The main limitations of this technique are related with the mold fabrication process, but the minimum dimensions of the microchannels vary from a few microns to a hundred nanometers. Further research works are focused on improving the limitation that injection molding has. For instance, a mold fabricated with a 3D printer which can mold up to 100 pieces [148]. However, the using of 3D printed molds does not imply an improvement in comparison with molds made of metal, which can be used more than a thousand times, since it is a low cost method for rapid prototyping. In the line of 3D printer, another option has been proposed by Lin et al. which consists on fabricating a 3D printed metal mold for hot embossing plastic microfluidic devices [149]. Other research works are focused on improving the functionality of the most used methods and materials. In this respect, a good example is the fabrication method through which a microtopography super-hydrophobic surface layer is deposited during the injection molding process [150]. Figure 2.17 shows an example of a mold made of metal and how it is assembled.

Hot embossing

Hot embossing is a process in which the thermoplastic is placed over a mold with a designed structure, heated over its T_g and subsequently pressed. During the heating and under a medium-high pressure, the shape of the mold is transferred to the thermoplastic, with a very high aspect ratio which depends on the fabrication method of the mold, varying from the microscale to the nanoscale [151, 152]. Most of the thermoplastics previously described are suitable for this technique, such as COC, PMMA or PC, among many others [153]. This technique has been widely developed due to its suitability for mass production, as well as for its usefulness for prototyping, if it is combined with other methods, such as micromilling [154]. Figure 2.18 presents the combination of hot embossing and micromilling for fabricating microfluidic devices.

Hot embossing advantages has made it one of the most used commercial method for fabricating microfluidic devices. Between these advantages, its low cost, precision and high aspect ratio are the most remarkable. Its main limitations are related to the material used, because not all the thermoplastics are suitable for hot embossing, and to the replication of complex three-dimensional structures [155]. Hot embossing technique shares a limitation with injection molding, which is the time needed and the cost of fabricating molds for perform the process. Despite this disadvantage, hot embossing is still a widely used method, both for prototyping and mass production of microfluidic devices, which continue to be a

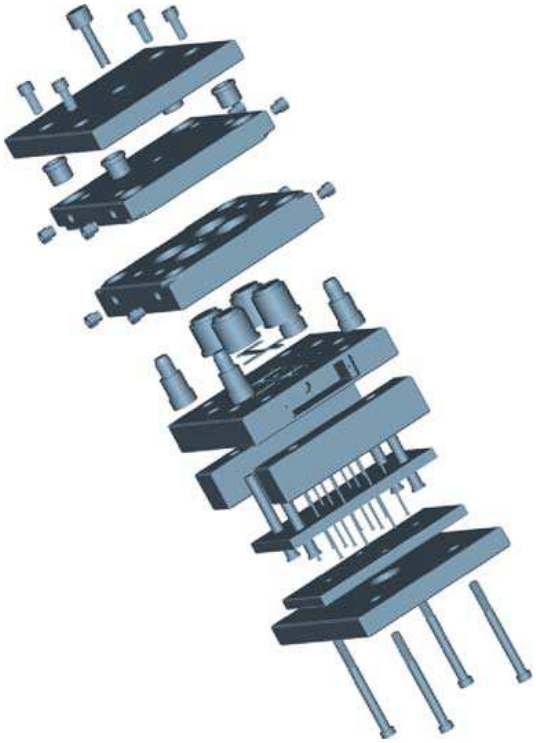

Figure 2.17 Modeling of the plastic injection mold. Copyright (2009) Springer.

technique to take into account in the upcoming years.

Micromilling

The two previously described method for fabricating microfluidic structures were focused on mass production. However, both methods exhibit some limitations for rapid prototyping, mainly due to the high cost of the mold. Micromilling consists on creating microscale features by using cutting tools which removes bulk material. This technique is often used for manufacturing the molds utilized in both injection molding and hot embossing techniques. However, it has some problems, such as the materials hardness and the high cost of the tools needed to mill these materials. This method can also be used directly with thermoplastics, becoming an effective method for the fabrication of microfluidic structures [156], specially for rapid prototyping [157, 158]. Figure 2.19 shows a comparison reported on [158], in which the same cell culture is developed on the same substrate but fabricated with different methods, demonstrating the adequacy of milled substrates for this type of applications.

The micromilling consists on removing bulk material by using cutting tools, and its suitability for the fabrication of microfluidic devices has been demonstrated in different

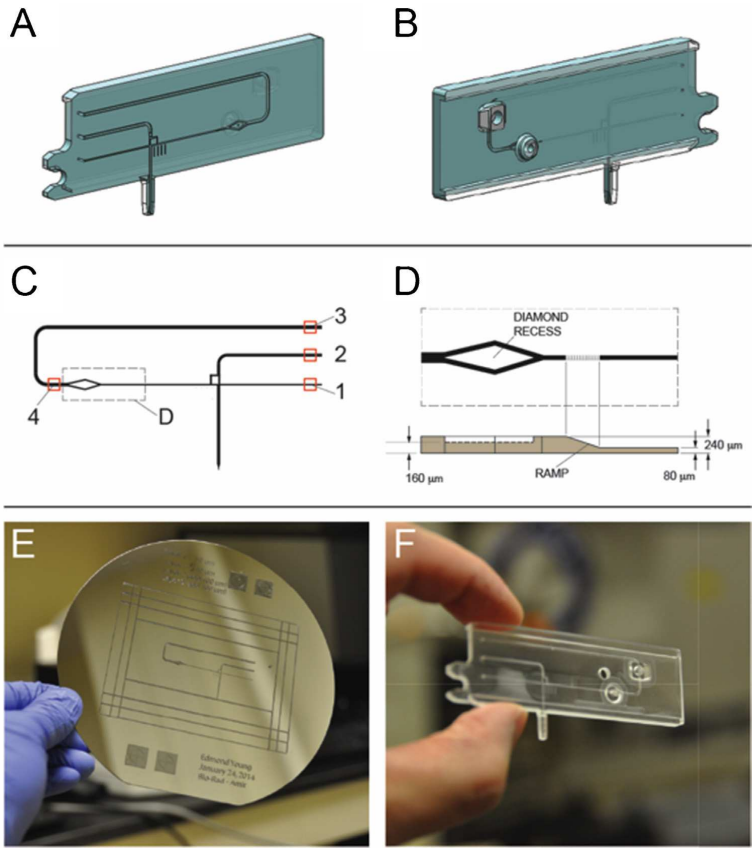

Figure 2.18 3D isometric views of the microfluidic chip design: (A) front view; (B) back view; (C) Microchannel layout; (D) Inset of diamond shape feature in (C); (E) Photograph of 6-in diameter primary master consisting of SU-8 microfeatures on a silicon wafer; (F) Final microfluidic chip after combined hot embossing and micromilling. Copyright (2016) Elsevier.

thermoplastics, such as PC [159] or PMMA [160]. Some research advances have demonstrated the possibility of fabricating microfluidic structures made of thermoplastics by using CNC milling machines. This option results in an efficient method for fabricating microfluidic prototypes with a high precision, a low cost and low manufacturing times, giving the possibility of testing many different geometries and functionalities, without the limitations of the other methods [161]. Other advantages of this technique are related to the ease to make modifications on the design through a 3D CAD model. However, the main disadvantage of micromilling is precisely that it is not suitable for mass production, becoming a better option injection molding or hot embossing.

Laser micromachining

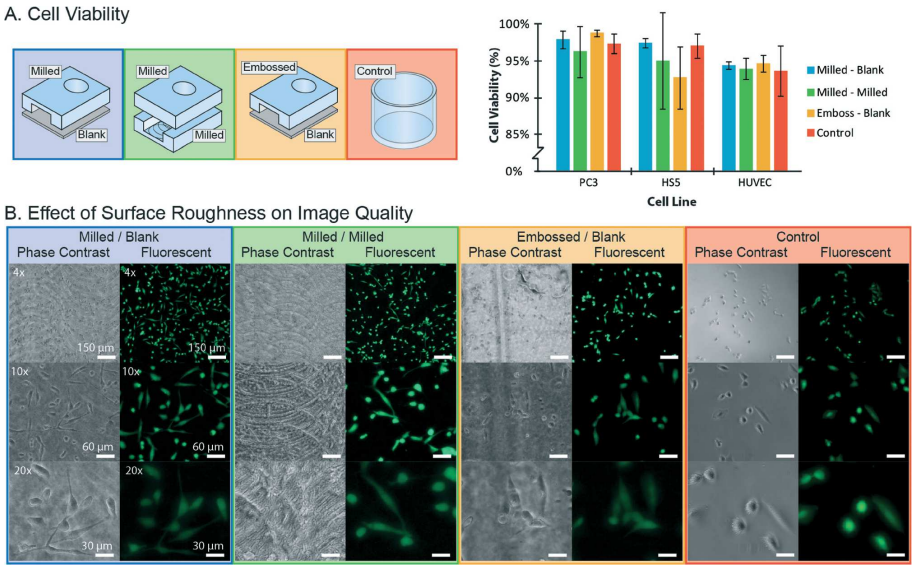

Figure 2.19 Cell culture and image analysis in milled microchannels: (A) Channels different assemblies; (B) Phase contrast and fluorescent images were taken of HS-5 stromal cells in each channel configuration using 4, 10, and 20× magnifications. Copyright (2015) The Royal Society of Chemistry.

As it happens with micromilling, laser micromachining is focused on rapid prototyping instead of mass production, mainly due to the cost of using the laser and the time needed to obtain a huge amount of pieces, in comparison with both injection molding and hot embossing techniques. This method is also utilized to fabricate the molds used for mass production. However, its applicability with thermoplastics has been demonstrated in many research works [162, 163]. Laser micromachining has many advantages, such as a high precision, low cost and low fabrication times. Similarly to micromilling, the design can be modified easily through a 3D CAD model, making possible the test of different designs without wasting time or money. There are different lasers which are suitable for micromachining thermoplastics, but the two main types are femtosecond lasers and CO_2 lasers [164, 165], whose results on PMMA microchannels are shown in figure 2.20. The first one is not the best option due to its high cost, while the second one is more used for obtaining microchannels on thermoplastics substrates. The limitations of this method are normally related to the diameter of the laser beam. A few research works report that it is possible to achieve dimensions close to 20 μm, but complicating the process [166]. Despite the use of lasers for fabricating microfluidic structures in thermoplastics is a reality, it is still needed a deeper investigations, specially characterizing the different materials and their interaction with the different existing lasers.

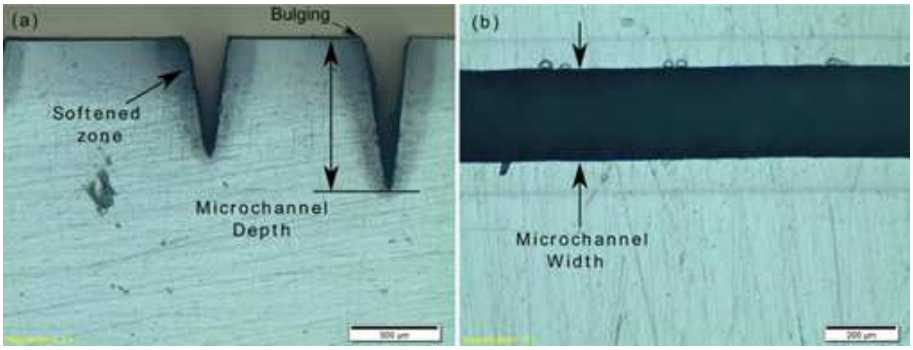

Figure 2.20 (a) Cross-sectional view and (b) Top view of microchannel. Copyright (2015) Springer.

Printed circuit boards (PCB)

After describing different materials for microfluidics in previous subsections, in this one the suitability of PCBs for microfluidics applications is described.

Printed circuit boards are normally made of FR4 and copper. FR4 is a type of fiberglass and it is covered with a flame resistant resin. The FR4 is hydrophobic, thus it requires a surface treatment to make it hydrophilic [167]. Regarding the copper, it can be placed on the top, on the bottom and between the FR4, and could have different heights, varying from several microns to a few hundred microns. The development of MEMS devices by using PCB-MEMS technologies is a low cost process that permits the integration in the same platform of both microfluidics and electronics. PCBs can be used both as substrates on which other materials are deposited or bonded to form the microfluidic structure, or as a structural material in which the microfluidic circuit is directly fabricated. Despite the main use of PCBs in this thesis work has been as a substrate, in this subsection both possibilities are described.

The concept of a microfluidic platform based on PCB-MEMS technology was succesfully tested for the first time in 1999 [168], demonstrating the suitability of this technology for the fabrication of microfluidic devices and creating a new type of lab on chip, named Lab on PCB, which will be fully described in following sections. The most important characteristic of PCBs, and what implies a significant improvement in microfluidics, is the possibility of integrating electronics, such as sensors or actuators, with the microfluidic structure. This issue, together with the huge experience accumulated over the last decades in PCB-MEMS technologies, make PCBs an indispensable option to take into account for fabricating microfluidic devices [169].

PCB is often used as a substrate to create microfluidic systems, mainly due to the good adhesion of FR4 to most of the photoresists. For instance, SU-8 is utilized in the fabrication of microfluidics structures over PCB [170]. In comparison with silicon, PCB

has the advantage of an easier manipulation and a lower cost. Moreover, FR4 exhibits a low thermal conductivity, which is very useful as an insulating substrate to perform heat transfer applications. Figure 2.21 shows a lab-protocol-on-PCB reported in [170]. This approach is particularly interesting because the liquids displacement is possible thanks to the integration of microvalves and pressure chambers on the same platform, as well as a sensor.

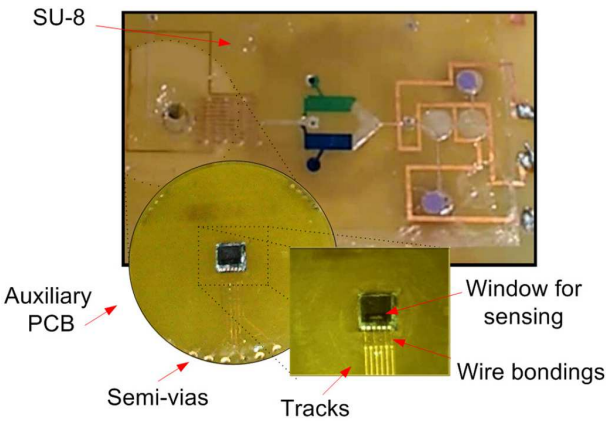

Figure 2.21 A silicon dummy sensor has been integrated as a proof of concept. Copyright (2015) Elsevier.

There are a wide range of applications for microfluidic platforms fabricated on PCBs as substrates. The photolithographic process of the copper layer offers the possibility of creating heaters, pressure or flow sensors or microelectrodes arrays, to name a few examples [171, 172, 173, 174]. Figure 2.22 presents a capacitive pressure sensor using de copper layer to define the gap. Moreover, PCB-MEMS technologies allow the development of more complex microfluidic systems through the integration of valves or pumps [175]. This presents a complexity that lies on the need of using auxiliary chambers to store the air which is pressurized using the copper tracks to heat the chamber, increasing the pressure inside it and releasing volume. To make this kind of devices suitable for biological applications, is indispensable to completely passivate the copper tracks, avoiding any contact between the copper and the biological samples.

Despite it is more extended the use of PCBs as substrate when developing microfluidic devices with PCB-MEMS technologies, it is also possible to fabricate microchannels directly on the PCBs. For instance, microchannels can be created bonding two PCBs with copper tracks [176]. The different existing thickness for the copper layers permits the fabrication of microchannels with different heights, while the width of the microchannels are limited by the photolithographic process performed. The bonding of the two PCBs is done with a low viscosity glue, depositing a thin layer of glue to avoid the blocking of the

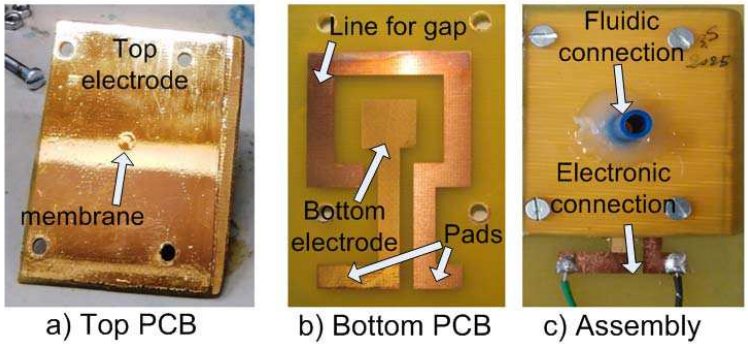

Figure 2.22 (a) The photograph shows the top PCB with SU-8 membrane and the sputtered gold. (b) The bottom PCB with the gold electrode and the copper lines to define the gap and the pads for electronic connections. (c) The final fabricated device as a result of the assembly of the bottom and top PCB, and the fluidic connection. Copyright (2015) IEEE.

channels. This kind of devices are easy to fabricate and low cost, but they are not suitable for biomedical or biological applications due to the non biocompatibility of copper, unless it is correctly isolated with a passive layer of a biocompatible material.

LOC systems development has been dominated by other technologies and materials, such as CMOS or polymers. However, it has been difficult to find a reliable low cost method to mass production of this type of devices, and most of them remain as proof-of-concept devices. This motivation of integration and micromanufacturing is fulfilled by PCB-MEMS which is becoming a re-emerging technology, even creating a new concept called Lab on PCB [177], presenting a huge potential and a bright future.

Regarding the industrial status of PCB-MEMS technology applied to microfluidics, to have a real possibility of growth and development in the LOC market it is indispensable to fulfill several objectives: low cost, highly integration and electronic functionality. In the last years, several companies have started to develop or commercialize useful microfluidic systems based on PCB-MEMS technologies. For instance, Dyconex Ltd. and Epigem Ltd. provides some products with the mentioned characteristics, or Tulip Group together with Bigtec Labs which are commercializing a PCB-based micro PCR system [177].

The huge possibilities that PCB-MEMS technology provides to the development of low cost microfluidic devices is a reality. However, this re-emerging technology has to face similar problems that LOC systems are facing in the present time. Among these problems, the most difficult to solve is the step from a prototype or proof-of-concept development to a mass production process and the commercialization of these devices in the market. The functionality of PCB-based microfluidic devices has been clearly demonstrated, as well as their applications in biology, chemistry or biomedicine. Nevertheless, the lack of a reliable mass production fabrication process is still the main objective that must focus the

Table 2.2 Most common uses of microfluidic building materials today.

	Substrates	Structural
Silicon	Yes	Yes
Glass	Yes	Uncommon
SU-8	No	Yes
PDMS	Uncommon	Yes
Thermoplastics	Yes	Yes
PCB	Yes	Yes

efforts in the near future.

Table 2.2 summarizes the different materials suitable for microfluidic fabrication and that are explained in this section. Each material is defined depending on if it is used as a substrate, which it is referred to a material that is use together with another one in which the microfluidic structure is fabricated, or if the material is used to directly fabricate the microfluidic circuit, named structural material.

2.2.3 Microfluidic functions and applications

This subsection is focused on the different functions and applications of microfluidic platforms used on the life sciences field. Most of the next functions can be useful not only in the biological or medical field, but also in many others. However, the motivation of this thesis work is close related to the life sciences area, so other areas of knowledge have been omitted. Microfluidic applications are wide and include, among others, the fluid manipulation, the sample preparation, the separation or the detection. In the next paragraph, some of the most important functions and applications of microfluidic platforms are detailed.

Fluid manipulation.

Fluid manipulation is an essential function in a microfluidic platform. Micropumps, microvalves and micromixers are the most common component integrated in a microfluidic platform to accomplish this task. Micropumps allow the flow of fluid all along the microchannels, and their integration in the whole microfluidic system avoid the use of an external pump, which would increase the cost and the dimensions of the device. There are lot of different micropumps used in microfluidics, but they are normally divided between active and passive micropumps. The most common passive micropumps use the capillarity for the fluid flow [178]. The active micropumps offer a huge range of types, among which are more used the electroosmotic (EO) pumps and the pneumatic peristaltic pumps. The main difference between these two types of micropumps are the actuation, being the first one non-mechanical, while the second one is mechanical. The EO pumps are very useful for biomedical applications [179]. The integration of pneumatic peristaltic pumps offers many

advantages for cell culture systems [180]. As well as micropumps, microvalves are another key elements in microfluidics, and their function is mainly the displacement of fluids all along the microchannels, specially when liquids need to be isolated or pressurized. Their correct integration has been a challenge for the research community, and the successful operation of a microfluidic structure often depends on that integration. Microvalves are also divided between passive and active components. The most representative passive microvalves consist on a cantilever or membrane which allow the fluid flow in one direction, by pressure changes on the structure [181]. The active microvalves need an external actuator to make them work, as the microvalve developed by Flores et al. which acts as a fuse and is activated through a high amperage peak during a very short period of time to break the fuse made of copper, resulting in a low consumption microvalve [182]. Figure 2.23 shows the active microvalve reported on [182]. This microvalve is a fuse made of copper which is broken when a high current peak crosses it, releasing the confined air of a pressurized chamber and displacing the liquids contained inside the microfluidic structure. The last component, but not less important, is the micromixer, which is responsible for the mixing of fluid at the microscale. This is not a negligible issue inside a microfluidic platform because the fluid flow is normally laminar, so if mixing occurs is by diffusion, but, with this type of components, two different liquids can be mixed or diluted or can generate a reaction, which is very useful for substances analysis. Micromixers are also divided between passive and active components. Passive micromixers benefit the diffusion of liquids inside the microchannels or implement complex geometries to facilitate the mixing of fluids along the microchannels [183]. Active micromixers can be activated in different ways: electrokinetic, acoustic or magneto-hydrodynamic, among many others [184]. The main problem of active micromixers are their complexity, which make them difficult to integrate within the microfluidic structure.

Sample preparation.

Sample preparation is a very difficult challenge in microfluidics, but researchers are making important progresses on the development of techniques to accomplish this task. Sample preparation includes filtration, extraction, purification and enrichment. The advantages of this function of microfluidic is reflected on a reduction of analysis time, automation and improved throughput [65]. Extraction, purification and enrichment are close related between them, and through the extraction the other two can be accomplished. In this respect, solid-phase extraction (SPE) results in a very useful method for purification and enrichment in which analytes are hold in a solid support and then eluted in a concentration form. SPE is easily integrable with other processes in a microfluidic platform, and the most common SPE modes are reversed-phase, which are normally developed on silica-based columns, demonstrating their reliability and reproducibility [185]. An application of SPE is for the extraction of DNA from biological samples in a post-based, high surface area poly(methyl methacrylate) (PMMA) microdevice DNA from blood [186]. The pre-concentration of samples also improves the functionalities of a microfluidic device, whose main advantages are the concentration detectability through optical methods or the detection of low-concentration analytes [187]. Exclusion methods for enrichment by using nanoporous filters reduce the complexity of the setup. The nanoporous filters can be

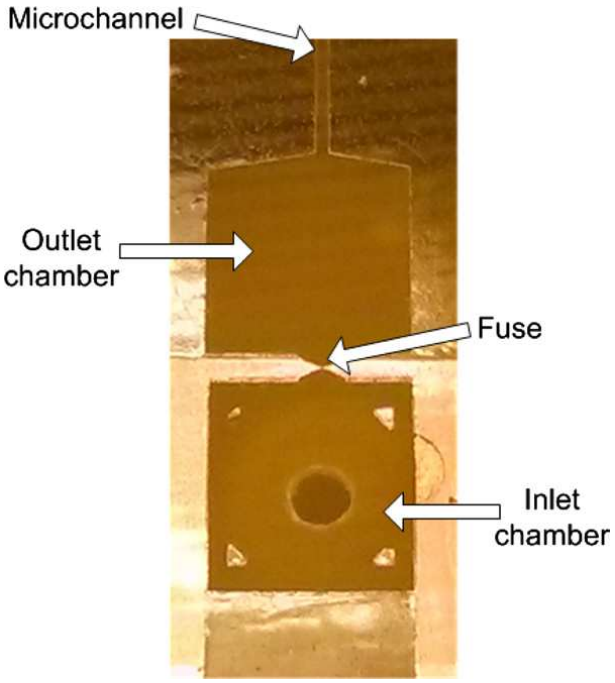

Figure 2.23 Fabricated microdevice. The main parts of the microvalve can be seen: the inlet chamber with the inlet port, the fuse, the outlet chamber and the microchannel. Copyright (2014) IOP Science.

fabricated with hydrogels membranes [188]. Sample labeling can also be integrated within the microfluidic structure, as it has been demonstrated by Yu et al. in protein analysis [189]. This device made of PMMA integrates on-chip labeling and parallel electrophoretic separation of up to eight samples. Figure 2.24 shows the microfluidic device reported on [189].

Separation methods.

The most extended methods used for separation fluids in microfluidic devices are electrophoresis and chromatography. Despite the first method has been used for longer than the other one, chromatography advances have increased in the recent years. Even so, both methods are widely used for separating liquids. Starting with electrophoresis, this technique is based on the liquid-phase separation, and can be applied in the separation of many different analytes. Electrophoresis microfluidic devices have demonstrated to be a reliable separation method, with good resolution and without moving parts, which simplifies the fabrication [190]. In free solution electrophoresis, stored analytes are moved by applying an electric field and, depending on their size and charge, are resolved as distinct bands. Figure 2.25 shows a microchip electrophoresis with laser-induced fluorescence detection for the analysis of N-glycans derived from disease-free individuals and patients

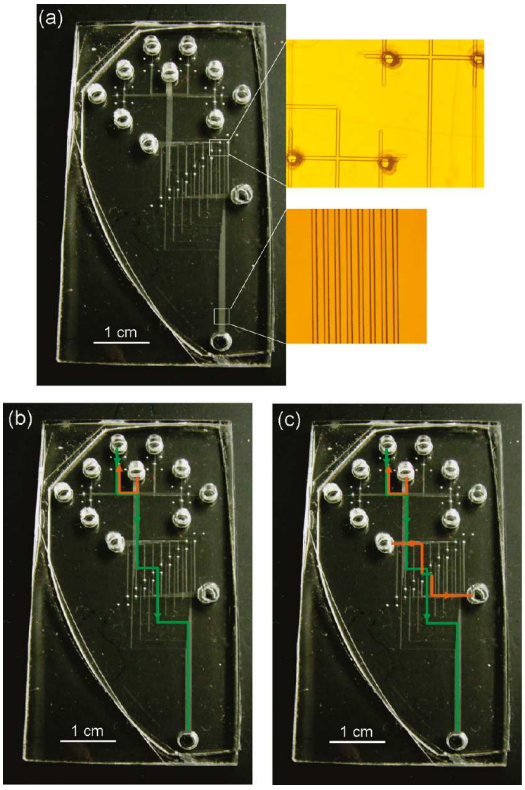

Figure 2.24 Multilayer microdevice photographs and operation. (a) Photograph of a complete device. Insets: photomicrographs of interlayer through-holes (upper) and detection region (lower). The channels are 40 μm wide and 13 - 15 μm deep. (b) The solution flow route during gated injection in one of the eight independent lanes is shown with arrows on green (bottom layer) and orange (top layer) solid lines. The interlayer through-holes are at the intersections of the green and orange lines. (c) The solution flow route during separation for the same lane is shown. Copyright (2011) American Chemical Society.

with Barrett's esophagus, high-grade dysplasia, andesophageal adenocarcinoma [191]. Normally, for electrophoresis as separation method, the longer the microchannel is the higher the efficiency of the separation is. The fabrication of a multilayer microfluidic system, for instance the one reported on [189], increase the functionality of this kind of devices. Regarding the chromathography as separation method of samples, this method has been developed more and more in the last years, becoming a reliable and versatile technique [65]. There are different options for separating liquids through chromathography. One of the most common one is by using columns to confine particles or peptides and protein, as reported on [192].

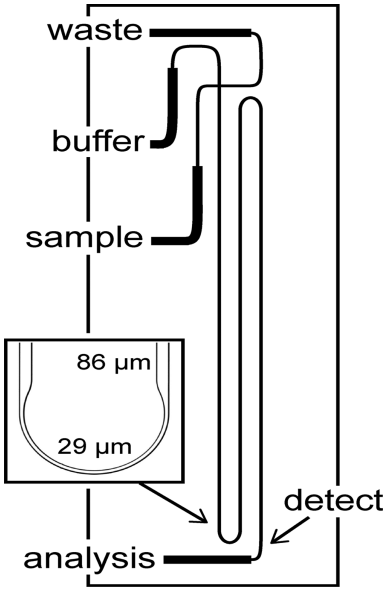

Figure 2.25 Schematic of the microfluidic device with a serpentine channel used for N-glycan analysis. The analysis channel is 22 cm long from the cross intersection to the detection point indicated by the arrow and has two asymmetrically tapered, 180 ° turns. The inset is a bright-field image of an asymmetrically tapered, 180 ° turn with taper ratio 3. The straight channel width and turn width are 86 and 29 μm,respectively. Copyright (2012) American Chemical Society.

Detection methods.

Among the different methods used for detecting or sensing substances inside a microfluidic device, the most extended are electrochemical and optical detection or biosensors. In the electrochemical detection, amperometry, conductivity and potentiometry are the most commonly used [193]. Amperometry is based on measuring the electrical current when a voltage is applied between two electrodes which are in contact with the sample. The main advantage of this method is the possibility of doing the detection inside the microchannel [194]. Potentiometry works in a similar way, but measuring the relative potential between two electrodes, being one of them an ion-selective electrode [65]. Electrochemical methods based on conductivity are the most common ones, and they consist on measuring the conductivity different between an electrolyte solution and the analyte. The electrodes can be integrated in a microfluidic device by using simple microfabrication techniques. Different electrochemical methods can be coupled together in the same system [195]. Regarding the optical detection methods, they offer several advantages, such as their good detection limits, the easy monitoring of many different substances or their isolation from the liquid samples [196]. Detection methods are normally divided depending on if they are label-based (fluorescence or chemiluminescence) or label-free. Laser-induced fluorescence

technique is the most common one, but it presents some problems when the sample does not have a natural fluorescence, needing to be derivatized [197]. Optics component are not usually integrated in the microfluidic device. However, some advances have been done by including a LED and a photodiode receptor inside a microfluidic system [198]. Chemiluminescence method main advantage relies on not requiring an excitation source because it is based on creating light through chemical reactions, being its most critical limitation the need of very sensitive detectors [65]. Regarding the label-free methods, UV absorbance is the most common one, offering less sensitivity than the previously commented label-based techniques. The last method mentioned at the beginning of this paragraph is based on biosensors, which are composed of a transducer to convert a biochemical signal into an electrical one [65]. The integration and development of biosensors within microfluidic structures are undergoing significant advances in the last decade [199]. This growth is due to the simple and versatile application of biosensors, which are more and more often used for detecting analytes. Surface plasmon resonance (SPR) is an extended optical biosensing method with a real-time, label-free and noninvasive nature, that allows a rapid and ultra sensitive detection of biological analytes [200]. Experimental setup of a surface plasmon resonance biosensors is presented in figure 2.26, and it is composed of a light source, a prism, a gold film and a detector, following the kretschmann configuration. Biosensors are based in many different methods, such as electrochemistry, amperometry or thermal, to name a few [65].

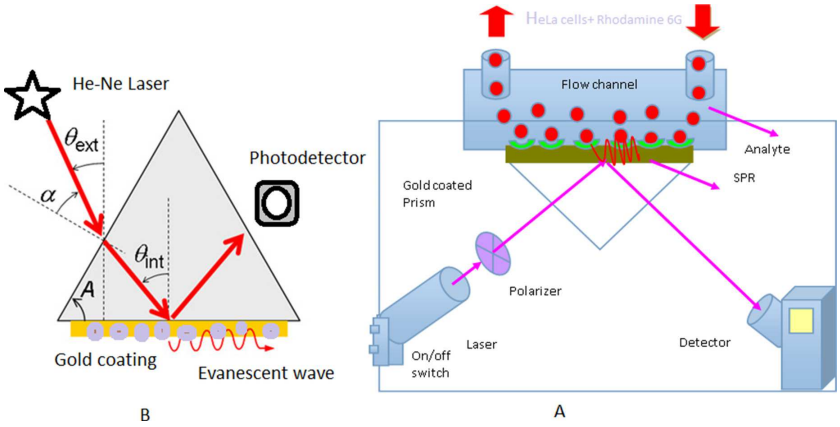

Figure 2.26 Experimental setup of surface plasmon resonance (SPR) biosensor, (Kretchmann configuration). Copyright (2018) IOP Science.

3 State of the art

After describing the basis and principles on which this thesis is based, the state of the art of lab on chip (LOC) devices are described, containing a brief introduction about their origins and main applications. Focusing on the biological applications of LOCs, an extended review of literature about LOCs and their application in life sciences, biology and medicine is presented. Finally, a detailed section is dedicated to LOC platforms for cell and tissue culture, including a summary to help to understand this research field of biology.

3.1 Lab on chip (LOC) devices for biological applications

In this section, lab on chip (LOC) devices are fully described. It starts with the origin of this concept and the need that bolstered its development, specially focused on its application on the biological and biomedical fields. In addition, in order to give a biological support to the presented work, organotypic and cell culture literature is presented. Consecutively, an overview about electrophysiology is given, explaining how can it fits with culturing applications. Finally, different LOC devices closed related to this thesis are explained in detail, including organs on a chip, microincubators or microelectrode arrays.

3.1.1 The miniaturization of a laboratory process. Approaching the Lab on chip concept

In previous sections, the importance and advantages of microelectronic and microfluidic has been explained, and how the miniaturization improves the functionality, reduces costs and opens new possibilities for many processes and devices. Thanks to all these research works related to microfluidic and microelectronics, a new concept emerges: "lab on chip

(LOC)", also know as "micro-total analysis systems" (μTAS), a term coined around the early 1990s [201]. These new devices include both microfluidic and microelectronics in the same platform, integrating different functions which normally needs a traditional laboratory to be done, but on a few square centimeters system [202].

Despite it is unquestionable that microfluidics advances have helped to promote the emergence and development of LOCs, it is important not to assume that they are only a group of microchannels forming some kind of network. Their functions go further than that. It is the integration of electronic and mechanical components together with those microfluidic structures what open a huge range of applications for LOCs, as well as imply many advantages in comparison with the same process performed in a traditional laboratory, such as the cost efficiency, the low volumes needed, the parallelization of several processes or the faster response and analysis time.

Notwithstanding all the improvements of LOCs, their development also implies some difficulties which are not easy to overcome. The concept lab on chip means to close and plug a lab inside a small chip, so the sealing and the interfacing become two of the most challenging problems to solve [203]. Related to the sealing of LOCs, the bonding methods or materials used can be influenced by the liquids used or by the temperatures needed to perform some processes, affecting negatively the sealing. Regarding the interfacing between sensors or actuators integrated in the LOC, specially when LOCs are disposable, low cost connectors become necessary, not only the electrical ones, but also the fluidic connectors. Apart from that, and close related to these two previously mentioned problems, the need of transparency for many applications, specially optical, requires specific materials, not only for the microfluidic platforms, which normally is made of plastic or elastomer, but also for the substrate, which make more difficult the integration of electronic components or metal tracks.

LOCs applications varies from simple laboratory processes performed inside a small device to very complex systems with different processes carried out sequentially or in parallel. The first μTAS that started to have a market were the test strips, during the late 1980s and 1990s. Some of them that can still be found in the market such as test strips for pregnancy, drug abuse or cardiac markers [204]. Over the last 20 years, LOC devices have increased exponentially their applications and their potential. In the present days, it is possible to find LOCs for applications as varied as point-of-care diagnostics [205], genomic and proteomic research [206], analytical chemistry [207] or environmental monitoring [208].

Among the different LOCs that can be found both in the market and in research, the present thesis work are going to be focused on those with a biomedical or biological applications. Therefor, in the following sections, LOCs with applications on the those fields, as well as the organ on a chip concept, are detailed. I will take special attention on those kind of systems related with cells and tissues cultures and the integration of microelectrode arrays together with microfluidic platforms.

3.1.2 LOC for cell and tissue cultures

Cells exist *in vivo* in a very specific and controlled environment, forming tissues or interacting between them [209]. It is precisely this interaction and communication with other cells what make cells growth inside living organisms. The phenotype of cells *in vivo* depends on several factors, such as the interaction with neighbor cells or with the extracellular matrix (ECM), among many others. For similar cells, for instance mammalian cells, there are some common aspects: the distance between cells, the nutrient supply or waste removal, or the set point temperature [210].

Regarding all of this, the utility and importance of cell cultures in cell biology, biomedical or tissue engineering and drug discovery is out of any doubt [210]. However, replicate this environment in an *in vitro* culture, with the exact same characteristics, is a very hard challenge for many researchers of different fields, specially Medicine and Biomedicine, Pharmacology or Biology. Many cell-based biological researches are carried out by isolating cells, which are placed inside a culture dish with medium but without any cellular structure to be adhered to or other type of cells with which interact or communicate [211]. This implies that *in vitro* cells often change their behavior, that is, their properties, morphology or growth rate.

In this framework, LOC devices play an important role as they make possible the replication of the *in vivo* cell culture environment but on an *in vitro* cell culture. Microfluidic cell culture devices are developed to provide a culture environment in which cells can be cultured and maintained in a controlled microenvironment for their analysis and experimentation in micro-scale volumes [212]. In the recent years, many different aspects of LOC system for cell culture have been studied, such as cell biology, surface modification, cellular microenvironment, apoptosis, drug research or 3D cell cultures, among many others [213]. These researches and improvements become more relevant as they can reduce considerably the experimentation on living animals, substituting these tests for others carried out on *in vitro* cell culture LOCs.

Compared to macroscopic cell culture, which means those performed on flask or well-plates, microfluidic cell culture devices have significant advantages. Firstly, and probably one of the most important advantages, LOC cell culture devices can be designed for specific type of cells, which make them very flexible to the needs of each culture. Moreover, and not less important, the possibility of adding different elements to the microfluidic structure allows the LOC cell culture to reproduce with more accuracy the cell's natural microenvironment, for instance with an external or integrated continuous perfusion system or by creating chemical gradients. Cell culture LOCs reduce significantly the amount of samples, culture medium or reagents used during a cell culture experiments, as well as the risk of contamination [213]. Despite the advantages of microfluidic cell culture devices, they also presents some disadvantages. In figure 3.1 the most relevant advantages and disadvantages of both micro-scale and macro-scale cell culture are shown (figure 3.1 has been taken from [213]).

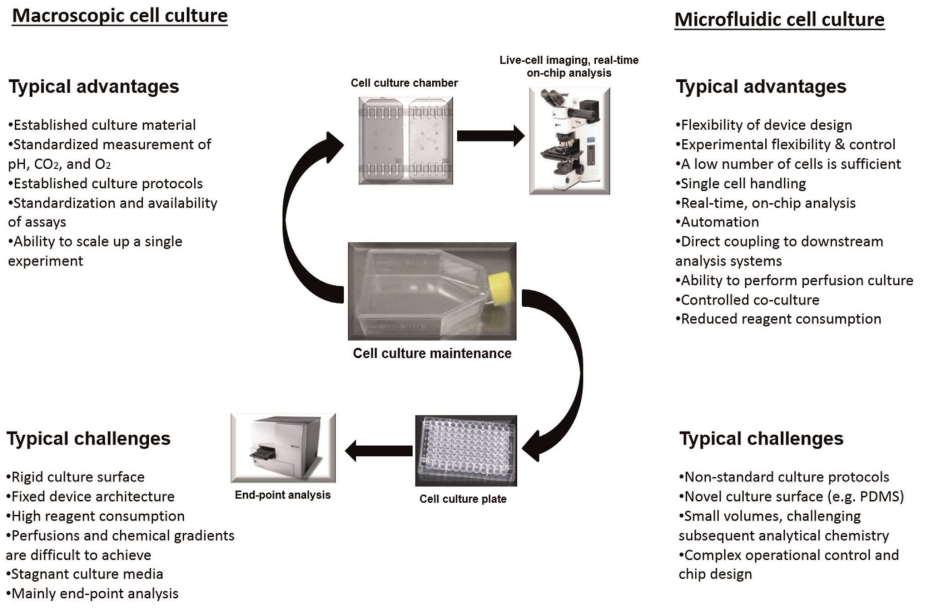

Figure 3.1 Overview of advantages and challenges of both macroscopic and microfluidic cell culture. Copyright (2014) Elsevier.

Regarding figure 3.1, the hardest limitation for microfluidic cell culture devices is the lack of standard culture protocols, which make more difficult the design of the LOC, and the choice of materials to fabricate the system. This issue is motivating lot of research works focused on finding a standard protocol for cell cultures in microfluidic devices. In the present days, PDMS or plastics, such as PMMA or polycarbonate, are widely used for the fabrication of this type of devices [213, 214]. For each material, is necessary to analyze different factors which can have an influence in the cells microenvironment, such as the adherence of the cells to the surface or the oxygen permeability.

Another important advantage that cell culture LOCs offer is the possibility of isolate a single cell for its study, which compare to macroscopic cultures in which a complex process is required to study a single cell. It has been demonstrated that single cell analysis can be applied in many situations, such as: gene and protein content and expression, PCR, cell culture and division, clone formation, differentiation, morphology, lysis, separation, sorting, cytotoxicity and fluorescence screens, antibody secretion [215]. Moreover, cell culture LOCs allow the monitoring of the culture in real time, giving accurate information at any moment during the experiment, such as the oxygen that is been consumed by the cells during the culture [216].

In figure 3.2 an example of what it has been previously explained is presented. It is a complex, versatile and fully automated microfluidic cell culture system [217]. This system has been designed to screen the effects of different mixtures of reagents on the behavior of

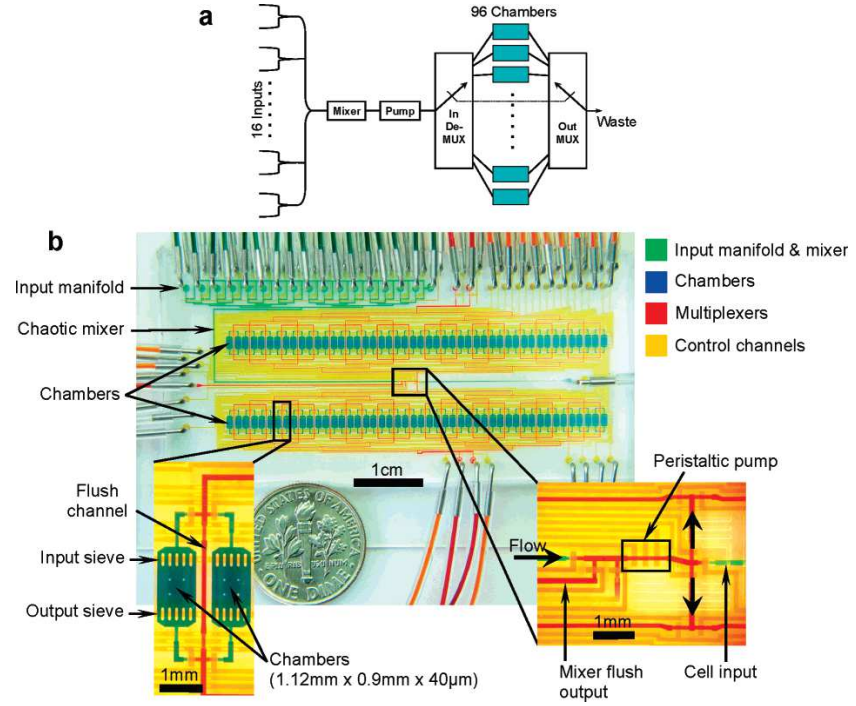

Figure 3.2 Design of the cell culture chip. (a) Simplified schematic diagram of the fluidic path in the chip (MUX, multiplexer). (b) Annotated photograph of a chip with the channels filled with colored water to indicate different parts of the device. The left inset gives a closer view of twoculture chambers, with the multiplexer flush channel in between them. The right inset shows the root of the input multiplexer, with the peristaltic pump, a waste output for flushing the mixer, and the cell input line. Copyright (2007) American Chemical Society.

cells on long-term cultures. The flexibility when designing a cell culture LOC is clearly demonstrated in this device, in which it is possible to test different reagents in each chamber, as well as the supply of nutrients can be fixed for each chamber.

3.1.3 Organ on a chip

Once the functioning of cell culture LOCs have been demonstrated, the next step in the development of LOC with medical or biological application lead researchers to the implementation of what has been called "organ on a chip". This type of devices continues the line that cell culture LOC starts, not only with cells but also with tissues, recreating in the most accurate possible way a human organ but in the micro scale. Thus, organ on a chip combines the microfluidic structures with complex 3D cell biology, providing "organ-like physiology and pathophysiological cellular and tissue level responses" [218].

The use of microengineering techniques in cell culture implies many advantages, such as the possibility of adding continuous flow, controlled drug delivery, sample or dilution preparation aspects, or sensors and actuators together with the culture system, being these processes indispensable to reproduce the organ functions. All of this makes easier to perform co-culture, 3D cultures or the application on controlled gradients [219].

Organ on a chip devices have had a considerable impact in medicine and biology in the last years, but their current and future significance is increasing over the years, mainly because they open a huge range of possibilities in these fields, specially for disease mechanisms, advance drug screening or personalized and precision medicine [218]. This has made organ on a chip to become a real alternative to conventional *in vitro* and animal models [220].

One of the most recent advances in organ on a chip is the reproduction of tissue barrier functions. This have been achieved in several ways based on the fabrication of microfluidic structures. Microfluidic membranes can be integrated together with the microfluidic channels of an organ on a chip, and are used to replicate interfaces of human tissue, such as intestine, brain or lung [221]. In figure 3.3, a reconstruction of the lung functions inside an organ on a chip is presented [222]. In this device, some complex responses to bacteria and inflammatory cytokines introduced into the alveolar space are reproduced. One of the target of this kind of systems which recreates tissue-tissue interfaces is to improve the capabilities of cell culture models and give a real alternative for drug discovery applications. Microfluidic scaffolds is another type of structure used to reproduce tissue barrier functions in organ on a chips. For instance, for the construction of vascularized functional tissues by using polymeric elastomers [223]. Another method to reproduce tissue barrier functions consists on using microfluidic hydrogels with a high concentration of water, such as collagen or gelatin. The main advantages of hydrogels are their permeability to biomolecules which, compared to PDMS, avoids the need of integrating porous membranes. However, this material is very fragile and not easy to manipulate at the microscale. Microfluidic hydrogels integrated with microchannels networks have been used to develop part of a human peritubular microvascular system [224].

In the last 15 years, different kinds of organ on a chip systems have been developed. These systems reproduce an organ of the human body, or sometimes more than one, in the same platform. Outline below, some examples of organ on a chip are described, highlighting their reliability, usability and potential for their applications in the biological, medical or biomedical fields. For each organ, a brief biological explanation of its functions is given, as well as a representative example found in the literature of an organ on chip recreating those functions.

Lung on a chip.

The lung is the main organ of the respiratory system, and alveoli are where the gas exchange takes place and the functional unit of the lung. A single layer of epithelial cells and endothelial cells compose the alveoli. The physiological complexity of the alveoli

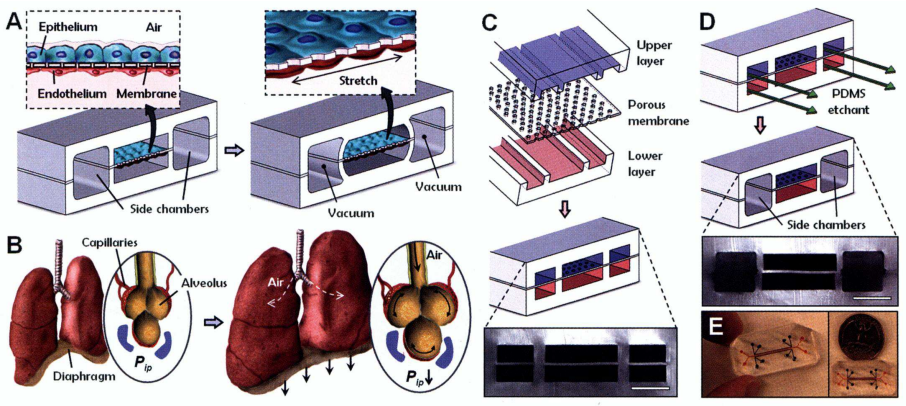

Figure 3.3 Biologically inspired design of a human breathing lung-on-a-chip microdevice. (A) The microfabricated lung mimic device uses compart- mentalized PDMS microchannels to form an alveolar-capillary barrier on a thin, porous, flexible PDMS membrane coated with ECM. The device recreates physiological breathing movements by applying vacuum to the side chambers and causing mechanical stretching of the PDMS membrane forming the alveolar-capillary barrier. (B) During inhalation in the living lung, contraction of the diaphragm causes a reduction in intrapleural pressure (P_{ip}), leading to distension of the alveoli and physical stretching of the alveolar-capillary interface. (C) Three PDMS layers are aligned and irreversibly bonded to form two sets of three parallel microchannels separated by a 10 μm thick PDMS membrane containing an array of through-holes with an effective diameter of 10 μm. Scale bar, 200 μm. (D) After permanent bonding, PDMS etchant is flowed through the side channels. Selective etching of the membrane layers in these channels produces two large side chambers to which vacuum is applied to cause mechanical stretching. Scale bar, 200 μm. (E) Images of an actual lung- on-a-chip microfluidic device viewed from above. Copyright (2010) American Association for the Advancement of Science.

structure makes more difficult to replicate with accuracy the lung functions in a traditional *in vitro* culture models [225], mainly because it is not possible to mimic how the lung tissue deforms during breathing. In this context, and how it has been previously explained, microfluidic techniques allow the fabrication of tissue barriers which, in the case of the lung, can reproduce the breathing of the human respiratory system [222]. In figure 3.3 it is shown the first lung on a chip developed by Huh et al. at Harvard University. The developed system is composed of two layer channel structure which is separated by a very thin membrane made of PDMS. The lung structure is reproduced culturing alveolar epithelial cells and vascular endothelial cells in the two different layers which are separated by the membrane, one in the upper and the other one in the lower surface of the membrane, and adding air flow and culture medium. The breathing is replicated with pressure changes in the channels, contracting and extending the membrane. Compared with traditional culture models, lung

on a chip systems mean a qualitative leap for drug testing and their chemical and biological effects in the human lung. Moreover, in the recent years, a microdevice fabricated by Yang et al. which recreates a lung on a chip has been used for anti-cancer drug testing, giving a new dimension and application to this type of organ on a chip systems [226].

Kidney on a chip.

The kidney is an important organ in humans which make the function of metabolism and excretion *in vivo*. Nephron is the basic functional unit of kidney and its role consists on removing metabolites and waste *in vivo* by producing urine, retaining nutrients by reabsorption function [225]. Drug discovery experiments in the kidney are carried out by animal testing, due to the lack of *in vitro* culture models of this organ. As can be deduced, the responses of animal kidneys and human kidneys is similar, but not the same, so the accuracy of these drug tests is clearly improvable [227]. Thus, the complexity of this organ in humans hampers the development of a kidney on a chip system that can reproduce its functions and its responses to drugs. Some successful approaches on the fabrication of a reliable kidney on a chip can be found in the bibliography [228]. One of the first chip was not exactly a kidney on a chip, but a nephron on a chip, in which the nephron functions are reproduced, included a filtration section, the reabsorption and an increasing in the urea concentration. This chip is composed of two layers with a membrane in between. Although this was a successful approach, many things could be improved. A subsequent step in the development of kidney on a chip systems was carried out by Jang et al. [229], including the culturing of renal cells of the tubule of the kidney. These cells were cultured on the microchannels and maintained alive by the appropriate conditions of fluidic shear stress. Another remarkable attempt was performed also by Jang et al. [230]. This kidney on a chip system was the first one on using primary human kidney proximal tubular epithelial cells, and its main application was on drug transport and nephrotoxicity assessment. Figure 3.4 shows this kidney on a chip in which a porous membrane separates the two layers of the microfluidic device, which is made of PDMS. On the upper surface of the membrane, primary human proximal tubule epithelial cells are cultured in the presence of physiological level of apical fluid shear stress. The system mimics the tissue-tissue interface of the living kidney proximal tubule

Liver on a chip.

The liver in the human body is located on the upper right side of the abdomen and is a metabolism organ. Its main functions are detoxification (removal of toxins), blood filtering and protein synthesis [230]. All the liver functions make it vulnerable to drugs, not only when overdosed but also in a controlled range. For that reason, liver is the main target for drug toxicity experiments and hepatoxicity. In this context, an accurate prediction of metabolic activity of livers becomes indispensable in drug discovery experiments. The traditional *in vitro* culture models of hepatocytes cannot reproduce all the functions and activity of livers *in vivo*. This is due to, especially, the lack of continuous perfusion and because hepatocytes degeneration *in vitro* cannot be avoided, while livers *in vivo* are able to regenerate. All of that can be solved, or at least improved, thanks to microfluidic

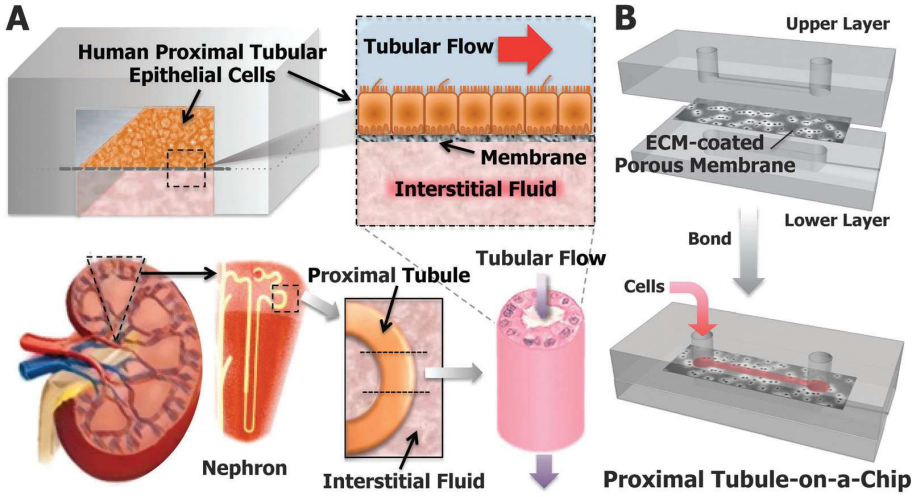

Figure 3.4 Design for the human kidney proximal tubule-on-a-chip. (A) The microfluidic device consists of an apical channel (intraluminal channel) separated from a bottom reservoir (interstitial space) by an ECM-coated porous membrane upon which primary human proximal tubule epithelial cells are cultured in the presence of a physiological level of apical fluid shear stress. The basolateral compartment is readily accessible for fluid sampling and addition of test compounds for the study of active and passive epithelial transport. This design mimics the natural architecture, tissue–tissue interface and dynamically active mechanical microenvironment of the living kidney proximal tubule. (B) Device assembly: the upper layer, polyester porous membrane, and lower layer are bonded together through surface plasma treatment. Human primary proximal tubular epithelial cells are seeded through device inlet onto the porous Extracellular matrix coated membrane. Copyright (2013), The Royal Society of Chemistry.

technology. One of the first approaches performed on microfluidics was the development of a 3D perfused bioreactor for liver tissue culture in which the perfusion conditions and the architectural properties present in *in vivo* hepatic tissue were reproduced [231]. Another approach carried out with lab on a chip techniques consists on a system with a continuous perfusion for stimulating expression and activity of detoxification genes. This research work was focused on evaluating how the culture medium flow can affect that liver on a chip model, demonstrating that a controlled medium flow has an influence in the xenosensors and the expression of detoxification genes in primary human hepatocytes [232]. In figure 3.5, a perfused multiwell plate for 3D liver tissue engineering is presented. This platform consists on the integration of multiple bioreactors in a multiwell plate format, allowing a continuous perfusion of medium thanks to pneamutic diaphragm micropumps and the formation on each bioreactors of 3D microscale tissue units thanks to scaffolds containing inside the bioreactors [233]. Another interesting platform developed by Seung-A et al. was a 3D liver on a chip to investigate the interactions of hepatocytes and hepatic stellate cells

co-cultured without direct cell-cell contact. One of the main advantages of this platform was the presence of a osmotic pumping which can assure a continuous perfusion of medium without the need of an external pump [234].

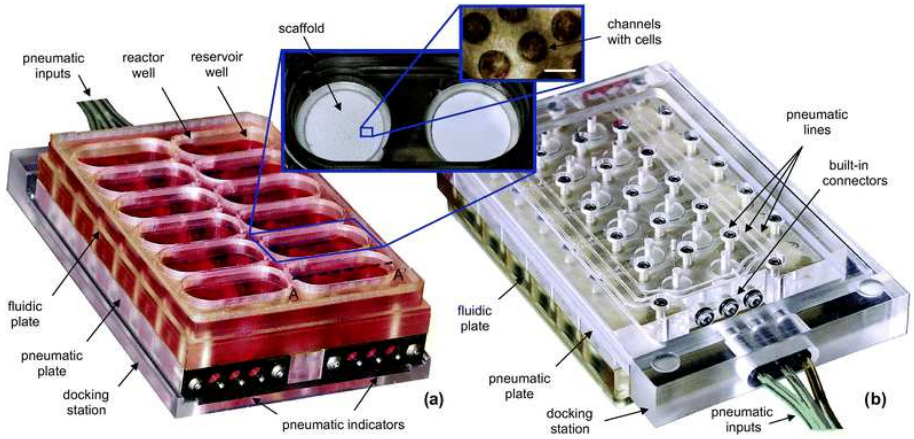

Figure 3.5 Photographs of a perfused multiwell with an array of 12 bioreactors. The size of the assembled multiwell plate is approximately 127.8 × 85.5 × 34 mm. The top view (a) includes inserted photographs of a bioreactor and a scaffold. The size of the white bar in the scaffold photograph is 300 μm. The bottom view (b) of a partially docked perfused multiwell shows the built-in connectors and pneumatic lines distributing positive and negative air pressure to individual valves and pump chambers. Copyright (2010), The Royal Society of Chemistry.

Heart on a chip.

The importance of cardiovascular system in the human body is unquestionable. Moreover, cardiovascular diseases are the main cause of death, representing almost a third of the total deaths in the world [235]. This system is composed of the heart, blood, blood vessels and the lymphatic system. Among their functions, the most important are those related to the transport of different substances, such as oxygen and carbon dioxide, nutrients or cellular waste. In mammals, the heart is responsible for pumping of blood, which is the key function of the cardiovascular system. Thus, the heart is in charge of making work the hole human body through the pumping of blood. The heart has two different cells, one of them permanent, including cardiac fibrolasts, cardiomyocytes and endothelial cells, and the others are transient cells, such as lymphocytes or mast cells [228]. Both groups of cells interact between each others. Traditional cultures of cardiac cells do not provide enough information, making the development of heart on a chip devices really important for cardiovascular research. The recreation of the cardiac microenvironment is the main obstacle that must be overcome for the fabrication of reliable heart on a chip platforms. One of the first approaches on the development of heart on a chip systems was carried out by Werdich et

al. and it consisted on a planar microelectrode array combined with a PDMS microfluidic network to measure extracellular potentials from cardiac myocytes [236]. In a similar way than the previous one, another system was developed integrating microelectrodes in a microfluidic platform for the acquirement of the electrical response of cardiomyocytes to study their metabolic profile and to optically measure the cell contractility [237]. An important advance in the fabrication of heart on a chip systems partly from the research work carried out by Grosberg et al., in which a system were developed for physiological and pharmacological studies of cardiac tissues [238]. In figure 3.6, the assembly and use of the heart on a chip platform reported on [238] is presented. This system has been designed "to measure contractility, combined with a quantification of action potential propagation, and cytoskeletal architecture in multiple tissues in the same experiment". The integration of cardiac tissue inside a organ on a chip platform was a fundamental step in the subsequent heart on a chip devices. Some recent studies that are worthy to highlight are related to the replication of the heart tissues and function as accurately as possible. For instance, by fabricating endothelialized myocardium with a 3D bioprinting strategy and embedding the biological sample into a microfluidic bioreactor with perfusion [239]. Another approach is based on engineered 3D cardiac tissue constructs (ECTCs) for the replication of cardiac physiology, but controlling the force applied to the tissue and analyzing the mechanical and electrical characteristics of the cultured tissue. This platform results very useful for many applications, such as drug screening or the study of cardiac diseases [240].

Retina on a chip.

This type of organ on a chip platforms are not the most developed or studied for the research community, so there is a field with lot of possibilities and a lot of work to do in the development of retina on a chip devices. This thesis work is partly focused on this kind of devices and, for that reason, this subsection is about different approaches found in bibliography about the characterization and fabrication of systems for the replication of the human eye, particularly the retina, functions inside a lab on a chip. The visual system is on charge of capturing and processing visual information which is acquired through the eye. This system is basically composed of three parts: eye, optic nerve and brain visual cortex [241]. There is a layer inside the eye which is called retina. In this component is where the light is received and then converted into neural signals which are sent to the brain. The retina is comprised of different layers, and one of them contains some photoreceptors cells which are responsible for the reception of light that is subsequently processed by the retina and sent to the brain through the optic nerve. The importance of the retina in the visual system is undoubted, and this is because retinal diseases, such as Startgardt disease, age-related macular degeneration or retinitis pigmentosa (RP) are some of the most common causes of vision loss in humans. Current animal models used for retinal experiments are not as accurate as could be expected, and, despite it is possible to reproduce some aspects of human visual system, some important characteristics, such as trichromacy, are not reflected. Traditional *in vitro* 2D cell culture are unable to mimic the architecture, cells interactions or blood perfusion of the human vision [242]. In this context, the tissue engineering emerges as a reliable option to replicate with high precision the *in vivo* function and environment of the human eye, which is called 3D retina organoids (ROs)

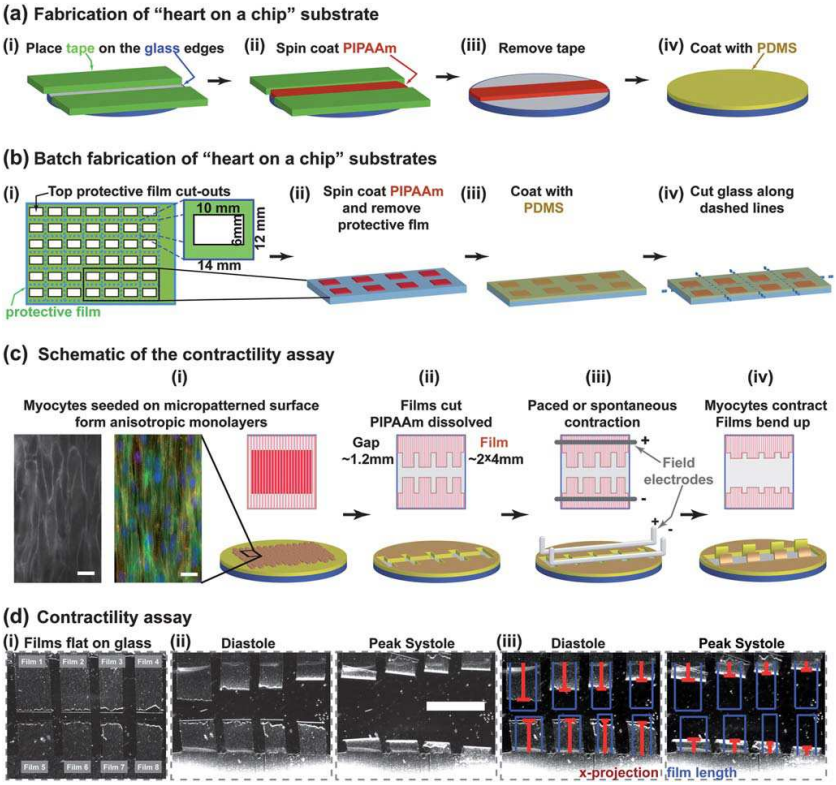

Figure 3.6 "Heart on a chip" assembly and use. (a) Fabrication of 25 mm round substrates; (b) schematic representation of batch fabrication of substrates with large glass sections for higher throughput; (c) contractility assay is run using anisotropic layers of myocytes; bottom row shows a 3D schematic representation, top row shows the view from above; the insets in (i): RH237 membrane dye stain (left) and an immunostain of a-actinin – red, actin – green, nuclei – blue (right), scale bar 20 mm; (d) Contractility experiment (PDMS layer ¼ 18.6 mm): (i) Brightfield images of films attached to the substrate, (ii) films bend up at diastole and peak systole, and (iii) the length of films (blue) and x-projection (red) overlaid on "heart on a chip" images – scale bar 5 mm. Copyright (2011), The Royal Society of Chemistry.

or "eyes on a dish" [243]. The development of 3D retina organoid requires the confluence of different complex disciplines, such as microfluidic or 3D tissue culturing, and the recent advances in this type of systems have led to important innovations [244, 245]. Nevertheless, 3D retina organoid presents some problems, most of them related to the growing of these tissues inside the device. One of the hardest disadvantage is the dissection of the tissue, which is normally performed manually. Other challenging problems of 3D retina organoid are the lack of essential cell types and physiological perfusion. The possibilities that organ

on a chip technologies offer have led to the development of some interesting platform for culturing retinas inside a lab on a chip. For instance, Dodson et al. have fabricated a microfluidic platform with the capability of point access reagent delivery through 100 μm diameter holes. The aim of this research work is to perform an organotypic culture of mice retinas for multiple days to probe the transport of signaling events [246]. Another remarkable investigation carried out by Mishra et al. consisted on the development of biomimetic microfluidic device to examine the concentration-dependent migration of retinal progenitors by using retinal lineage cells in biomimetic geometries of human and mouse retinas [247]. One of the most recent studies found in bibliography was performed by Achberger et al. and it consists on "a physiologically relevant 3D *in vitro* model of the human retina by combining human induced pluripotent (hiPSC) stem cells-ROs with hiPSC-derived retinal pigment epithelia in a retina-on-a-chip" [242]. The main advantages of this device are the enhancement in the formation and preservation of inner and outer segment, a direct interplay between photoreceptors and RPE and a controllable perfusion. Figure 3.7 shows the microfluidic retina on a chip platform of [242]. The applicability of this system for drug screening was demonstrated, becoming an important step in the development of retina on a chip devices.

Summarizing what has been explained in this section about organ on a chip, it is possible to make som affirmations. Firstly, its growth in the las 10 years is out of any doubt, attracting the interest of the pharmaceutical industry, many regulatory agencies or even national defense agencies. In addition, The appearance of this new market niche has been the trigger for the creation of many companies which have emerged to develop organ on a chip systems [221]. Drug testing is probably the organ on a chip application that have motivated the creation of more companies. Pharmaceutical industry is well known for being a very powerful industry, with a remarkable market volume. Besides, there is a real need to develop reliable systems to validate drug efficacy in humans. This need can be fulfill by organ on a chip system, creating an independent market inside the pharmaceutical one. In figure 3.8, some companies of recent creation whose main activity is based on the development of organ on a chip systems are presented [248].

3.1.4 Microelectrodes array for *in vitro* cultures

Microelectrode arrays (MEAs), also known as multielectrode arrays, are devices composed of a substrate, such as silicon, glass, plastic, FR4, etc. and a group of microelectrodes made of metal, mostly gold or biocompatible metals. The number of microelectrodes depends on the size of the substrate and the microelectrodes themselves, but it normally ranges from tens to thousands of them. Through these microelectrodes, electrical signal can be acquired or emitted, being the main applications of these devices those related with the electrical activity of cells, neurons and biological samples in general. There are two main types of MEAs: the implantable MEAs, which are used *in vivo* but are not related with this thesis work; and the non-implantable MEAs, which are normally used on *in vitro* cultures. The subsequent sections are focused in this last type of MEAs, their fabrication processes,

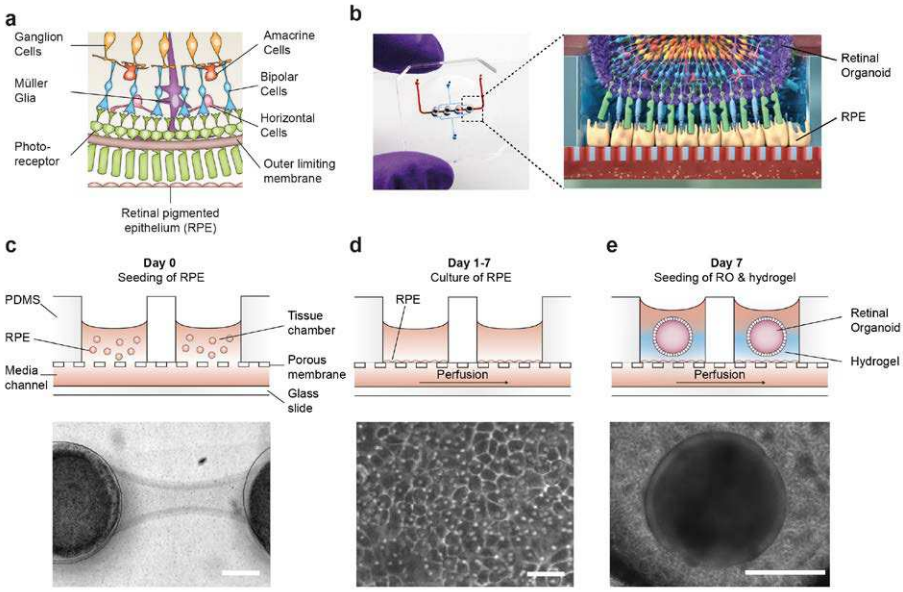

Figure 3.7 Microfluidic RoC. a) Schematic representation of the human retinal composition and cell types in vivo. b) Photo (left) of the RoC and (right) representation of the RO photoreceptor and RPE interaction. c) RPE cells are seeded into the device, d) forming a densely packed monolayer after 24 hours of culture. e) ROs and the hyaluronic acid-based hydrogel are directly loaded from the top into the well and onto the RPE. Bars indicate c) 500 μm, d) 80 μm, e) 400 μm. Copyright (2019), Achberger et al.

materials and applications, specially electrophysiological applications in cell and tissue cultures.

The first MEA device used for recording extracellular activity from cells was developed by Thomas et al. in 1972. This MEA contained 30 element microelectrode arrays fabricated by etching metal deposited on glass as substrate, and was used for recording the electrical activity of heart cells [249]. Since then, many advances have been done in the fabrication and applicability of MEA devices, developing MEAs in different substrates, including flexible ones, and using them for culturing and recording activity of many different cells, such as ganglion cells, and tissues, such as brain slices, among many others [250].

There are different types of MEAs, and depending on that, the fabrication processes differ from one to another. The first thing that should be taken into account is the materials chosen, not only to fabricate the electrodes but also for the substrate. Different materials can be useful for some applications but not for others, thus this choice must be correctly substantiated. For biological and medical applications, such as cell culture or electrophy-

Figure 3.8 Summary of organ on a chip start-ups and their core products. Copyright (2017) The Royal Society of Chemistry.

siology, some characteristics such as biocompatibility or the durability to cell culture conditions become indispensable [250]. For the fabrication of planar microelectrodes, the most common materials used for creating the metal pattern are gold, platinum or indium-tin oxide, being normally used over glass or silicon substrates. Gold and platinum need an intermediate metal layer to improve their adherence to the substrate, such as chromium or titanium [251, 252]. The metal deposition on the substrate is done using sputtering, thermal evaporation or e-beam evaporation [250], and because some of those methods require very high temperature, not all materials are adequate for all processes. The dimensions of the metal pattern, such as width, height or inter-electrode spacing, influence the number of electrodes that are included in a MEA, but in commercial MEAs, the number of electrodes is about 32 up to 256 (based on Multichannel Systems products, a division of Harvard Bioscience, Inc. [253]), being reported in bibliography higher densities of microelectrodes [254]. In figure 3.9b a commercial MEA with 60 microelectrodes made of gold on glass substrate is shown. Together with the metal pattern, the deposition of a passivation layer is needed, which normally is made of silicon dioxide or silicon nitride, as it is made the

one shown in figure 3.9b. This type of insulator layers are deposited through chemical vapor deposition (CVD) techniques. However, polymers such as PDMS or SU-8 can also be used as insulators layers [255, 256]. Once the insulator layer is deposited over the metal pattern, a hole must be opened at the end of the metal track, defining the microelectrode itself. To do this, photolithographic processes are commonly used, and the minimum size of the electrode strongly depends on the limitations of the fabrication techniques. Different solutions must be utilized to etch the insulator layer according to the material, such as hydrofluoric acid for silicon oxide or reactive etching with sulfur hexafluoride and fluoride ions for silicon nitride [250]. In figure 3.9a a brief scheme is shown in order to describe the different step of the MEA fabrication process previously explained.

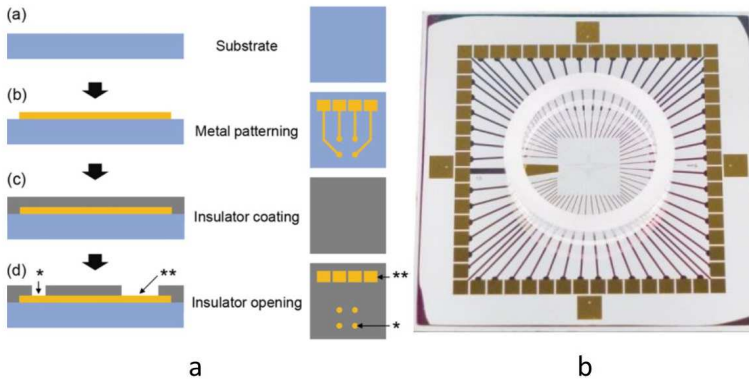

Figure 3.9 a) MEA Fabrication process. Copyright (2014) Springer. b) Commercial MEA with 60 microelectrodes made of gold on glass substrate developed by the company Multichannel Systems. Copyright (2019) Multichannel Systems, a division of Harvard Bioscience, Inc.

One of the most extended application of MEA devices is related to neural network studies. This is because of the possibility of recording and stimulating cells and tissue cultures through a few microelectrodes; and also because of the non-invasive cell-electrode interface which permits the recording and stimulation of the culture for large periods of time, if the culture microenvironment is correctly controlled. Regarding the use of MEAs for cell culturing, the working principle can described as follow. In the case of neurons cultured on a MEA, but it can be extended to many other type of cells with electrical activity, they adhere to its surface, which include the substrate and the electrodes. Those neurons which are directly in contact with the electrodes emit extracellular action potentials which are recorded through those electrodes, which can be also used for the stimulation of the cultured neurons. The extracellular action potentials are very low signals that ranges from tens to hundred microvolts, requiring an additional electronic system to detect and process those signals [250]. Many research works about neurons electrical activity recorded with MEAs can be found in the bibliography [257, 258].

In the recent years, the addition of microfluidic structures to MEA devices is growing considerably. This type of MEAs results very useful for developing *in vivo* cell culture systems with recording and stimulation of the biological samples. For instance, Moutaux et al. have developed and integrated a MEA with a microfluidic structure to record and control the electrical activity allowing "to decipher the cellular events that are involved in synaptic transmission and plasticity within neuronal networks" [259]. One of the hardest challenges for researchers to face when fabricating MEAs for cellular cultures is to have high spatial and temporal resolution on *in vivo* cultures. In this respect, some recent researches approach this problem, highlighting the work developed by Moutaux et al. who have integrated a matrix of electrodes with a microfluidic platform. This on-a-chip system can be used together with a high-resolution video-microscopy, allowing to record intracellular dynamics and electrical activity of neurons, including presynaptic axonal projections and their postsynaptic neuronal targets, as well as the electrical stimulation of the neurones cultured [260]. Figure 3.10 shows the design of a MEA with an integrated microfluidic platform, reported on [260].

Despite the main application of MEAs is related to the acquirement of neural activity, this kind of devices have been used with other type of cells, such as cancer cells, or for testing platforms for retinal diseases. For instance, and as a part of this thesis work, microelectrode arrays have been used for monitoring the electrical activity of prostate cancer cell [261], obtaining a pattern of the behavior of prostate cancer cell by using a MEA fabricated on silicon with gold electrodes. These electrodes were previously characterized by Rocha et al. by measuring their electrochemical noise and impedance, and subsequently detecting the extracellular activity of glioma cell populations [262]. With respect to retinal prostheses some research works report the use of MEAs to study the electrophysiological characteristics of retina slices. For instance, Sekirnjak et al. use microelectrode arrays to stimulate ganglion cells in the peripheral macaque retina [263], or Gautam et al. have developed a polymer optoelectronic interface which provides visual cues to a blind retina, using the MEA developed by Multichannel Systems [250][264]. Based on this type of devices, during this thesis work an autonomous culture systems with microelectrodes embedded in PDMS has been developed to study the electrical stimulation of mouse retinas with retinitis pigmentosa [265].

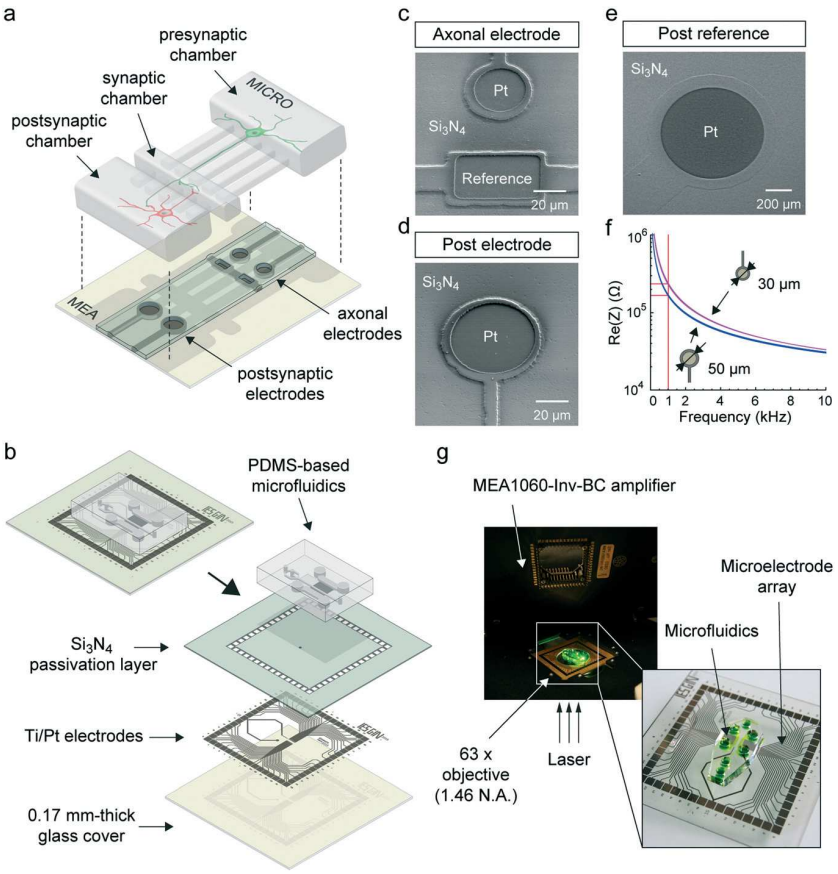

Figure 3.10 Design of the microMEA platform. (a) Scheme showing the microfluidic (micro) and microelectrode (MEA) components of the platform. (b) Exploded view depicting the different lithography layers for the fabrication of the MEA. (c–e) Electron microscopy images of axonal (c), postsynaptic (d) and reference (e) electrodes. Pt = platinum. (f) Impedance measurements of axonal electrodes (30 μm) and of postsynaptic electrodes (50 μm). (g) Mounting of the microMEA platform inside the MEA1060-Inv-BC amplifier.. Copyright (2018) The Royal Society of Chemistry.

4 Autonomous LOP for retinal culture and electrostimulation

Once the literature related to this thesis has been presented in chapter 3, in the following sections, the different systems and their applications developed during this PhD work are explained. The first one, which is fully described below, is a lab on PCB (LOP) system for culturing and electrostimulating organotypic cultures, particularly mice retinal explants, being able to culture and incubate the samples for longer than 7 days inside the developed device. The electrostimulation effect has been proved on mice retinas with retinitis pigmentosa disease, demonstrating the neuroprotection of the biological material due to the electrical stimuli. In addition, the electrical characterization of the microelectrodes have also been carried out. Thus, our main objective is the development of a culture system which clusters this characteristics: reliability, high integrability, autonomous functioning, cost effective and user-friendly.

4.1 Introduction to the problem

This thesis work has been supported by the Spanish Ministry of Science and Innovation, thanks to a national project named BIOLOP (project TEC2014-54449-C3-2-R, BIOLOP), in collaboration with the Andalusian Health Ministry (Fundacion Publica Andaluza Progreso y Salud, CABIMER) and Dr. Isabel Relimpio, a renowned ophthalmologist of Virgen de la Macarena Hospital, in the city of Seville. Moreover, it was the previous work of Dr. Relimpio on patients with retinitis pigmentosa what mainly motivated the development of the presented Lab-on-PCB (LOP). Dr. Relimpio inserted a retinal implant to patients to electrically stimulate their retinas and induce the vision in those patients. When this microchip is working the patients restore part of their vision. However, Dr. Relimpio

realized that, when the microchips were not working, the patients lost their vision, not at the same level than before inserting the microchips but at a little higher level than before the electrostimulation. These unexpected results make the doctor investigate what could have been the reasons why the electrical stimulation affected the retinitis pigmentosa patients. In this point is where Berta de la Cerda and her team, from the Andalusian Molecular Biology and Regenerative Medicine Centre (CABIMER), and the microsystem group, from the University of Seville, of which I am a member, started this research work as part of the previously mentioned national project. The main objective was to develop an autonomous lab-on-chip based on PCB-MEMS technologies for the culture and electrostimulation of mice retinas with the retinitis pigmentosa disease.

In order to understand the importance of it, a short description of retinitis pigmentosa (RP) disease is given in the following lines. RP is a hereditary retinal disease which degenerates the rod and cone photoreceptors, being the most common manifestation of retinal dystrophies. This disease affects to 1 in 4000 for a total of more than 1 million patients [266]. The effects of this disease vary depending on the mutation (there are up to 100 different mutations). The onset of RP can happen both to young people, even in the first years of life, and to adults, developing the symptoms significantly later. These symptoms includes a progressive deterioration of the ability to see in dim light, followed by loss of peripheral vision, and finishing with a complete blindness. The photoreceptors affected by RP suffer apoptosis [267]. Figure 4.1 shows the gradual lost of the photoreceptors. Nowadays, there is a real option to treat this disease by implanting a microchip inside the eyes. The American company Second Sight Medical Products has developed the product Argus retinal prosthesis (version II) and as it is said in their website, this implant "is intended to provide useful vision to blind individuals severely impacted by RP". Through the electrostimulation of the human retina, this bionic eye can induce vision in RP patients. The functioning of the whole system is complex. Together with the implant, the Argus II also includes a video-processing unit and a microcamera, which is integrated in a pair of glasses. The microcamera captures the images, sending them to the processor in which they are transformed into instructions and resend to the glasses. Those instructions are transmitted to the implant in which they are converted by a group of microelectrodes in electrical stimuli that are sending to the living cells inside the human retina directly connected to the optic nerve which sends the information to the brain, creating the perception of light patterns. Patients must learn how to interpret these light patterns.

It is possible to find some studies about the efficiency and functioning of the Argus II, being one of the most representative the one developed by Ahuja et al [268]. The aim of that study was "to determine to what extent subjects implanted with the Argus II retinal prosthesis can improve performance compared with residual native vision in a spatial-motor task". Their results conclude that a 96 % presented an improvement in accuracy and a 93 % of them an improvement in repeatability with the system than without it, concluding that the retinal implant increment information from existing vision in a spatial-motor task. As it has been previously mentioned, it has been clinically observed that the RP disease can be decelerated with the electrical stimulation of the photoreceptors by using this retinal implant, even when it is not working. However, there is no certain

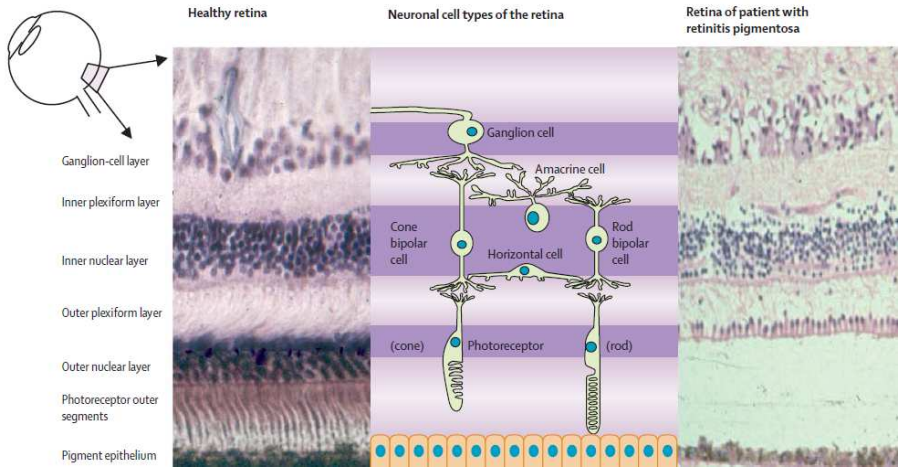

Figure 4.1 Histological appearance of healthy human retina (left) and retina of a patient with retinitis pigmentosa at a mid-stage of disease (right). The space between the retinal pigment epithelium and the outer nuclear layer in the diseased retina is a processing artifact. Copyright (2006) Science Direct.

research works with *in vitro* culture experiments that confirms this fact. Nevertheless, it is possible to find some *in vivo* experiments on patients with retinal diseases by using electrostimulation, which are related with this thesis work [269], but *in vivo* not *in vitro*. The development of an autonomous system such as the one presented here, open new possibilities on the RP *in vitro* research, by optimizing the electrostimulation or carrying out drug delivery experiments on the cultured samples.

There are some differences between human retinas and mice retinas, specially in the lack of fovea and macula in mice retinas, or in the photoreceptors ratios and the ganglion cell types. Despite those differences, and in order to have a higher numbers of experiments under controlled conditions, our tests have been carried out using mice retinas. For our experiments, wild-type pigmented mouse C57BL/6 (WT) was used as a healthy control; albino CD1-IGS (CD1) and two RP models with a C57BL/6 background such as $Pde6b^{rd10}$ (rd10) and $Pde6b^{rd1}$ (rd1) were used as diseased-tissue models. Rd1 and rd10 are the most widely used model animals for the study of RP, displaying spontaneous apoptotic degeneration of the photoreceptor cell layer that starts from the first or second week after birth respectively. Cell death in these mouse models is caused by mutations in the Pde6b gene, expressed specifically in the photoreceptor cells. Mutations in this gene also cause RP in humans [270, 271].

4.2 Proposed solution

Under these circumstances, we have developed an autonomous LOP for organotypic retinal culture able to provide electrical stimuli to retinal explants of mouse models of retinal dystrophy. Moreover, we have tested the histological effect of electrostimulation in a degenerating retina. The development of a LOP to carry out a medium-long term organotypic culture requires to take into account many different aspects, which are introduced below.

The first one is related to the choice of materials. Due to part of the device is going to be directly in contact with biological samples (mice retinas), those materials must be biocompatible. Due to our system is intended to be used on a inverted microscope, the part of it that is going to use for culturing must be transparent. Looking at those requirement, PDMS and thermoplastics fit perfectly as materials that are going to be used during the fabrication.

Another critical point is the placement of the microelectrodes through which the stimulation is going to be applied, including not only the PCB for these microelectrodes, but also the microfluidic structure and the bonding of both pieces. These microelectrodes are integrated with sensors and actuators for heating and measuring the temperature (37 $^{\circ}$C) inside the culture chambers, as well as the electronic to control the environmental conditions. The rest of the electronic circuits, those that control the LOP and connect it to the software which monitor the whole system, are also an indispensable part of the development. The assembly of the different parts and its correct functioning is not a minor aspect, that is taken into account in this chapter.

Finally, performing cultures on autonomous system is not trivial. Normally, cultures are carried out inside a CO_2 chamber, with temperature and oxygen and CO_2 levels perfectly controlled. However, what we propose is to keep the culture alive outside an incubator, which has been demonstrated as a possible option on literature [272], and as it is also demonstrated in this PhD. The continuous flow in LOP culture devices is not a minor aspect, being the maintenance of oxygen and carbon dioxide the limiting elements. In this thesis work, CO_2 has been more constraining than oxygen and it has influenced the flow rate applied to the culture, as it will be explained in following sections.

In figure 4.2 the different parts that comprise the whole system are shown. Each of them will be detailed in the next sections. Moreover, according to the context which has been previously presented, for each part, the different approaches until obtaining the final device are explained, as well as a detailed description of the developed LOP, including the design of each part, the materials used, the fabrication process and the experimental results. In figure 4.2, a conditioning LOP is included and it works as an independent system. Regarding the culture LOP, it is composed of several structures which are fabricated separately and subsequently joined. There are two main parts in this LOP: a MEA device fabricated on PCB and microfluidic structure.

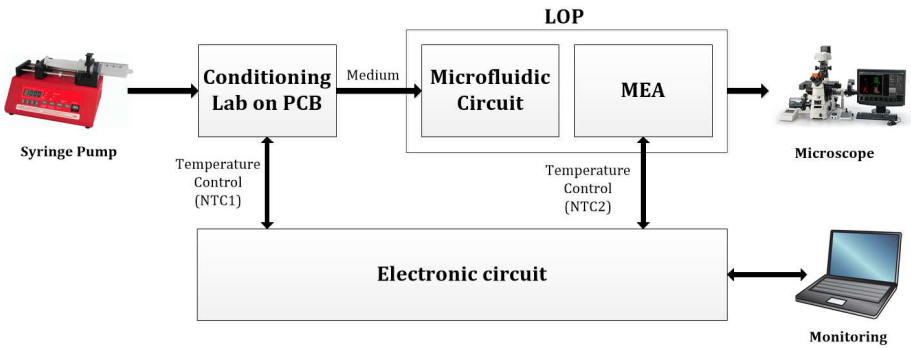

Figure 4.2 General scheme of the whole system.

During the development of this LOP, there are two main issues which have resulted specially critical. The first one is the fabrication of the MEA device, which implies a real novelty due to the manufacturing process. This MEA is composed of a group of gold wires embedded on PDMS, whose ends connect the MEA with the biological samples culture inside it. The other one is the integration of the MEA device with the microfluidic structures and the electronic circuits, without which the whole system would not have worked properly well. Particular mention deserves the microfluidic circuit, which must be perfectly watertightness, assuring sterility, but allowing an easy insertion and extraction of the samples cultured inside the LOP, maintaining a transparency enough to its used on an inverted microscope. Apart from all of this, a software to monitor the system has also been developed. Through this software it is possible to control the temperature, the heating and even the electrostimulation, with a user-friendly program. Summarizing, we have developed an autonomous LOP that works as a microincubator, inside which a medium-long term mice retinas culture can be carried out and electrostimulated, while it can be observed through an inverted microscope and monitor with a user-friendly program. Each part of the system is described in an independent section. The functioning of the whole system, with the experimental results, the biological test and the conclusions are explained at the end of this chapter.

4.3 Lab-on-PCB

In this section, the design and fabrication of the different parts of the LOP are explained. The LOP is composed of several structures which are fabricated separately and subsequently joined. There are two main parts in this LOP. Firstly, a printed circiut board (PCB) of FR4 and copper has been chosen as a substrate. The use of PCBs offers many advantages for the developed LOP, such as the possibility of integrate sensors and actuators or it low cost fabrication process. The microelectrodes are integrated in the PCB and embedded in PDMS, as it will be outlined below. The other important part of the LOP is the microfluidic structure. During this thesis work, there have been different approaches before obtaining

the final design of the microfluidic device. The major changes on its design has affected the material used, the channels distribution and the assembly with the substrate. In this section the most important approaches are detailed, paying special attention on the final design.

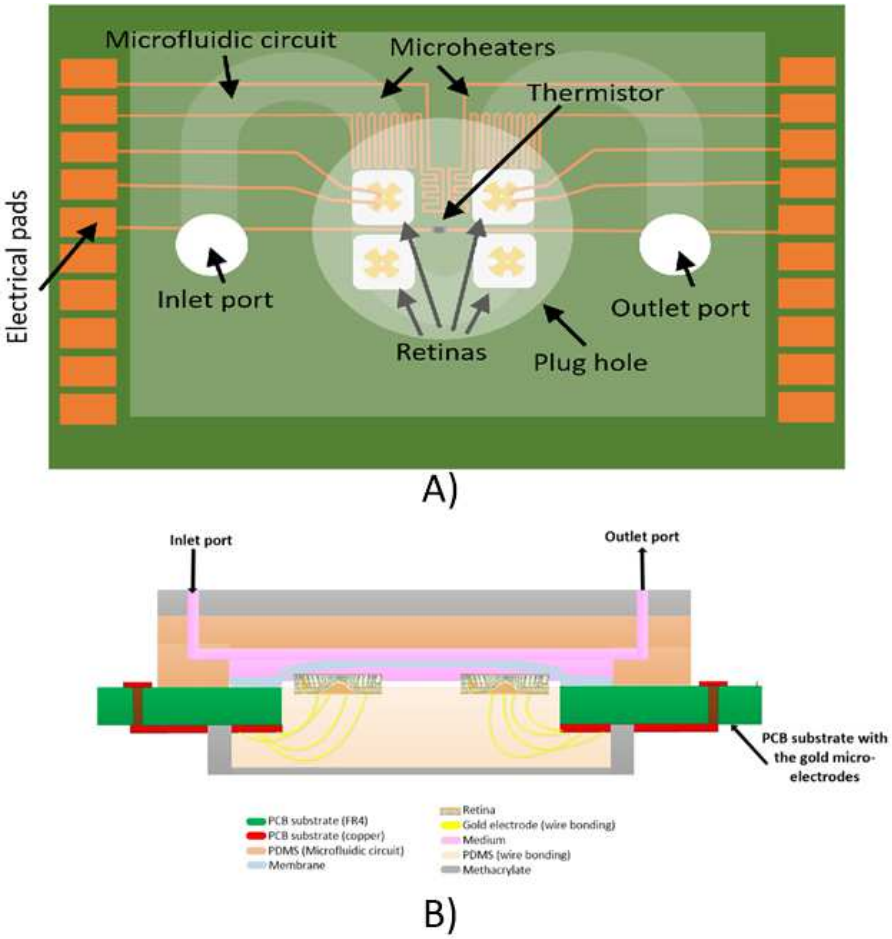

Figure 4.3 Scheme of the LOP design: A)Top view; B)Front view.

In figure 4.3 the scheme of the LOP design using a PCB as a substrate is shown. As it is shown in figure 4.3A, there are four different wells in which a mice retina is cultured. For each retina, a group of microelectrodes are embedded in PDMS with their ends directly in contact with the retinas, as can be seen in figure 4.3B. A microfluidic circuit is bonded to the MEA, to distribute the medium and feed the culture. This circuit is just indicative, but in section 4.3.2 the different approaches are explained. Regarding this short explanation,

in following subsections the each part of the LOP is described in detail.

4.3.1 Microelectrode array on PCB

In this section, the design and fabrication of the microelectrode array (MEA) on PCB is fully described. It includes the different approaches until obtaining the final design, as well as some explanations about the used materials.

Design

This part of the LOP has been designed in such a way that the development of the other elements depend on it. The function of the MEA is to stimulate the biological samples which are placed over the microelectrodes embedded in PDMS, a biocompatible material widely used for culturing cells and tissues. These microelectrodes are gold wires which connect the biological sample with the PCB. The use of a PCB as a substrate offers lot of possibilities, among which the integration of sensors and actuators has been used in the presented design. Thus, the microheaters can be integrated in the LOP by using the copper tracks of the PCB as actuators, heating the LOP through heat dissipation by Joule effect when a constant current is applied. A NTC thermistor is also included to measure and control the temperature of the device. Both heaters and NTC thermistor are embedded on PDMS.

Despite PCB technologies have many advantages, during the development of this LOP it has been necessary to face the fact that FR4 is not transparent, and that this device is intended to be used on an inverted microscope, with substances such as fluorophore that needs transparency to be observed with that type of microscope. For that reason, we have decided to use PDMS, which is integrated on the PCB, embedding the gold microelectrodes and acting as a passive layer for the NTC thermistor and the microheater. Hence, there are four squares milled in the PCB filled with PDMS and embedding up to 10 microelectrodes in each one, making a total of 40 of them in the MEA. These microelectrodes are made of a thin gold wire placed by using the wire bonding technique. In the presented design, the retinas are going to be placed over these areas, called from now on "effective working areas", made of PDMS with the embedded electrodes, being possible to culture four retinas in the same device.

In figure 4.4 the layout of the presented LOP is shown. The milled squares are represented in green color, while the copper tracks of the top and the bottom layers are in red and blue color respectively. The end of the red copper tracks, in the top layer, are on the edge of each milled square (in green color) coated with a thin gold layer, to improve the adherence of the gold wire during the wire bonding technique. The copper thickness is 35 μm and the FR4 thickness is 800 μm. The use of a PCB with two copper layers avoids the contact between the medium and the heaters or the NTC thermistor. The pads in blue color are made of copper with a gold coating, and through those pads is how the MEA is connected

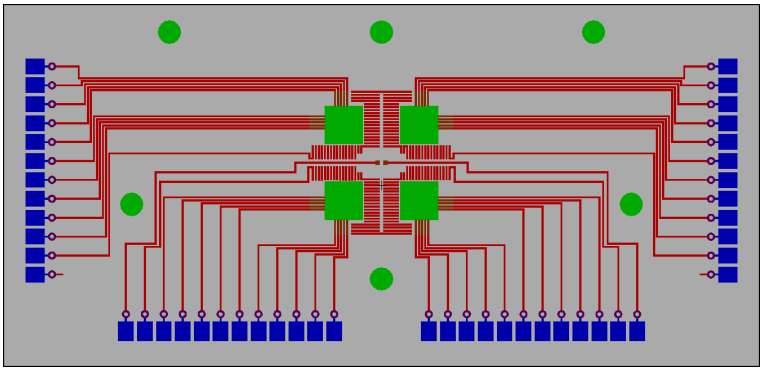

Figure 4.4 PCB Layout of the LOP. In green color, the milled squares where the microelectrodes are embedded; in red color the copper tracks of the top layer; in blue color the copper pads of the bottom layer.

to an external electronic circuit which controls the LOP. The dimensions of the PCB are 100 mm x 50 mm and the milled squares are 5 mm x 5 mm each.

The most critical aspect on the design of this part of the LOP is how the microelectrodes are going to be placed and subsequently embedded in the PDMS. The wire bonding technique requires two metal surface to place each end of the gold wire. The copper tracks close to the edges of the milled squares are coating with a thin gold layer, to improve the adhesion with the gold wire. The other end of the gold wire is bonded to an auxiliary PCB, which acts as a sacrificial layer and that is assembled to the main PCB with screws. Once the gold microelectrodes are placed, the next step in the design of the LOP is how these microelectrodes are going to be embedded on PDMS. To achieve that, and taking into account that the PDMS is deposited in liquid state, a frame is located around the effective working areas to contain the PDMS. Once the PDMS is deposited embedding the microelectrodes, a glass cover slide is placed over the PMMA frame, to hold the elastomer maintaining the transparency of the LOP. Figure 4.5 represents the final design of the LOP with the gold microelectrodes embedded. The different steps of the fabrication process will be detailed on section 4.3.1, as well as the problems which were solved during that process.

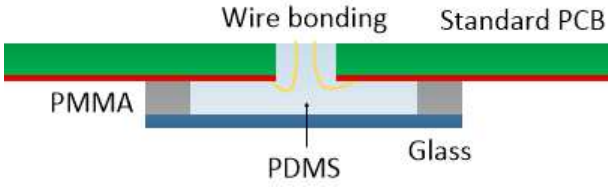

Figure 4.5 Final design of the LOP with the gold microelectrodes embedded in PDMS.

To summarize this section about the design of the MEA on PCB, some aspects need to be highlighted. Firstly, the materials which are in direct contact with the culture must be biocompatible and transparent, to allow the used of this LOP on an inverted microscope. That is the reason why PDMS and gold has been chosen. The used of a PCB as substrate allow the integration of sensors (NTC thermistor) and actuators (copper tracks as heaters) which allow the heating and temperature control of the LOP. In order to make possible the culture of several samples in each experiment, four different effective working areas are included, each one with 10 microelectrodes, which has been placed through the wire bonding technique. To control the PDMS deposition, a PMMA frame and a glass cover is needed, this last one to maintain the transparency.

Fabrication

Despite on previous paragraphs some little clues were given about the fabrication process of the MEA on PCB, it is much more complex and deserves a whole subsection to be explained. For that reason, along the next paragraphs, the different attempts until obtaining the final MEA are going to be explained. The main problems which have been faced and solved, in one way or another, were normally related with the placement of the microelectrodes and the adherence of the ends of them to the metal surface. The deposition of the PDMS and the possibility of embedded the whole electrode on PDMS are other important issues of the fabrication process. This part is specially critical because if the end of the microelectrode is completely covered with PDMS, the electrostimulation is not possible. However, every problem during the process has been successfully solved and has led to a final LOP with good functioning and results.

Once the material for manufacturing the MEA are chosen, now we are going to focused on describing how the fabrication process has been performed, including some figures with the steps of that process and some real images with the final devices as a result of the manufacturing.

The fabrication process of the MEA includes an innovative procedure to create a low cost microelectrode array, as it is shown in figure 4.6. A novel microelectrode array fabrication process has been developed, embedding the gold electrodes in PDMS. The PCB used to create the MEA is composed of FR4 of 800 μm thick and double side copper layer, of 35 μm thick. The cavities where the gold microelectrodes are embedded in PDMS have been obtained by micromilling the PCB (step (a)). After the micromilling, a typical photolithographic process has been implemented to pattern the copper and create the paths, that are completely covered by a resin layer with the exception of the part of the copper pads where the electrodes are located, which have a gold coating. The wire bonding technique has been conducted to place the gold microelectrodes in the cavities. This is the most critical part of the process because the gold wires must be correctly located before the deposition of the PDMS. Thus, another piece of PCB with one side of copper, named from now on auxiliary PCB, is put under the main PCB that contains the MEA, with the objective of using the copper layer to execute the wire bonding technique (step

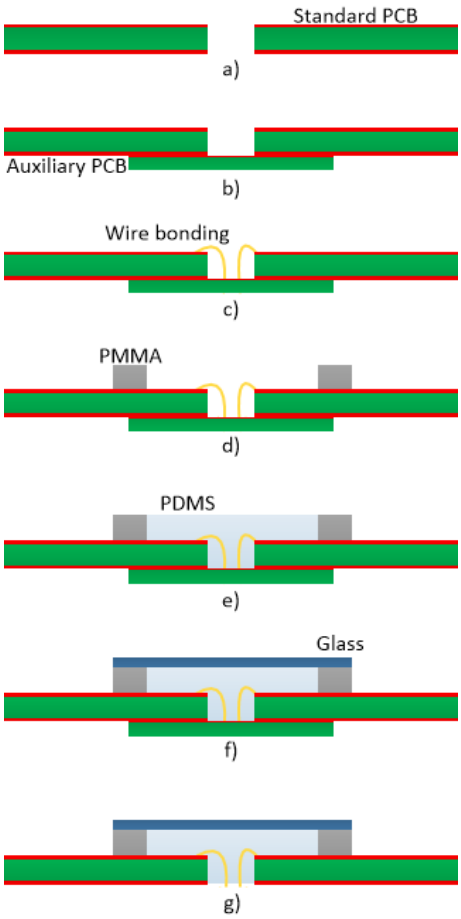

Figure 4.6 Steps of the fabrication process, using the wire bonding technique: a) Commercial PCB of FR4 and copper; b) A auxiliary PCB is bonded to the commercial PCB; c) Gold microelectrodes with a diameter of 25 μm are placed using the wire bonding technique; d) A frame of PMMA surrounds the gold microelectrodes; e) The gold microelectrodes cavity is filled with PDMS, embedding them; f) A glass coverslip is placed over the PDMS; g) Once the PDMS is cured, the auxiliary PCB is released.

(b)). The two PCBs are assembled with screws in such a way that the gold wire is bonded between the copper paths of the MEA, with a gold coating, and the copper side of the auxiliary PCB. The gold microelectrodes have a diameter of 25 μm (step(c)). Once the wire bonding technique is completed, a Poly methyl methacrylate (PMMA) frame of 2 mm thick is bonded to the MEA, with the purpose of controlling the deposition of the PDMS. This frame is bonded to the PCB with a biocompatible two component glue (step (d)). The next step is the deposition of the PDMS to embedded the electrodes (step(e)).

Immediately after the deposition of PDMS, a glass coverslip is placed over the PMMA frame to hold the PDMS maintaining the transparency of the LOP (step (f)). The next step consists on introducing the device inside an oven to perform the curing of the PDMS, which needs 90 minutes at 65 °C to be completely cured. Once the PDMS is cured, the auxiliary PCB can be released (step (g)), whereupon the MEA is completely fabricated and the gold electrodes are correctly embedded in the PDMS, with the end of the electrode out of the PDMS.

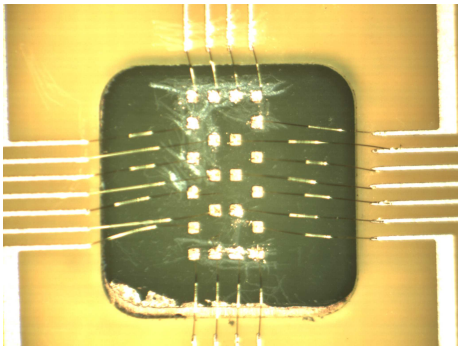

Figure 4.7 First attempt for the microelectrodes placement. The auxiliary PCB includes some copper pads in which one of the end of the wire bonding is placed, allowing a controlled position of each one.

Despite the different steps of the fabrication process were fixed in a very early stage of this PhD work, there were different approaches for the microelectrodes placement, which corresponds to the fabrication step (c) of figure 4.6. One of the first attempts consisted on performing a photolithographic process on the auxiliary PCB before the wire bonding technique. This allows a controlled placement of the microelectrodes in the effective working area, as it is shown in figure 4.7.

This first attempt seemed to be a good solution. However, the fabrication steps (f) and (g) present some problems related with the transparency. The deposition and curing of PDMS on FR4 result to be translucent due to the roughness of the FR4, denying the pass of enough amount of light to be used on an inverted microscope. Figure 4.8 shows the problem previously described.

The results of the first approach, shown in figure 4.8, was not as good as it was expected, so a new solution is needed. The best results were obtained with this second attempt. It consists on performing the wire bonding technique between the copper track with the thing gold layer and the copper of an auxiliariy PCB, but without a previous photolithographic process. That is to say: microelectrodes are not exactly in the same position in each effecting working area, because the end of the microelectrode which is placed on the auxiliary PCB does not have an exactly pad to place it, as it happened with the first attempt. Figure 4.9

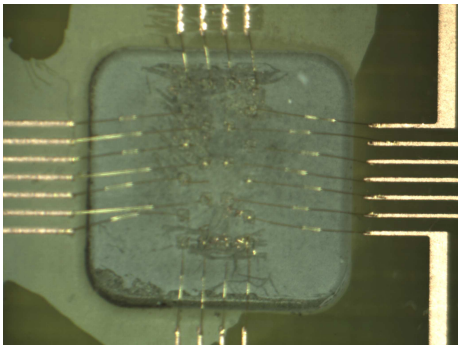

Figure 4.8 Results of the first attempt for the microelectrodes placement after the curing of the PDMS. Transparency is not enough to allow the pass of light on an inverted microscope.

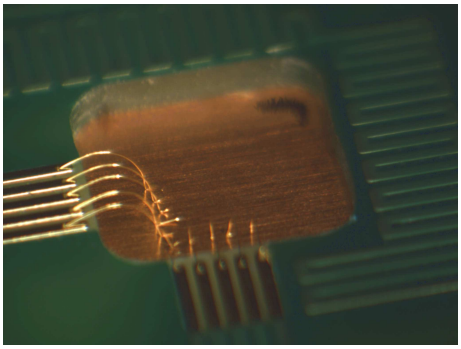

Figure 4.9 Second attempt for the microelectrodes placement. The auxiliary PCB is completely made of copper, so the exact position of the end of the wire which is placed on the auxiliary PCB cannot be controlled as it was in the first attempt.

shows the placement of the microelectrodes in one of the effective working area before depositing the PDMS. As it can be seen, the gold wire is placed between the gold patterned copper track and the copper of the auxiliary PCB, but not in a certain position.

Despite this solution could seem worse than the first approach previously explained, the placement of the electrodes is not as important as we though at the beginning. As it was explained in the design section, the MEA device includes four effective working areas of 5 mm x 5 mm each one, in which 10 gold microelectrodes are embedded in PDMS. Being the diameter of a mice retina of about 3 mm and the diameter of the gold wire of 25 μm, the retinas can be easily placed over the area of actuation of the microelectrodes, so the position of them is not critical. The insertion protocol of the mice retinas are fully described in other section. Moreover, the main problem of the first attempt is solved in this second approach and, as it is shown in figure 4.10, the effective working area is more transparent than in the first approach. This demonstrates that the deposition of PDMS

directly on copper instead on FR4 increase the transparency, making the MEA device suitable for its use on an inverted microscope.

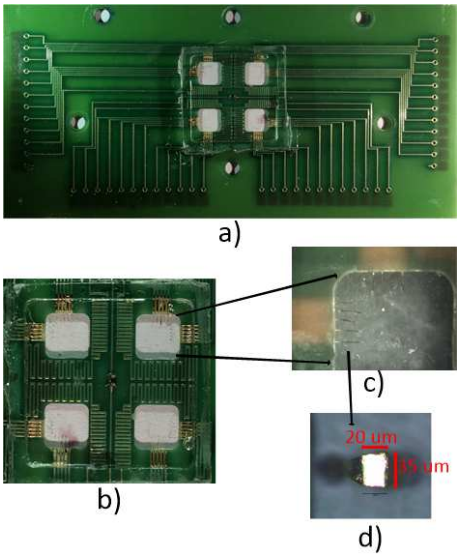

Figure 4.10 a)Top view of the complete MEA; b) Top view of the four effective working areas, the microheater and the NTC thermistor; c) One of the effective working area with gold microelectrodes embedded in PDMS; d) End of a gold microelectrode with dimensions: 20 x 35 μm.

The final result of a fabricated MEA is shown in figure 4.10a). The four effective working areas are presented on figure 4.10b), each of them with 10 gold microelectrodes embedded in PDMS. Figure 4.10c) corresponds to an enlarged image of one effective working area. Finally, figure 4.10d) is a zoomed image of the end of the electrode which is placed on the auxiliary PCB. It can be seen how the end of the electrode deforms, being rectangular instead of perfectly circular. This fact does not affect the functionality of the MEA.

Summarizing this subsection, the MEA on PCB which has been finally used for our experiments is the second approach described in this section and shown in figure 4.10. It consists on a group of 10 microelectrodes in each effective working area, of a total of 40 microelectrodes, which are placed by using the wire bonding technique between a copper track coated with gold and the copper layer of an auxiliary PCB. The deposition of PDMS over the copper instead of FR4 improves the transparency of the effective working areas. The PMMA square and the glass cover slide hold the PDMS and maintain the transparency of the LOP. The biocompatibility of the materials used on this process makes the presented MEA suitable for biological or biomedical applications.

4.3.2 Microfluidic structure. Design and fabrication

In this section, the design and fabrication of the microfluidic structure is presented. This part of the system has had different approaches until obtaining the final design, so the most representative are explained, including some experimental and simulation results, and the reasons why they have been finally discarded or chosen.

It is important to remember that the previously explained MEA on PCB is part of a more complex LOP for culturing biological samples. The development of the microfluidic structure has needed more different approaches until obtaining the final design. This is mainly because of the difficulties found for integrating it with the MEA on PCB. To handle liquids, the watertighness is an indispensable requirement, as well as the correct distribution of the liquid all along the microfluidic circuit. This issue has been the main bone of contention during the development of the microfluidic structure.

The first decision to take is the material of the microfluidic structures. Taking into account the importance of the biocompatibility in the chosen material, the different options considered for the microfluidic circuit were thermoplastics and PDMS, which are typically used for fabricating microfluidic devices with biological applications, as it has been explained in the state of the art section. Thus, different approaches were attempted varying the structure of the microfluidic circuit, the materials used and the way the microfluidic is assembled to the MEA. In the following paragraphs, the most representative attempts until obtaining the final model of the LOP presented in this thesis work are explained, including the layout and some simulation results carried out with COMSOL Multiphysics, highlighting their advantages and disadvantages.

PDMS microfluidic structure based on vanes

Design

The main problem to solve during the design of the microfluidic circuit was to assure an uniform distribution of the culture medium all along the LOP, with a reliable watertightness, but allowing the insertion and extraction of the mice retinas at the beginning and at the end of each experiment. Regarding these non-negotiable requirements, a closed microfluidic circuit made of a thermoplastic and directly bonded to the MEA on PCB was the first idea which was discarded, because the insertion and extraction resulted impossible to carried out. Under this circumstances is how the idea of using screws to assembly the MEA and the microfluidic circuit appeared as a good option for the development of the presented LOP. In this first approach, PDMS was the material chosen to fabricate the structure with the microchannels, and a screws made of plastics were used to join both parts of the LOP.

Once the problem related to the insertion and extraction of the biological samples was solved, the next step was to assure a correct distribution of the culture medium. For that

purpose, different microchannel distributions were studied. The first design was based on vanes to distribute the culture medium once it has been introduced through the inlet port. With this design, the goal was to obtain an uniform flow all along the microfluidic circuit, assuring that the culture medium fed the four retinas cultured inside the LOP. Figure 4.11 shows the design of the microfluidic distribution based on vanes, in which the microfluidic channels are represented in white color, while the structure is represented in blue color. The presented design was conceived to be fabricated on PDMS by using an aluminum mold with the shape of the figure 4.11. The height of the microfluidic circuit is 500 μm.

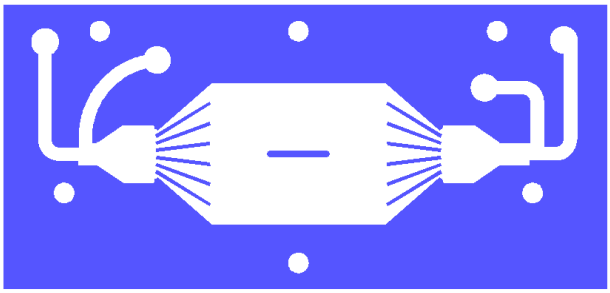

Figure 4.11 Microfluidic structure design based on vanes to obtain an uniform distribution of the culture medium.

Before fabricating the proposed design, some simulations were carried out on COMSOL Multiphysics. Figure 4.12 shows the simulation of the culture medium distribution in the designed microfluidic structure based on vanes. As can be seen, the distribution of culture medium seems to be uniform. However, the fluid flow is too slow, becoming almost standing, which could cause some problems in the culture if the flow is not continuous.

The fluid distribution does not show good results, not being possible to assure an homogeneous fluid flow all along the microfluidic structure. Moreover, there are some points in which the medium can remain standing, specially on the corners. For that reason, this first attempt was discarded before fabricating it.

PDMS microfluidic structure based on fractals

Design

Due to the results previously described, the microfluidic design was changed to obtain a better one without the standing of culture medium inside the microfluidic circuit. Thus, a new design was proposed, which was based on fractals. Its functioning is very simple: the microfluidic circuit is divided in different fractals, being bigger in the closest part to the inlet port and becoming smaller when approaching the zone in which the mice retinas are

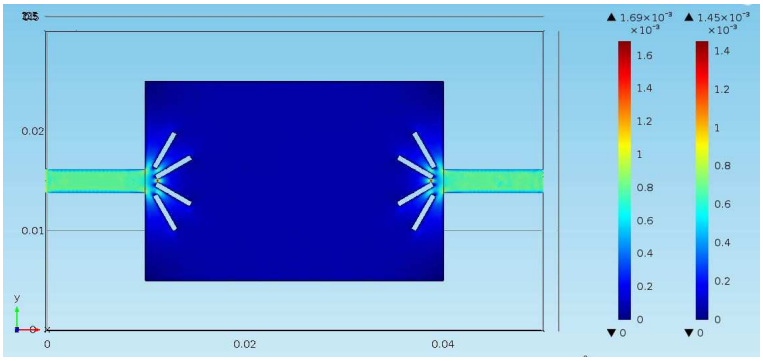

Figure 4.12 COMSOL Multiphysics simulation of the microfluidic structure design based on vanes. The distribution of culture medium is uniform, but the fluid flow is too slow provoking the standing of liquid in some parts of the microfluidic circuit.

supposed to be cultured. In the middle of the culture zone, a pillar is added, to make the fluid flow divide and assure the correct feeding of all the mice retinas cultured in the LOP. Figure 4.13 shows the design of the microfluidic distribution based on fractals, in which the microfluidic channels are represented in white color, while the structure is represented in blue color. The presented design was conceived to be fabricated on PDMS by using an aluminum mold with the shape shown in figure 4.13. The height of the microfluidic circuit is 500 μm.

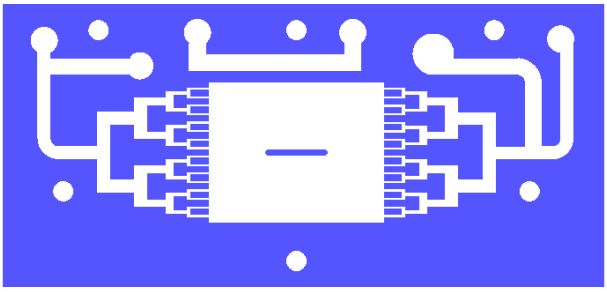

Figure 4.13 Microfluidic structure design based on fractals to obtain an uniform distribution of the culture medium.

As it was explained above, once the design is decided, the next step consist on simulating with COMSOL Multiphysics the fluid distribution inside the new microfluidic structure. Figure 4.14 shows the simulation of the culture medium distribution in the designed microfluidic structure based on fractals. As can be seen, the distribution of culture medium seems to be uniform, and the integration of a pillar just in the middle of the culture zone

improves the fluid flow where the mice retinas are supposed to be placed.

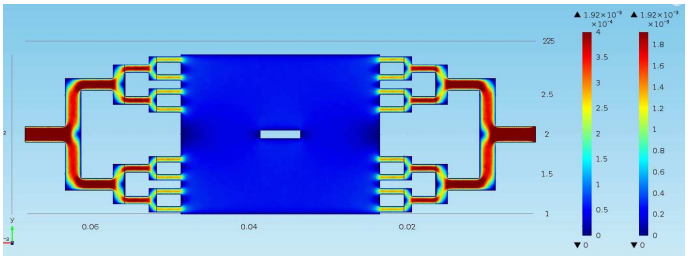

Figure 4.14 COMSOL Multiphysics simulation of the microfluidic structure design based on fractals. The distribution of culture medium is uniform and the pillar assures the correct fluid flow in the culture zone.

Fabrication process

The step by step fabrication process of the microfluidic structures made of PDMS is the same for each one, but modifying the shape of the aluminum mold which is filled with PDMS. Thus, this process is explained just once, on this the first approach based on fractals. However, the final result of the microfluidic circuit and its assembly with the MEA device is shown, paying more attention in those which have been used to perform experiments with mice retinas.

As it is shown in figure 4.15A and 4.15B, a aluminum piece is micromilled to obtain the designed structure. To fabricate the mold, a CNC machine of high precision is used. The height of the microfluidic channel is 500 μm. The next step consist on filling the mold with PDMS in liquid state, as it is shown in figure 4.15C. The aluminum mold filled with PDMS is introduced inside an oven at 65 $^{\circ}$C for 1 hour and 30 minutes for its curing. After that time, the microfluidic structure made of PDMS is demoulded, fig. 4.15D. After the demoulding, the inlet and outlet ports are holed, as it is shown in figure 4.15E. After this step, the microfluidic structure is fabricated and ready to be assembled to the MEA on PCB thanks to the screws included for that end.

Following the steps of the fabrication process explained in figure 4.15, the aluminum mold and the resulting microfluidic platform made of PDMS are shown in figure 4.16. This structure improves the microfluidic distribution of the culture medium compare to the one based on vanes, as it was shown in the simulations, but it presents some problems related with the watertightness and the appearance of bubbles. The disadvantages of this microfluidic structure based on fractals made us to discard it and find a new approach to fulfill our requirements.

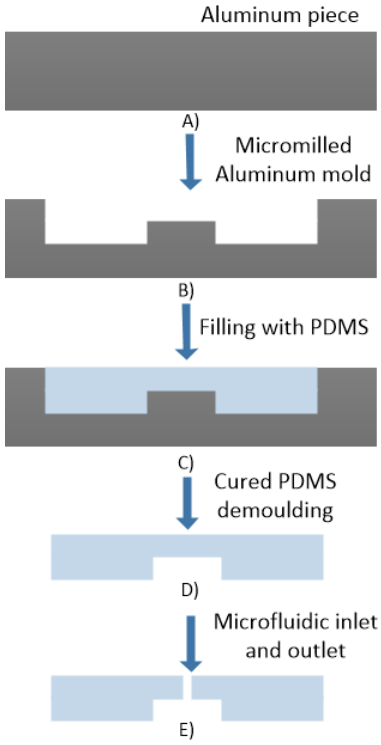

Figure 4.15 Step by step fabrication process of the microfluidic structure made of PDMS: A) Aluminum piece; B) Micromilled aluminum mold; C) PDMS deposition; D) Demoulding; E) Inlet and outlet ports.

PDMS microfluidic structure based on a continuous channel

Design

The proposed model to solve the problems presented in the microfluidic structure based on fractals is a platform whose design is shown in figure 4.17, in which the fractals have been substituted for a continuous microfluidic channel of the same width all along the structure. This width of the microfluidic channel is the same than the effective working area of the MEA, that is to say 5 mm. Thus, the alignment between the MEA and the microfluidic structure results crucial for a correct functioning. That alignment is possible thanks to six screws which assembly the MEA and the microfluidic platform.

To demonstrate the correct distribution of fluid inside the presented structure before its fabrication, figure 4.18 shows the COMSOL Multiphysics simulation of the proposed microfluidic structure. As can be seen, the fluid flow is homogeneous along the microfluidic channel, assuring the feed of each retina culture inside the LOP. With this design, the

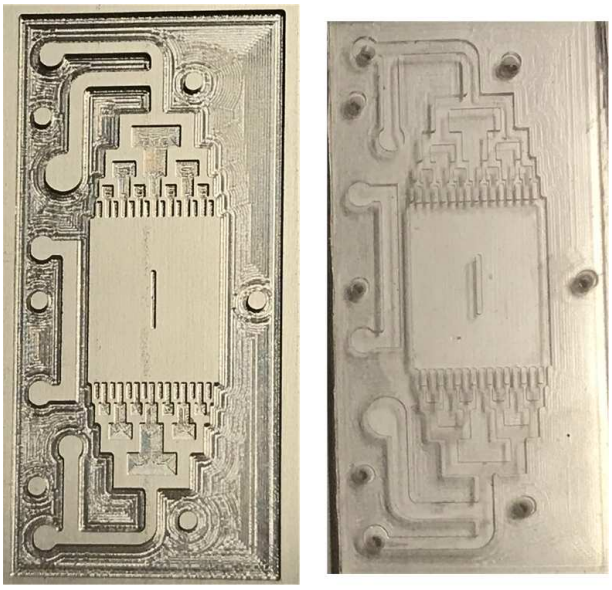

Figure 4.16 Aluminum mold and microfluidic structure based on vanes, entirely fabricated on PDMS.

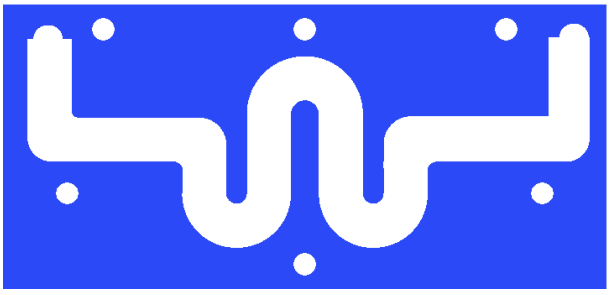

Figure 4.17 COMSOL Multiphysics simulation of the microfluidic structure design based on a continuous microfluidic channel. The distribution of culture medium is uniform and the four effective working areas are perfectly fed with culture medium.

problem with bubbles is minimized in comparison with the others.

Fabrication process

The fabrication process of the PDMS microfluidic structure based on a continuous channel is the same that the one based on fractals. Thus, step by step process is shown in

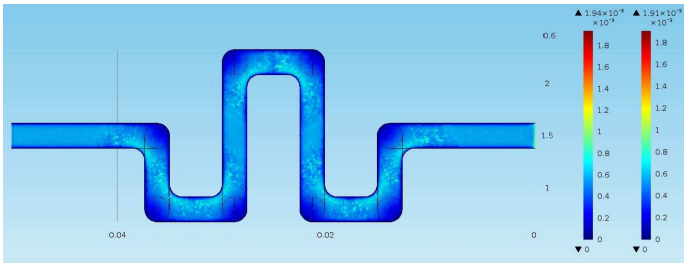

Figure 4.18 Design of the PDMS microfluidic structure based on a continuous channel to obtain an uniform distribution of the culture medium.

the previous figure 4.15. This new structure improve not only the fluid distribution, but also considerably decreases the onset of bubbles. However, the watertightness problem remains. Figure 4.19 shows the aluminum mold and the microfluidic circuit made of PDMS with the continuous microfluidic channel.

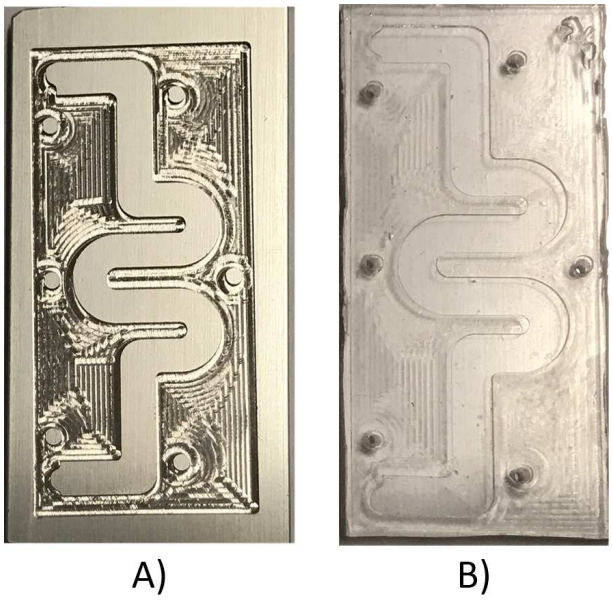

Figure 4.19 Aluminum mold and microfluidic structure based on a continuous microfluidic channel, entirely fabricated on PDMS.

The watertightness is a recurring problem which cannot be solved by using a microfluidic structure completely made of PDMS. The assembly between the MEA and the microfluidic circuit by using screws does not assure a perfect seal, mainly due to the flexibility of the PDMS and the warping of the PCB. These watertightness problems also appeared in some

occasions in the previous models made of PDMS and assembled to the MEA with screws. Thus, we conclude that the lack of watertightness was not a problem of the distribution, but a problem of the material and the assembly of both parts of the LOC.

PMMA microfluidic structure based on a continuous channel with a removable plug of PDMS

Design

Hence, the microfluidic structure made of PDMS and joined to the MEA with screws was substituted by another one made of PMMA and bonded to the MEA with biocompatible glue, but maintaining the continuous microfluidic channel, which has demonstrated a good distribution of culture medium. Notwithstanding, and as it was explained at the beginning of this section, the LOP needs to be removable to allow the insertion and extraction of the mice retinas culture inside. Thus, the microfluidic structure is not a closed circuit, but a semi-closed one, in which the microfluidic channel is made of PMMA, but there are a plug made of PDMS, which can be easily inserted and extracted, in the zone of the effective working areas. This plug made of PDMS has the exact dimensions to assure the watertightness of the LOP, while its shape continue the microfluidic channel of the PMMA, connecting the microfluidic circuit and feeding the mice retinas culture inside the LOP. Figure 4.20 shows the design of the microfluidic circuit based on a continuous microfluidic channel and made of PMMA, with a removable plug made of PDMS which is represented in gray color.

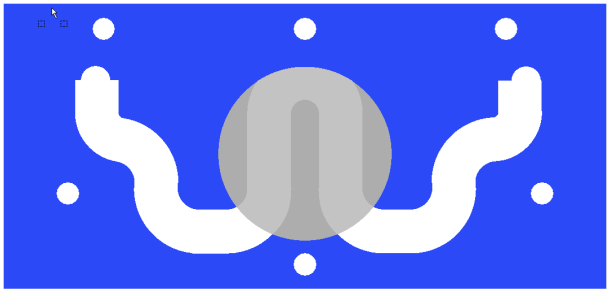

Figure 4.20 Design of the PMMA microfluidic structure, with a plug made of PDMS, based on a continuous channel to obtain an uniform distribution of the culture medium.

The design presented in figure 4.20 is the one which is finally used during this thesis work to develop the autonomous culture of mice retinas inside a LOP. This design solves the problems which occurred in the other microfluidic structures, specially those related with the appearance of bubbles and the watertightness, allowing an easy insertion and

extraction of the biological samples cultured inside. The removable plug made of PDMS is a great advantage during the experiment, allowing a perfect watertightness and facilitating the assembly of both parts of the LOP. In the next subsection, the fabrication process of each microfluidic structure is presented.

Fabrication

The watertighness problem was the main reason why the PDMS microfluidic structure was discarded and another attempt, which resulted the final one, was proposed. This last approach is made of PMMA, with a removable plug of PDMS. Two main changes are included in this final microfluidic structure. Firstly, the main material is PMMA, which is directly bonded to the MEA instead of using screws to join both parts. The second modification is the fabrication and integration of a plug made of PDMS to cover the effective working areas. The fabrication processes of both the microfluidic circuit made of PMMA and the plug made of PDMS are outlined below.

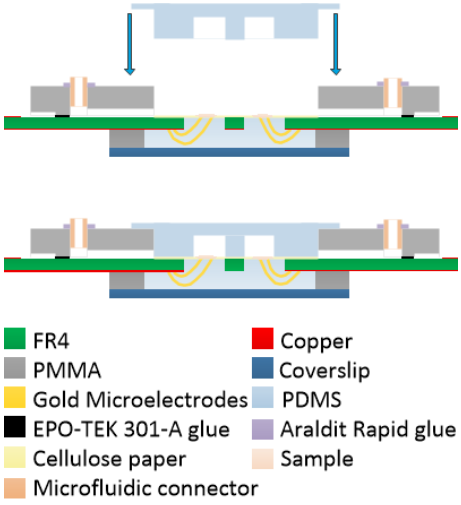

Figure 4.21 Insertion of the plug made of PDMS in the microfluidic structure made of PMMA.

The two different parts of the microfluidic structure and how they are integrated in the MEA are described in figure 4.21. The PMMA platform is bonded to the MEA as a fixed part, while the plug is inserted on it as a removable part to allow the extraction and insertion of the mice retinas cultured in the LOP. The use of PDMS to fabricate the plug facilitates the watertightness of the microfluidic, as well as it allows the continuous flow all along the channel, thanks to the shape of the mold in which the PDMS is deposited and cured. Both parts, the microfluidic structure and the plug are fully described below.

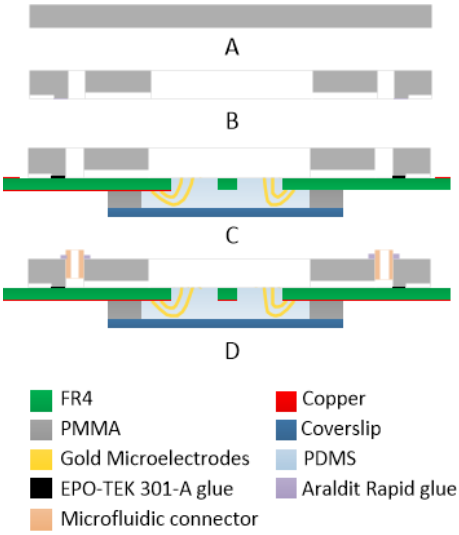

Figure 4.22 Steps of the fabrication process and bonding of the microfluidic structure: (A) Piece of PMMA of 5 mm thick; (B) Micromilling of the piece of PMMA; (C) Bonding of the microfluidic structure to the MEA; (D) Bonding of the microfluidic connector to the microfluidic structure.

The step by step fabrication process of the microfluidic structure and its bonding to the MEA is shown in figure 4.22. This microfluidic structure is made of PMMA (step (a)). The fabrication process consists on micromilling the piece of PMMA according to the previously designed microfluidic circuit. The milling tool used has a diameter of 2 mm, and the channel dimensions are 1 mm of depth and 5 mm of width, the same width than the effective working area. A circular hole, with the dimensions of the plug, is located in the center of the microfluidic structure (step (b)). A thick wall of 2 mm of width surrounds the fluidic channels and the hole, in order to facilitate the bonding between the microfluidic structure and the MEA, being assembled by using a biocompatible, two component, room temperature curing epoxy (EPO-TEK 301, Epoxy Technology). The thickness of the epoxy glue layer is 86 μm, and it is deposited in a planar surface with a roller that assures that thickness. Then, the epoxy glue is transferred to the microfluidic structure by the stamping method and bonded to the MEA. To obtain an optimal bonding, both the MEA and the microfluidic circuit must be joined for 24 hours at room temperature (Step (c)). Once the PMMA structure is bonded to the MEA, the last step consists on bonding the microfluidic luer connectors to the microfluidic structure with a two component epoxy (Araldit Rapid) for one hour, for what there are two holes, one for the inlet port and another one for the outlet port (step (d)).

The step by step fabrication process of the plug is shown in figure 4.23. This fabrication process is independent from the fabrication process of the LOP shown in figure 4.22. This plug is made of PDMS to obtain the transparency required for its use in an inverted

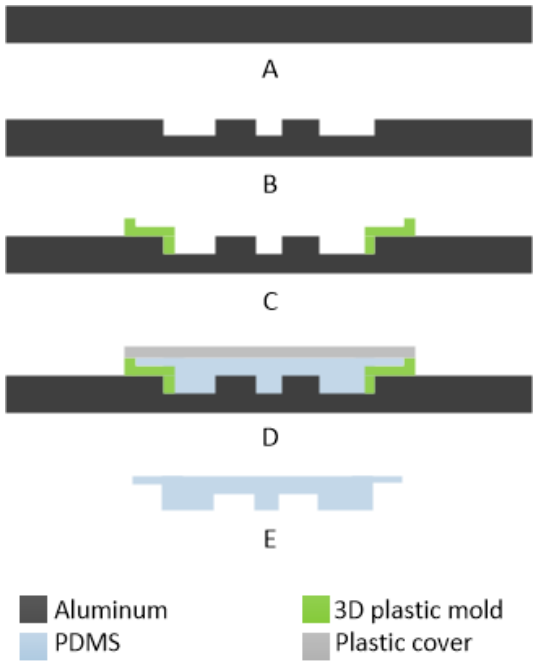

Figure 4.23 Steps of the fabrication process of the plug: (A) Aluminum sheet; (B) Micromilling of the mold made of aluminum; (C) 3D structure to control the deposition of PDMS; (D) Deposition of PDMS inside the mold; (E) De-molding of the plug.

microscope and to assure the biocompatibility of the LOP. Moreover, the PDMS has a flexibility and workability which make it ideal for this application. PDMS is deposited in a liquid state and, after a curing time, it becomes a silicone-like solid. The mold substrate is an aluminum sheet of 5 mm thick (step (a)). This aluminum sheet is micromilled with a 1 mm mill tool, obtaining the desired design of the microfluidic circuit (step (b)). Once the mold is fabricated, it is necessary an additional part which controls the PDMS deposition and assures the desired height of the plug. Thus, a structure made of plastic and fabricated with a 3D printer is located inside the cast (step (c)). After the PDMS deposition, the mold is covered with a plastic sheet, to avoid the leakage of the PDMS (step (d)). Finally, the mold with the deposited PDMS is cured inside an oven at 70 $^{\circ}$C for 90 minutes. After PDMS curing, we can release it from the mold, resulting in the final plug which is ready to be used together with the rest of the LOP (step (e)).

Figure 4.24 shows the aluminum mold and the plug made of PDMS. As can be seen, the mold is micromilled using the negative layout that continues the microfluidic channel of the PMMA structure. The piece in green color is used to hold the PDMS deposition to assure a defined height of the plug, to make it fix perfectly when it is inserted in the LOP. This piece is made of plastic (PLA) and has been fabricated with a 3D printer. The plug

Figure 4.24 Final result of the fabricated plug made of PDMS. The shape of the mold make the plug fit with the microfluidic channel.

made of PDMS fixes in the PMMA microfluidic structure with a complete watertightness, allowing the fluid flow all along the effective working areas.

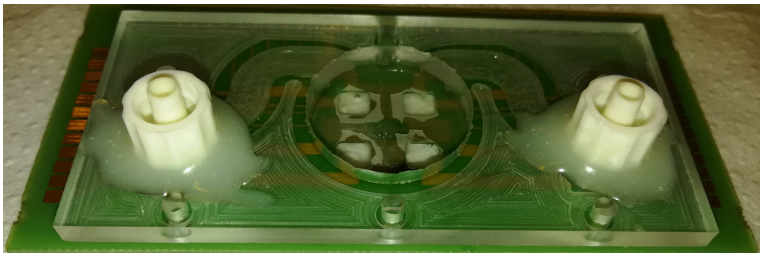

Figure 4.25 Final result of the fabricated microfluidic structure bonded to the MEA. The circle in the center is where the plug made of PDMS is inserted.

The final result of the fabrication process of the microfluidic structure bonded to the MEA is shown in figure 4.25. As can be seen, the microfluidic circuit includes two ports, one inlet and one outlet, and a circle surrounded the effective working areas, in which the plug made of PDMS is inserted. The inlet and outlet ports are bonded to the piece of PMMA with biocompatible glue, as well as the microfluidic circuit is bonded to the MEA in the same way.

4.4 Pre-conditioning circuit

The pre-conditioning circuit is an independent module developed in this thesis work, and that is fully described in this section. The main function of the pre-conditioning circuit is to maintain the appropriate conditions of the culture medium before introducing it in the LOP, assuring a temperature of $37^{\circ}C \pm 0.5^{\circ}C$. This platform is also able to mix other fluids with the culture medium, if it is necessary. Despite it has not been used in the final system, its development has led this thesis work to some important conclusions that have resulted useful for the design and fabrication of other parts. Thus, in this section the design and fabrication process of the conditioning circuit are included, as well as some experimental results which demonstrate its correct functioning.

4.4.1 Design

The initial idea of developing this pre-conditioning circuit was to pre-heat the culture medium before introduce it inside the LOP device with the mice retinas. Despite this circuit has been designed, fabricated and tested, and as such it is explained in this section, it has not been finally used together with the other parts of the system, because its function results useless for a low continuous fluid flow as it is needed in this type of organotypic cultures. However, the heating by joule effect when a current is applied to a copper track and the temperature measurement and control have resulted really useful when designing the heating and temperature control of the MEA device, and for many other applications not directly related to this thesis work. In fact, the heating and temperature control has been included in the final LOP as it was designed in this pre-conditioning circuit. Figure 4.26 shows a scheme of the different parts of the pre-conditioning circuit and their connections.

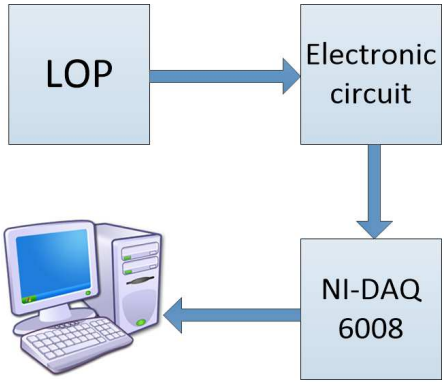

Figure 4.26 Different parts of the system.

The pre-conditioning LOP is divided into three different parts, each of which with a specific function. Firstly, a microfluidic circuit made of PDMS, with three inlet ports, one outlet port, and microchannels, which enables the flow and mixing of fluids. PDMS is the only material which is directly in contact with the samples, assuring the biocompatibility of the presented device. Secondly, a PCB, which is used as a substrate, with a microheater made of copper and a NTC thermistor to temperature measurements. A PDMS layer covers the copper tracks as a passive layer, in order to avoid the contact between the liquids and the metal tracks. The last part of the system is an electronic circuit for signal conditioning and control. This electronic circuit performs the temperature measurements through the NTC thermistor as well as controls the external power supply that provides 5V/1A to the microheater, working as a PWM. The system is controlled with a user friendly program developed with LabView software, from National Instruments. a data acquisition device (NI-DAQ, from National instruments) make possible the connections between the pre-conditioning circuit and the Labview software.

Due to its biocompatible properties, the microfluidic circuit is made of PDMS, making it suitable for preparing a culture medium for biological applications. The microfluidic circuit makes possible the distribution and mixing (if necessary) of the medium. Regarding the mixing, it is particularly interesting for drug discovery. For that purpose, three inlet ports and one outlet port are included. The mixing is achieved by diffusion inside the serpentine. The fabrication of the microchannels has been carried out by using a mold made of aluminum, which has been previously designed for its fabrication in a CNC milling machine. The microfluidic circuit is closely related to the PCB module since it has to be aligned with the microheater to optimized the temperature control. Hence, the microfluidic structure is located over the PCB module that contains the microheater and the NTC thermistor covered with a PDMS layer, facilitating the adhesion between the PCB and the microfluidic circuit. The design of the microfluidic circuit assures the optimal conditions and mixing of the fluid when it passes through the outlet port.

The PCB contents a NTC thermistor, EPCOS B572xxV5, and a heater patterned in its copper layer, which has the shape of a serpentine to assure an homogeneous temperature along the microfluidic channel. As it has been mentioned beofre, it has to be aligned just below the microchannel of the microfluidic circuit to allow the correct heating of the fluid, as it is shown in the layout of figure 4.27. In order to improve the accuracy of the temperature measurement, the NTC thermistor is placed near the outlet port assuring the established conditions of the culture medium.

The NTC thermistor and the microheater are controlled by an external electronic module. There are different parts included in this module, as described below. The first one is necessary for the correct operation of the NTC thermistor. It consists on a voltage divider. It has been characterized in such a way that the output voltage (captured by the DAQ card) is converted, via LabView software, from National Instruments, into the real temperature. The NI-DAQ 6008 also supplies the 5V that are needed by the NTC thermistor to operate. The heater contained in the pre-conditioning circuit requires a 5V/1A external power source. The activation of this external source is also controlled via LabView software. The

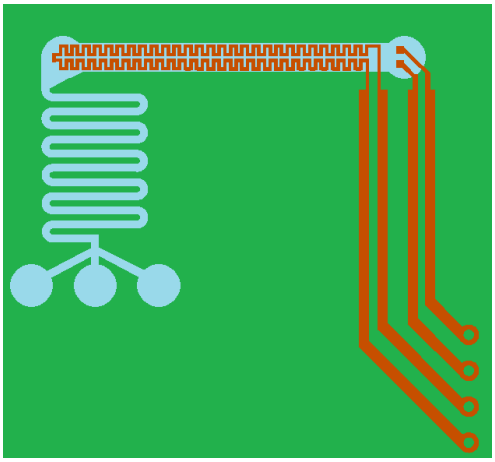

Figure 4.27 Layout of the pre-conditioning circuit: in blue color the microfluidic circuit; in red color the copper paths; in green color the FR4 of the PCB.

electronic circuit needed in this case includes a transistor that controls the pass of current from the external power supply to the heater. The transistor is activated, allowing the pass of current, when the temperature is under 36.5°C, and it will be off when the temperature is over 37.5°C, operating as a Pulse Width Modulation (PWM).

4.4.2 Fabrication

In this section the fabrication process of each part of the pre-conditioning circuit is described. It includes the manufacturing process of the microfluidic circuit made of PDMS and the PCB with the NTC thermistor and the microheater made of copper, as well as the assembly of both parts.

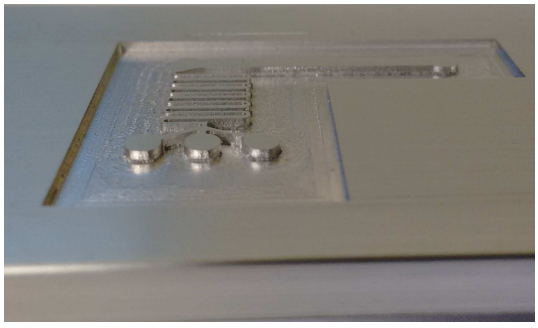

Figure 4.28 Mold made of aluminum utilized to create the microfluidic circuit with PDMS.

For the fabrication of the microfluidic circuit, a mold made of aluminum has been designed and fabricated, as it is shown in figure 4.28. This mold is manufactured by using a CNC milling machine. The microchannels have a width of 1 mm and a height of 0.5 mm, needing a milling tool with a diameter of 1 mm. This mold is filled with PDMS, resulting in the final microfluidic structure of the pre-conditioning circuit with the shape of the microfluidic channels.

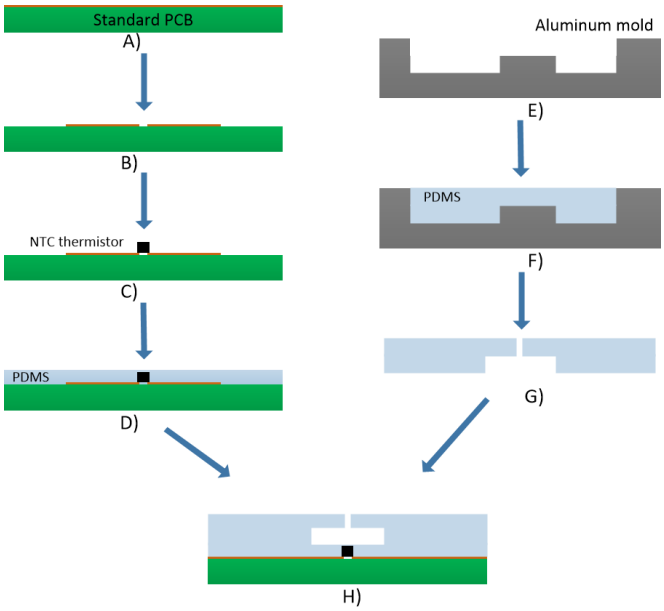

Figure 4.29 Fabrication process of the PCB module: A) Standard PCB of FR4 and copper; B) Photolithographic process; C) NTC thermistor welded to the copper; D) PDMS layer over the copper and the NTC thermistor, half cured in the oven. Microfluidic circuit: E) Aluminum mold; F) PDMS deposition in the aluminum mold; G) PDMS releasing when it is half cured. H) pre-Conditioning circuit after bonding the microfluidic circuit to the PCB module.

As can be seen in figure 4.29, the fabrication processes of both the PCB and the microfluidic structure are carried out simultaneously. That means that the curing of PDMS, deposited on both the mold and the PCB, must be performed at the same time, to obtain an appropriate bonding between both parts. Starting with the PCB manufacturing, a standard PCB of FR4 standard thickness of 1,6 mm and a copper standard thickness of 35 μm has been chosen, figure 4.29A. Then, the typical photolithographic process is performed to fabricate the PCB module, that includes the copper paths and the NTC thermistor, figure 4.29B. The NTC thermistor is welded into the copper pads and it is located close to the outlet port to assure that the temperature of the culture medium is accurate, figure

4.29C. Then a passive layer of PDMS of 500 μm, in a proportion of 20:1, is deposited on the PCB using a spin-coater, covering the heater and the NTC thermistor, but releasing the connections to the external electronic circuit, figure 4.29D. In parallel to step A, the fabrication of the microfluidic circuit must be performed. Thus, the aluminum mold, figure 4.29E, is filled with PDMS, in a proportion of 10:1, figure 4.29F, and introduced in a belt vacuum chamber for 30 minutes, in order to remove the possible bubbles that may appear during the deposition. When there are no bubbles, PDMS is cured with temperature, so the mold with PDMS is introduced in a oven at 65°C for 45 minutes. The PCB with the PDMS layer must be introduced at the same time than the aluminum mold filled with PDMS, to assure the same curing of PDMS in both parts. After that time, PDMS deposited in the mold is released, figure 4.29G, resulting in the final structure of the microfluidic circuit. The last step consists of drilling the holes of the inlet and outlet ports with a punch and bonding this part with the PCB with the PDMS layer half cured and, finally, the resulting device is introduce inside the oven for 1 hour at 80°C, figure 4.29H.

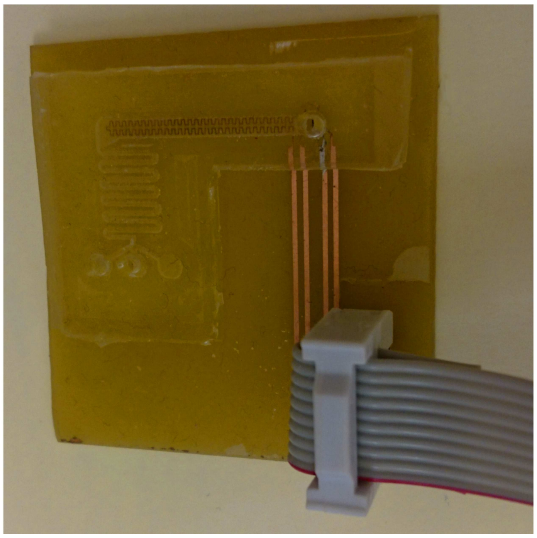

Figure 4.30 Top view of the LOP after its fabrication.

Top view of the pre-conditioning LOP already fabricated (Microfluidic circuit and PCB module) is presented in figure 4.30. The curing and bonding needs to be accurate to avoid the blocking of the microchannels when the second curing of PDMS after the assembly is accomplished.

4.4.3 Experimental results

In this section, the experimental results carried out to test the functioning of the pre-conditioning circuit are presented. The first objective is to demonstrate the correct distribution of fluids and its mixing once they are introduced into the microfluidic platform made of PDMS. Through the second experiment, the adequate operation of the microheater with the NTC thermistor that measures the temperature has been successfully tested, as well as the external electronic and the Labview software to monitor the system.

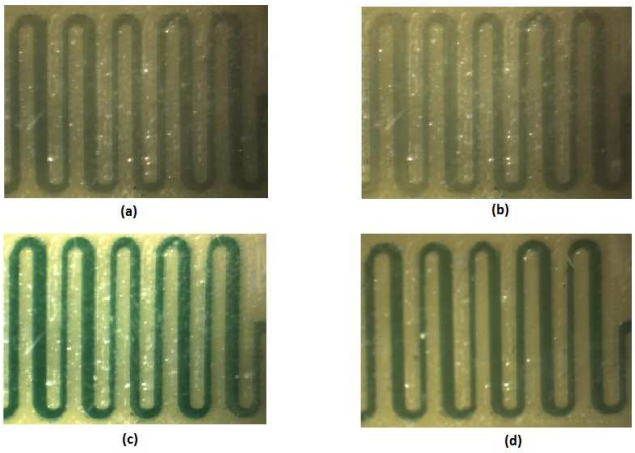

Figure 4.31 Mixing of fluids inside the microchannel: (a) Blue ink; (b) Blue ink mixed with water; (c) Green ink; (d) Green ink mixed with water and blue ink.

The first experiment carried out tests the correct operation of the microfluidic circuit to mix fluids, as it is shown in figure 4.31. It is crucial to have a correct fluids mixing inside the microchannel, in case different substances need to be mixed with the culture medium. In order to achieve this goal, three different inlet ports are included in the microfluidic platform. The microfluidic circuit shows a good behavior when different liquids are introduced in the microfluidic circuit. The microchannel distribution is based on a traditional serpentine to facilitate the mixing of different fluids. In figure 4.31 the mixing of three different liquids is shown, exhibiting an appropriate functioning of this part of the pre-conditioning circuit. One of the most important aspects of this first experiment is the verification of a complete isolation and watertighness between the electronic and the microfluidic circuits, which is correctly demonstrated.

Once the mixing inside the microfluidic circuit presents successful results, the next experiment consists on testing the microheater operation and the NTC thermistor that measure the fluids temperature. An external power supply (5V/1A) feeds the microheater. A

program that implements a PWM model developed with Labview software, from National Instruments, controls the heating. Hence, a Mosfet transistor allows or denies the pass of current through the microheater depending on the temperature. Figure 4.32 shows the front panel of the Labview program which monitor the pre-conditioning circuit, in which the system temperature is measured through the NTC thermistor and its conversion through the DAQ device connected to the electronic circuit.

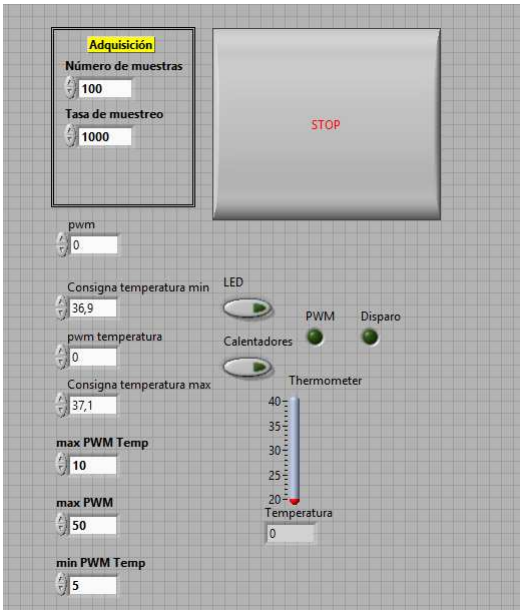

Figure 4.32 Labview software panel by mean which it is possible to control the temperature of the LOP.

A simulation on COMSOL multiphysics demonstrates the theoretical good behavior of the developed heater and how the temperature inside the microchannel placed over it assure the desired temperature. As it is shown in figure 4.33, the temperature inside the microchannel is around 37°C. To be more exact, the results given by COMSOl were as follow: the average temperature of the fluid inside the microchannel is 37.45°C; the temperature of the fluid in the outlet port is 36.85°C; the temperature measure in the NTC is 37.1°C.

The next step is to test the functioning of the device in a real experiment. As it has been said, the objective is to assure a constant temperature of the culture medium of 37°C, which is the usual temperature needed in a culture. This make the presented pre-conditioning circuit suitable for this type of biological applications. The NTC thermistor is located as close as possible to the outlet port to improve the accuracy of the temperature measurement

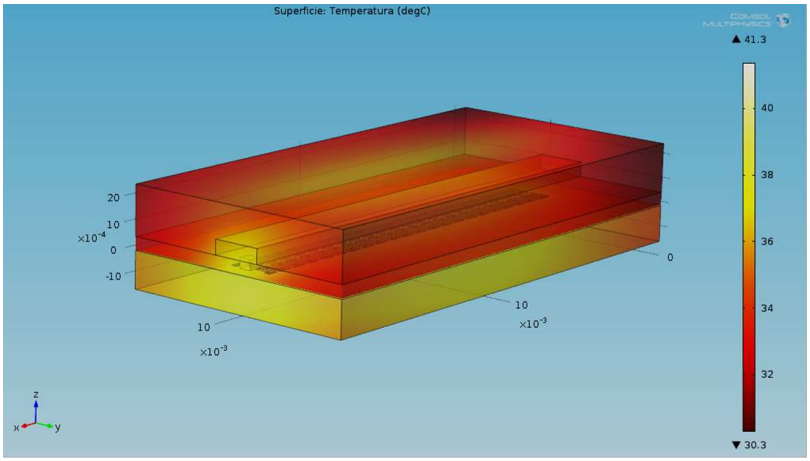

Figure 4.33 Temperature simulation of the fluid flow inside the microchannel over the heater.

of the fluid. The program which monitors the temperature operates as a PWM, in such a way that, if it is over 37.5°C the power supply is disconnected, and, if it is under 36.9 °C the heater is fed with current. It is demonstrated that the temperature is correctly controlled and it is possible to keep it on a constant temperature of 37°C ± 0.5°C. Figure 4.34 shows the graph of time Vs temperature depending on the fluid flow velocities.

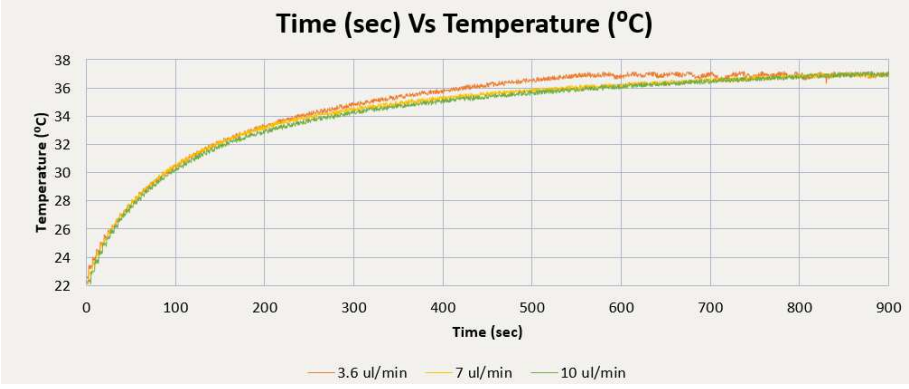

Figure 4.34 Heating process for different inlet flows.

Regarding the presented experimental results of this pre-conditioning circuit to pre-heat and mix the culture medium, it has been demonstrated its correct functioning. The microfluidic structure permits the mixing of fluids and the use of a PCB implies some advantages, such as its low cost and the possibility of including sensors and actuators. The Labview

software and the electronic circuit have presented an appropriate behavior being possible to ensure a constant temperature of 37°C ± 0.5°C. The use of biocompatible materials make this pre-conditioning circuit suitable for biological and biomedical applications. As it has mentioned at the beginning of this section, this pre-conditioning circuit has not been finally included in the final system, because the fluid flow is too slow and it has been demonstrated that it can be heated in the LOP culture module. However, its development has led this thesis work to some important conclusions which have resulted very useful in the development of the LOP, such as the characterization of the heater or the software to monitor the temperature and control the heating.

The development of the previously described pre-conditioning circuit has led to a oral conference in the 2017 Spanish Conference on Electron Devices (CDE), and its publication in the proceeding with the same name published by IEEE.

4.5 Electronic circuit

In this section, the electronic circuit module, which is shown in the general scheme of the system in figure 4.2, is fully described. This electronic circuit has been designed as an interface between the MEA and the data acquisition devices (NI-DAQmx series, from National Instruments), which allow the connection and control with the Labview software.

The electronic circuit is composed of some conditioning circuits, in order to fulfill the main functions of the presented LOP, such as the temperature measurement or the heating control. Some components have been included to allow the connection of the electronic circuit with both the MEA and the data acquisition devices. In addition, some INA amplifiers have been included to acquire and amplify electrical signals obtained through the gold microelectrodes.

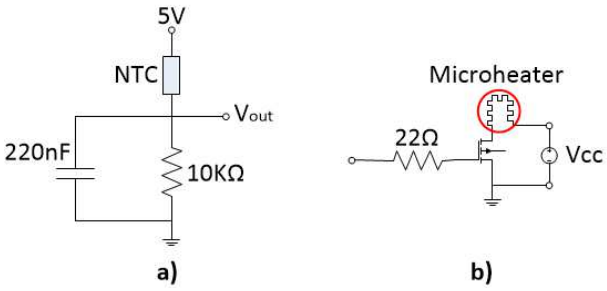

Figure 4.35 a) Voltage divider to measure temperature through a NTC thermistor; b) MOSFET transistor that allows or denies the pass of current to the microheater.

Thus, the conditioning circuits consist on a voltage divider to measure the temperature through a NTC thermistor, figure 4.35a, and a MOSFET transistor that works as a switch, allowing or denying the pass of current depending on the temperature, figure 4.35b. The microheater integrated in the MEA is fed with an external power supply of 5V/1A, while the INA is fed by the data acquisition device, which includes different supply ports of 5V and 2.5V. The temperature measurement through the voltage divider is characterized following the datasheet of the NTC thermistor chosen by translating the changes on the NTC resistor into voltage values, which are sent to the Labview software through the data acquisition device. Both conditioning circuits for temperature control and heating are the same than those developed and explained on section 4.4.

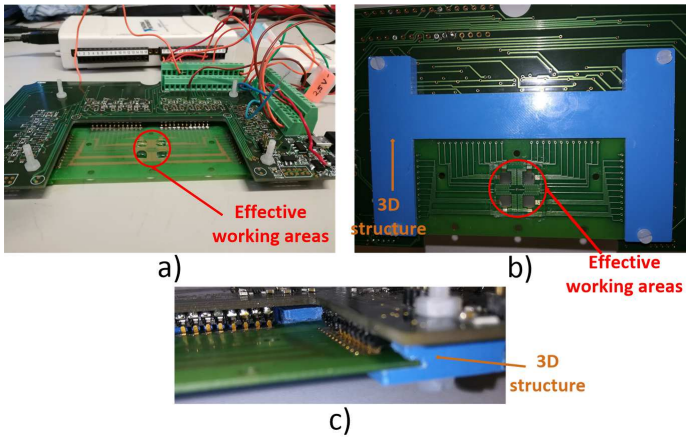

Figure 4.36 a) Complete setup of the MEA, the electronic circuit and the NI-DAQ devices; b) Bottom view of the electronic circuit and the MEA, with the 3D structure in blue color c) Contact between the MEA and the electronic circuit by using battery contact.

The electronic circuits are fabricated on a commercial printed circuit board of 1.6 mm of thickness of FR4 and 35 μm of thickness of copper. The complete setup of the MEA and electronic circuit is shown in figure 4.36a. The electrical connection between the MEA and the electronic circuit is possible thanks to a group of male 4 way battery contacts soldered to the electronic circuit and a plastic structure fabricated with a 3D printer, as can be seen in figures 4.36b and 4.36c.

A low power precision instrumentation amplifier (INA 333) has been used to amplify the signal acquired from the effective working area through the gold microelectrodes. This amplifier has a low consumption, with high precision and an adjustable gain. For a portable and autonomous system such as it is described in this thesis work, the INA 333 becomes one of the most interesting options. The use of an INA allows the easy modification of the amplification that could be needed depending on the application, simply varying the value

of R_{gain}. According to its datasheet, the INA's gain is shown in equation 4.1:

$$G = 1 + \frac{2R_1}{R_{gain}} \tag{4.1}$$

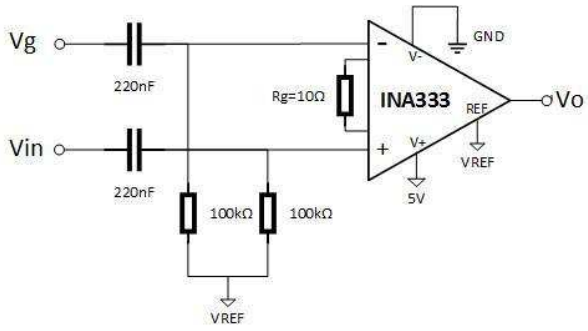

Figure 4.37 INA 333 conditioning circuit.

To obtain a clear and clean electrical signal with the INA amplifier, results indispensable to include a conditioning circuit to reduce the noise that could affect the electronic components, Fig. 4.37. The signal is captured through the gold wires and transmitted to the electronic circuit, where it is amplified by the INA, which is connected to the data acquisition device through which it is possible to plot the amplified signal or write the values in a text file. A differential measure is done between two gold microelectrodes from the effective working area, being one of them common to all the amplifiers of the same effective working area, which has been named in figure 4.37 as V_{in}. The voltage V_g comes from a different electrode in each amplifier. Two capacitors and two resistors filter the acquired signal, as a high pass filter. The symmetry of the conditioning circuit helps to avoid the noise in the loop. A decoupling capacitor between the power supply and the ground is included to reduce the electromagnetic interferences (EMI).

4.6 Monitoring software of the LOP

In this section, the program to monitor the functioning of the whole system is presented. Labview, from National Instruments, is the software used to control the whole system. This software offers a powerful tool with many applications, fitting perfectly with the purpose of this thesis work, which is the control and signal acquisition/stimulation of the system described all along this chapter. To connect the computer with the Labview program with the electronic circuits which monitor the system behavior, some external data acquisition

devices, developed for National Instruments, becomes indispensable. These NI-DAQmx series devices allow the generation of electrical signals, that could be used as a stimulus in each effective working area through the gold electrodes, as well as the acquisition of electrical signals, providing also power supply for low consumption components, such as the INA amplifier.

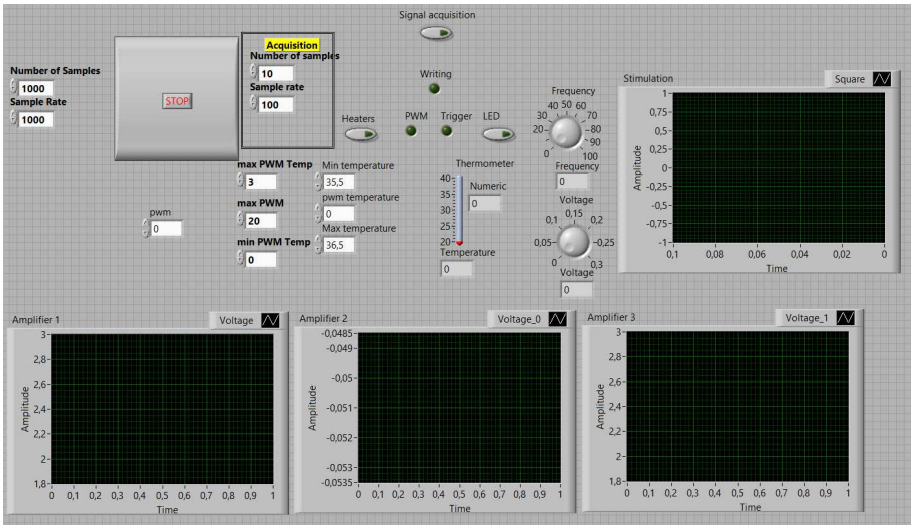

Figure 4.38 Front panel window of the Labview program.

In figure 4.38 all the elements that allow the complete control of the whole system are represented. In this panel, the user can monitor the functioning of the PWM, fixing the time during which the current is passing or not through the mosfet transistor toward the microheater, depending on the temperature measured with the NTC thermistor. The minimum and maximum temperature values between which the temperature of the LOP is going to range, can be also fixed in this front panel, being the current temperature of the LOP represented in the red bar. The heaters can be activated by pulsing a button, which will initiate the working of the PWM. Some LEDs are placed to indicate if the PWM is working or not, and if the current is passing through the mosfet transistor or not. Another button is included to acquire the signal and write the values in a text file, if necessary. The acquisition can be controlled by fixing the sample rate and the number of samples displays. There are two different dials to introduce the stimulation signal, one for the frequency (from 0 Hz to 100 Hz) and the other one for the voltage (from 0 V to 1 V). The graph next to these dials plots the signal which is introduced to the LOP through one of the microelectrodes. Finally, three different graphs plot the signal acquire from three different INA amplifiers, but we can add as many as amplifiers are included in the electronic circuit. The inlet of these graph corresponds to the outlet of those INAs connected through the NI-DAQ device.

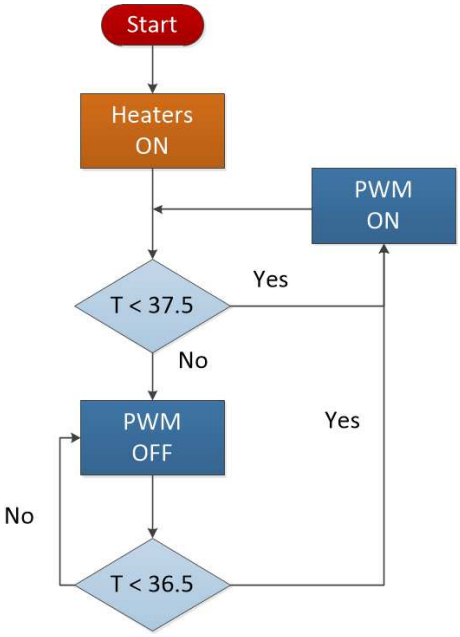

Figure 4.39 Flow chart of the PWM operation.

The flow chart of the PWM operation is shown in figure 4.39. The target temperature is 37°C ± 0.5°C. Once the heaters button is pressed, the PWM starts working. If temperature is under 37.5°C the Mosfet transistor allows the pass of current and increasing the temperature, while if temperature is over 37.5°C the Mosfet transistor denied the pass of current and decreasing the temperature. If temperature goes under 36.5°C, the Mosfet transistor allows again the pass of current and the PWM is working, increasing the temperature again. The temperature must be maintained between 36.5°C and 37.5°C.

4.7 Experimental results and discussion

In this section, the different experiments carried out to test each part of the system are presented, as well as the test which demonstrates the correct functioning of the whole system and the integration of each part between them. The integration results particularly important for this thesis work, due to there are different elements which are fabricated separately and then assembled between them. The experiments have been carried out as follow: firstly, the electrical characterization of the gold microelectrodes and the INA amplifier circuit are described; then, the biological experiments are fully explained, including some biocompatibility test to confirm the suitability of this system for culturing tissues and the electrostimulation experiment in which we have obtained successful results by providing neuroprotection to mice retinas with the retinitis pigmentosa disease.

4.7.1 Microelectrodes electrical characterization and temperature experiments

In this subsection, the electrical characterization of the gold microelectrodes embedded in PDMS is presented. Thus, the different experiments presented in this subsection are focused on characterizing not only the microelectrodes but also the INA 333 amplifier. The aim of these tests is the detection and subsequent amplification of electrical signals. The noise and the losses ratio during the acquisition of the electrical signals are the most recurrent problems to solve during these tests, mainly due to stimulation and detection through the gold microelectrode, which has a diameter of 25 μm. According to the equation 4.2, for a fixed value of R_1 of 50$K\Omega$, the gain of the INA only depends on the value of R_{gain}, which could be modified easily by changing the resistor. For the following experiments, the value of R_{gain} have been modified in order to obtain these gains: 3.13, 11, 101, and 213. Figure 4.40 shows a scheme to understand how the measurements have been obtained.

$$G = 1 + \frac{100K\Omega}{R_{gain}} \tag{4.2}$$

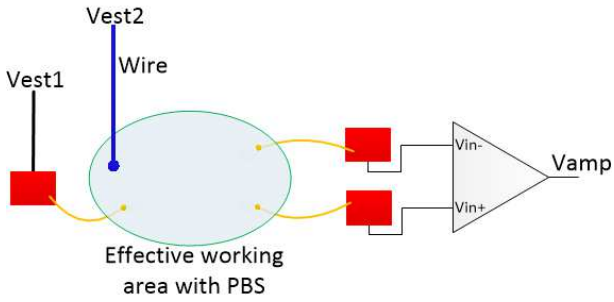

Figure 4.40 Brief scheme of the MEA, in order to understand how the detection of signals has been carried out.

The experiments performed with the MEA consist on introducing the electrical signal (V_{est}) through one of the gold microelectrode and detecting it through another gold microelectrode (V_{in}), which is connected to the inlet of the INA where it is amplified (V_{amp}) depending on the gain, as it is shown in figure 4.40. A Phosphate Buffered Saline (PBS) is the medium utilized to allow the transmission of the signal from the emitter to the receiver gold microelectrode. For this test, the introduced signal is a sine waveform. Once this signal is received by the gold microelectrode, it is passed through the conditioning circuit of the INA, where its peak-to-peak voltage is measured. The INA 333 is a low power amplifier, so it needs to be fed with 5V and the reference voltage must be 2.5 V, which is the same reference voltage of the effective working area where the signal is introduced. Both voltages are supplied through the 5 V power supply by the NI-DAQ device.

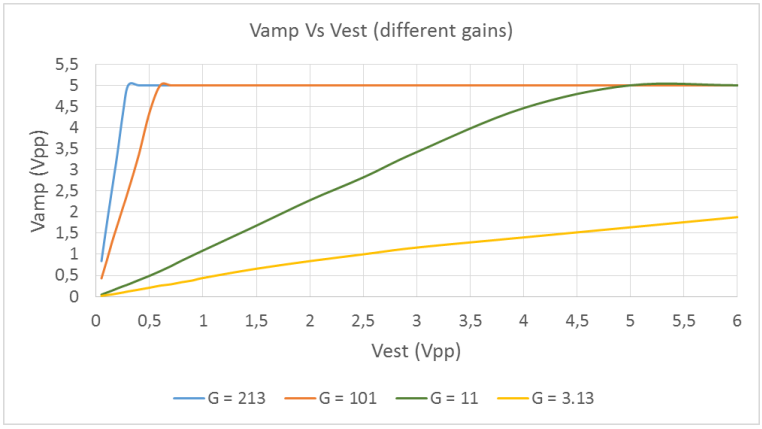

Figure 4.41 Characterization of the system depending on the amplifier gain.

The behavior of the INA for different gains and different voltages is shown in figure 4.41. As can be seen, for a higher gain the amplifier saturates earlier. Despite the saturation of the amplifier for low level signals when the gain is high, the wide range is useful for the lower gains. Figure 4.41 is useful as a characterization of the system behavior for an amplifier gain ranging between 3.13 and 213.

Figure 4.42 System losses ratio depending on the amplifier gain.

The losses ratio results of dividing V_{est} and V_{in}, and the results are shown in figure 4.42. To perform the characterization of the system losses ratio according to the gain, the peak-to-peak input voltage V_{in} that reaches the amplifier needs to be calculated by dividing the peak-to-peak amplified voltage (V_{amp}), measured in the INA output, and the gain of the amplifier. Once this voltage has been obtained, the losses ratio can be calculated, Fig.

4.42. Figure 4.42 exhibits the influence of the gain in the losses ratio. Therefore, it has been demonstrated that the higher the gain is, the higher the losses ratio is.

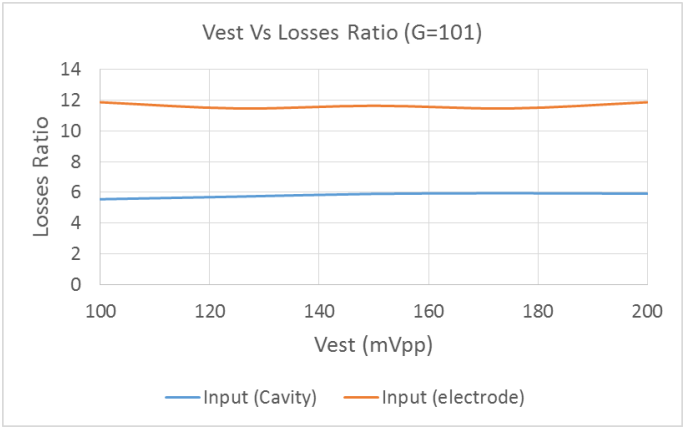

Figure 4.43 Relation of the losses ratio and the way the signal is introduced in the effective working area.

The electrical signals is introduced via a gold microelectrode (V_{est1} in figure 4.40) and transmitted through the PBS, which fills the effective working area, to another gold microelectrode which is connected to the INA. However, a hypothesis started to rise up in our mind: the losses ratio are mostly due to the gold microelectrodes and the influence on the losses of the PBS is negligible. For that reason, in order to demonstrate that the main losses are due to the gold microelectrodes, the signal is introduced in the PBS through a wire which is directly connected to the stimulus generator (V_{est2} in figure 4.40). Despite the introduction of the signal is different in this experiment, it is also transmitted through the PBS and detected by a gold microelectrode, and subsequently amplified. With this experiment we have demonstrated that the way the electrical signal is introduced affects the losses ratio. As it is shown in figure 4.43, when the signal is input through a gold microelectrode (the signal would pass through two gold microelectrodes), the losses ratio is approximately double in comparison with the one obtained when the signal is introduced directly through a wire connected to the waveform generator (the signal would pass through one gold microelectrode), which losses are almost negligible. This result confirms the initial hypothesis: the losses ratio is mostly due to the gold microelectrodes, and the medium or the electronic circuits barely have an influence on these signal losses.

Temperature measurement and heating control were explained on section 4.6, in which its good functioning was also demonstrated, as well as the user-friendly labview program to monitor these parameters. That program has also been implemented for the culture system, but adding some graph to plot both the introduced signal and the recorded one. Figure 4.44 shows the Labview interface used to monitor the system, in which the temperature is

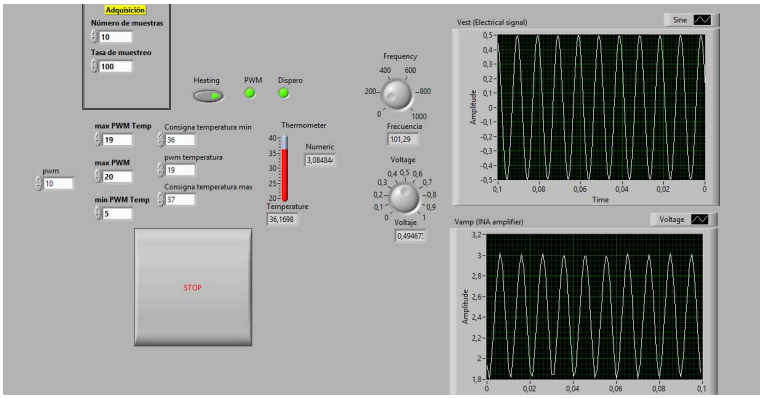

Figure 4.44 Labview interface to control both the temperature,and the heating velocity; and to perform the electrical stimulation and signal detection.

shown in the red bar, while the stimulation signal and the acquired signal are both plotted in different graphs. In this case, the gain of the INA amplifier is 11, and the signal is introduced and acquired through a gold microelectrodes, resulting in a losses ratio of about 10, which explains why the acquired signal is similar to the introduced signal.

4.7.2 Biological experiments

In this section, an organotypic culture has been carried out inside the culture LOP presented in this thesis work as one of the possible applications of this system in the biological and biomedical fields. The organotypic culture developes inside the presented LOP is a mice retinas culture with different types of mice, including those with the retinitis pigmentosa disease. These experiments have been carried out together with a biological research group of the Andalusian Molecular Biology and Regenerative Medicine Centre (CABIMER), in which the PhD Berta de la Cerda has been our connecting link with the "biological world". The final goal of these experiments is to demonstrate how the electrostimulation of mice retinas with the retinitis pigmentosa disease can provide a neuroprotection on the mice retinas, being possible a slowdown of the degeneration of the mice retina.

Thus, in the following paragraphs, a detailed explanation about the materials and methods used to perform the biological experiments is included. Moreover, the biocompatibility tests of the LOP are fully described in order to demonstrate that this system is suitable for its use for biological applications. Finally, electrical stimulus are applied to the biological samples, obtaining a neuroprotection of the mice retinas with the retinitis pigmentosa disease, which are the confirmation of the utility of the presented LOP for developing organotypic cultures of mice retinas.

Materials and methods

In this subsection, the materials and methods established to perform the biological experiments are detailed. As it has been previously mentioned, we have had the immeasurable help of the biological research group from CABIMER to perform all these experiments. They have provided us with biological samples (mice retinas), which were extracted from the mice in their facilities, and subsequently cultured in our LOP. Once the culture was finished, the extraction and histological studies of the mice retinas were also carried out in the CABIMER facilities, which was mostly done by the PhD Berta de la Cerda, to whom I cannot be grateful enough.

Hence, the different processes needed to correctly develop the mice retina culture inside of the presented LOP are outlined below. That includes not only the biological preparation of the culture, that is the dissection, insertion and extraction of the mice retinas, but also the complete setup of the system, which implies the external tubes and pumps, the electrostimulation, the histological studies or the tunnel staining to confirm the results obtained.

Fluidic connections and culture medium feeding

A combination of male Luer to 10-23 threads screwed inside the PMMA and female Luer to 1/16" ID tubing (45505-84 and 45508-01 respectively, Cole-Parmer Instrument) have been used, assuring the proper connection with the culture device. Tubing is Tygon 2375, with an internal diameter of 1.6 mm (RS). The media reservoir used is a sterilized 60 mL syringe, in which the total volume of media needed for the whole culture experiment is stored. If the media contains any photosensitive substance, the syringe and tubing are completely covered in black insulating. A 0.22 μm-pass filter (Millex-FG, Merck Millipore) is inserted between the tube and the syringe to keep the sterility of the culture medium. A syringe pump (New Era Pump Systems, Inc.) is the impulsion method used for the continuous media flow.

Biological material

Four biocompatibility tests were performed with adult WT C57BL/6J mice and models of degenerating retina such as albino CD1 and the retinitis pigmentosa models *Pde6b*^{rd10} (rd10) and *Pde6b*^{rd1} (rd1). One retina of each type was used for each test, with a total of 16 animals used and 16 retinas analyzed. Four electrostimulation assays were performed with 7 day-old WT and rd1 mice. In each experiment two retinas of each type were used, with a total of 8 animals used and 16 retinas analyzed. Two electrostimulation experiments were also performed with 14 day-old WT and rd10 mice providing similar results to the rd1, using 8 retinas from 4 animals. The complete set of experiments used 40 retinas from 28 animals. All mice were provided by Jackson Laboratory, and were maintained in-house in cyclic 12:12 hour light cycles in a pathogen-free animal facility and sacrificed using CO_2 inhalation. All experimental procedures have been previously approved by the local

"Animal Care and Use" ethical committee.

Explant culture

Aseptic technique has been used to dissect the neuroretinas. Once the eyes are enucleated, the procedure is performed in a sterile cell culture hood. Regular retinal dissection is performed. Eyes are rinsed in 1 % penicillin-streptomycin before dissection. Anterior segment is removed and neuro-retinas peeled from retinal pigmented epithelium. Deposition for culture in the wells of the device in their final position is helped with the support of a PVDF membrane (Amersham Hybond-P, GE Healthcare) as scaffold and explants are covered with 0.4 μM Millicell membrane (Millipore) with the ganglion cell layer downwards for electrostimulation. The culture medium used is Neurobasal A supplemented with 2 % B27, 1 % N2, 1 % penicillin-streptomycin solution and 0.4 % glutamax (all media components from Gibco). The transparency of the device allows the visualization of the cell viability using FITC-conjugated Cholera toxin subunit B (FITC-CTB; C-1655, Sigma-Aldrich) used according to the manufacturer's instructions.

Electrostimulation

The starting model for the retinal stimulation in humans is the Argus II retinal prosthesis [273]. The impedance of the electrodes has been calculated, the current values has been converted to voltage values and the pattern of the stimulation frequency has been adapted from the bibliography [269]. The electrical stimulation consists on a biphasic square signal of 0.5 V_{pp}, with a frequency ranging between 10 Hz and 40 Hz. Work from Zrenner lab [274] reports stimulation for 30 minutes one day per week during a total of six weeks, directly in patients with RP. According to these calculations, the retinal explant culture for seven days gives an estimation of 3 stimulation periods of 5 minutes distributed along the week of culture. Thus, the electrical stimulation has been applied in 3 alternative days, starting the second day of culture, a total of 5 times per day, 1 minute per cycle. Between every repetition, the stimulation frequency is changed in order to achieve different response thresholds, as it is shown in table 4.1. The voltage is fixed to 0.5 V_{pp}, and the output current to 2 mA, due to the specifications of the NI DAQ 6211 used to control the system and stimulate the culture.

Table 4.1 Electrical stimulation of the culture.

Repetition	Frequency (Hz)	Voltage (V_{pp})
1	30	0.5
2	15	0.5
3	20	0.5
4	40	0.5
5	10	0.5

Histological studies

After the finalization of the culture, tissues are fixed in paraformaldehyde, washed in phosphate buffered saline (PBS), embedded in 4 % agarose and cryopreserved by sequentially equilibrating in a solution with increasing sucrose concentration [275]. Blocks for cryostat sectioning are prepared in molds with OCT (Tissue Tech) and 18 μm sections are used for subsequent staining with hematoxylin-eosin or specific antibodies. In both cases, standard staining and immunostaining protocols have been used. For immunofluorescent staining, anti-opsin (AB 5407 Millipore) and anti-rhodopsin (ab190307 Abcam) have been used as primary antibodies; anti-rabbit (emission 488 nm, A-21206 Life technologies) and anti-mouse (emission 633 nm, A-21052 Life technologies) have been used as secondary antibodies, and DAPI for nuclei staining.

TUNEL staining

Retinal sections obtained from electrostimulated and non-electrostimulated explants are subjected to TUNEL staining following manufacturer's instructions (In Situ Cell Death Detection kit, Fluorescein; Roche). As a positive control of cell death, DNase I treatment is provided to a WT retinal section. DAPI has been used for nuclei staining.

Imaging and image treatment

Optic microscopy is used for the imaging of hematoxylin-eosin stained sections using a Leica DM 2500 apparatus with 10x magnification. Microscopy in a confocal Leica TCS SP5 apparatus is used for the imaging of immunostained and TUNEL-stained sections with 40x magnification. ImageJ (FIJI version) software is used for the image treatment and for the calculation of signal intensities. For the counting of nuclei per layer, 12 rows of nuclei are counted in five consecutive sections for each of the retinal layers. For the calculation of TUNEL vs. DAPI fluorescence ratio, intensities from 10 sections are measured for each condition. Mean and standard deviation are calculated and represented using Excel.

Biocompatibility tests

Once the materials and methods for performing the biological experiment are set, the next step consists on testing the biocompatibility of the developed LOP to demonstrate its suitability for organotypic cultures. As it has been previously explained in sections 4.3.1 and 4.3.2, all the materials which are directly in contact with the biological samples are biocompatible.

Therefore, after the fabrication of the LOP, the following experiments consist on demonstrating the surveillance of retinal explants inside the presented LOP, as well as the conditions of tissue placement and organotypic culture. The biological material used to test the culture conditions has been WT mice retinas. The placement of the retinal explants is more important than it could seem, because the ganglion cell layer has to be deposited facing the PDMS substrate with the gold microelectrodes, to assure a good reception of the electrical stimuli. The specific deposition method used is described in [276]. Controlled

levels of O_2, CO_2 and a balanced pH are indispensable to keep the culture alive. For that reason, nutrients are supplied by a continuous flow of culture media (Neurobasal-A, Gibco) [277, 246, 272], being the flow rate one of the most critical parameter of this experiment. Hence, the initial flow of culture media has been decided according to data from the bibliography [278, 279], which means a constant flow of 3.6 μL/min for the correct maintenance of four retinal explants in our device. Figure 4.45 shows the whole setup needed to perform an experiment with our culture system. As can be seen, the LOP is placed on an inverted microscope, through which it is possible to control the culture with death-live markers.

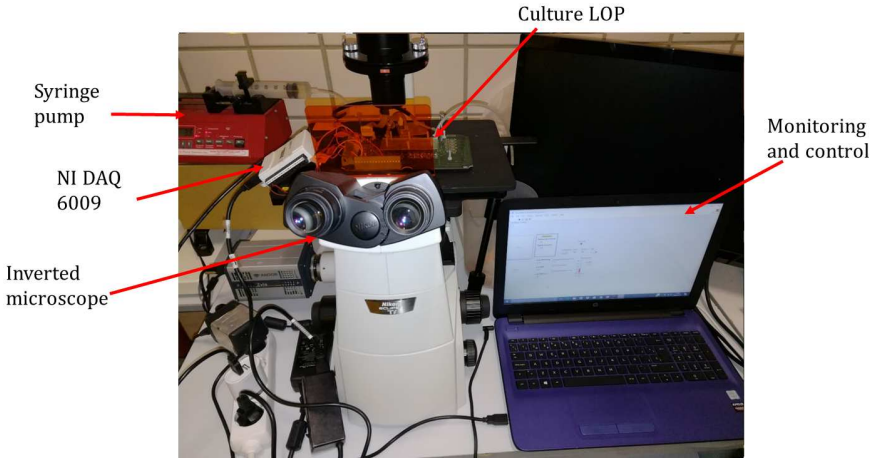

Figure 4.45 Experimental setup in the microsystem group laboratory.

The use of PDMS to fabricate the plug and to embedded the gold microelectrodes of the effective working areas allows the monitoring of the biological material along the 7-day explant culture by using a microscopy and live-fluorescence staining. FITC-conjugated cholera toxin subunit B (CTB) provides specific staining of ganglion cells due to its affinity for the ganglioside GM1. Fluorescence emission requires active transport of the product inside the cell [246], thus labeling only living cells. In this setting, the fluorophore is added to the culture medium every two days, because fluorescence peaks after 24 hours of incubation and decays after 48 h. The viability of CTB as a live-cell marker has been validated by damaging the cells with temperature or with different concentrations of hydrogen peroxide and we have found a good correlation between CTB fluorescence and live-dead status of the retinal tissue (Fig.4.46).

Once the suitability for culturing retinal explants inside the presented LOP is demonstrated and the culture conditions are set, several biocompatibility tests have been performed, maintaining the retinal explants for seven days inside the LOP without electrical stimulation. As source of biological material, WT mice and animal models of degenerating retina

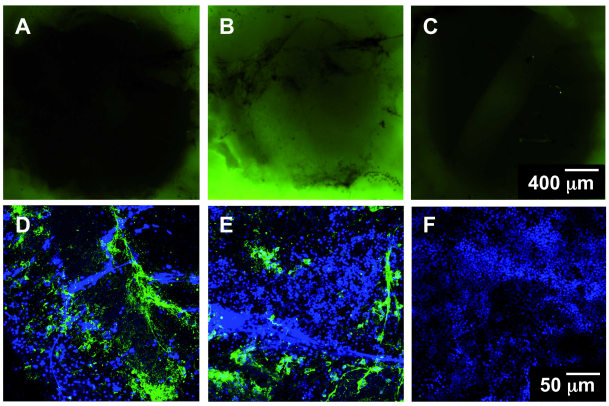

Figure 4.46 Viability of CTB as a marker of living ganglion cells in the device. Upper row: Direct microscopy visualization of CTB staining of retinal explants in the LOP system; (A) Retinal explant without CTB; (B) Retinal explant after 24h of CTB incubation in the culture medium; (C) Retinal explant with added CTB and cell death induced by heating of the sample. Bottom row: Confocal microscopy images of ganglion cell fibers stained with CTB (in green) and DAPI for nuclear staining (in blue). CTB signal depends on live-dead status of cells: (D) Healthy tissue; (E) Tissue treated with 600 μM H_2O_2 for 15 min inducing mild cellular damage; (F) Tissue treated with 600 mM H_2O_2 for 15 min inducing complete cell death.

such as albino CD1, and the RP models rd10 and rd1, have been used.

Figure 4.47 shows a foreground picture of the LOP after culturing retinal explants from different type of mice. In each effective working area is placed a mouse retina and the tubes and luer fittings are connected to the external pump in the inlet port and to the waste in the outlet port. This setup corresponds to the data shown in figure 4.48.

Results of the biocompatibility test for WT and CD1 retinas are shown in figure 4.48. After seven days of organotypic culture, retinas are taken off the device, fixed and prepared for histological analysis, making sections and immunostaining. The results confirms that after one week both WT and CD1 retinas maintain their respective natural structure in layers. Like in the human tissue, mouse retina is a tightly structured tissue in which any distortion of the cell layers can be related to disease. From the outer to the inner side of a retinal section, a structure conformed by cell layers can be found; first, the outer nuclear layer (ONL) constituted by photoreceptors (rods and cones), which sense the light and transmit the neural signal to the processing neurons in the second layer, formed by bipolar, amacrine and horizontal cells, named altogether as inner nuclear layer (INL). The last layer is the ganglion cell layer (GCL), whose axons transport the visual information to the brain. Figure 4.48A and figure 4.48E, DAPI staining of nuclei shows from top to bottom the integrity of the three retinal layers. To further visualize tissue preservation, the

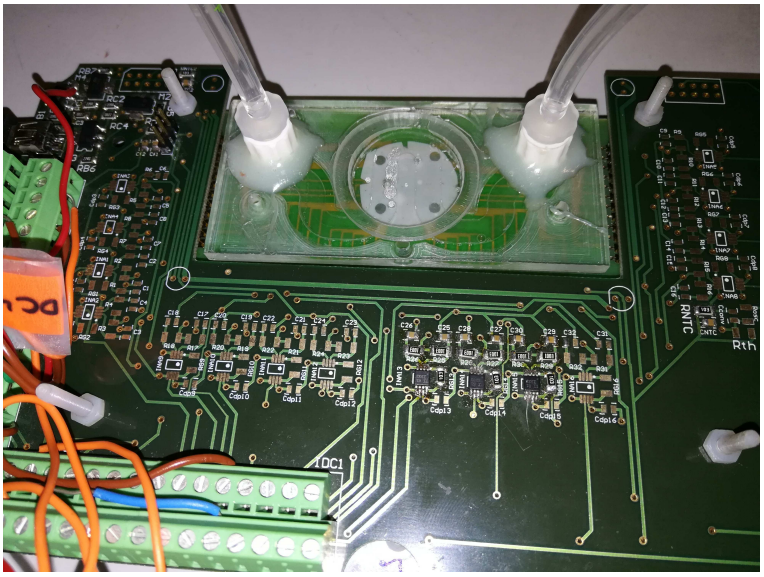

Figure 4.47 Foreground picture of the LOP with the retinal explants cultured inside.

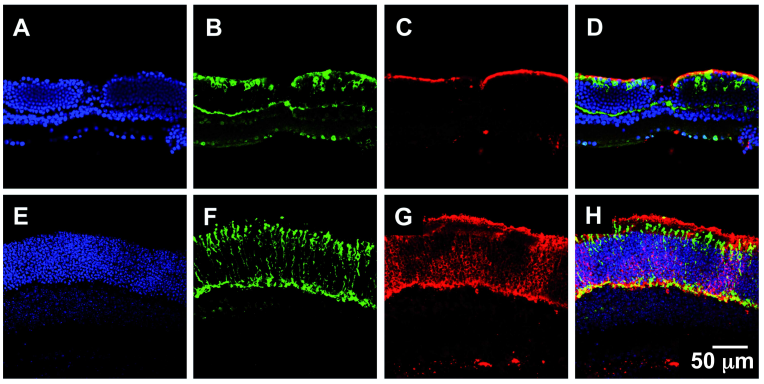

Figure 4.48 Biocompaibility of the autonomous device with retinal explant culture from different mouse models. (A-D) Upper row shows pigmented-mouse WT retina sections depicting normal morphology and photoreceptor immunostaining; (E-H) bottom row corresponds to albino CD1 retina showing abnormal localization of rhodopsin and opsin. (A, E) DAPI staining for nuclei in blue; (B, F) immunostaining for opsin (cones) in green; (C, G) immunostaining for rhodopsin (rods) in red; (D, H) composite images.

immunostaining of sections has been performed with specific antibodies for cones (opsin, in green, in figure 4.48B and figure 4.48F) and for rods (rhodopsin, in red, in figure 4.48C and figure 4.48G) to verify the correct localization of photoreceptor pigments in the retina.

Visual pigments of rods and cones in the healthy retina are located in the outer segments of the photoreceptor cells, on top of the ONL (figure 4.48B-D) as can be seen for WT retinas. Localization of the pigment signals in the bodies of the photoreceptor layer is shown for CD1 retina (figure 4.48F-H) compatible with the mild degenerative state naturally found in the albino retina. These results suggest that culturing retinal explant in the proposed LOP keeps the natural features of the retinal tissue for at least one week, both for healthy and dystrophic retinas, demonstrating its biocompatibility and suitability not only for healthy retinas but also for ill ones.

Electrostimulation of retinal cultures

During the experiments, it has been possible to follow up the health of the retinal explants thanks to the CTB live-staining. The culture lasts for 7 days. After that time, tissue is collected from the culture system, prepared for histological examination, sectioned and stained using different approaches to check for the preservation of the retinal structure, as well as the correct localization of photoreceptor markers and the quantification of cell death. For each case, all these parameters have been compared between treated and non-treated rd1 retinas, while a healthy WT retina has been used as control for normal tissue. The results presented are representative of four independent experimental replicates.

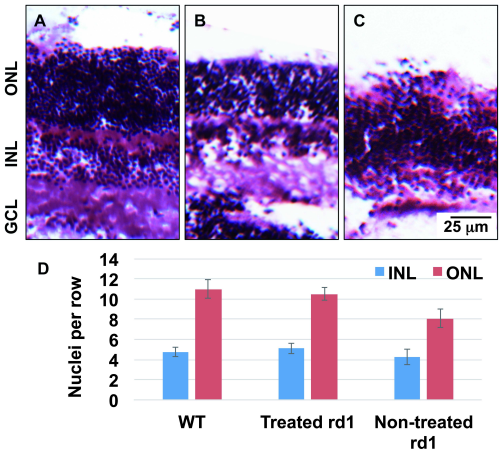

Figure 4.49 Effect of electrostimulation in the tissue histology. Eosin-hematoxylin staining of retinal explant sections. (A) WT control; (B) Rd1 treated with electrostimulation; (C) Rd1 non-treated control; (D) Quantification of nuclei per row in the ONL and INL of (A), (B) and (C) experimental conditions. ONL: Outer nuclear layer; INL: Inner nuclear layer; GCL: Ganglion cell layer.

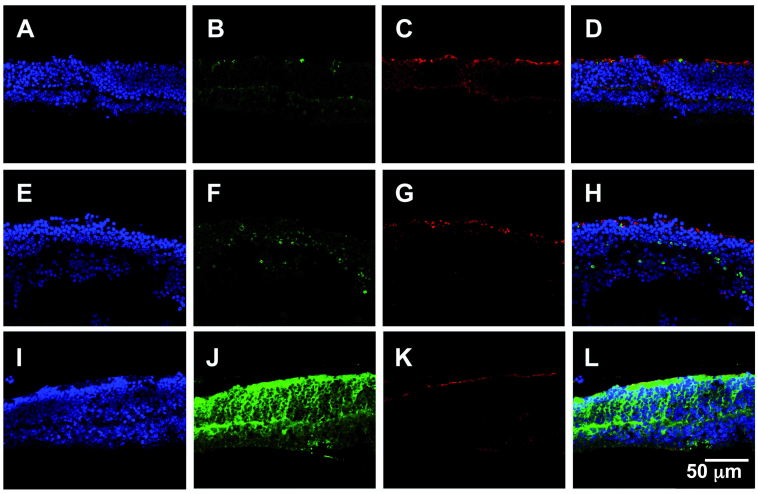

Figure 4.50 Effect of electrostimulation in the disorganization of photoreceptor cells in the retinal explants. (A-D) Upper row is WT retina; (E-H) middle row is rd1 electrostimulated retina; (I-L) lower row is rd1 non-treated retina. (A, E, I) DAPI staining for nuclei in blue; (B, F, J) immunostaining for opsin (cones) in green; (C, G, K) immunostaining for rhodopsin (rods) in red; (D, H, L) composite images.

Firstly, the histological structure of the retinal layers is checked using the classic eosin-hematoxylin staining, which stains all cells and nuclei. In figure 4.49, it can be seen that retinal structure is completely distorted in the untreated rd1 sample (figure 4.49C) compared to the healthy control (figure 4.49A), cultured simultaneously in an adjacent well of the device. The electrostimulated rd1 retinal explant presents an intermediate state, with mild degenerative changes only in the ONL. Rd1 degeneration is specific for photoreceptors, so it is expected to see changes mainly in the ONL. A typical measurement for retinal degeneration is the quantification of the number of nuclei per row in the retinal layers. We have calculated the mean number of nuclei from 12 rows per layer, counted in five different retinal sections for each experimental condition, and we have observed that the electrostimulation in the device protects the ONL of the rd1 treated retina from loosing cells, as the number of nuclei in this layer is not significantly different from healthy control, while there is a notable difference with the untreated rd1 retina (figure 4.49D).

Secondly, retinal sections have been used to localize the visual pigments of rods and cones. Delocalization of these pigments is one of the hallmarks of retinal degeneration indicating cell dysfunction preceding cell death.

In the presented experimental results, retinas are dissected the day before the degenerative process starts, and are cultured for 7 days inside the LOP. After one week of culturing, the disease progress is compared in treated and non-treated rd1 retinas, using a healthy WT

retina as a negative control. Figure 4.50 shows the confocal microscopy images of retinal sections stained for nuclei and immunostained for opsin and rhodopsin. These images are organized in three rows, from top to bottom: WT (figures 4.50A-D), treated rd1 (figures 4.50E-H) and non-treated rd1 (figures 4.50I-L). Last picture of each row is a composite image. The main differences between the treated and untreated retinal explants can be seen in the opsin staining pattern, which shows a slight delocalization in figure 4.50F, corresponding to a treated rd1 retina, compared to WT (figure 4.50B), but the staining pattern is really distorted in the amount of labeling and the localization of the signal in figure 4.50J, corresponding to a non-treated rd1 retina. For rhodopsin, a signal decreasing can also be seen, as expected, in the non-treated rd1 retina (figure 4.50K), while the treated rd1 retina (figure 4.50G) shows the same staining and localization pattern as in WT control (figure 4.50C). In summary, composite images (figures 4.50D, H, L) depict a normal immunostaining for visual pigments in both WT and treated-rd1 retinas cultured for one week inside the presented LOP, while a dystrophic staining pattern and morphology is shown for the non-treated rd1 retina cultured in the same conditions, as expected for a diseased and degenerating tissue.

Regarding the results previously presented, it is demonstrated how the electrical stimulation has an influence on the rd1 RP model retina cultured inside the autonomous LOP, providing a protective effect from the delocalization of visual pigments that occurs during the natural degenerative course of the RP disease.

In order to endorse the successful results presented and to gain some insight on the biological effect of the electrical stimuli provided to the retinas cultured in this device, a TUNEL staining has been carried out for the visualization and quantification of apoptosis (programmed cell death) at the single cell level [280, 281]. The experiment has been performed to sections of rd1 retinal tissue subjected or not to electrical stimulation along the organotypic explant culture. WT retina is used as a negative control and a retinal explant with DNA damage pre-treatment before staining as a positive control. In figure 4.51 data is presented in columns in which, from left to right it is shown: firstly, the DAPI staining of cell nuclei; in the middle, the FITC labeling of DNA strand breaks due to TUNEL reaction and, at the right, a composite image to visualize co-localization, marking individual apoptotic cells. WT negative control (figures 4.51A-C) depicts absence of cell death, showing just background fluorescence (figure 4.51B). Figures 4.51D-F displays the positive control, with a clear co-localization of FITC with the cell nuclei. Figures 4.51G-I corresponds to rd1 retina treated with electrostimulation, in which only a few disperse nuclei show some apoptotic-related fluorescence compared to images of the non-treated rd1 retina in figures 4.51J-L which exhibit the natural course of retinal degeneration with a very high intensity of fluorescence in figure 4.51K and the co-localization of apoptotic signal with nuclei in figure 4.51L.

The quantification of relative fluorescence is shown in figure 4.51M, presenting similar values for the positive control (WT with induced DNA damage) and for non-treated rd1 retina. Both WT control and electrostimulated rd1 retina present a very low level of relative intensity, indicating that the number of cells undergoing programmed cell death in treated

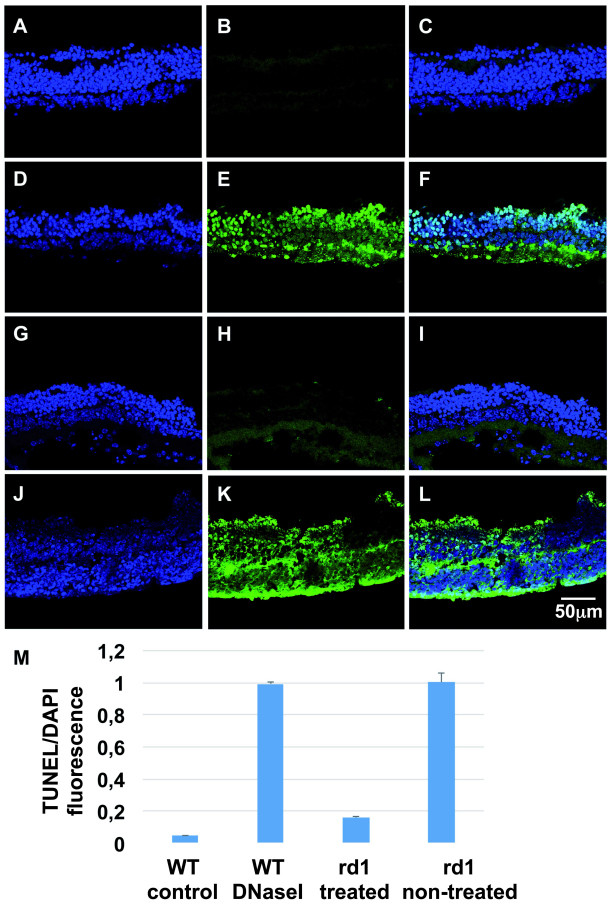

Figure 4.51 Effect of electrostimulation in programmed cell death. (A-C) Upper row is WT sample used as negative control; (D-F) second row is WT sample with induced DNA damage used as positive control for TUNEL labeling; (G-I) third row is rd1 retina treated with electrostimulation; (J-L) lower row is non-treated rd1. For all the samples: left column is nuclear DAPI staining; central column is TUNEL fluorescence reflecting DNA damage associated to cell death; and composite images are shown at the right column. (M) Quantification of mean intensity for TUNEL fluorescence relative to DAPI staining.

rd1 retinas is similar to the healthy control.

In the light of the results presented in this section, it is possible to concluded that the stimuli provided to the retinal explants in the autonomous device has protected the photoreceptors from their normal course of apoptotic cell death in an organotypic model of RP, demonstrating the suitability of the proposed LOP not only for organotypic cultures,

but also for electrostimulating the biological samples.

4.8 Conclusions of the LOP for retinal explant culture

In this chapter, an autonomous LOP for organotypic cultures and electrostimulation is presented. In addition, the electrical characterization of a MEA on PCB with gold microelectrodes embedded in PDMS is described. The main goals to achieve during this part of the thesis work was to obtain a biocompatible, cost effective, reliable and autonomous system. Regarding those conditions, the proposed LOP has been designed, fabricated and characterized to fulfill all the objectives fixed at the beginning of this PhD.

The characterization of the electrical behavior of the gold microelectrodes has been carried out with good results. Moreover, the temperature and heating control to recreate the microenvironment needed to perform a culture inside the presented LOP has been also demonstrated, including the program to monitor its operation.

The biocompatibility and suitability of this system to function as an autonomous tissue culture setting for retinal explants independent of standard CO_2 incubator has been succesfully demonstrated, being possible to carried out retinal cultures during, at least, 7 days inside the proposed LOP.

In addition, After many experiments, we have observed that retinas provided with periodic electrical stimuli along the whole-tissue culture in the proposed LOP display a better preservation of the tissue structural features and lesser apoptotic cell death in the photoreceptor cell layer compared with non-treated RP retinal explants.

The results presented in this chapter has given rise to two publication in a high impact factor journal, Sensors and Actuators B: Chemical [174, 265], as well as another publication in the Spanish Conference on Electron Devices (CDE) [282].

Cabello, M., Aracil, C., Perdigones, F., Mozo, M., de la Cerda, B., & Quero, J. M. (2018). Gold microelectrodes array embedded in PDMS for electrical stimulation and signal detection. Sensors and Actuators B: Chemical, 257, 954-962.

Cabello, M., Mozo, M., De la Cerda, B., Aracil, C., Diaz-Corrales, F. J., Perdigones, F., ... & Quero, J. M. (2019). Electrostimulation in an autonomous culture lab-on-chip provides neuroprotection of a retinal explant from a retinitis pigmentosa mouse-model. Sensors and Actuators B: Chemical, 288, 337-346.

Cabello, M., Aracil, C., Perdigones, F., & Quero, J. M. (2017, February). Conditioning lab on PCB to control temperature and mix fluids at the microscale for biomedical applications. In 2017 Spanish Conference on Electron Devices (CDE) (pp. 1-4). IEEE.

5 Cell culture and electrical recordings application

After the development of the LOP and its evaluation for a particular application, in this case the culture and electrostimulation of RP mice retinal explants, the next step of this thesis is focused on improving the MEA device and including cell culture applications. In this respect, all along this chapter, new approaches and experiments with MEAs and cell culture are outlined below.

The first part of this chapter includes the work carried out by the PhD student during his stay in the University of Bath. The aim of this collaboration was to continue the development of MEA devices for culturing applications, particularly the fabrication of microelectrode arrays for cell culture and electrical signal acquisition. PhD Paulo Rocha, as a member of the Centre for Biosensors, Bioelectronics and Biodevices (C3Bio) of the Department of Electronic and Electrical Engineering of University of Bath, has been the responsible on charge of the research work described on this chapter. Dr. Rocha has a wide experience in the development of MEAs for signal acquisition of cell populations, with some publications in high impact factor journal [262, 283, 284, 285]. Despite the previous research of Dr. Rocha was focused mostly on glioma cell populations and their electrical activity, the cells cultured and electrically characterized in the experiments outlined below are prostate cancer cells (PC-3). Moreover, after the good results obtained during the stay, the research work has been continued in the University of Seville with the fabrication and testing MEAs on PCB, glass and plastic for performing cell cultures.

Thus, in the following sections the experiments with PC-3 cells carried out in the University of Bath, as well as the continuation of this type of cultures in the University of Seville, are fully described. In section 5.1 results are conclusive and successful, while section 5.2 is more focused on the design and fabrication of MEA devices for its used in cell culture applications.

This collaboration has produced successful results which has led to several publications in both conference and high impact factor journal.

5.1 Prostate cancer cells (PC-3): culture and extracellular electrophysiology

Prostate cancer is one of the most common malignancy cancer diagnosed in men [286], especially in Western countries [287, 288]. This cancer develops when prostate cells grows and spreads out of control. Early prevention of cancer becomes indispensable to improve the analysis of this disease. In that sense, studying the electrical behavior of the prostate cancer cells and how it is related to its proliferation and growth could be a good approach to find better and more efficient treatments. However, electrophysiology researches of the prostate cancer cells are still in a very early stage and its understanding is, to say the least, improvable. If electrical patterns of this type of cells can be found, as well as a electrical relation between proliferation or metastasis and cell growth, this would be really useful for drug delivery of for exploring new treatments for prostate cancer.

Similarly as it has been explained in chapter 4 for study the mice retinal explants, *in vitro* cultures are one of the most widely used techniques to study cell growth and proliferation. In the case of prostate cancer cells, it can be found in bibliography some successful *in vitro* models [289]. There are three main types of cancer cell lines which are most commonly use for *in vitro* cultures: LNCaP, DU-145 and PC-3 [290, 291], being this last type of prostate cancer cell line the one used for this research work. Among the different characteristics of PC-3 cells, its reliability for growth rate and its behavior as a xenograph [292], as well as the fact that they maintain its genotype and phenotype when injected into mice [293, 294], result particularly interesting. Moreover, PC-3 cell lines are hormone insensitive and exhibit no AR or PSA mRNA/protein. As a highly aneuploid line, its proliferation duplicates after approximately 33 hours and leads to high levels of oxidative stress [295], being the oxidative stress close related to the ionic channels of calcium (Ca^{2+}). Another parameter that could give relevant information is the PH sensitivity, being insignificant in malignant cells in comparison with non-malignant cells. thus, PH sensitivity is used for developing novel anticancer drugs [296]. However, the expensive Ca^{2+} dyes toxicity and the incapability to carried out long term Ca^{2+} imaging, make the cited method unfeasible.

Regarding the ionic channels, they can be defined as follow: "Ionic channels are gated aqueous pores whose conformational changes are driven by the electric field in the membrane"[297]. Thus, ionic channels are proteins which control the pass of ions through the cell membrane, being the primary ion channels: K^+ N^+, Cl^- and Ca^{2+}. Moreover, fluctuations of the membrane potential, which are caused by those ion channels, have a key effect on cells of the nervous system. Different diseases on humans are demonstrated to be related with gradients in ion channels, such as: cardiac arrhythmias [298], brain illnesses

[299] or the development of cancer [300, 301, 302].

This relation between ion channels and cancer is specially interesting for the presented PhD work, particularly with the prostate cancer. In this respect, several imaging and single cell studies focused on the connection between the K^+ N^+ and Ca^{2+} channels and the prostate cancer basal activity and proliferation have provided some promising results [303, 304]. Nevertheless, a common agreement can be found in most of the research works found in literature about the influence that Ca^{2+} channel has during prostate cancer proliferation. For instance, different investigation have demonstrated a relation between the prostate cancer cells proliferation and the Ca^{2+} permeable channel TRPM8 [305, 306]. In addition, other research works have found a relation between the PC-3 cells proliferation and the Ca^{2+} permeable channel TRPC6 [307] and other oxidative stress [308].

Electrical fluctuations on cell membranes can be acquired thanks to these ions passing through those membranes [309]. Dr. Rocha et al. have already measured those fluctuations in glia cells, giving rise to several publications [262, 283, 284, 285]. In the light of this successful results, our hypothesis is based on the possibility of monitoring the electrical activity of prostate cancer cells, not using invasive and toxic methods, which normally results expensive and complicated, such as fluorescence, but by acquiring their electrical activity with a low cost, ultra-sensitive electrical recording setup to measure a whole population of non-neuronal cells.

As it has been explained in chapter 3, MEA devices are normally used for acquiring or emitting electrical signal. In our case, the electrical activity of a population of PC-3 cells is recorded through one of these MEAs. For this kind of applications, minimizing the impedance and maximizing the capacitance of the electrodes become priority goals in the fabrication process. These two parameters directly influence in the signal to noise ratio, being desirable values as high as possible. Focusing our attention in the impedance, to achieve a low value is particularly challenging when the electrodes are fabricated on the microscale. In this respect, one of the approaches consists on modifying the electrodes to increase the effective surface area by using porous conducting materials such as gold nanostructures, Pt black or carbon nanotubes, or increasing the electrode area. With these methods, the modification of the surface implies a decreasing of the impedance, resulting in an improvement of the electrical acquisition. In our case, the MEA that has been used for our experiment is fabricated with large areas electrodes of about mm^2, obtaining a very low noise level of 0.3 μV_{pp} [262]. This low noise system makes possible the recording of membrane capacitive current oscillations across large population of cells. This system has been successfully tested with C6 glioma cells [284].

Thus, what it is described in this section is the electrically characterization of prostate cancer cell model PC-3. The electrical activity is measured by using the previously mentioned electrophysiological recording system. The experiments carried out consist on recording the electrical activity of large populations of PC-3 cells over time. The obtained results show that this type of cells present two recurrent behaviors. The first one is close related to the basal activity and it is expressed as asynchronous and sporadic electrical

spikes. The second behavior is a collaborative event which is manifested as quasi-periodic electrical spikes. As it has been explained before, the influence of the Ca^{2+} channel on prostate cancer has been proved in many researches. Thus, we have used specific inhibitors of the Ca^{2+} channel to demonstrate that the quasi-periodic spike pattern is related to Ca^{2+} ions passing through a large populations of cells. The obtained results encourage to continue this research work by using the presented electrical recording system for *in vitro* PC-3 cells cultures or other cancer cells, and its subsequent application on *in vivo* experiments.

5.1.1 Materials and methods

In this subsection, the materials and methods established to perform the experiments are detailed. As it happened with the mice retinas experiments explained in chapter 4, these tests have been developed in a multidisciplinary environment, working together with specialist biologist in cell culture. Thus, the biological material has been provided by Sofia I. Pascu and Haobo Ge of the department of Chemistry of the University of Bath. The experiments with the electrical recording system have been carried out in the laboratory of department of Electronic and Electrical Engineering of the University of Bath by myself, with the supervision of Dr. Rocha. Therefore, in this subsection are included: the general cellular culturing method for PC-3 cells; the standard cellular viability assays of PC-3 cells in water; and finally, a short explanation of the MEA chip fabrication and the experimental details of the test performed with the PC-3 cells cultured in the MEA.

General cellular culturing method

PC-3 cells were cultured using standard methodologies, at 37 °C in a humidified atmosphere in air and harvested once a confluence of over 70 % had been reached. PC-3 cells were cultured in Roswell Park Memorial Institute (RPMI) 1640 medium. The media contained 10 % foetal calf serum (FCS), 0.5 % penicillin/streptomycin (10,000 IU mL^{-1} / 10,000 mL^{-1}) and 1 % 200 mM L-glutamine. All culturing and imaging steps were performed in the absence of phenol red-based additives. The supernatant containing dead cell matter and excess protein were aspirated. The live adherent cells were then washed with 10 mL of phosphate buffer saline (PBS) solution twice to remove any remaining media containing FCS, which may inactivate trypsin. Cells were incubated in 3 mL of trypsin solution (0.25 % trypsin) for 5 to 7 min at 37 °C. After trypsinisation, 6 mL of medium containing 10 % serum was added to inactivate the trypsin and the solution was centrifuged for 5 min (1000 rpm, 25 °C) to remove any remaining dead cell matter. The supernatant liquid was aspirated and 5 mL of cell medium (10 % FCS) was added to the cell matter left behind. Cells were counted using a haemocytometer and then seeded as appropriate, either on a microchip, or on a cellular plate suitable for optical imaging.

Standard Cellular Viability Assays in Water

To assess the cellular viability over the duration of experiment, in a parallel setting, standard MTT assays (i.e., colorimetric assays for measuring cell metabolic activity) were performed. For this, PC-3 cells were plated (7 x 10^3 cells per well) in a 96-well plate and left for 48 h to adhere fully. For a cellular viability estimation (denoted IC50 estimations by MTT assays), cells were incubated with aqueous gadolinium chloride and tested for 20 min at 37 °C. Concentrations used were 250, 100, 50, 10, 1, 0.5, 0.1 μM, 0.001 μM (1 % water, 99 % RPMI medium containing 10 % FCS at standard concentration of the cell line). Subsequently, cells were washed three times with PBS and 100 μL of MTT was added (0.5 mg mL^{-1}, 10 % PBS:SFM), followed by a 2-h incubation. Following aspiration, 100 μL of DMSO was added and the 96 well plates were read at an ELISA plate reader (Fluostar Omega BMGLabTech, Aylesbury, UK). Data emerged from at least three consistent results and IC_{50} values were calculated using Origin 9 (Wellesley Hills, MA, USA). However, when the effect of $GdCl^3$ was evaluated in aqueous conditions, the IC_{50} value at 20 min could not be determined because no significant cytotoxicity effect is induced by aqueous gadolinium chloride in 20-min incubation with given concentrations.

MEA fabrication and cell culture

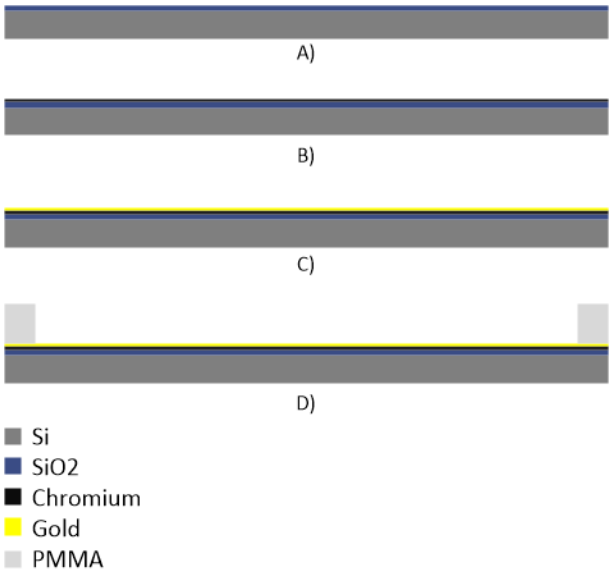

Figure 5.1 Step by step fabrication process of the MEA chip used for the experiments: A) Silicon/silicon oxide substrate; B) Chromium deposition; C) Gold deposition; D) Square piece of PMMA bonded to the MEA.

The MEA design and characterization is based on the previous research work developed by Dr. Rocha et al [285]. The step by step fabrication process of the MEA used for the

experiments with PC-3 cells is shown in figure 5.1. This MEA has been fabricated on a silicon/silicon dioxide wafer of 1 mm thick as substrate (figure 5.1A), on which surface round shaped gold electrodes have been patterned. The fabrication of the electrodes has been performed by the typical physical vapor deposition (PVD) process by evaporation of both chromium and gold. Firstly, a shadow mask made of metal with the pattern of the electrodes is placed over the substrate. Both the mask and the substrate are introduced in the PVD system inside which a thin layer of 8 nm of chromium, which works as an adhesion layer, is evaporated and deposited on the substrate surface (figure 5.1B). Then, a layer of 50 nm of gold is evaporated and deposited to create the electrodes (figure 5.1C). Their area is 1 mm^2 and they are connected to the contact pad with a small strip line of 0.2 mm width. After the fabrication of the gold electrodes, a milled piece of PMMA is glued to the substrate with the deposited metals, surrounding the gold electrodes but leaving out most of the strip line and the contact pad, which have no influence on the electrical recordings(figure 5.1D). This piece of PMMA act as well to contain the solution. The strip lines placed inside the well can be disregarded with respect to the electrodes area.

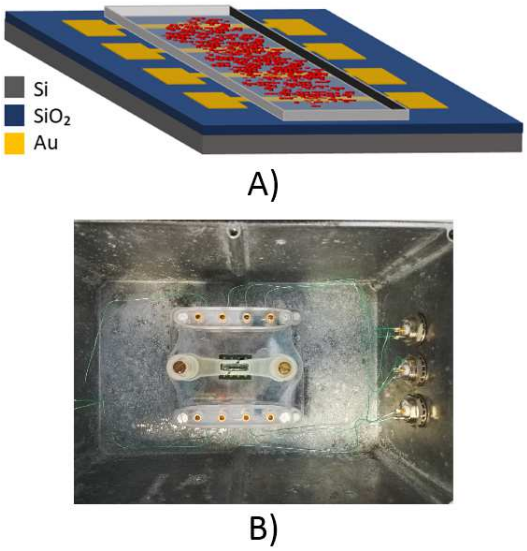

Figure 5.2 A) Drawing of the transducer used for PC-3 cells culture. The red circles represent the PC-3 cells within the culture medium; B) PC-3 cells deposited in the MEA chip and placed inside the shielded box.

The MEA chip is connected to the measurement equipment through gold plated contact pins located outside the well. These pins were purchased from Distrelec (Bremen, Germany), rated at 3 A with a length of 24.64 mm and type SPA-2D. In order to assure a complete sterility, the whole system is autoclaved before its use. Then, the PC-3 cells with medium are deposited inside the PMMA well, covering all the electrodes. Due to the

volume of the PMMA well, 0.1 million cells with 280 μL of medium are deposited on the MEA chip. To allow the correct deposition and adhesion of cells to the electrodes, the cell culture chip is introduced inside a CO_2 incubator (Midi 40, Thermo Scientific, Schwerte, Germany) for three hour before starting the electrical recordings. The experiment is running for three days while it is continuously monitored. This experiment has been repeated three times with the same conditions. Possible problems of medium evaporation are avoided by partially covering the PMMA well with a lid. The amount of medium inside the well is enough to maintain the cell culture for more than 24 hours without changing the medium. Figure 5.2A shows a drawing of the MEA with the cultured cells insite it, while figure 5.2B presents a real image of that MEA chip with the PMMA well glued to its surface and placed inside the shielded box before introducing it in the CO_2 incubator.

Electrical recordings

The electrical recordings of PC-3 cells activity is carried out by measuring the current between two gold electrodes. The acquired signal is transmitted through a low noise current amplifier (SR570, Stanford Research, Sunnyvale, CA, USA) to a dynamic signal analyzer (35670A, Agilent, Frankfurt, Germany). The data recorded is passed from the signal analyzer to a Labview software using a high speed USB/GPIB interface converter from Keysight Technologies (Frankfurt, Germany). This signal is then processed with Matlab R2017b. Two hours before the starting the measurements, the current amplifier is calibrated, as well as the setup is stabilized, to minimize the drift. The current is recorded as a function of time with zero bias on the electrodes. In addition, in order to minimized any external interference, both the current amplifier and the signal analyzer are covered with a Faraday cage, and the wires used are low noise. Figure 5.3A) shows the current amplifier and the signal analyzer inside the faraday cage; and figure 5.3B) presents the Labview interface in which the recorded signal is plotted in real time. To check if the PC-3 cells are adhered or not to the substrate and the electrodes, some optical micrographs taken with an epifluorescence microscope (Nikon, Surrey, UK) demonstrate an appropriate cells adhesion to the chip surface. As it has been previously said, the electrode area is 1 mm^2, which is a large area. Hence, our intention is to record not a single cell electrical activity but a superposition of signals from different cells directly in contact with the gold electrode, that is, we have recorded the activity of a PC-3 cell population.

5.1.2 Results and discussion

In this section, the experimental results obtained from the PC-3 cell culture and its electrical activity are fully described. Firstly, results extracted from the cell adhesion and viability in the MEA chip are presented. Then, results of the electrical activity of PC-3 cells cultured in the MEA, which has been recorded with the equipment explained in subsection 5.1.1, is shown. Finally, the use of $GdCl^3$ as a Ca^{2+} channel inhibitor and its influence in the electrical activity is detailed.

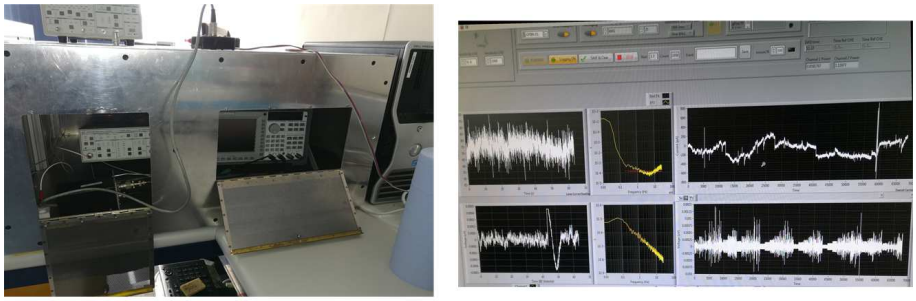

A) B)

Figure 5.3 A) Current amplifier and signal analyzer covered by the Faraday cage; B) Labview interface to monitor and plot the electrical recordings.

Cell adhesion and viability

In the following paragraphs, the first tests carried out during this work are described. These consist on demonstrating the adhesion of PC-3 cells to the substrate and the gold electrodes, and the viability of PC-3 cells cultured in the MEA chip.

As it has been previously explained, the MEA chip used for these experiments is composed of a silicon/silicon dioxide wafer with gold electrodes evaporated on its surface with the PVD process. There are a total of four pairs of circular electrodes on the MEA, which are optimized to record the electrical signals of the cell populations adhered to them [258, 310].

For an accurate electrical recording through the gold electrodes, cells adhesion to them results indispensable. In this respect, figure 5.4A shows a real amplified images of the cells adhesion to both the substrate and the gold electrodes after three days of their deposition, which demonstrates that, PC-3 cells perfectly adhere to almost the whole surface of the electrode. Finally, once the cells adhesion is confirmed, the next step consists on testing the cell viability of the MEA. For this experiment, 1 x 10^5 cells are deposited in the chip and incubated for 24 hours. Cells growth is monitored every day and the number of them is quantified and averaged on every electrode of the MEA. Results are shown in figure 5.4C, in which normalized cell numbers in 1, 2, 3, 4 and 8 days are represented. These results demonstrate the absence of toxicity in the presented chip, as well as PC-3 cells can attach and proliferate in normal conditions. For each post, the average of the eight different electrodes was calculated. The error reported was the standard error of the mean and is shown as $\pm$S.E.M. Table 5.1 illustrates the numerical results of the cell viability tests.

PC-3 cells electrical activity

Once the MEA chip has been described and the cell viability has been demonstrated, in order to give a deeper insight of the recording system, a brief description of the recording

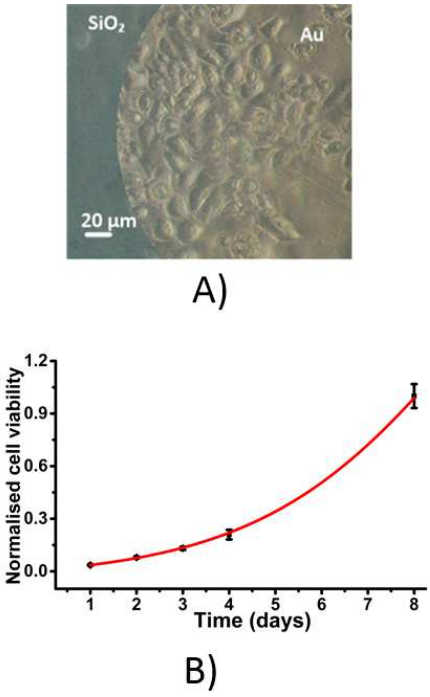

Figure 5.4 A) PC-3 cells adhered to the gold electrodes 3 days after being deposited. B) Cell viability describing a typical exponential PC-3 cell growth in the MEA device.

Table 5.1 Average, S.E.M, normalized average and normalized S.E.M..

	Day 1	Day 2	Day 3	Day 4	Day 8
Average	42.0000	93.7500	156.6250	285.0000	1193.6250
S.E.M	4.5591	9.4449	16.8395	43.4133	128.5749
Normalized average	0.0352	0.0785	0.1312	0.2089	1.0000
Normalizeed S.E.M	2.42 x 10^{-3}	5.02 x 10^{-3}	8.95 x 10^{-3}	2.75 x 10^{-2}	6.84 x 10^{-2}

system is outlined below. The equivalent circuit based on the charge transfer resistance (R_D) is modeled in parallel with the Helmholtz-Gouy-Chapman double layer capacitance (C_D) which is in series with the spreading resistance (R_C). A similar circuit is implemented for the counter electrode. Figure 5.5 represents the equivalent circuit of the model used for the electrical recordings, which is based on the one reported on [311].

In that model, an important parameter called seal impedance (Z_{seal}) is taken into account, and so it is done in our recording system. Z_{seal} "is usually defined as the resistance between

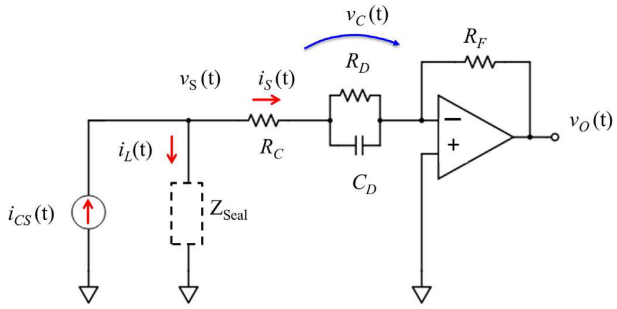

Figure 5.5 Equivalent circuit. i_{cs}(t) is the signal generated by the cell. When Z_{seal} is very high, i_{cs}(t) = i_s(t). Copyright (2016) Elsevier Ltd.

the cell and the surrounding solution (ground)". In our case, this Z_{seal} is very high due to the large distance between the sensing and the counter electrode. Our system, instead of measuring the voltage generated by cells (v_s(t)), measures the current (i_s(t)) using a transimpedance amplifier. The output voltage (v_o(t)) is then given by equation 5.1:

$$v_o(t) = R_F i_s(t) \tag{5.1}$$

According to equation 5.1, R_F is the feedback resistance. According to the model explained on [311], the detected current is given by:

$$i_s(t) = \frac{dv_s}{dt} \cdot C_D(1 - e^{\frac{t}{\tau}}), with \tau = R_C R_D \tag{5.2}$$

In equation 5.2, τ is the time constant for the charging or discharging of the network. C_D plays the role of a multiplying factor, influencing the spatial resolution and allowing the signal amplification. This is possible due to the use of large area electrodes which permit the rescaling of C_D. As it has been defined on 5.2, i_s(t) is the derivative of the acquired voltage signal, hence any change on the extracellular potentials affect i_s(t).

On this basis, the electrical activity of PC-3 cells has been monitored over time. This experiment has been repeated three times to demonstrate its reproducibility and reliability. The first test consists on measuring the baseline signal which results of recording the electrical signal of the MEA chip with only medium. Once the baseline is characterized, the next tests are focused on recording the electrical activities of PC-3 cells cultured in the chip. Finally, this electrical signal recorded with our system is post-processed with a Matlab software, where the acquired spikes are analyzed depending on their amplitude, their width and the distance, in time, between them.

Figure 5.6a shows the baseline signal of the MEA chip. As it has been previously mentioned, this baseline signal has been recorded with only medium, that is, it has been acquired before the PC-3 cells were deposited. As can be seen in figure 5.6a the baseline signal is around 1 pA or even lower, which is in accordance with the results reported on [262]. The expected spikes amplitude of PC-3 cells is about 100 pA, or higher. Thus, the baseline signal is low enough to assure a reliable recordings.

Once the baseline is characterized and being its value low enough, PC-3 cells are then cultured and monitored in our system. Figure 5.6b presents part of the electrical recordings of PC-3 cells, corresponding to a period of time of about 12 hours, during which the two common patterns of the electrical measurements at zero bias are shown. These two common patterns are associated to two behaviors clearly differentiated. During the first hours after culturing the cells, a basal sporadic and asynchronous activity is recorded. However, in less than 24 hours after the cells deposition, the electrical activity becomes quasi-periodic. Figure 5.6c represents the typical unipolar asynchronous electical spike of the PC-3 cells population culture during the extracellular recordings. On the other hand, figure 5.6d shows a zoomed image of a quasi-periodic spikes train related to the electrical activity of PC-3 cells. In addition, figure 5.6e presents a more detailed image of those quasi periodic spikes. Comparing the obtained results, according to figure 5.6c, we have noticed that, during the first hours of the experiment, about the 70 % of the recorded spikes are unipolar, fast (below 100 ms) and with lower amplitudes (about 100 pA or lower) than those with a synchronous behavior. Regarding the quasi-periodic spikes shown in figures 5.6d and 5.6e, it can be seen how the recorded spikes are biphasic, with higher signal amplitudes (about $\pm$150 pA) and a longer width than the unipolar spikes (normally over 100 ms). Moreover, the inter-spike intervals recorded for the quasi-periodic activity are about a few seconds.

In addition to the electrical signal recordings from the PC-3 cells, a detailed statistical analysis of the quasi-periodic activity is presented in figures 5.6f, 5.6g and 5.6h. The analysis of the recorded spikes have been carried out depending on three different parameters: the spikes amplitude, the spikes width and the distance between spikes. The results obtained from this statistical analysis, correspond to what the recorded spikes suggested in figures 5.6b-e. In the histograms presented in figure 5.6f, only the spikes with an amplitude over $\pm$50 pA have been taken into account. As it can be seen, almost half of the recorded spikes present an amplitude between $\pm$100 pA and $\pm$200 pA, while a considerable number of spikes have an amplitude over $\pm$200 pA or even over $\pm$300 pA. These results confirm what was previously suggested, that quasi-periodic spikes recorded from PC-3 cells electrical activity during the synchronous behavior show higher amplitudes than those spikes recorded during the asynchronous activity. Moreover, regarding the histograms presented in figure 5.6g, the spike widths corresponding to the quasi-periodic activity show a distribution which is broader and with larger widths than those acquired during the asynchronous behavior, in which most of the acquired spikes exhibit a width between 30 and 200 ms. These results are in accordance to what it was shown in figures 5.6b-e. Finally, figure 5.6h represents the inter-spike interval, that is the distance between spikes during the quasi-periodic activity. In this case, events with a distance larger than 10 seconds are

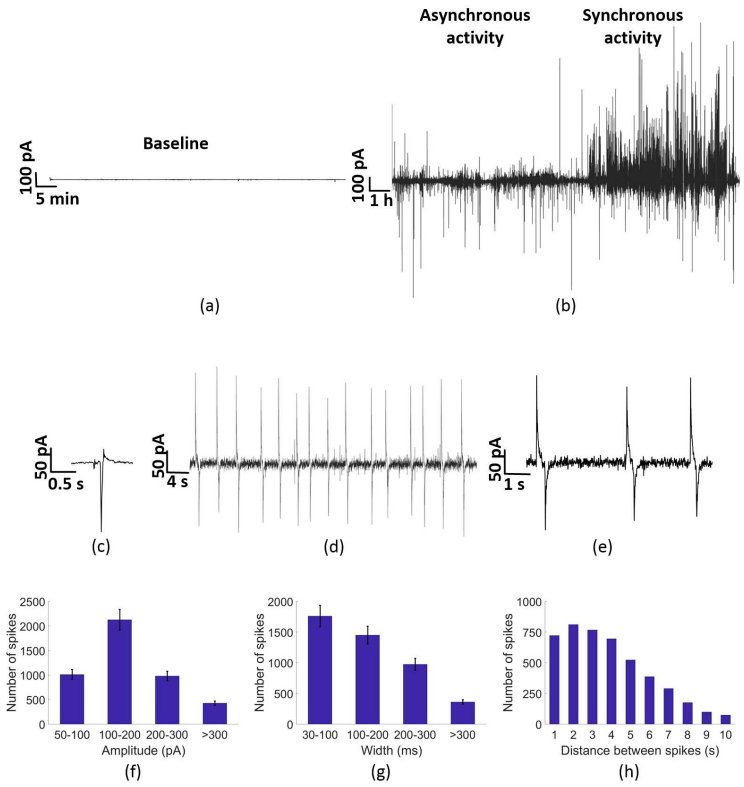

Figure 5.6 Electrical activity of a PC-3 cells culture on a Si/SiO2/Au substrate chip. (a) Baseline measured on the chip with only cell medium; (b) Most representative electrical activity of PC-3 cells during the experiment, showing on the left side of the graph the sporadic and mostly unipolar electrical activity, and on the right side the quasi-periodic behavior; (c) Zoom-in to the sporadic and asynchronous regime showing a typical unipolar negative spike; (d) Quasi-periodic activity of PC-3 cells, presenting biphasic spikes. (e) Biphasic pulses corresponding to the quasi-periodic activity, with a measurable distance between the positive and the negative spike of about 0.3s; (f-h) represent the characterization of the quasi-periodic activity of PC-3 cells: (f) Number of spikes depending on its amplitude; (g) Number of spikes depending on its width; (h) Number of spikes depending on the distance between them. The inter-spike intervals are distributed into time slots with a resolution of 1s..

not taken into account because they are barely representative. As it is shown in figure 5.6h, most of the recorded spikes have a distance between them which ranges between 1 and 4 seconds, being not negligible but less meaningful those spikes with a distance between them of 5 to 10 seconds.

Based on the results obtained from the spikes recordings and analysis, some conclusions could be extracted. Firstly, in the first part of the experiment, which corresponds to the asynchronous behavior of PC-3 cells electrical activity, the number of spikes detected is much lower (around ten times lower) than during the quasi-periodic behavior. In addition, according to the works reported on [262, 284], as it was expected for cooperative signals, spikes recorded during the quasi-periodic activity exhibit higher amplitudes and larger widths than those spikes from the asynchronous behavior. Our explanation about the asynchronous behavior of PC-3 cells electrical activity during the first part of these experiments are based on the research works reported on [312, 313, 314], in which the known expression of K^+ channels of the Kv1.3 family for prostate cancer cell lines is shown via patch clamp experiments. As it was previously explained, our recording system acquires the electrical activity of cells population, which is the sum of all individual cell contributions, by using large area electrodes. Thus, there is not enough spatial information to record the individual cell signals, which makes that the uncorrelated cell activity is interpreted as noise and low magnitude asynchronous spikes. Hence, based on our conclusions, we argue the asynchronous behavior of PC-3 cells in the first hours of culture is mainly caused by uncorrelated single cell activity.

Calcium channel inhibition

In the following paragraphs, the effect of a calcium channel inhibitor in the electrical activity of PC-3 cells is described. Additionally, a viability test to confirm that the inhibitor do not disturb the cell viability is presented. Through these experiments, we want to demonstrate the influence of Ca^{2+} channels in the electrical activity of prostate cancer cells.

In the previous subsection, the electrical activity of a PC-3 cells population has been demonstrated to be sporadic and asynchronous during the first hours of experiment, becoming quasi-periodic over time. Furthermore, we have shown how those quasi-periodic spikes are slow and how they occurs prostate cancer cells proliferation. In addition, according to the literature, this quasi-periodic activity is related with an extracellular traveling wave across the large electrode area. When this wave reaches the sensing electrode, a potential relative to the counter electrode is risen, forcing a large displacement current through the double layer capacitance, which results in upward and downward current spikes corresponding to the wave entrance and exiting on the recording electrode [262, 284, 312]. Regarding the obtained results explained before, by using electrodes with and area of 1 mm^2, we have recorded upward and downward spikes with a separation between 0.7 and 2 seconds. It means that we are able to record a wave speed of a few hundreds of micrometers per second, which is, in accordance with some research works reported on [315, 316], the Ca^{2+} waves propagation speeds. Hence, having explained that, our hypothesis is focused on demonstrating that Ca^{2+} channels are directly involved in PC-3 cells electrical activity. In this respect, we have used a widely known Ca^{2+} inhibitor, gadolinium (Gd^{3+}), to block the electrical spikes of the PC-3 cells culture in our MEA chip [317].

As it has been said before, Gd^{3+} has been used as a Ca^{2+} inhibitor during the experiment. The inhibitor has been added to the medium with cells for 20 minutes. After that time, the medium with Gd^{3+} has been washed up to three times to eliminate any possible remnant of the inhibitor. According to [310], Gd^{3+} has been diluted in deionized (DI) water, in concentrations between 10 and 40 μM. Taken into account that the medium contained in the MEA chip at the beginning of the experiment was 280 μL, the amount of Gd^{3+} added has been 3 μL in a concentration of 1 mM, resulting in a final concentration of Gd^{3+} of between 10 and 20 μM.

Figure 5.7 presents the results obtained on the experiments carried out before, during and after the use of Gd^{3+}. Figure 5.7a (black color on the left side) shows the quasi-periodic electrical activity of PC-3 cells before adding the inhibitor, which is the same behavior of the electrical activity of fresh PC-3 cells fully described in figure 5.6, as it was expected. Figure 5.7a (red color) presents the absence of electrical activity of PC-3 cells after the addition of 20 μM of Gd^{3+} together with the medium. The inhibitor has an immediate effect, so in less than one minute the current spikes are almost negligible, under $\pm$5 pA of amplitude. 20 minutes after the addition of Gd^{3+}, the cells are washed with phosphate buffer saline (PBS) a total of three times to assure the elimination of the inhibitor, and then the culture is filled with fresh medium. Figure 5.7a (black color on the right side) shows how the electrical activity of PC-3 cells is completely recovered after removing the Gd^{3+}, showing similar spikes to those recorded before the use of the Ca^{2+} inhibitor. Spikes magnitude recorded before and after the use of Gd^{3+} were about $\pm$100 pA, which is in accordance with the results provided on the first PC-3 cells experiments. Figure 5.7b shows the number of spikes detected before, during and after the use of the Ca^{2+} inhibitor. The histograms exhibit a similar number of spikes recorded before and after the use of Gd^{3+}, but not a single spike when Gd^{3+} was added, strengthening the conclusions extracted from figure 5.7a.

These results guide our hypothesis to a possible claim: Ca^{2+} channels are directly involved in the electrical activity of PC-3 cells population. However, in order to reassure our conclusions, an acute Gd^{3+} viability test has been performed. Results are illustrated in figures 5.7c and 5.7d. Histograms represented in figure 5.7c correspond the MTT assays with Gd^{3+} in different concentrations, which show that the cell viability of all concentrations are around or above 90 %. Apart from the MTT assays, in figure 5.7d, a positive and negative control results are compared with the Gd^{3+} results. 250 μM triton has been used as a positive control, while water is used as the negative control. The amount of Gd^{3+} used is 250 μM during 20 minutes of incubation. As can be seen in figure 5.7d, Gd^{3+} presents a very close cell viability to the negative control, which is non-cytotoxic. However, in the positive control, a cytotoxic reagent in the same concentration of Gd^{3+} is added to the PC-3 cells with medium, resulting in a meaningful reduction in the cell viability. Thus, it has been demonstrated that the use of Gd^{3+} during 20 minutes, together with PC-3 cells and medium, do not cause a cytotoxic effect on PC-3 cells, confirming that the reduction of the electrical activity described in figure 5.7a is due to the inhibition of Ca^{2+} channels instead of cell death.

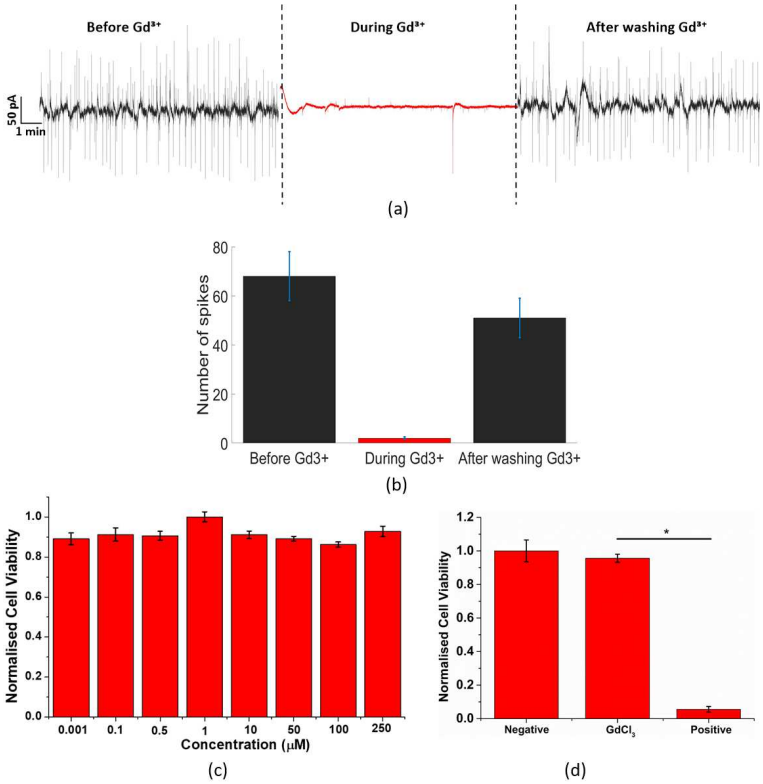

Figure 5.7 (a) Electrical activity of PC-3 cells culture before, during and after using Gd^{3+} as a Ca^{2+} inhibitor; (b) Number of spikes detected before, during and after the use of Gd^{3+}; (c) gadolinium chloride MTT assays. The results of (c) are reported as means ±S.E.M. The data were analysed by one way ANOVA, $p<0.05$, which means there is a significant difference between results of different concentrations (n=3). Error bars represent standard error with respect to the repeated six measurements of the same concentration; (d) Positive and negative control test of gadolinium chloride. The results are reported as means ±SEM. (*, $p < 0.05$, Student's t-test). There is a significant difference between results of GdCl3 and positive control at 250 μM concentration (n=3). Error bars represent standard error with respect to the three independent experiments.

5.1.3 Conclusions of the PC-3 cells experiments

In this subsection, a short summary of the conclusions extracted from these experiments are described. The aim of this research work was to characterized the electrical activity of a prostate cancer cell line (PC-3) by using a MEA chip on silicon/silicon oxide substrate with circular gold electrodes. The obtained results show that PC-3 cells exhibit a low frequency electrical activity, between 0.1 Hz and 10 Hz, with two clearly differentiate

patterns: one sporadic and asynchronous and the other synchronous and quasi-periodic. The sporadic activity mainly occurs during the first hours of the experiment and it consists on weak and fast spikes with a width shorter than 100 ms. Quasi-periodic activity is acquired during the rest of the experiment and the recorded spikes presents amplitudes around $\pm$150 pA, width between 50 and 300 ms and inter-spike intervals of between 1 and 4 seconds. Moreover, the use of Gd^{3+} as a Ca^{2+} inhibitor has proved the involvement of Ca^{2+} in the electrical activity of PC-3 cells population. Hence, for the first time, we have characterized the electrical activity of a PC-3 cells population by using a feasible, real time and highly sensitive system for electrical recordings. These results are useful to understand the signaling pathways of prostate cancer cells, as well as the utilized system can be considered to its application with many other type of cells. This work has led us to improve our knowledge on MEA devices, as well as on the electrical recordings of cells. In addition, it has resulted in a publication in a high impact factor journal [261].

Cabello, M., Ge, H., Aracil, C., Moschou, D., Estrela, P., Manuel Quero, J., ... & RF Rocha, P. (2019). Extracellular electrophysiology in the prostate cancer cell model PC-3. Sensors, 19(1), 139.

5.2 Microelectrode array for cell culture applications

Taken into account the experience acquired during the stay at the University of Bath and the huge potential of this field, the following step on this thesis work is focused on improving the MEA design and fabrication process, to develop suitable MEAs for electrical recording by increasing the contact between the electrode and the biological material, as well as to enable the electrical recordings of cell cultures through these MEA devices. Thus, the migration of the original MEA for the retinal explants culture towards a device with electrodes for electrical recordings of cells or tissue cultures is explained in this section. In subsection 3.1.4, a detailed view of the state of the art of MEAs for *in vitro* cultures was given, so it is not repeated once again in this section.

Despite the successful results obtained with the MEA for organotypic culture applications presented on chapter 4, the microelectrodes of this device presents some problems for its use for electrical recordings of biological samples. In this respect, some approaches of MEA devices are outlined below, in order to improve their functionality for this application.

In the following paragraphs, different fabricated devices are presented, as well as some biological tests which are not completely conclusive. The materials used as substrates for the fabrications of these MEAs includes non-transparent materials such as PCB of FR4, and transparent substrates such as thermoplastics or glass. Both 3D and planar electrodes have been manufactured following different processes depending on the substrate and the shape. Due to its proved biocompatibility, the material used to grow the electrodes is gold. Most of the approaches shown in this subsection are focused on the fabrication

processes. However, some experiments of their biocompatibility are also included. These initial approaches are the connecting link between the work developed on the national project named BIOLOP (project TEC2014-54449-C3-2-R, BIOLOP), to which this thesis work is associated, and the continuation project focused on the development and integration of opto-electrostimulation and signal processing for *in vitro* culture devices to study the neuronal behavior (RTI2018-100773-B-C33), which has just been recently started.

5.2.1 3D MEA fabricated on PCB of FR4 as substrate

In this subsection, a 3D MEA fabricated on PCB of FR4 as substrate is presented. In addition, the impedance measurement and its comparison with the microelectrodes described in 4 are included. The aim of this research work is the development of a 3D MEA for electrical recordings of biological samples cultured on it. The 3D shape allow its use not only with cells but also with tissues, thanks to a better contact between the microelectrodes and the sample than in planar MEAs. The 3D MEA was firstly designed and fabricated before starting the stay at the University of Bath, as a preliminary approach to improve the microelectrodes fabricated on PCB.

Design and fabrication process

The 3D MEA developed on this work is fabricated by using a PCB of FR4 and copper as substrate. Copper is well-known to be biologically incompatible. For that reason, in order to minimize the amount of copper, the PCB chosen has a thin layer of copper of 5 μm thick, which is the base of the microelectrodes and their lines and pads. These microelectrodes has been designed as micro- pillars which are grown on the copper by gold deposition through the electroplating technique (Spa Plating, Bath, UK). These pillars have a diameter of 100 μm and a height ranging between 25 μm and 40 μm, and the minimum copper width is 50 μm. Microelectrodes and copper tracks and pads distribution is based on the commercial MEA of Multichannel Systems (Multichannel Systems, a division of Harvard Bioscience, Inc. [253]). Figure 5.8 shows the layout of the described 3D MEA. The effective area of the electrodes is a square of 3.5 mm x 3.5 mm. Despite the use of copper, a non biocompatible material, it will be covered with gold, and passivated with a thin SU-8 layer, making the designed 3D MEA suitable for biological applications.

Once the microelectrodes and tracks distribution is designed, the fabrication process is carried out. Before starting it, it is necessary to print the mask which will be used during the process, based on the design shown in figure 5.8.

The step by step fabrication process of the 3D pillars MEA is shown in figure 5.9. The substrate used for fabricating the 3D MEA is a standard PCB of 1.5 mm of FR4 and 5 μm of copper (figure 5.9A). The first step consists on obtaining the copper tracks through the typical photolithographic process by using the mask previously designed (figure 5.9B). Then, a first gold layer is grown through the gold electroplating method (figure 5.9C). With

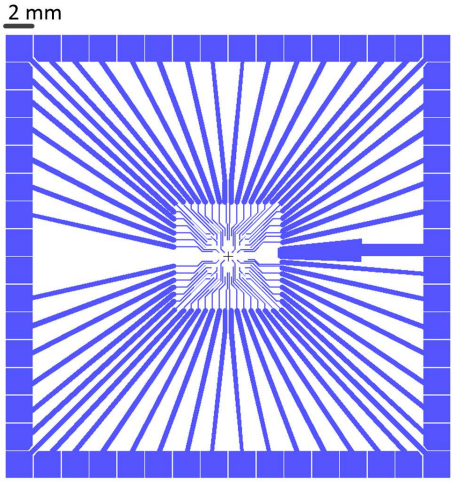

Figure 5.8 Layout of the 3D MEA.

this layer any possible contact between the biological sample and copper is completely avoided. Then, a SU-8 layer of 15 μm thick is deposited, acting as a passive layer and covering the metal tracks (figure 5.9D). The next step is a photolithographic process of the SU-8, relasing the holes to allow the growth of the 3D pillars (figure 5.9E). Later on, a layer of 50 μm of AZ 125nXT, which is used as a sacrificial layer, is deposited over the SU-8 (figure 5.9F). By repeating the same photolithographic process that was done for the SU-8, the holes for growing the 3D pillars are released (figure 5.9G). The next step consists on growing the gold on the released holes to fabricate the 3D pillars (figure 5.9H). In this respect, the electroplating kit company (Spa plating, Bath, UK) provides users a calculator to estimate current and time needed to grow a gold layer depending on the area. For the fabrication of these gold 3D pillars, we have grown around 40 μm of gold on a surface of around 0.01 cm^2 (the sum of all the electrode areas), being necessary up to 5 hours and 40 minutes with a current of 0.1 mA. After that time in which the MEA is immersed in the electroplating solution, the device is properly clean with a non-corrosive cleaner. The last step is the removal of the sacrificial layer of AZ 125nXT, leaving the end of the gold microelectrode, that is around 25 μm, above the SU-8 layer (figure 5.9I). Finally, a squared piece of PMMA is bonded to the MEA, surrounding the 3D microelectrodes.

Following the step by step fabrication process previously described, the resulting 3D MEA with gold pillars is shown in figure 5.10A. The gold microelectrodes are surrounding by a squared piece of PMMA necessary to hold the solution. There are up to 60 electrodes in an area of about 12 mm^2. Thanks to the SU-8 passive layer, only the gold pillars are directly in contact with the solution and the biological samples, assuring the biocompatibility of the presented MEA.

In figure 5.10B, an enlarged image of one of the 3D gold pillars is shown. The resulting pillar it is not a perfect cylinder, but a "mushroom". This is due to the gold deposition

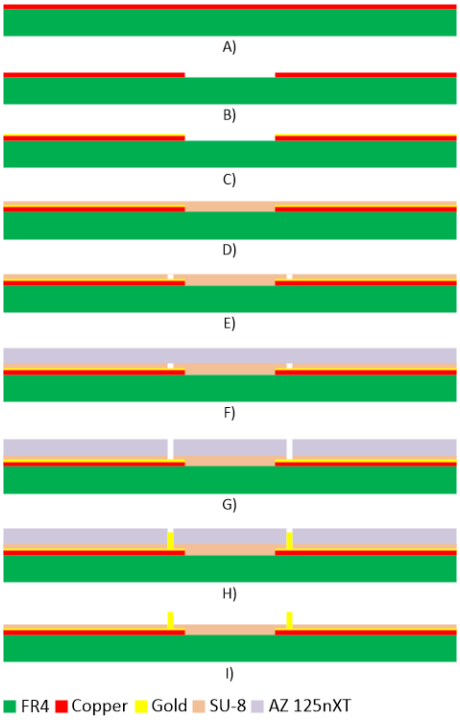

Figure 5.9 Fabrication process of the 3D gold pillars MEA. A) PCB of FR4 and copper; B) Photolithographic process; c) First gold coating; D) SU-8 deposition; E) SU-8 UV light exposition and developing; F) AZ 125nXT deposition; G) AZ 125nXT UV light exposition and developing; H) Second gold coating to obtain the 3D pillars; I) Elimination of AZ 125nXT layer.

process through electroplating. The total height of the microelectrode is about 40 μm. However, regarding that the heigh of the SU-8 layer is about 15 μm, the gold pillar is approximately 25 μm above the passive layer, with a diameter of 100 μm. One of the main advantages of the presented MEA is it cost effective fabrication process. Apart from using a non-expensive substrate, the amount of gold needed to create those pillars is less than 30 mg, which implies a cost of about 1.5 euros for each MEA. All of this makes this device a good alternative to fabricate disposable MEA devices with 3D microelectrodes.

Experimental results and discussion

In the following paragraphs, different experiments has been performed to characterized the 3D MEA previously described. The aim of this work is to develop a group of microelectrodes to improve the contact between the biological samples and the electrodes, which is, in the case of planar MEAs, a challenging issue. A better contact implies more accurate recordings of the electrical activity. Hence, in order to demonstrate the improvements of

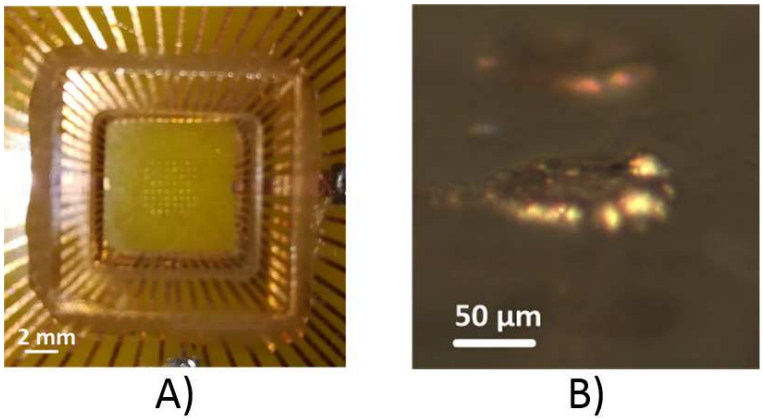

Figure 5.10 A) Fabricated 3D Gold pillars MEA; B) Amplified view of a 3D gold pillar. The gold is around 25 microns above the SU-8 layer.

the presented MEA in terms of electrical behavior, we have compared this 3D MEA with the previously MEA described in chapter 4 and used for culturing mice retinal explants.

Firstly, the characterization of the 3D MEA has been carried out by measuring the impedance of the microelectrodes. This has been performed with an impedance spectroscopy provided by Dr. Rocha in the University of Bath. The impedance was measured by using different concentrations of a potassium-chloride (KCl) solution. The concentrations were: 100 μM, 1 mM and 1 M. As it is shown in figure 5.11A, the impedance decreases over the frequency, as it was expected, presenting values between $10^6\Omega$ and $10^7\Omega$ at low frequencies, turning into a lower impedance, around $10^2\Omega$, specially for 1 M concentration, at higher frequencies. These impedance measurements have been obtained following the previous research work of Rocha et al. reported on [262].

For low concentrations of KCl, the relaxation frequency (F_r) appears around 10^3 Hz, occurring close to the 10^6 Hz for higher concentrations of KCl.The Maxwell-Wagner relaxation effect occurs when a current passees an interface between two dielectrics. This effect can be simplified by using the Randles equivalent circuit, consisting in a two RC circuit in series, as can be seen in the schematic shown in figure 5.11B. This circuit recreates the electrode interface (R_{ct} and a constant phase element, CPE) and the solution (R_{sol} and C_{sol}), and it can be modeled as it is described in equation 5.3.

$$F_r = \frac{1}{2\pi}\frac{QR_{ct}R_{sol}}{R_{ct}+R_{sol}}^{-1/n} \tag{5.3}$$

Where Q is a frequency independent, phenomenological parameter. R_{ct} is the charge transfer resistance of the gold electrode. R_{sol} is the resistance solution due to the spreading

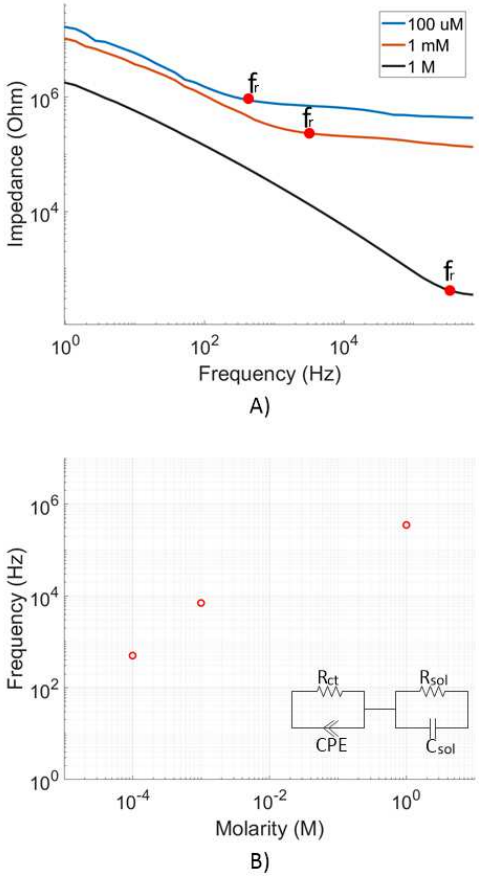

Figure 5.11 A) 3D gold pillars impedance as a function of molarity of the KCl solution. Red circles represent the relaxation frequencies in each case; B) Relaxation frecuency as a function of molarity obtained from the experimental results.

of current from the localized electrode to a distant counter electrode in the solution, and depends on the conductivity of the solution and the radius of the electrode. The solution capacitance (C_{sol}) is negligible.

Figure 5.11B presents the relaxation frequency as a function of the molarity, resulting from the impedance measurements of the 3D gold pillars. As can be seen, the relaxation frequency strongly depends on the molarity of the KCl solution, being higher for higher concentrations. According to the theoretical calculations of the Randles equivalent circuit, the obtained results are the expected ones. Moreover, these conclusions are in the line of what is reported on [262]. Thus, we can conclude that, for the impedance measurements, the main influence of the microelectrodes occurs at low frequencies, while at higher frequencies the impedance depends more on the KCl solution.

Once the 3D MEA is correctly characterized, the next experiment carried out consists on comparing the impedance of these 3D gold pillars with those microelectrodes fabricated with the wire bonding technique (WB MEA) and used for mice retinal culture applications (chapter 4).

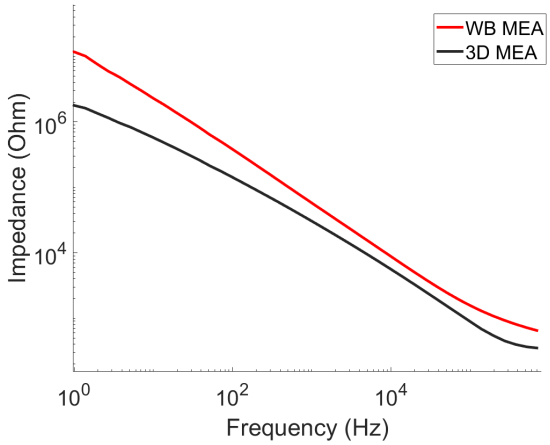

Figure 5.12 Comparison between the impedance measurements, in a KCl solution of 1 M, of both the WB MEA and the 3D pillars MEA for a frequency between 100 Hz to 10^6 Hz.

As it is shown in figure 5.12, there is a significant difference between the impedance of the WB MEA and the 3D MEA. In the previous paragraphs, the influence of the electrodes at low frequencies was highlighted. Thus, as it is described in figure 5.12, the main differences appear at low frequencies, which means that the electrodes fabricated on the 3D MEA present an impedance almost two orders of magnitude lower than the wire bonding electrodes impedance. Furthermore, as the frequencies increase, the difference in the impedance measurements between both MEAs becomes less evident.

In order to enforce the results obtained through the impedance measurements, the baseline of both MEAs has been measured and compared between them, as it can be seen in figure 5.13.

According to figure 5.13, the 3D MEA baseline is significantly lower than that of the WB MEA, which is a consistent results with those obtained for the impedance measurements. Thus, it is demonstrated that the WB MEA it is not ideal for its application on electrical recordings, due to its high baseline noise. On the other hand, values obtained for the 3D MEA exhibit a baseline noise of about 10 μV_{pp}, which is in the line of other research work, such as the one reported on [258]. Despite it is still not possible to reach the values

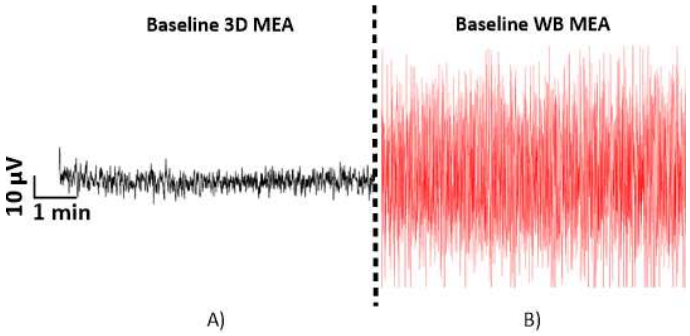

Figure 5.13 Baseline of both 3D MEA and WB MEA measured using a KCl solution of 1 M.

reported on [262], in which the electrodes have larger areas, we are able to provide a high concentration of gold microelectrodes with an impedance and baseline low enough to perform electrical recordings.

The results obtained from the characterization of the 3D MEA demonstrate a considerable improvement with respect to the previous MEA developed with the wire bonding electrodes embedded in PDMS. In this point, the reader is probably thinking that it is fine to have good results during the characterization, but it is needed a real experimental with cells to confirm the suitability of this 3D MEA for its application in electrical recordings of cell activity. Thus, during the stay in the University of Bath, we have measured the electrical activity of the PC-3 cells, as it was done in section 5.1, but cultured inside the 3D MEA.

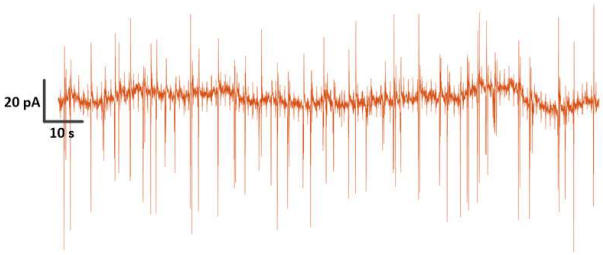

Figure 5.14 Current extracellular recordings of cancer prostate cells cultured on the 3D MEA.

The experimental results from the electrical recordings of PC-3 cells activity are shown in figure 5.14. As it was previously explained, the most representative activity of PC-3 cells is recorded several hours after depositing the cells in the MEA chip. This activity

presents a synchronous and quasi-periodic behavior, which is a consistent result compared to that obtained with the silicon/silicon oxide chip used on subsection 5.1.2. Despite it would be necessary to carry out more tests, such as a cell viability one, or replicate the cell culture and electrical recordings, these preliminary experiment guide us to consider that our 3D MEA is a good first approach for the development of cell culture devices for electrical recordings.

Conclusions of the 3D MEA

Summarizing what is has been previously explained, we can confirm that the presented 3D MEA is a step forward in the development of cell culture devices suitable for electrical recording of cells activity, if we compare it with the WB MEA described in chapter 4. The fabrication process has been demonstrated to be reliable, cost effective and biocompatible, thanks to the use of materials such as SU-8 or gold. The use of a PCB of FR4 and copper as substrate facilitates the integration of other components such as electronics or microfluidic together with the microelectrodes array. Moreover, the impedance and baseline noise show similar values to those found in the literature. In addition, an experiment with PC-3 cells has been carried out with the 3D MEA, being able to replicate the experiment presented on subsection 5.1.2 with similar results and electrical patterns. This work has resulted on a publication on an international congress [318].

Cabello, M., Aracil, C., Perdigones, F., Quero, J. M., & Rocha, P. R. (2018, November). Lab-on-PCB: Low Cost 3D Microelectrode Array Device for Extracellular Recordings. In 2018 Spanish Conference on Electron Devices (CDE) (pp. 1-4). IEEE.

5.2.2 Design and fabrication of planar MEAs on transparent substrates

Once the development, fabrication and characterization of the 3D MEA fabricated on PCB as substrate have been successfully carried out, the next step of this thesis work is focused on the obtaining a low cost MEA for cell culture in a transparent substrate, to make it suitable for optical applications. Hence, in this section, some new approaches of MEA chips designed and fabricated on transparent substrates are described in order to follow-up the development of these devices for electrical recordings of cells activity. The materials used to fabricate this chips are glass and PMMA as substrates, gold to pattern the electrodes and SU-8 to improve their adherence with the substrate and to passivate them.

Thus, in the following subsections, the development of two MEAs on glass and PMMA as substrates with gold electrodes are described. In addition, some preliminary experiments with neuroblastoma cells (SK-N-SH) cultured on these MEAs are included.

Design and fabrication of a MEA on glass substrate

In this subsection, the first approach of a MEA fabricated on transparent substrate is described. As it has been mentioned many times during this thesis work, the biocompatibility of the chosen materials is indispensable. For that reason, the substrate of this first MEA is made of glass, while SU-8 is used as a passive layer and the electrodes are made of gold. These electrodes are designed with different areas, to test how far our current technology can lead us in the development of microelectrodes.

Figure 5.15 shows the design and distribution of the electrodes, tracks and pads which will be fabricated on gold. In this case, each electrode has a different area, ranging between 0.002 and 0.785 mm^2, which means a radius between 25 and 500 μm. In figure 5.15 the gray color represents the substrates, which has the standard dimensions of a glass slide, that is 25 x 75 mm with 1 mm thick. The blue color represents the electrodes, tracks and pads which will be made of gold. This design is the same for both MEAs on glass and PMMA substrates.

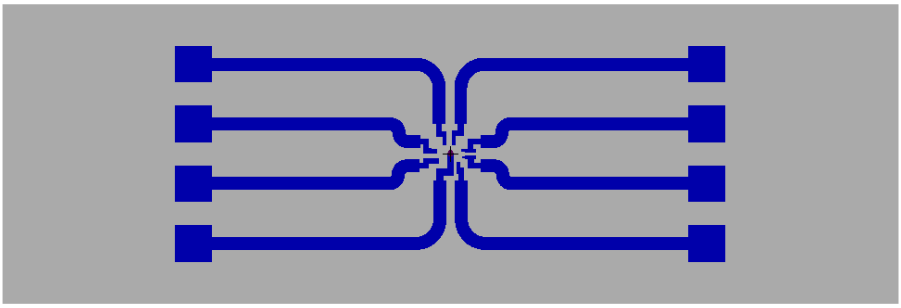

Figure 5.15 Design of the MEA on transparent substrates.

Once the design is finished, the fabrication process of the MEA on glass substrate can be carried out. Before manufacturing the MEA, the glass substrate is properly cleaned to eliminate any particle of dust. Firstly, the glass slide is rinsed on an isopropyl alcohol solution and introduced inside an ultrasonic cleaner for 20 minutes. Then, the glass slide is rinsed on DI water and put once again inside the ultrasonic cleaner for 30 minutes. Finally, the glass slide is taken out from the DI water and dry at room temperature for 15 minutes. Once the glass slide is completely dry, the step by step fabrication process is performed, as it is described in figure 5.16.

Figure 5.16 illustrates the step by step fabrication process of a MEA with gold electrodes patterned on glass substrate. Firstly, the glass slide has been properly cleaned (figure 5.16A). Once the substrate is neat, a SU-8 layer of 10 μm thick is deposited by using the spin coater (figure 5.16B). Following the typical photolithographic process of the SU-8 described on

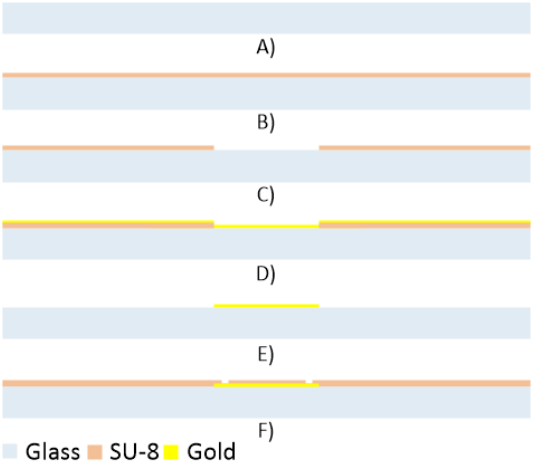

Figure 5.16 Step by step fabrication process of the MEA on glass substrate. A) Glass slide; B) Deposition of a SU-8 layer; C) Photolithographic process on the SU-8; D) Sputtering of a gold layer on the substrate with SU-8; E) Lift-off process to release the SU-8 with gold; F) Deposition of SU-8 as a passive layer.

subsection 2.2.2, the SU-8 is removed from those parts of the substrate in which the gold is going to be deposited (figure 5.16C). In this point, the glass slide is covered with cross-linked SU-8, except those parts corresponding to the electrodes, tracks and pads. Thus, the next step consists on the deposition of gold on the glass slide with SU-8 (figure 5.16D). The gold deposition is performed by the sputtering technique, depositing nanoparticles of metal over the substrate. In our case, the gold layer has a thickness of 100 nm. After the gold sputtering, the SU-8 with gold which is on the glass slide is released through the lift-off technique. To facilitate the lift-off, the glass slide with SU-8 and gold is heated to temperatures over 120 °C for at least 15 minutes. After that time, the SU-8 layer can be easily removed from the glass slide, remaining only the gold deposited directly on the substrate (figure 5.16E). Finally, a new SU-8 layer of about 5 μm thick is deposited over the glass slide with gold, acting as a passive layer. This SU-8 layer is covering the whole glass slide but releasing the squared pads and small holes at the end of each gold track to create the electrode, allowing the contact of the metal part with the outside (figure 5.16F).

Figure 5.17 shows a fabricated MEA on glass substrate. Figure 5.17A) correspond to an intermediate step of the fabrication process, particularly the step D, just before the lift-off process, and, as can be seen, the SU-8 is starting to detach from the glass due to the high temperature we expose it. Figure 5.17B shows the final result of the MEA after the last step of the fabrication process. There is a very thin layer, almost unnoticeable, over the glass and the gold tracks, releasing just the squared pads and the tips of the electrodes. Finally, figure 5.17C shows an enlarged image of one of the electrodes with SU-8 covering it, except that little circle of about 100 μm of diameter which makes possible the contact between the electrode and anything sample deposited on it.

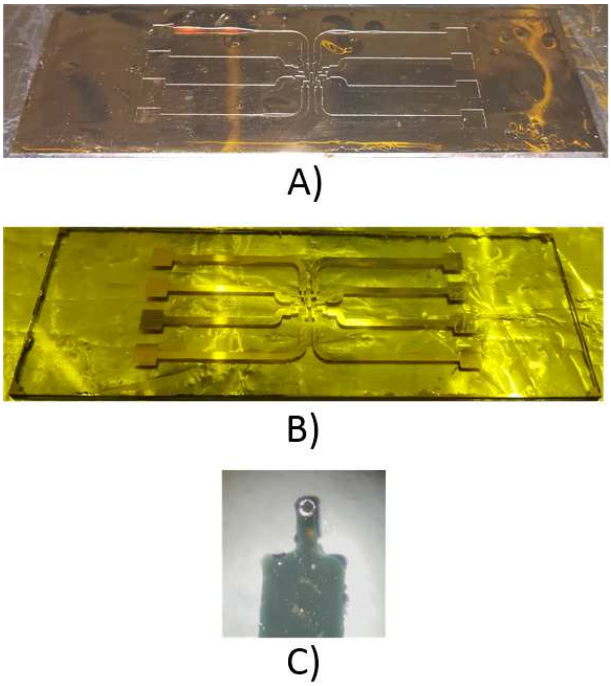

Figure 5.17 Real image of the MEA on glass substrate. A) Before the lift-off process; B) Final result after the whole fabrication process; C) Enlarge image of the SU-8 with a hole of 100 μm of diameter to create the electrode.

Regarding the design and fabrication process of this MEA, and the results obtained, our intention is to culture cells inside this device. To hold the medium with cells and keep the samples in contact with the gold electrodes, a squared piece of PMMA is bonded surrounding the electrodes but not the pads, allowing a possible electrical recording of the biological material by using external equipment. A first attempt with cells is outlined below.

Design and fabrication of a MEA on PMMA substrate

In this subsection, an alternative approach to the MEA fabricated on glass substrate is presented. Despite the MEA on glass substrate was apparently enough for our purpose, we had some problems with the adhesion between SU-8 and glass. The issue was that the passivation layer tends to lift away from the substrate. Thus, the electrodes become useless as long as the medium make contact not only with the tip but with the whole gold track. Furthermore, the use of glass as substrate makes the MEA chip more restrictive in terms of fabricating devices with different shapes. For that reason, our next attempt is focused on development MEA with gold electrodes patterned on PMMA as substrate. The main advantages of using a thermoplastic as a substrate is its low cost, not only the material

itself but also the fabrication process. In addition, through micromilling or laser cutting techniques it is possible to obtain many different shapes depending on our necessities.

Despite we have commented the flexibility of the presented MEA on PMMA substrate, in this approach we have followed the same design and electrodes distribution than those used for the MEA on glass substrate, described on figure 5.15. Hence, this MEA on PMMA substrate have a dimensions of 75 mm x 25 mm and a thickness of 2 mm. Each electrode has a different area, ranging between 0.002 and 0.785 mm^2. Before starting the fabrication process, the PMMA is cleaning. Firstly, it is rinsed on an isopropyl alcohol solution and introduced inside an ultrasonic cleaner for 20 minutes. Then, the piece of PMMA is rinsed on DI water and put once again inside the ultrasonic cleaner for 30 minutes. Finally, the it is taken out from the DI water and dry at room temperature for 15 minutes. Regarding the fabrication process, it has some similarities with that used to make the MEA on glass substrate, but there are some significant differences.

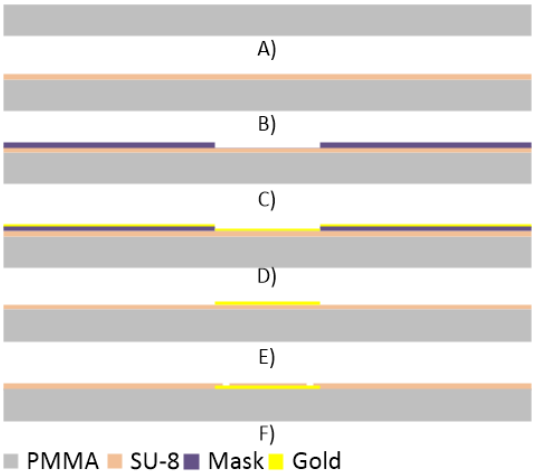

Figure 5.18 Step by step fabrication process of the MEA on PMMA substrate. A) PMMA piece; B) Deposition of a SU-8 layer; C) Use of an adhesive vinyl mask before the gold deposition; D) Sputtering of a gold layer on the substrate with SU-8 and the vinyl mask; E) The vinyl mask is peeled off; F) Deposition of SU-8 as a passive layer.

Figure 5.18 illustrates the step by step fabrication process of a MEA with gold electrodes patterned on PMMA substrate. Firstly, the PMMA piece has been properly cleaned (figure 5.18A). Once the substrate is neat, a SU-8 layer of 10 μm thick is deposited by using the spin coater (figure 5.18B). Following the typical photolithographic process of the SU-8 described on subsection 2.2.2, the SU-8 is cross-linked over the PMMA substrate, acting as a seed layer to improve the adherence between gold and PMMA. Once the SU-8 is

crosslinked, an adhesive vinyl mask is placed over the substrate with SU-8. This vinyl mask has been cut with a laser to obtain the desired design of the gold tracks, allowing the gold deposition in the correct place (figure 5.18C). The next step consists on the gold deposition through the sputtering technique (figure 5.18D). The thickness of the gold layer is about 100 nm. After the gold sputtering, the vinyl mask is peeled off from the substrate with SU-8, revealing the final disposition of the gold tracks, according to the designed mask. (figure 5.18E). Finally, a new SU-8 layer of about 5 μm thick is deposited over the PMMA slide with SU-8 and gold, acting as a passive layer. Similarly to what was done to fabricate the MEA on glass substrate, this SU-8 layer is covering the whole PMMA piece but releasing the squared pads and small holes at the end of each gold track to create the electrode, allowing the contact of the metal part with the outside (figure 5.18F).

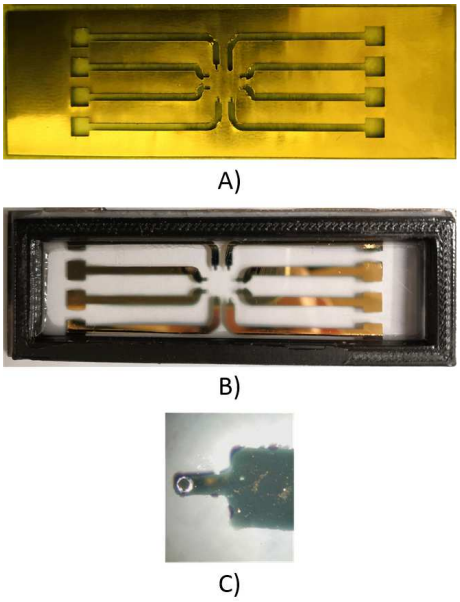

Figure 5.19 Real image of the MEA on PMMA substrate. A) PMMA substrate with the vinyl mask before gold deposition; B) Final result after the whole fabrication process, including the square piece of plastic glued to the MEA; C) Enlarge image of the SU-8 with a hole of 100 μm of diameter to create the electrode.

Figure 5.19 shows a fabricated MEA on PMMA substrate. Figure 5.19A) illustrates the vinyl mask used on the fabrication process step C. As it was previously explained, this mask is cut with a laser to allow the gold deposition with the desired distribution. Figure 5.19B shows the final result of the MEA on PMMA substrate with the PMMA square bonded to the MEA with a biocompatible, two component, room temperature curing epoxy (EPO-TEK 301, Epoxy Technology). This square permit to hold the cell culture with

medium. Finally, figure 5.19C is very similar to figure 5.17C, in which an enlarged image of the electrode covered by the SU-8 is shown. The hole that release the gold electrode is about 100 μm. This image demonstrates that the aspect-ratio of SU-8 does not depend on the MEA substrate.

The MEA on PMMA substrate presents several advantages with respect to the MEA on glass substrate. Firstly, the adhesion between SU-8 and PMMA is much stronger than between SU-8 and glass. Thanks to that, the seed layer of SU-8 can be used as an intermediate layer on PMMA substrate to improve the adherence of gold to the substrate, which is not good neither on glass nor PMMA. Moreover, the passivation layer of SU-8 over PMMA substrate has also a good adherence, but not over glass substrate. Despite the best results during the fabrication process have been obtained for the MEA on PMMA substrate, both chips, on glass and PMMA substrates, has been used for the experiments carried out with cells.

SK-N-SH experiments: results and preliminary conclusions

According to what has been explained at the beginning of this section, the described MEAs on transparent substrates, glass and PMMA, have been preliminary tested by performing some cell culture experiments with neuroblastoma cells (SK-N-SH) to demonstrate their biocompatibility and cell viability. However, these tests are still running and obtained results are not definitive. Nevertheless, what it is included below is a proof of concept of the presented devices, to demonstrate its potential as the starting point of the national project which continues the part of this thesis work related with cell culture and electrical recording of cells activity.

As it has been previously mentioned, neuroblastoma cells (SK-N-SH) have been cultured in the presented MEAs on transparent substrates. Neuroblastoma is a tumor formed by neuronal precursors of the sympathetic nervous system (SNS), derived from the neural crests. Neuroblastoma differentiated cells present larger nuclei and cytoplasm than those undifferentiated, which are normally round and small with scant cytoplasm. Particularly, SK-N-SH cell line result interesting because it contains cells with three different phenotypes: sympathoadrenal neuroblasts (N), substrate-adherent non neuronal (S), and intermediate (I) [319].

Hence, in the following paragraphs, as it was done in the other biological experiments, a material and methods subsection is included to explain the cell line, incubation protocols, experimental setup, etc. Then, some experimental results are given as images of the cells growing over the MEA chip substrates. Finally, some comments about these preliminary results are explained, as well as the ongoing and future works.

Materials and methods

As it happened with other biological experiments, these tests have been developed in a

multidisciplinary environment, working together with specialist biologist in cell culture. Thus, the biological material has been provided by professor Inmaculada Domínguez of the department of Cell Biology of the University of Seville. The cell culture has been carried out by professor Domínguez and Clara Macias, a biochemical student, in the facilities of the department of Cell Biology.

MEA Sterilization method

The sterilization method carried out for these experiments is carried out as follow. Firstly, MEA chips are rinsed on ethanol 70 % prepared from ethanol 96 % (EMSURE). Then, the culture devices are rinsed on DI water (Thermo Scientific) for 15 minutes, changing the DI water for fresh solution and rinsing the chips 30 more minutes to eliminate any rest of ethanol. Finally, MEAs are exposed to UV light for 30 minutes, for their subsequent drying at 37°C inside an oven during, at least, 8 hours, for a complete evaporation of any rest of ethanol absorbed by the substrate.

Cellular culturing method

SK-N-SH cells were cultured in a petri dish of 78 cm^2 of area using standard methodologies, at 37°C in a humidified atmosphere in air with a 5 % of CO_2. DMEM (1x) + GlutaMAX (Dulbecco's Modified Eagle Medium, Gibco) complemented with 10 % fetal bovine serum (FCS) and 1 % penicillin/streptomycin has been used. Once the cell culture shows a confluence of over 75 %, cells are sub-cultured in the MEA chips. Firstly, the medium is removed from the petri dish and the cells are washed twice with 2 mL of PBS (Gybco). Then, 1.5 mL of sterile HyClone Trypsin Protease (GE Healthcare Hyclone) is added to the petri dish with cells for their incubation during 7 minutes at 37°C inside the incubator, to disaggregate the cells from the petri dish bottom. Next step consists on neutralizing the trypsin by adding 3.5 mL of DMEM (1x) + GlutaMAX (Dulbecco's Modified Eagle Medium, Gibco) complemented with 10 % fetal bovine serum (FCS) and 1 % penicillin/streptomycin. Cells are then deposited on a 15 mL conical centrifuge tubes (Corning Falcon) and shaken to avoid the aggregation of cells. Finally, cells are counted using a Neubauer chamber (Brand). The number of cells cultured in each MEA is 900000, being the effective culture area of each chip of 10.20 cm^2. The chip is filled with 2.8 mL of DMEM (1x) + GlutaMAX (Dulbecco's Modified Eagle Medium, Gibco) complemented with 10 % fetal bovine serum (FCS) and 1 % penicillin/streptomycin, placed on a petri dish and introduced in the incubator at 37°C in a humidified atmosphere in air with a 5 % of CO_2. The duration of the experiment is three days.

Cellular Viability Assays

To assess the cellular viability over the duration of the experiment, a standard MTT assays were performed. For preparing the MTT solution, MTT (3-(4.5-Dimethylthiazol-2-yl)-2.5-Diphenyltetrazolium Bromide, Molecular Probes) is dissolved in a proportion of 5 mg/mL in 50 mL of PBS. The resulted solution is filtered inside the laminar flow cabinet and kept in a sterile tube of 50 mL for its freezing. In our experiments, the MTT solution is

mixed with DMEM (1x) + GlutaMAX (Dulbecco's Modified Eagle Medium, Gibco), in a proportion of one part of MTT for 4 parts of medium (MTTd). Once the MTTd is prepared, medium is removed from the MEA chips. Then, 1 mL of MTTd is added to each MEA and incubated at 37°C in a humidified atmosphere in air with a 5 % of CO_2 for 3 hours. After that time, 0.8 mL of Sodium Dodecyl Sulfate (SDS), White Powder, Electrophoresis (Fisher BioReagents) is added to each MEA. After one night of incubation, the solution contained inside the chip is deposited in a 96 multiwell plate (Thermo Scientific) which is analyzed inside the multiskan sky microplate spectrophotometer (Thermo Scientific).

Results and discussion

Despite the experiments are still running and the obtained results are not already conclusive, a first approach of what has been done and achieved is presented. Thus, in the following paragraphs, both MEAs, on glass and PMMA substrates, are compared to test their biocompatibility and cell viability with SK-N-SH cells. The different experiments carried out are focused on demonstrating the cell viability of each material used to fabricated these MEAs, as well as to test the suitability of each fabrication method for cell culture applications. In this respect, we have used many different variation of the presented MEAs, including two controls (one on glass and another one on PMMA), another pair of MEAs on glass and PMMA substrates with electrodes but without SU-8, and two more completes MEAs on glass and PMMA substrates, that is with gold and SU-8, following the whole fabrication process explained before. The aim of these experiments is to check if there are any critical material which can affect the normal proliferation of cells during the culture. Each experiment has lasted for three days, being monitored each day by taking pictures of the culture with a microscope. At the end of the experiment, the MTT assays described on "Materials and methods" has been performed to test the cell viability. However, while the pictures taken during the experiments are presented, there are not enough data to show the MTT assays results.

Experimental results from a SK-N-SH cell culture in a MEA chip on glass substrate is shown in figure 5.20. Two types of MEA have been used, one with glass and no gold electrodes, and the other one with gold electrodes patterned on its surface. Cells proliferation and growth after one day of culture in a MEA chip on glass substrate is shown in figure 5.20A, in which a normal growth and proliferation of cells can be seen. Figure 5.20B represents the cell culture on glass substrate after three days of experiment, time during which the SK-N-SH have reached a high confluence and are extended all along the MEA surface. Figure 5.20C and 5.20D presents a SK-N-SH cell culture inside a MEA chip made of glass as substrate and gold as electrodes. Similarly as it was previously explained, figure 5.20C corresponds to the cell culture after one day of experiment, while 5.20D is related to the same culture but after three days of experiment. Finally, figures 5.20E and 5.20F represents the negative and positive control, respectively. According to the images, obtained results are very similar in both MEAs on glass substrate with and without gold electrodes patterned on its surface and the negative control, with good cell proliferation and morphology, and reaching a cell confluence in both cases in about three days of culture. There are no images of SK-N-SH cell cultures on glass substrate with SU-8 and gold,

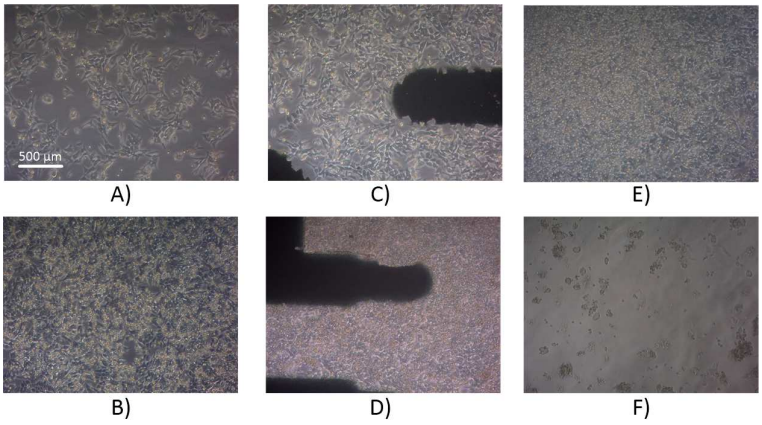

Figure 5.20 Cell proliferation and growth on glass substrate: A) Cells growth after one day of culture on glass substrate; B) Cells growth after three days of culture. Cells are in high confluence, filling the whole surface of the substrate; C) Cells growth after one day of culture on glass substrate with gold; D) Cells growth after three days of culture. Gold patterned on glass does not have a negative effect on cells growth and high confluence is achieved; E) Negative control; F) Positive control.

because several problems of adherence between SU-8 and glass provoke the detachment of the SU-8 layer from the glass, causing leakage and contamination in the culture.

All of this, have made us to find other alternatives, such as the MEA fabricated on PMMA substrate, whose fabrication process has been explained before. The main difference between both MEAs is related with the adherence of the SU-8 to the substrate, being much better on PMMA than on glass. For that reason, on the MEA on PMMA substrate, the adherence of gold to the substrate is improved by using a thin layer of SU-8 between the substrate and the metal, as well as the passive layer is also made of SU-8, which is deposited over the first layer of SU-8 and the gold patterned on it, demonstrating a good adherence and avoiding the contact between the cells and the gold tracks.

Experimental results from a SK-N-SH cell culture in a MEA chip on PMMA substrate is shown in figure 5.21. Up to three types of MEA have been used for these tests, being one of them a MEA made of PMMA, but without gold nor SU-8. Another MEA does include gold electrodes patterned on PMMA surface. The last one is a "complete" MEA with gold electrodes and SU-8 on PMMA substrate. Cells proliferation and growth after one day of culture in a MEA chip on PMMA substrate without gold or SU-8 is shown in figure 5.21A, in which cells are growing and proliferating as expected. Figure 5.21B represents the cell culture on PMMA substrate after three days of experiment, time during which the SK-N-SH have reached a high confluence and are extended all along the MEA surface. Figure 5.21C and 5.21D presents a SK-N-SH cell culture inside a MEA chip made of PMMA as substrate and gold as electrodes. Similarly as it was previously explained,

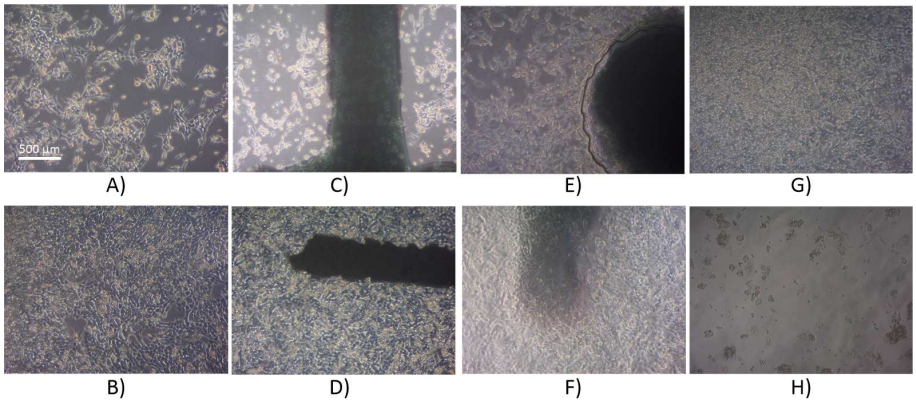

Figure 5.21 Cell proliferation and growth on PMMA substrate: A) Cells growth after one day of culture on PMMA substrate; B) Cells growth after three days of culture. Cells are in high confluence, filling the whole surface of the substrate; C) Cells growth after one day of culture on PMMA substrate with gold; D) Cells growth after three days of culture. Gold patterned on PMMA does not have a negative effect on cells growth and high confluence is achieved; E) Cells growth after one day of culture on PMMA substrate with SU-8 and gold; F) Cells growth after three days of culture. SU-8 deposited on PMMA with gold does not have a negative effect on cells growth and high confluence is achieved; G) Negative control; H) Positive control.

figure 5.21C corresponds to the cell culture after one day of experiment and, as can be seen, cells are growing over PMMA and gold indistinctly. Figure 5.21D is related to the same culture but after three days of experiment. Finally, figures 5.21E and 5.21F exhibits a SK-N-SH cell culture inside a MEA chip made of PMMA as substrate, with gold and SU-8, after one day and three days of experiment, respectively. In both images, cells are growing and proliferating with a correct morphology. Moreover, in figure 5.21F, as can be observed, cells are growing over both the gold electrodes and the SU-8 layer. Negative and positive controls are also included for these experiments in figures 5.20G and 5.20H. According to the images, obtained results are very similar in the three types of MEAs on PMMA substrate used for these tests. Cell proliferation and morphology is very similar between the cell culture performed on our fabricated MEAs on PMMA substrate and the negative control. In addition, cell confluence is reached in all cases in about three days of culture, which suggests a good behavior of the presented MEA for cell culture.

Table 5.2 summarizes the different MEAs used for the SK-N-SH cells experiments and the figure which corresponds to the experimental results of each one.

Table 5.2 MEAs used on SK-N-SH cells experiments.

Type of MEA	Figure
Glass substrate	Figures 5.20A and 5.20B
Glass substrate with gold	Figures 5.20C and 5.20D
Negative control	Figures 5.20E and 5.21G
Possitive control	Figures 5.20F and 5.21H
PMMA substrate	Figures 5.21A and 5.21B
PMMA substrate with gold	Figures 5.21C and 5.21D
PMMA substrate with gold and SU-8	Figures 5.21E and 5.21F

Conclusions of the MEAs on transparent substrates

Obtained results on glass substrate suggest that, despite it is possible to keep alive and proliferate cells inside our MEA on glass substrate, gold adhesion to glass is not reliable, as well as it is difficult the use of SU-8 as a passive layer to cover the gold tracks due to the lack of adherence between SU-8 and glass. On the other hand, our MEA fabricated on PMMA as substrate also show similar results in terms of cell proliferation and cell morphology. However, there are some important advantages with respect to the MEA on glass substrate. Firstly, the adherence between the substrate and gold, as well as between the substrate and SU-8, has been considerable improved. Secondly, the use of PMMA as substrate allows modifications on its shape by simple micromilling or laser cut processes, being possible even the integration of microfluidic structures on the substrate through those methods.

6 Conclusions and future works

6.1 Conclusions

This thesis work has resulted on the **creation of valuable knowledge** for the design and development **LOC** platforms for biomedical applications related with the culture of **cells and tissues** and their **electrical treatment and behavior**. The different systems presented in this PhD involve components or functions with high impact in the state of the art. Main contributions of this thesis work are summarized as follows.

Design, fabrication and electrical characterization of a MEA on PCB

The main novelty of this device lies on its innovative **cost effective process** which uses biocompatible materials that make it suitable for biological applications. Moreover, the **integration** of microheaters, by using the copper tracks as actuators, and temperature sensors in the same PCB of the MEA, improves its functionality.

In addition, the **electrical characterization** of the MEA has been performed, demonstrating the correct behavior of the gold microelectrodes. Successful experiments have been carried out in relation to the detection of low level electrical signals and their subsequent amplification. The possibility of controlling the MEA through a user-friendly Labview program, including the electrical behavior and the **temperature and heating control**, makes this device very attractive for its use on cell and tissue culture applications.

System for retinal culture and electrostimulation

The main novelties of this system lie on: the LOP, which integrates both parts, the MEA and the microfluidic structure, in the same platform; the cost effective fabrication process of the MEA with **gold microelectrodes of 25 μm** of diameter; its **user-friendliness** thanks

to an easy experimental setup, including the insertion and extraction of the biological sample, and the control of the system through an intuitive interface; the **recreation of the culture conditions**, including heating, temperature control and fluid flow, assuring the **sterility and watertightness**; and the possibility of **electrostimulating** the culture through the gold microelectrodes.

The presented system has been demonstrated to be suitable for its application on **organotypic cultures**. Particularly, several experiments with mice retinal explants have been entirely carried out inside our LOP for, **at least, 7 days**, presenting similar results to those obtained for the same culture, but performed through traditional methods inside a CO_2 incubator. In addition, after many experiments, we have observed that **RP retinal explants** provided with periodic **electrical stimuli** along the whole-tissue culture in the proposed LOP display a **better preservation** of the tissue structural features and **lesser apoptotic cell death** in the photoreceptor cell layer, compared with non-treated RP retinal explants.

In comparison with other devices reported in the literature presenting LOCs or microfluidic culture platforms, this system integrates all the components needed to carry out an autonomous organotypic culture, with perfusion, heating, temperature control and electrostimulation, conjointly controlled through a user-friendly program. The obtained results demonstrate the suitability and reliability of the presented LOP for culture and electrostimulation applications.

PC-3 cells culture and extracellular electrophysiology

The contributions obtained from this work are as follows. It has been demonstrated for the first time the feasibility of a real time and highly sensitive system to understand the **signaling pathways among prostate cancer cells**. The obtained results show that PC-3 cells exhibit a low frequency electrical activity, between 0.1 Hz and 10 Hz, with two clearly differentiate patterns: one sporadic and asynchronous and the other synchronous and quasi-periodic. In addition, the use of Gd^{3+} as a Ca^{2+} inhibitor has proved the **involvement of** Ca^{2+} **channels** in the electrical activity of PC-3 cells population.

This work was entirely developed during the stay at the University of Bath. The extracellular electrophysiology in the prostate cancer cell model PC-3 has resulted in a successful collaboration between this University of Bath and the University of Seville.

Microelectrode array for cell culture applications

The main novelty of this MEA is its reliable and cost effective fabrication process to create **3D gold microelectrode** with 100 μm of diameter and about 25 μm of height. The use of a **PCB** of FR4 and copper as substrate facilitates the integration of other components such as electronics or microfluidic together with the microelectrodes array.

The impedance of both the WB MEA and the 3D MEA have been characterizing, demonstrating how the 3D MEA improves considerably the electrical behavior of the WB

MEA. The impedance and baseline noise, around 10 μV_{pp}, show similar values to those found in the literature. Moreover, its suitability to carried out a PC-3 cells culture and acquire their electrical signals has also been demonstrated.

The need of transparency lead us to evolve from the PCB to transparent substrates to fabricate the MEA. For that reason, we have presented some approaches of MEAs on transparent substrates. The best results were obtained for the **MEA fabricated on PMMA substrate**. The main advantage is the cost effective fabrication process and its biocompatibility. There are not enough data to confirm the cell viability of this MEA made of PMMA, but several successful cultures of SK-N-SH cells performed inside this MEA suggest its biocompatibility and suitability for cell culture applications.

Main conclusions

During this thesis work we have developed a culture LOC system with gold microelectrodes, which has been successfully tested with a mice retinal explants culture. We are able to maintain the culture for, at least, 7 days, as well as we have provided neuro-protection through electrical electrostimulation to mice retinal explants with RP. In order to make this device suitable for its application on cell culture, the MEA has been enhanced by improving the electrical behavior of the microelectrodes. We have characterized for the first time the electrical activity of prostate cancer cells (PC-3). To improve our WB MEA, we have fabricated a 3D MEA on PCB, which improve the impedance and baseline noise with respect to the WB MEA. The last part of this thesis work has been focused on developing MEAs in transparent substrate to allow its use for cell culture with optical applications. These transparent MEAs have been tested with neuroblastoma cells, whose preliminary results suggest a good biocompatibility and cell viability.

6.2 Future works

In this thesis work, there are two main research lines which can be continued in different ways: one related with the culture and electrostimulation on RP mice retinal explants; the other one about the development of MEAs for cell culture and electrical recordings. The proposed future works of this thesis are outlined below:

LOC for retinal explants: future works

- Deepen the understanding of neuroprotection mechanisms elicited by electrical stimuli on RP retinas, by optimizing the electrical stimuli and its effect on the biological material.

- Integrate sensors inside the LOP to carry out metabolic studies or drug discovery experiments.

- Study the effect of light stimulation on retinal cultures carried out in the LOP.

- Expand the applicability of the LOP to develop cultures of more types of tissues on which the electrical stimulation, metabolic studios or drug administration experiments can be performed.

- Improve our system by integrating a closed perfusion circuit, instead of a external pump, to feed the biological material.

- To continue the work with the retinal explant cultures, there is a granted project named: "Lab-On-Chip de Electro-Estimulación, Para El Estudio In-Vitro de Cultivos de Retina de Larga Duración: Retina-On-A-Chip" (US-1265983). This project started at the beginning of 2020.

MEAs for cell culture and electrical recordings: future works

- Enhance the fabrication process to obtain microelectrodes with a lower impedance, on both PCB and transparent substrates. The approaches presented on this thesis work have a huge potential and its development is still in a early stage.

- Improve the electronic circuit to reduce noise and minimize losses ratio.

- Develop a reliable fabrication process to obtain 3D microelectrodes on transparent substrates.

- Integrate a microfluidic circuit together with the MEAs fabricated on transparent substrates, as well as heating and temperature control to perform a cell culture with electrical recordings without using a CO_2 incubator.

- Isolate single neurons, connecting those neurons between them and with a computer program to learn their behavior or even "talk" to the neurons through that program.

- To follow-up the development of MEAs for cell culture and electrical recordings applications there is also a granted project named "Integración de Opto-Electroestimulación y Procesamiento de Señales para el Estudio in-Vitro de Larga Duración del Comportamiento Neuronal" (RTI2018-100773-B-C33). This project is running since December 2019.

Thanks to the creation of a recent spin-off named **"Biodevices Technologies"**, we are able to transfer all this technology and find a real application with **high impact on society**. Thus, I am continuing this thesis work through this company, of which I am co-founder, by **developing marketable devices** based on this PhD.

Annex A

Publications

In this appendix, the scientific publications directly related with this thesis work are presented. There have been up to three publications in high impact factor journals, as well as two publications on international congress.

International journal publications

Cabello, M., Aracil, C., Perdigones, F., Mozo, M., de la Cerda, B., & Quero, J. M. (2018). Gold microelectrodes array embedded in PDMS for electrical stimulation and signal detection. Sensors and Actuators B: Chemical, 257, 954-962.

Cabello, M., Ge, H., Aracil, C., Moschou, D., Estrela, P., Manuel Quero, J., ... & RF Rocha, P. (2019). Extracellular electrophysiology in the prostate cancer cell model PC-3. Sensors, 19(1), 139.

Cabello, M., Mozo, M., De la Cerda, B., Aracil, C., Diaz-Corrales, F. J., Perdigones, F., ... & Quero, J. M. (2019). Electrostimulation in an autonomous culture lab-on-chip provides neuroprotection of a retinal explant from a retinitis pigmentosa mouse-model. Sensors and Actuators B: Chemical, 288, 337-346.

Congress contributions

Cabello, M., Aracil, C., Perdigones, F., & Quero, J. M. (2017, February). Conditioning lab on PCB to control temperature and mix fluids at the microscale for biomedical applications. In 2017 Spanish Conference on Electron Devices (CDE) (pp. 1-4). IEEE.

Cabello, M., Aracil, C., Perdigones, F., Quero, J. M., & Rocha, P. R. (2018, November).

Lab-on-PCB: Low Cost 3D Microelectrode Array Device for Extracellular Recordings. In 2018 Spanish Conference on Electron Devices (CDE) (pp. 1-4). IEEE.

Sensors and Actuators B 257 (2018) 954–962

Contents lists available at ScienceDirect

Sensors and Actuators B: Chemical

journal homepage: www.elsevier.com/locate/snb

Gold microelectrodes array embedded in PDMS for electrical stimulation and signal detection

Miguel Cabello*, Carmen Aracil, Francisco Perdigones, Marta Mozo, Berta de la Cerda, José M. Quero

University of Seville, Avda de los Descubrimientos sn, 41092, Spain

ARTICLE INFO

Article history:
Received 25 May 2017
Received in revised form 24 October 2017
Accepted 5 November 2017
Available online 9 November 2017

Keywords:
Sensors
MEA
Micro-electrodes

ABSTRACT

In this paper, an innovative low cost fabrication process of a biocompatible MEA, composed of a group of gold microelectrodes embedded in a cavity filled with PDMS is presented. This MEA is part of a more complex system, which has been designed to stimulate, detect and amplify electrical signals. It is possible to control the temperature and heat the MEA, with the purpose of making this system suitable for biomedical application, such as cell or tissues culture, or monitoring neuronal activity. A deeply characterization of the MEA has been performed. The main experiment carried out consists in the introduction of an electrical signal through a gold microelectrode. This electrical signal is transmitted between microelectrodes through a water-based salt solution, in particular with Phosphate Buffered Saline (PBS). In order to have the possibility of amplifying a wide range of signals, different INA 333 amplifiers with different gains, between 3.13 and 213, have been included. Nevertheless, the gain could be easily modified. The behavior of the system is controlled via Labview software, provided by National Instruments. This program allows for detecting the stimulus, the stimulation and an accurate measurement of the temperature's system. An electronic circuit, which includes the conditioning circuits needed to run the whole system, is used as an interface between the MEA and the Labview software. The proper functioning of the system introduced, and the stimulation and detection of electrical signals, as well as its amplification through a water-based salt solution, using gold microelectrodes embedded in PDMS, have been demonstrated. A survival test with mice retinas has been performed to demonstrate the biocompatibility of the MEA.

1. Introduction

The development of microelectrode arrays (MEAs) is a well-stablished field for measuring a plenty biological and chemical parameters [1–4]. Microelectrode arrays have been used for many applications. Some of them that could be highlighted are: neurotechnology field, for instance, for in vitro screening of metal oxide nanoparticles for effects on neural functions using cortical networks on MEAs [5]; drug discovery, for example, in drug evaluations using neuronal networks cultured on MEAs [3,6]. The configuration of MEAs makes possible the study of variables in a small area. Thanks to this, MEAs are an interesting sensing method to be integrated on Lab-on-Chip (LOC) applications [7,8].

There is a high number of fabrication materials of MEAs. This variety implies different fabrication processes. Regarding these materials, silicon is the most widely used as base material [9]. The use of silicon is logically related with the typical fabrication process of microelectromechanical systems (MEMS), for example, photolithographic processes, wet etching or reactive ion etching (RIE). Not only the silicon, but also, and especially, the expensive facilities, with very demanding requirements needed to manipulate silicon, have led to use new materials and processes. For instance, the use of Parylene C is an alternative to silicon as base material [10,11]. In addition, silicon is a rigid material, making it not suitable for those applications which require flexibility. This fact together with the cost makes the elastomer polydimethylsiloxane (PDMS) [12] a good choice to fabricate flexible and inexpensive MEAs [13]. In the previously commented fabrication processes, metal or conductive lines have to be integrated. For instance, gold is frequently utilized when biocompatible characteristics are necessary.

Microelectrode arrays are often used for in vivo applications in order to record biological activity [14,15]. However, they can also be used for studying the properties of biological or chemical fluid samples [16,17]. Regarding this last application, together with the commented small-size characteristic, the integration of MEAs with microfluidic circuits means a necessary step in the fabrication processes to develop a complete system. Many often, a MEA requires the management of multitude electronic signals, that is, every sin-

* Corresponding author.
E-mail address: mcabellov@gte.esi.us.es (M. Cabello).

https://doi.org/10.1016/j.snb.2017.11.026
0925-4005/

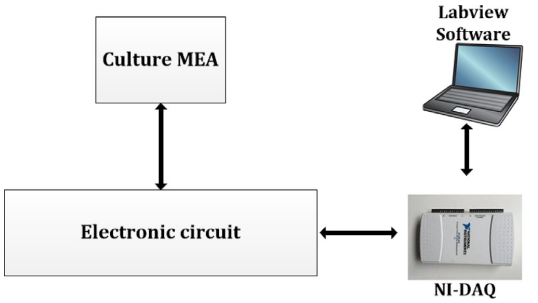

Fig. 1. Brief scheme to understand how each part of the whole system is connected among them.

gle microelectrode of the array has a conductive line towards the signal processing circuit. All these conductive lines have to be integrated with the MEA and the rest of the system. This implies an additional effort in the integration to achieve a complete system. The previously commented microelectrode array could be used, not only for measuring, but also for actuating over the sample under study, and reading its response.

Electronic circuits can be used together with optical systems for biological or chemical applications [18–20]. If the system has to be actuated using light, an important requirement to be fulfilled is the transparency. In this case, the transparency of the PDMS or glass makes possible to use these materials with optical applications. The optical sensing is usually dependent on conventional microscopes or fluorescence inverted microscopes to certain studies [21]. For this last sensing method, the requirement of transparency is even more demanding, because the light has to cross the whole system.

The system outlined in this paper is divided into three different parts: a MEA, an electronic circuit and the control software. The aim of this research work is to develop a MEA which could be used in biological applications. An inexpensive fabrication process of a MEA, where a group of gold microelectrodes are embedded in polydimethylsiloxane (PDMS), is described. In addition, the configuration and transparency of the structure of the MEA makes possible the use of different combinations of optical and electronic actuations and sensing, including conventional or inverted fluorescence microscopes. Some conditioning circuits has been implemented in an electronic PCB. Finally, with the purpose of controlling the behavior of the whole system, Labview software, provided by National Instruments, has been used to execute a program.

Fig. 1 shows a brief scheme with the different parts of the system connected to each other. As can be seen, the MEA is connected to the electronic circuit, which is controlled by a computer through a NI-DAQ device. A Labview software program allows for monitoring the whole system. These parts are explained in the following sections.

The rest of the paper is structured as follows. In Section 2, the design and fabrication of the MEA is described. Next, in Section 3, the electronic circuit and the software are explained. After that, the experimental results to characterize the behavior of the system are shown and discussed in Section 4. And finally, the main conclusions of this research work are summarized in Section 5.

2. MEA: design and fabrication process

2.1. Design

This is the main part of the system, and that influences in the design of the others parts of the system. The function of the MEA is the recording and stimulation through gold wires embedded in PDMS. This MEA is intended to be part of a more complex system for biological applications, such as cell or tissue culture, or monitoring neuronal activity. The fluid samples are placed over the effective working area, which is the surface where the end of the gold microelectrodes embedded in PDMS are in contact with the sample, allowing the transmission and measurement of the electrical signal. The dimension of the effective working area is 5 mm × 5 mm. As can be seen in Fig. 2 (step g), this structure has been designed in such a way that the end of the gold wires is not covered by the PDMS, just to allow a good contact between the fluid and the gold microelectrodes. The gold microelectrodes have been made by the wedge bonding technique [22]. Four different effective working areas, that permit separated measurements, have been designed. To improve the functionality of the MEA, a temperature control module is implemented. For this purpose, a microheater and a Negative Temperature Coefficient (NTC) ther-

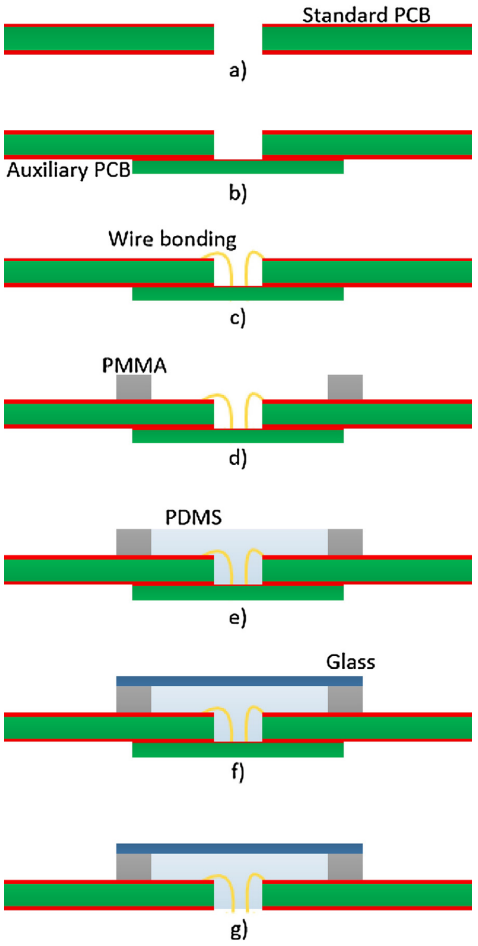

Fig. 2. Steps of the fabrication process, using the wire bonding technique: (a) commercial PCB of FR4 and copper; (b) a auxiliary PCB is bonded to the commercial PCB; (c) gold microelectrodes with a diameter of 25 μm are placed using the wire bonding technique; (d) a frame of PMMA surrounds the gold microelectrodes; (e) the gold microelectrodes cavity is filled with PDMS, embedding them; (f) a glass coverslip is placed over the PDMS; (g) once the PDMS is cured, the auxiliary PCB is released.

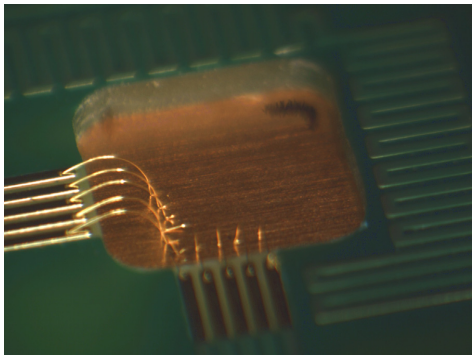

Fig. 3. Gold microelectrodes placed using the wire bonding technique.

mistor have been integrated in the MEA. In this way, the heating and the temperature measurement could be performed.

2.2. Fabrication process

The fabrication process of the MEA includes an innovative procedure to create a low cost microelectrode array, Fig. 2. A novel microelectrode array fabrication process has been developed, embedding the gold electrodes in PMDS. For this purpose, a printed circuit board (PCB), composed of FR4 of 800 μm thick and double side copper layer, of 35 μm thick, has been used. A micromilling machine has been utilized to obtain the cavities where the gold microelectrodes will be embedded in PDMS (step (a)). After the micromilling, a typical photolithographic process has been implemented to pattern the copper and create the paths that are completely covered by a resin layer, with the exception of the part of the copper pads where the electrodes are located, which have a gold coating. The wire bonding technique has been conducted to place the gold electrodes. This is the most critical part of the process because the gold wires must be correctly located before the embedding step. Thus, another piece of PCB with one side of copper, named from now on auxiliary PCB, is put under the main PCB that contains the MEA, with the objective of using the copper layer to execute the wire bonding technique between both metals (step (b)). The two pieces of PCBs are assembled with screws in such a way that the gold wire can be placed between the copper paths of the MEA, with a gold coating, and the copper side of the auxiliary PCB. Fig. 3 shows how the gold microelectrodes are placed using the wire bonding technique, whereby a 25 μm diameter gold wire is placed (step (c)).

Once the wire bonding technique is completed, a Poly methyl methacrylate (PMMA) frame of 2 mm thick is bonded to the MEA,

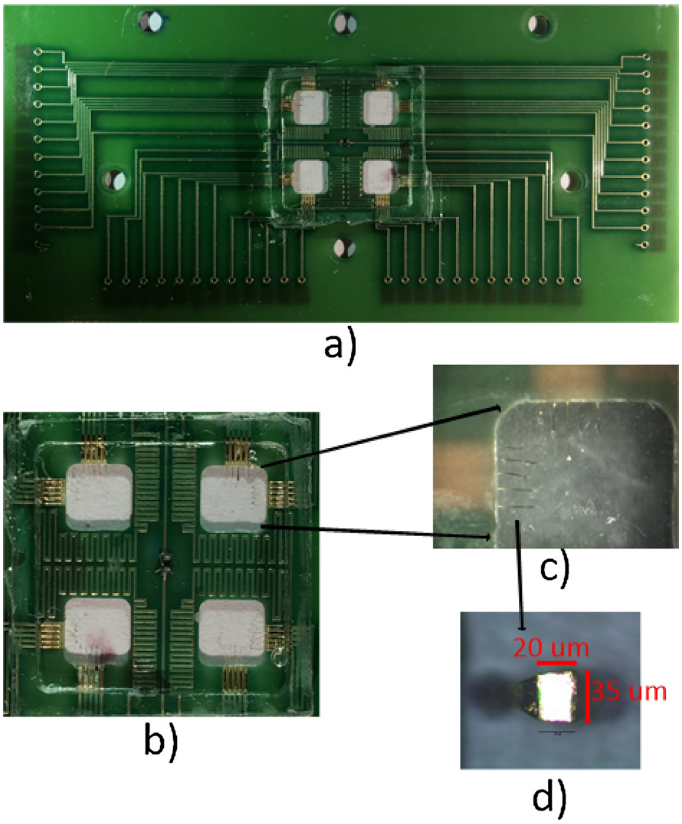

Fig. 4. (a) Top view of the complete MEA; (b) top view of the four effective working areas, the microheater and the NTC thermistor; (c) one of the effective working area with gold microelectrodes embedded in PDMS; (d) end of a gold microelectrode with dimensions: 20 × 35 μm.

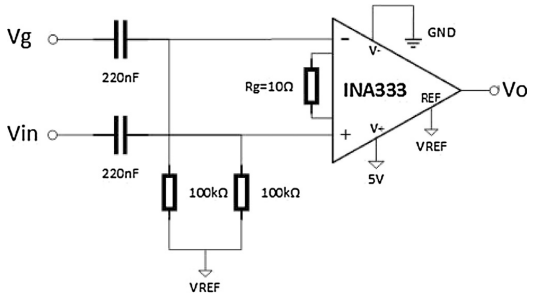

Fig. 5. INA 333 conditioning circuit.

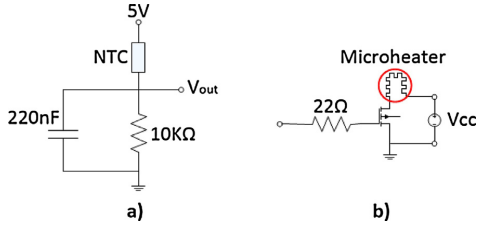

Fig. 6. (a) Voltage divider to measure temperature through a NTC thermistor; (b) MOSFET transistor that allows or denies the pass of current to the microheater.

with the purpose of controlling the deposition of the PMDS (step (d)). The next step is the deposition of the PDMS to embedded the electrodes (step (e)). Immediately after the deposition of PDMS, a glass coverslip is placed over the PMMA frame (step (f)). PDMS needs 90 min at 65 °C inside an oven to cure completely. After PDMS is cured, it is possible to release the auxiliary PCB (step (g)), whereupon the MEA is completely fabricated and the gold electrodes are correctly embedded in the PDMS, with the end of the electrode out of the PDMS, what is called in the paper "effective working area".

The result of the fabrication process can be seen in Fig. 4. This figure shows the whole MEA, including an extended picture of the gold microelectrodes.

3. Electronic circuit and software

3.1. Electronic circuit

The electronic circuit has been designed as an interface between the MEA and the software. Some conditioning circuits are included in order to amplify the voltages obtained through the gold microelectrodes, measure the temperature and control the heating. There are also some components that permit the connection with the MEA and with the computer.

A low power precision instrumentation amplifier [23] has been used to amplify the signal received from the effective working area through the gold microelectrodes. According to its datasheet, the INA's gain is:

$$A_d = 1 + \frac{2R_1}{R_{gain}} \tag{1}$$

The use of an INA allows the easy modification of the amplification that could be needed depending on the application, simply varying the value of R_{gain}.

A conditioning circuit is necessary for the correct operation of the amplifier, indispensable to reduce the noise that could affect the electronic components, Fig. 5. The signal is captured through the gold wires and transmitted to the electronic circuit, which amplifies the signal through the INA. A differential measure is done between two gold microelectrodes from the effective working area, one of them is common to all the amplifiers of the same effective working

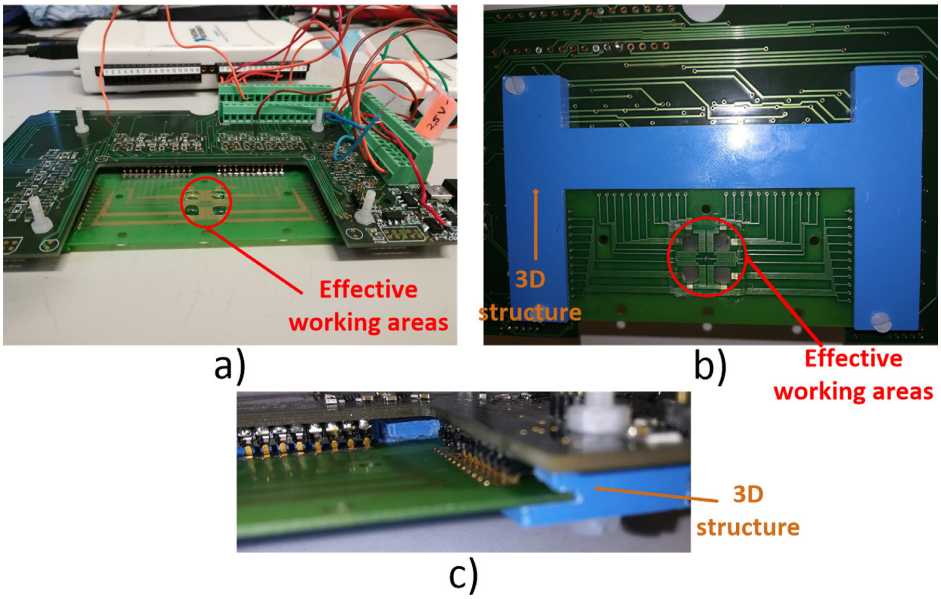

Fig. 7. (a) Complete setup of the MEA, the electronic circuit and the NI-DAQ devices; (b) bottom view of the electronic circuit and the MEA, with the 3D structure in blue color; (c) contact between the MEA and the electronic circuit by using battery contact. (For interpretation of the references to color in this figure legend, the reader is referred to the web version of the article.)

area and give the voltage V_{in}. The voltage V_g comes from a different electrode in every amplifier.

The others conditioning circuits consist of a voltage divider to measure the temperature through a NTC thermistor, and a MOSFET transistor that works as a switch, allowing or denying the pass of current depending on the temperature, Fig. 6. An external power source is used to supply the electronic circuit and the microheater contained in the MEA. Specifically, 5 V/1 A are needed to power the electronic circuit.

The typical photolithographic process is performed to fabricate the electronic circuit. A commercial printed circuit board (PCB) of 1.6 mm of thickness of FR4 and 35 μm of thickness of copper has been chosen. The MEA and the electronic circuit are joined through male 4 way battery contacts. A structure fabricated with a 3D printer makes possible a good contact between both parts, as it is shown in Fig. 7b and c.

3.2. LabView control software

LabView, provided by National Instruments, is the software chosen to implement the program that controls the system. Two data acquisition devices, NI-DAQmx series, have been programmed in order to control the system. These NI-DAQmx series devices permit the generation of electrical signals, that could be used as a stimulus in each effective working area through the gold electrodes, and the reception of electrical signals. They could also monitor the temperature of the system thanks to a NTC thermistor included in the MEA. This NTC thermistor is connected to the electronic circuit and, consequently, to the LabView program, where a bar that indicates the temperature inside the MEA is implemented. With this software, it is also possible to control the operation of the microheater. A MOSFET transistor is activated, allowing the pass of current through the microheater, when the temperature is under a pre-defined temperature, and it will be off when the temperature is over a pre-defined temperature, operating as a Pulse Width Modulation (PWM). Temperature control permits the maintenance of a specific temperature, which could be indispensable for some kind of samples. Nevertheless, the temperature may not be higher than the maximum temperature the used materials can withstand.

4. Experimental results and discussion

The system is tested to show its behavior. The main objective of these experiments is to demonstrate the correct functioning of the gold electrodes. For this purpose, an electrical signal is introduced through one microelectrode and captured through other electrode

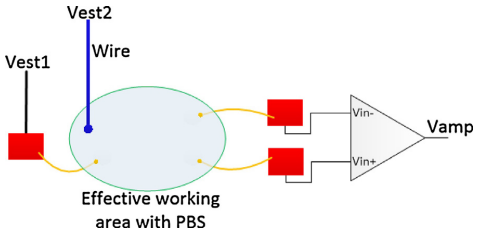

Fig. 8. Brief scheme of the MEA, in order to understand how the detection of signals has been carried out.

of the same effective working area. Then, this signal is amplified. It is also tested the operation of the NTC thermistor to control, via LabView software, the temperature of the microheater included in the MEA. The complete setup used during experiment is shown in Fig. 7a.

The most critical part of the electronic circuit is the low power precision instrumentation amplifier (INA 333). To assure a correct behavior of the amplifier, different tests have been done modifying the gain of the INA. The objective of this system is to detect a signal and amplify it. One of the most recurrent problems to solve during these tests is the noise and losses produced due to stimulation through a gold microelectrode that is intended to capture and amplify. According to the Eq. (1), for a fixed value of R_1 of 50 KΩ, Eq. (2) demonstrates how the gain of the INA only depends on the value of R_{gain}, and this value could be modified easily by choosing the adequate resistor. For the next experiments, different values of R_{gain} have been chosen, in order to obtain these gains: 3.13, 11, 101, and 213. Fig. 8 shows a scheme to understand how the measurements have been obtained.

$$G = 1 + \frac{100\ \text{K}\Omega}{R_{gain}} \tag{2}$$

The experiments carried out with the MEA consist on the introduction of an electrical signal (V_{est}) through one of the gold microelectrode and the detection of that signal through another gold microelectrode (V_{in}) and the amplification of it through the amplifier (V_{amp}), Fig. 8. In this case, a sine waveform is introduced, and its peak-to-peak voltage is measured. A Phosphate Buffered Saline (PBS) is the medium utilized to allow the transmission of the signal from the emitter to the receiver gold microelectrode. Once the signal is received by the gold microelectrode, it is passed through the conditioning circuit of the INA, where it is correctly amplified. The amplifier is fed with 5 V and needs a reference volt-

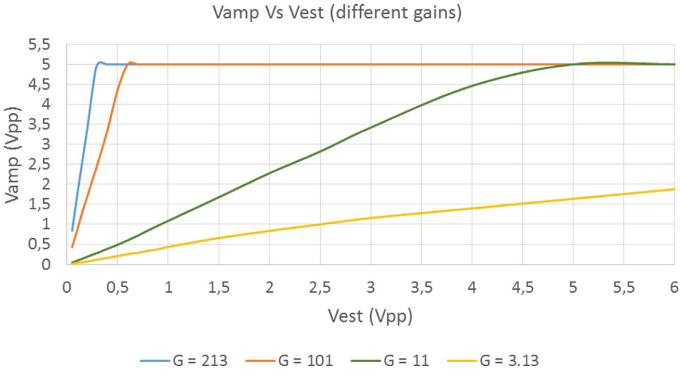

Fig. 9. Behavior of the system depending on the gain of the amplifier.

age of 2.5 V that is also the reference voltage of the effective working area where the measurement is done. Both voltages are supplied by the NI-DAQ.

The system has been evaluated for a wide range of values of voltages and gains, as can be seen in Fig. 9. The higher the gain, is the earlier the amplifier saturates. Despite the fact that in some cases the amplifier saturates for a low level signal (higher gains), the wide range is useful for the lower gains. Fig. 9 can also be used to have an approximated behavior of the system for a gain between 3.13 and 213.

The losses ratio results of dividing V_{est} and V_{in}, Fig. 10. The characterization of the losses ratio of the system according to the gain has been carried out. In order to obtain the value of the losses ratio through the experimental measurements, the peak-to-peak input voltage V_{in} that reaches the amplifier is needed. V_{in} is calculated by dividing the peak-to-peak amplified voltage (V_{amp}), measured in the INA output, and the gain of the amplifier. Once this voltage has been calculated, the losses ratio is calculated, Fig. 10. Fig. 10 demonstrates how the gain influences in the losses ratio. Therefore, it has been demonstrate that the higher the gain is, the higher the losses ratio is.

The way the electrical signal is transmitted to the fluid sample (PBS) placed over the effective working area is carried out through one of the gold microelectrode embedded in PDMS. (V_{est1} in Fig. 8) Nevertheless, in order to demonstrate that the main losses are due to the gold microelectrode, and not because of the PBS, a wire, which is directly connected to the stimulus generator, and whose end is immersed in the PBS, has also been used to transmit the electrical signal. (V_{est2} in Fig. 8) Once the signal is introduced into the effective working area, it is always detected through a gold microelectrode, and subsequently amplified. The experiment demonstrates that the losses ratio is different depending on the way the electrical signal is introduced. As can be seen in Fig. 11, if the signal is transmitted to the effective working area with the PBS through a gold microelectrode (the signal would pass through two gold microelectrodes), the losses ratio is approximately double than if the signal is introduced to the PBS, not through the gold microelectrode, but directly through a wire (the signal would pass through one gold microelectrode), which adds no losses in compari-

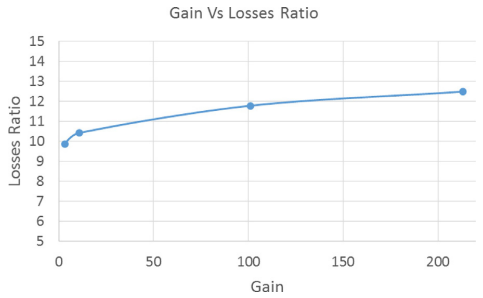

Fig. 10. Losses ratio of the system depending on the gain of the amplifier.

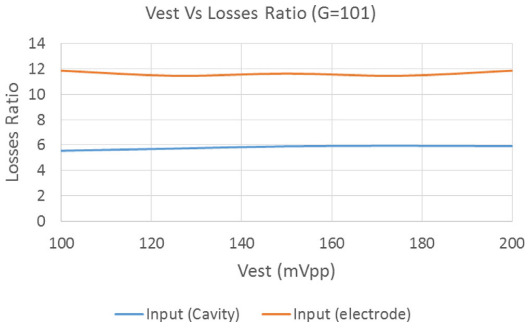

Fig. 11. The losses ratio depends on how the signal is introduced into the effective working area with the PBS.

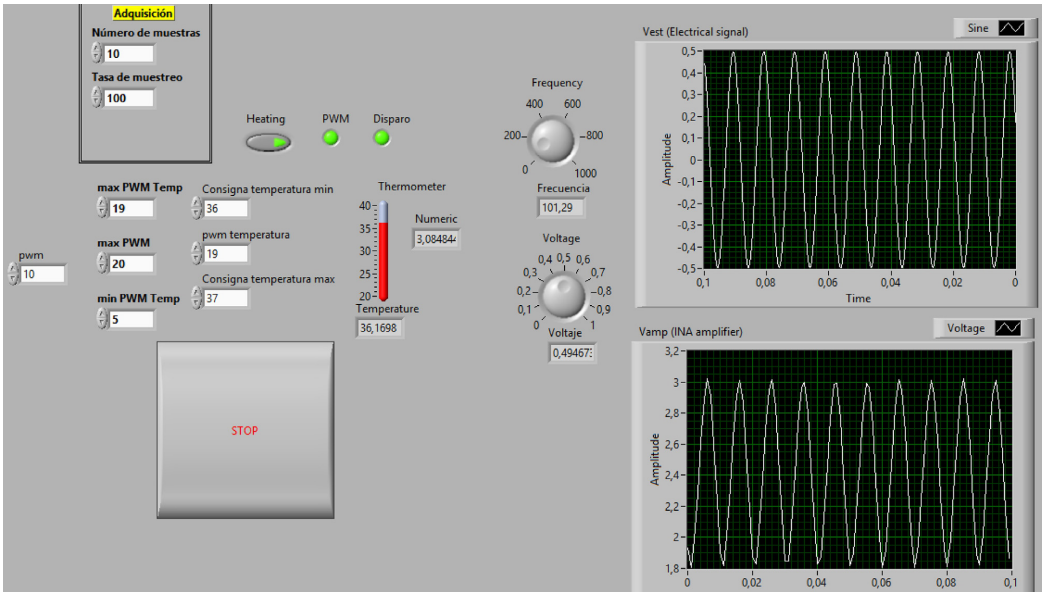

Fig. 12. Labview interface to control both the temperature, and the heating velocity; and to perform the electrical stimulation and detect the signals.

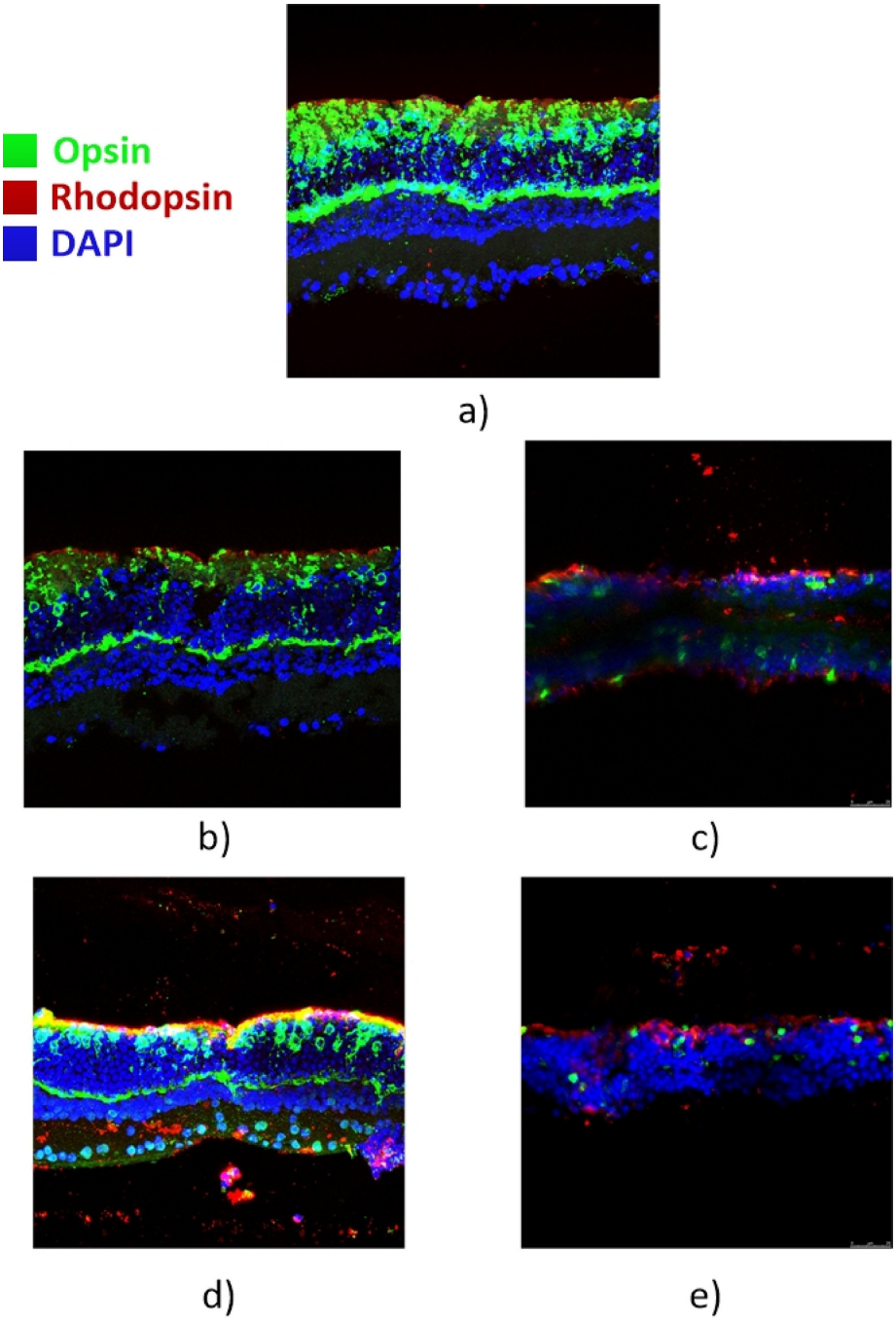

Fig. 13. Immunohistological study: (a) wild-type mice retina after its extraction; (b) wild-type mice retina after seven days of culture in a cell culture plate; (c) albino mice retina after seven days of culture in a cell culture plate; (d) wild-type mice retina after seven days of culture inside the MEA; (e) albino mice retina after seven days of culture inside the MEA.

son with the gold microelectrode. This result confirms that the main losses are due to the gold microelectrodes, and that the medium barely have an influence on the signal losses. In any case, this losses ratio could be easily characterized.

Labview software program allows the stimulation and acquisition of the amplified signal from the effective working area by the use of the a NI-DAQ device, from National Instruments. This NI-DAQ feeds the electronic components that are necessary, such as the INA amplifier, supply the voltage used as a reference (2.5 V) and could also acquire more than one signal at once. Temperature and heating velocity are also controlled with Labview software, and its behavior has also been demonstrated. It is possible to monitor the functioning of the whole system with the interface of Labview software. In other words, this system can be controlled with only a computer and the previously mentioned NI-DAQ. Fig. 12 shows the Labview interface used to monitor the system.

In order to validate the biocompatibility of the MEA, a survival test has been performed inside the presented device. This test consists on an organotypic retinal culture which has been kept alive for seven days. During this culture, a constant temperature of 37 °C is assured. Wild-type mice (C57BL/6, Jackson's Laboratory) have been used for the tissue dissection; albino mice (CD1, Jackson's Laboratory) have been used as a negative control for damaged tissue. The used culture media for the survival experiment has been Neurobasal-A (Gibco), which is the preferred culture media for retinal cultures [24,25]. The retinas have been placed over the MEA, one in every effective working area. To assure a correct grip between the retinas and the PDMS, a polyvinylidene fluoride (PVDF) membrane is placed on top of the tissues. A cell culture membrane (Millipore Millicell) is located over the PVDF membrane to allow the appropriate absorption of culture medium by the retinal explants.

The result of this survival test has been confirmed through an immunohistological study after seven days of culture. As a control, an organotypic culture of mice retinas has been carried out in a cell culture plate, and it has been compared to the same type of mice retinas, but cultured inside the MEA. Fig. 13a shows the normal structure of a healthy retina right after its dissection, in which the photoreceptors are marked specifically for the visual pigments, opsin in green and rhodopsin in red, and the nuclei of all the cells in the tissue are marked in blue with DAPI, which is a DNA stain. Fig. 13b and c shows a healthy (wild-type mice) and a damaged (albino mice) retina, respectively, after seven days of culture in a cell culture plate. Fig. 13d and e shows a healthy (wild-type mice) and a damaged (albino mice) retina, respectively, after seven days of culture inside the proposed MEA.

In the control retinal explants cultured in cell culture plates it is shown a clear difference in retinal structure, number of nuclei and photoreceptors between the healthy and the damaged retina. The same difference is observed when the retinas were cultured inside the proposed MEA. Moreover, in the albino mice retina cultured in a cell culture plate, the tissue bended over itself during the immunohistological study due to its higher degeneration, while the same type of mice retina cultured inside the MEA did not suffer that kind of damage. This demonstrates that the MEA is suitable for organotypic cultures, in this case mice retinas, without adding any additional damage to the tissues, in comparison with a traditional culture method. Thus, the biocompatibility of the presented MEA has been successfully demonstrated.

Concerning the fabrication process it is demonstrated the low cost of the whole system. All the materials that could be in contact with the PBS medium or with cells, neurons or cellular tissue are biocompatible. Only the MEA is disposable and must be replaced if it is going to be used in cell culture. Furthermore, due to the transparency of the PDMS utilized to fabricate the MEA, the system could be suitable for its implementation with a microscope.

5. Conclusions

A prototype system to receive and amplify an electrical signal has been developed and characterized. An innovative fabrication process is presented and carried out to make a microelectrode array (MEA) based on gold electrodes embedded in PDMS.

The low cost fabrication process allows the possibility of making a disposable MEA. The materials utilized are biocompatible, therefore, the MEA is suitable for bio-medical applications. Survival tests carried out with mice retinas demonstrate that this MEA could be used for medium-long term organotypic cultures.

A deeply characterization of the MEA has been performed, demonstrating the correct behavior of the gold microelectrodes. The experiments carried out in relation to the detection of a low level electrical signal and the subsequent amplification have been a success. The used water-based salt solution (PBS) allows the transmission of the signal from the emitter gold microelectrode to the receiver gold microelectrode.

The control and acquisition via Labview software make the whole system easy to implement and use. The possibility of seeing the waveform in a graph and compare it with the original signal introduced in the effective working area permits an easy monitoring of the behavior of the MEA. The parameters needed to maintain cells or tissues alive, such as temperature, could also be easily modified.

In future work, some applications of the proposed MEA will be performed in order to obtain biological parameters of organotypic cultures.

Acknowledgements

This work was supported by the Spanish Ministry of Economy, Industry and Competitiveness under grant TEC2014-54449-C3-2-R, BIOLOP.

The biological part of this paper has been possible thanks to Cabimer (Centro Andaluz de Biología Molecular y Medicina Regenerativa).

References

[1] A.F. Johnstone, G.W. Gross, D.G. Weiss, O.H.-U. Schroeder, A. Gramowski, T.J. Shafer, Microelectrode arrays: a physiologically based neurotoxicity testing platform for the 21st century, Neurotoxicology 31 (4) (2010) 331–350.
[2] X.-J. Huang, A.M. O'Mahony, R.G. Compton, Microelectrode arrays for electrochemistry: approaches to fabrication, Small 5 (7) (2009) 776–788.
[3] A. Stett, U. Egert, E. Guenther, F. Hofmann, T. Meyer, W. Nisch, H. Haemmerle, Biological application of microelectrode arrays in drug discovery and basic research, Anal. Bioanal. Chem. 377 (3) (2003) 486–495.
[4] J.P. Seymour, N.B. Langhals, D.J. Anderson, D.R. Kipke, Novel multi-sided, microelectrode arrays for implantable neural applications, Biomed. Microdev. 13 (3) (2011) 441–451.
[5] J.D. Strickland, W.R. Lefew, J. Crooks, D. Hall, J.N. Ortenzio, K. Dreher, T.J. Shafer, In vitro screening of metal oxide nanoparticles for effects on neural function using cortical networks on microelectrode arrays, Nanotoxicology 10 (5) (2016) 619–628.
[6] S. Morefield, E. Keefer, K. Chapman, G. Gross, Drug evaluations using neuronal networks cultured on microelectrode arrays, Biosens. Bioelectron. 15 (7) (2000) 383–396.
[7] F. Morin, N. Nishimura, L. Griscom, B. LePioufle, H. Fujita, Y. Takamura, E. Tamiya, Constraining the connectivity of neuronal networks cultured on microelectrode arrays with microfluidic techniques: a step towards neuron-based functional chips, Biosens. Bioelectron. 21 (7) (2006) 1093–1100.
[8] H. Lu, M.A. Schmidt, K.F. Jensen, A microfluidic electroporation device for cell lysis, Lab Chip 5 (1) (2005) 23–29.
[9] R. Biran, D.C. Martin, P.A. Tresco, Neuronal cell loss accompanies the brain tissue response to chronically implanted silicon microelectrode arrays, Exp. Neurol. 195 (1) (2005) 115–126.
[10] X. Kang, J. Liu, H. Tian, B. Yang, Y. NuLi, C. Yang, Sputtered iridium oxide modified flexible parylene microelectrodes array for electrical recording and stimulation of muscles, Sens. Actuators B: Chem. 225 (2016) 267–278.
[11] A. Mondal, B. Baker, I. Harvey, A.P. Moreno, Perflexmea: a thin microporous microelectrode array for in vitro cardiac electrophysiological studies on

hetero-cellular bilayers with controlled gap junction communication, Lab Chip 15 (9) (2015) 2037–2048.
[12] Y. Xia, G.M. Whitesides, Soft lithography, Ann. Rev. Mater. Sci. 28 (1) (1998) 153–184.
[13] L. Guo, G.S. Guvanasen, X. Liu, C. Tuthill, T.R. Nichols, S.P. DeWeerth, A PDMS-based integrated stretchable microelectrode array (ISMEA) for neural and muscular surface interfacing, IEEE Trans. Biomed. Circ. Syst. 7 (1) (2013) 1–10.
[14] J.C. Barrese, N. Rao, K. Paroo, C. Triebwasser, C. Vargas-Irwin, L. Franquemont, J.P. Donoghue, Failure mode analysis of silicon-based intracortical microelectrode arrays in non-human primates, J. Neural Eng. 10 (6) (2013) 066014.
[15] N.F. Nolta, M.B. Christensen, P.D. Crane, J.L. Skousen, P.A. Tresco, Bbb leakage, astrogliosis, and tissue loss correlate with silicon microelectrode array recording performance, Biomaterials 53 (2015) 753–762.
[16] F.-L. Meng, L. Zhang, Y. Jia, J.-Y. Liu, Y.-F. Sun, T. Luo, M.-Q. Li, J.-H. Liu, X.-J. Huang, Electronic chip based on self-oriented carbon nanotube microelectrode array to enhance the sensitivity of indoor air pollutants capacitive detection, Sens. Actuators B: Chem. 153 (1) (2011) 103–109.
[17] J.-H. Lee, A. Jang, P.R. Bhadri, R.R. Myers, W. Timmons, F.R. Beyette, P.L. Bishop, I. Papautsky, Fabrication of microelectrode arrays for in situ sensing of oxidation reduction potentials, Sens. Actuators B: Chem. 115 (1) (2006) 220–226.
[18] A. Scott, K. Weir, C. Easton, W. Huynh, W.J. Moody, A. Folch, A microfluidic microelectrode array for simultaneous electrophysiology, chemical stimulation, and imaging of brain slices, Lab Chip 13 (4) (2013) 527–535.
[19] M.M. Chernov, G. Chen, L.A. Torre-Healy, R.M. Friedman, A.W. Roe, Microelectrode array stimulation combined with intrinsic optical imaging: a novel tool for functional brain mapping, J. Neurosci. Methods 263 (2016) 7–14.
[20] N.M.M. Pires, T. Dong, U. Hanke, N. Hoivik, Recent developments in optical detection technologies in lab-on-a-chip devices for biosensing applications, Sensors 14 (8) (2014) 15458–15479.
[21] S. Fukuda, T. Uchihashi, R. Iino, Y. Okazaki, M. Yoshida, K. Igarashi, T. Ando, High-speed atomic force microscope combined with single-molecule fluorescence microscope, Rev. Sci. Instrum. 84 (7) (2013) 073706.
[22] M.J. Madou, Fundamentals of Microfabrication and Nanotechnology, vol. III, CRC Press, 6000 Broken Sound Parkway NW, Suite 300, Boca Raton, FL 33487-2742, 2011, pp. 197–198.
[23] INA333 Micro-Power (50 μA), Zero-Drift, Rail-to-Rail Out Instrumentation Amplifier.
[24] R. Sappington, T. Sidorova, D. Long, D. Calkins, Trpv1: contribution to retinal ganglion cell apoptosis and increased intracellular Ca^{2+} with exposure to hydrostatic pressure, Invest. Ophthalmol. Vis. Sci. (2009).
[25] K. Dodson, F. Echevarria, D. Li, R. Sappington, J. Edd, Retina-on-a-chip: a microfluidic platform for point access signaling studies, Biomed. Microdev. (2015).

Biographies

Miguel Cabello was born in Córdoba, Spain, in 1988. He received M.Sc. degree in Telecommunication Engineering from University of Seville, Seville, in 2014, where he is currently pursuing the Ph.D. degree with the Electronic Engineering Department. His research interests include PCB-MEMS, microelectrode arrays for biomedical and biological application, microfabrication, and lab-on-chip technologies.

Carmen Aracil received the M.Sc. degrees in physics and electronics engineering, and the Ph.D. degree in electronics engineering from the University of Seville, Seville, Spain, in 2001, 2003, and 2010 respectively. She joined the Department of Electronic Engineering, University of Seville, in 2003, where she is currently a Research and Teaching Assistant. Her current research interests include BioMEMS, polymer microsystems, PCB-MEMS, and microfluidics.

Francisco Perdigones was born in Huelva, Spain, in 1979. He received the M.Sc. and Ph.D. degrees in electronics engineering from the University of Seville, Seville, Spain, in 2006 and 2010, respectively. He joined the Aerospace Engineering and Fluid Mechanics Department in 2006. In 2009, he joined the Electronic Engineering Department, where he is currently working. His research interests include polymer microstructures, sensors, actuators, and lab-on-chip devices.

Marta Mozo was born in Seville, Spain, in 1996. She received the M.Sc. degree in Biomedical Sciences in 2016, and the MA in Molecular Genetics in 2017. She joined the Electronic Engineering Department in 2016 while doing her degree's final project, where she is now working on her Ph.D. degree. Her research interests include lab-on-chip technologies and their application in the biomedical field.

Berta de la Cerda Biology grade in 1993 and PhD in Biology "cum laude" in 1999, Seville University. Researcher in Biochemistry Department, Seville University 2000–2005. Junior postdoctoral researcher, Spanish Research Council (CSIC) 2005–2008, working mainly in protein interactions and structure–function relationships in macromolecules. Senior postdoctoral researcher, Andalusian Molecular Biology and Regenerative Medicine Centre (CABIMER), Seville, 2009. Focused in disease modelling and advanced therapies for retinal diseases. Currently leading a project on cellular modeling for monogenic retinal diseases, participant on EU Eye-risk project for the study of age-related macular degeneration, member of European Retinal Disease Consortium (ERDC) and European Retinal Therapeutics Consortium (ERTC) and member of the scientific advisory board of "Fundación Macula Retina".

José M. Quero received the M.Sc. and Ph.D. degrees in electrical engineering from the University of Seville, Spain, in 1988 and 1991, respectively. He has been a Full Professor with the Department of Electronic Engineering, Universidad de Sevilla, since 2000. He is also a Senior Researcher within AICIA, a non-profit research organization. He has been an Evaluator and Reviewer for the European Commission in the Information Society Technology program since 2002. He is currently the CEO of Solar MEMS Technologies, a spin-off company, specialized in MEMS applications for space. His research interests include MEMS sensors and actuators and their application in microfluidics, BioMEMS, RF, and space.

sensors

MDPI

Article

Extracellular Electrophysiology in the Prostate Cancer Cell Model PC-3

Miguel Cabello [1], Haobo Ge [2], Carmen Aracil [1], Despina Moschou [3], Pedro Estrela [3], Jose Manuel Quero [1], Sofia I. Pascu [2] and Paulo R. F. Rocha [3,*]

[1] Department of Electronic Engineering, Escuela Superior de Ingenieros, University of Seville, 41004 Seville, Spain; mcabellov@gte.esi.us.es (M.C.); caracil@gte.esi.us.es (C.A.); quero@us.es (J.M.Q.)

[2] Department of Chemistry, University of Bath, Claverton Down, Bath BA2 7AY, UK; H.Ge@bath.ac.uk (H.G.); S.Pascu@bath.ac.uk (S.I.P.)

[3] Centre for Biosensors, Bioelectronics and Biodevices (C3Bio), Department of Electronic and Electrical Engineering, University of Bath, Claverton Down, Bath BA2 7AY, UK; D.Moschou@bath.ac.uk (D.M.); P.Estrela@bath.ac.uk (P.E.)

* Correspondence: P.Rocha@bath.ac.uk; Tel.: +44-(0)-1225-386051

Received: 31 October 2018; Accepted: 20 December 2018; Published: 3 January 2019

Abstract: Although prostate cancer is one of the most common cancers in the male population, its basic biological function at a cellular level remains to be fully understood. This lack of in depth understanding of its physiology significantly hinders the development of new, targeted and more effective treatment strategies. Whilst electrophysiological studies can provide in depth analysis, the possibility of recording electrical activity in large populations of non-neuronal cells remains a significant challenge, even harder to address in the picoAmpere-range, which is typical of cellular level electrical activities. In this paper, we present the measurement and characterization of electrical activity of populations of prostate cancer cells PC-3, demonstrating for the first time a meaningful electrical pattern. The low noise system used comprises a multi-electrode array (MEA) with circular gold electrodes on silicon oxide substrates. The extracellular capacitive currents present two standard patterns: an asynchronous sporadic pattern and a synchronous quasi-periodic biphasic spike pattern. An amplitude of $\pm$150 pA, a width between 50–300 ms and an inter-spike interval around 0.5 Hz characterize the quasi-periodic spikes. Our experiments using treatment of cells with Gd^{3+}, known as an inhibitor for the Ca^{2+} exchanges, suggest that the quasi-periodic signals originate from Ca^2 channels. After adding the Gd^{3+} to a population of living PC-3 cells, their electrical activity considerably decreased; once the culture was washed, thus eliminating the Gd^{3+} containing medium and addition of fresh cellular growth medium, the PC-3 cells recovered their normal electrical activity. Cellular viability plots have been carried out, demonstrating that the PC-3 cells remain viable after the use of Gd^{3+}, on the timescale of this experiment. Hence, this experimental work suggests that Ca^{2+} is significantly affecting the electrophysiological communication pattern among PC-3 cell populations. Our measuring platform opens up new avenues for real time and highly sensitive investigations of prostate cancer signalling pathways.

Keywords: prostate cancer signalling; PC-3 cells; electrical activity; calcium channel inhibitor

1. Introduction

Prostate cancer is one of the most common malignancy cancers diagnosed in men [1], especially in Western countries [2,3]. In the UK alone, about 50,000 men per year are diagnosed with prostate cancer [4]. The disease can develop when cells in the prostate start to grow and spread in an uncontrolled way. Also, owing to its difficulty in diagnosis, there is an urgent need for early prevention

and efficient treatment to stop it spreading. Nonetheless, there is still little scientific understanding on the electrophysiology of the prostate cancer growth and metastatic patterns, thus delaying the development of new, targeted drugs for confinement and treatment of the tumour [5].

Currently, a reliable and useful in-vitro model for prostate cancer is cell culture [6]. Along with LNCaP and DU-145, PC-3 cells are considered the gold standard of prostate cancer cell culture lines [7,8]. PC-3 cells are proven to be reliable for growth rate and behaviour as a xenograft [9], and maintain genotype and phenotype when injected into mice [10,11]. Finally, PC-3 cell lines are hormone insensitive and present no AR or PSA mRNA/protein. As a highly aneuploid line, it duplicates after approximately 33 h. This proliferation is known to lead to high levels of oxidative stress [12]. Concomitantly, the scientific community has routinely attributed the transduction of oxidative stress to the universal second messenger Ca^{2+}. The pH sensitivity in comparison to non-malignant cells is noticeable and being utilized in the development of novel anticancer drugs [13]. The routine use of this methodology is hindered by the expensive Ca^{2+} dyes toxicity and inability to perform long term Ca^{2+} imaging.

Fluctuations of the membrane potential play a central role in cells of the nervous system. They are caused by the flux of primarily Na^+, K^+, Cl^-, and Ca^{2+} ions along the gradient, controlled by the function of ion channel proteins. Gradients in ion channels are closely related to brain illnesses [14] cardiac arrhythmias [15] and the development of cancer [16–21]. Previous imaging and single cell studies investigated K^+, Na^+ and Ca^{2+} channels in human prostate cancer basal activity and proliferation [22,23] Consensus on the role of Ca^{2+} channels during prostate cancer proliferation seems to exist as demonstrated by Zhang and colleagues through the use of Ca^{2+}-permeable channel TRPM8 [24,25] and by others trough a permeable channel to Ca^{2+}, TRPC6 [26] and other oxidative stresses [27].

Moving ions across the membrane of cells gives rise to minute electrical fluctuations, even in electrically quiescent cells such as Glia cells [28–32]. Hence, we hypothesize that electrical monitoring of prostate cancer cells would also be possible, not through using expensive and sometimes toxic methods such as fluorescence, but instead using a low cost, ultra-sensitive electrical recording setup to measure a whole population of non-neuronal cells.

To electrically detect a population of living cells, multi-electrode arrays (MEAs) are used as the technology of choice. A MEA consists of a group of electrodes on a substrate which allow a close contact with cells in culture medium. The first MEA used to monitor the electrical activity of cells culture was created around 1970 [33]. Since then, most of the efforts related to MEAs have been focused on improving the concentration of electrodes and their electrical characteristics [34–38]. A major goal of electrode fabrication for application in MEAs is to achieve a low impedance and high capacitance, as it results in a higher signal-to-noise ratio; low impedance becomes particularly challenging when the planar electrode dimensions are miniaturized down to the micrometre scale. Therefore, researchers are focusing on increasing the effective surface area by modifying the electrode with porous conducting materials such as Pt black, Au nanostructures and carbon nanotubes. By modifying the surface, the impedance of the electrode is reduced, leading to improved electrical recordings. In this respect, we have decreased the impedance by using extreme large electrode areas of mm^2 and have shown a noise level as low as 0.3 μV_{pp} [31]. An extremely low-noise measuring system allowed us to detect minute, yet constantly occurring and functional, membrane capacitive current oscillations across large populations of cells, such as e.g., C6 glioma cells [32].

In this paper, we show that the reliable prostate cancer cell model PC-3 can be electrically monitored using the same extremely high signal-to-noise electrophysiological recording system. We recorded the electrical activity of populations of PC-3 cells over time and show that two typical and consistent behaviours occur. The first one relates to the basal activity and is manifested as asynchronous and sporadic electrical spikes. The second is a collaborative event and is manifested through the observation of a quasi-periodic electrical spike-pattern. By using specific inhibitors, we show that the routinely observed quasi-periodic spikes relate to Ca^{2+} ions cooperatively traveling through a population of thousands of cells. Our findings also suggest the applicability of our cells-on-a-chip

system for reliable in-vitro testing of human-relevant prostate cancer models such as PC-3 cells for in-vivo applications.

2. Materials and Methods

2.1. General Cellular Culturing Method

PC-3 cells were cultured using standard methodologies, at 37 °C in a humidified atmosphere in air and harvested once a confluence of over 70% had been reached. PC-3 cells were cultured in Roswell Park Memorial Institute (RPMI) 1640 medium. The media contained 10% foetal calf serum (FCS), 0.5% penicillin/streptomycin (10,000 IU mL^{-1}/10,000 mg mL^{-1}) and 1% 200 mM L-glutamine. All culturing and imaging steps were performed in the absence of phenol red-based additives. The supernatant containing dead cell matter and excess protein were aspirated. The live adherent cells were then washed with 10 mL of phosphate buffer saline (PBS) solution twice to remove any remaining media containing FCS, which may inactivate trypsin. Cells were incubated in 3 mL of trypsin solution (0.25% trypsin) for 5 to 7 min at 37 °C. After trypsinisation, 6 mL of medium containing 10% serum was added to inactivate the trypsin and the solution was centrifuged for 5 min (1000 rpm, 25 °C) to remove any remaining dead cell matter. The supernatant liquid was aspirated and 5 mL of cell medium (10% FCS) was added to the cell matter left behind. Cells were counted using a haemocytometer and then seeded as appropriate, either on a microchip, or on a cellular plate suitable for optical imaging.

2.2. Standard Cellular Viability Assays in Water

To assess the cellular viability over the duration of experiment, in a parallel setting, standard MTT assays (i.e., colorimetric assays for measuring cell metabolic activity) were performed. For this, PC-3 cells were plated (7×10^3 cells per well) in a 96-well plate and left for 48 h to adhere fully. For a cellular viability estimation (denoted IC50 estimations by MTT assays), cells were incubated with aqueous gadolinium chloride and tested for 20 min at 37 °C. Concentrations used were 250, 100, 50, 10, 1, 0.5, 0.1 μM, 0.001 μM (1% water, 99% RPMI medium containing 10% FCS at standard concentration of the cell line). Subsequently, cells were washed three times with PBS and 100 μL of MTT was added (0.5 mg mL^{-1}, 10% PBS:SFM), followed by a 2-h incubation. Following aspiration, 100 μL of DMSO was added and the 96 well plates were read at an ELISA plate reader (Fluostar Omega BMGLabTech, Aylesbury, UK). Data emerged from at least three consistent results and IC_{50} values were calculated using Origin 9 (Wellesley Hills, MA, USA). However, when the effect of $GdCl^3$ was evaluated in aqueous conditions, the IC_{50} value at 20 min could not be determined because no significant cytotoxicity effect is induced by aqueous gadolinium chloride in 20-min incubation with given concentrations.

2.3. MEA Experimental Details

The MEA chip used for the experiments consists of a 1 mm thick silicon/silicon dioxide substrate and round shaped Au electrodes of 50 nm thickness and 2 mm apart. Au was evaporated on top of a 8 nm Cr adhesion layer through a shadow mask. The electrode area is 1 mm^2. Then, a previously drilled piece of PMMA was glued to the substrate with the electrodes, which is used as a well to contain the solution. The gold electrodes, which have an area of 1 mm^2, are located inside the well and connected with a small strip-line of 0.2 mm to the contact pad outside the well. The area of the strip-line can be disregarded with respect to the area of the electrodes. The Au plated contact pins outside the well were purchased from Distrelec (Bremen, Germany), rated at 3 A with a length of 24.64 mm and type SPA-2D, allowing the connection to the chip with the measurement equipment. After autoclaving the whole system, cells are deposited with the medium over the electrode. Recordings start at least 3 h after cell deposition. A total of 0.1 million cells were prepared for its culture in the described MEA. The whole system was autoclaved before each experiment. A total of 280 μL (0.1 M) were

loaded onto the MEA chip. Devices were placed in the incubator and monitored continuously up to 3 days. The whole experiment was repeated three times with the same conditions. The well was loosely covered with a lid to prevent evaporation of the medium. After filling, the system was put into an incubator (Midi 40, Thermo Scientific, Schwerte, Germany). This system assures the presence of enough cell culture medium to keep the cells viable over more than 24 h without medium change.

The current between two Au electrodes was measured using a low-noise current amplifier (SR570, Stanford Research, Sunnyvale, CA, USA) and a dynamic signal analyser (35670A, Agilent, Frankfurt, Germany). The data from the signal analyser was extracted with a homemade LabVIEW acquisition software using a high speed USB/GPIB interface converter from Keysight Technologies (Frankfurt, Germany) and processed using Matlab R2017b. To minimize drift, the current amplifier was calibrated and the setup was stabilized for at least 2 h before measuring. The current was recorded as a function of time by using zero bias on the electrodes. The use of a Faraday cage and low noise wires assure a minimized external interference.

Optical micrographs taken with an epifluorescence microscope (Nikon, Surrey, UK) showed that the PC-3 cells adhered and covered the whole electrode and substrate. Because of the large electrode area, the recorded current was not from a single cell but from the superposition of signals of all cells coupled to the electrode. Hence, we recorded the activity of a PC-3 cell population, and findings are discussed below.

3. Results and Discussion

3.1. Sensor, Cell Adhesion and Viability

Figure 1a illustrates the MEA chip used during the experiments, in which red circles represent the cells inside the chip. The chip is composed of four pairs of circular electrodes, which are optimized to record the electrical signals of cells populations adhered to them [39,40]. Pairs of electrodes comprise one measuring electrode and one counter electrode. To better understand the recording system, we have modelled the equivalent circuit based on the charge transfer resistance, R_D, in parallel with the Helmholtz-Gouy-Chapman double layer capacitance, C_D, which is in series with the spreading resistance, R_C. The counter electrode has a similar circuit. The path between the sensing and the counter electrode is large, making the impedance, Z_{seal}, very high. Cells generate a voltage, $v_s(t)$. Our approach measures the current $i_s(t)$ using a transimpedance amplifier. The output voltage is then given by $v_o(t)$:

$$vo(t) = -R_F\, i_s(t) \tag{1}$$

where R_F is the feedback resistance. The model used in these experiments has been explained by Medeiros et al. [39]. The detected current is given as:

$$i_s(t) = \frac{dv_s}{dt} \cdot C_D\left(1 - e^{-\frac{t}{\tau}}\right), \text{ with } \tau = R_c R_D \tag{2}$$

In this case, τ is the time constant for the charging or discharging of the network. C_D acts as a multiplying factor, which affects the spatial resolution, but also allows the amplification of the signal thanks to the rescaling of C_D due to the use of large-area electrodes. Changes on the extracellular potentials affect the current, which is the derivative of the acquired voltage signal [41].

Figure 1b shows the adhesion of cells to the substrate and the gold electrodes. Figure 1c shows cell viability in the developed sensors. For cell viability experiments, $1 \times 10_5$ cells were added and incubated for 24 h. The growth of cells was monitored every day. The number of cells on eight different electrodes were counted and averaged. The results show the normalized cell numbers in 1, 2, 3, 4 and 8 days. It shows no toxicity in our recording system and that PC-3 cells can attach and proliferate in normal conditions. Each spot was calculated from the average of the eight different electrodes on the chips. The error reported was the standard error of the mean and is shown as ±S.E.M (see Table 1).

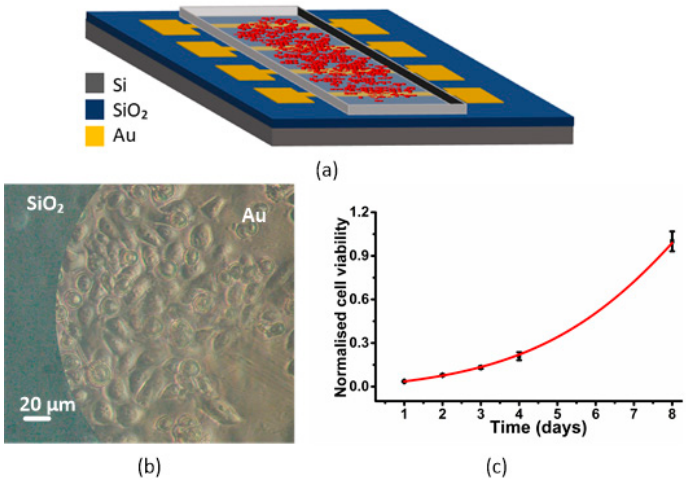

Figure 1. (**a**) Drawing of the transducer used for the culturing of PC-3 cells. PC-3 cells are represented as red circles within the culture medium. (**b**) PC-3 cells adhered to the gold electrodes 3 days after being deposited. (**c**) Cell viability describing a typical exponential PC-3 cell growth in the MEA device.

Table 1. Average, S.E.M, normalized average and normalized S.E.M.

	Day 1	Day 2	Day 3	Day 4	Day 8
Average	42.0000	93.7500	156.6250	285.0000	1193.6250
S.E.M	4.5591	9.4449	16.8395	43.4133	128.5749
Normalized average	0.0352	0.0785	0.1312	0.2089	1.0000
Normalized S.E.M	2.42×10^{-3}	5.02×10^{-3}	8.95×10^{-3}	2.75×10^{-2}	6.84×10^{-2}

3.2. Electrical Activity of PC-3 Cells

The electrical activity of PC-3 cells has been monitored over time. We repeated all electrical recordings at least three times for reproducibility. A baseline signal was obtained by performing electrical recordings only with medium. This experiment was made before the electrical recordings with cells took place. This results in a baseline of less than 1 pA as depicted in Figure 2a in close agreement to previous reported results [31].

PC-3 cells were then monitored in our system. Figure 2b describes the two common patterns of the current measurements at zero bias. Two typical behaviours were recorded through the experimental recordings. A basal sporadic and asynchronous activity and a quasi-periodic behaviour. A zoomed of the quasi-periodicity is presented in Figure 2c and an even larger zoom to the spike shape is given by Figure 2d. We note that the basal sporadic activities are characterized by faster and smaller magnitudes of about 100 pA, and by their asynchronous and sporadic behaviour. Yet, when quasi-periodic spikes appear, they are mostly characterized by larger signal magnitudes, slower widths ranging from 0.03 to 0.3 s and inter-spike intervals in the range of few seconds. We present a detailed statistical analysis of the recorded synchronous activity in Figure 2e–g.

Figure 2c depicts a typical unipolar asynchronous spike observed in PC-3 cell cultures during extracellular recordings. We note that about 70% of the electrical spikes were unipolar, fast (below 200 ms) and with lower magnitudes than that of the synchronous regime. Figure 2d,e shows that quasi-periodic spikes are biphasic, and that the spike amplitude during the more intense period of electrical activity is about $\pm$150 pA. We further analyse our data by plotting the histograms of all our synchronous signals during 3 different experiments. Figure 2f–h shows the statistics of the time between consecutive spikes, signal magnitudes and spike widths during the synchronous activity.

Due to a low number of events, the histograms in Figure 2f–h shows only spikes over ±50 pA. Near half of the spikes accounted have an amplitude between ±100 and ±200 pA, and a remarkable amount of spikes exist with an even higher amplitude with maximums over 300 pA. Interestingly, we note that in most cases the quasi-periodic spikes observed in the synchronous period have larger widths than those appearing in the asynchronous regime. About 80% of the analysed spikes in the asynchronous regime had widths between 30 and 200 ms, whereas in the synchronous regime the distribution was broader and with widths larger as depicted in Figure 2g. The time between synchronous events is depicted in Figure 2h. Here we see that the distance between spikes reaches a peak around 2–3 s although the variation expands from 1 to 10 s of interval between biphasic spikes.

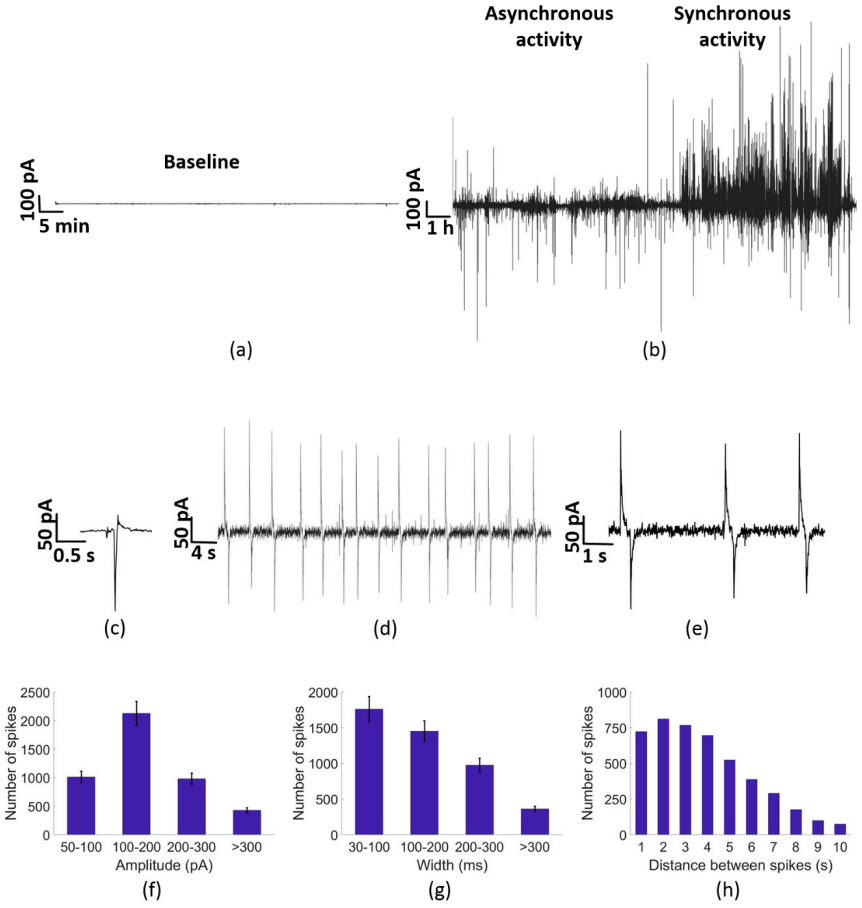

Figure 2. Electrical activity of a PC-3 cells culture on a $Si/SiO_2/Au$ substrate chip. (**a**) Baseline measured on the chip with only cell medium. (**b**) Most representative electrical activity of PC-3 cells during the experiment, showing on the left side of the graph the sporadic and mostly unipolar electrical activity. (**c**) Zoom-in to the sporadic and asynchronous regime showing a typical unipolar negative spike. (**d**) Quasi-periodic activity of PC-3 cells, presenting Biphasic spikes. (**e**) Biphasic pulses of the electrical activity of PC-3 cells, with a measurable distance between the positive and the negative pulse of about 0.3 s. (**f**–**h**) represent the characterization of the quasi-periodic activity of PC-3 cells: (**f**) Number of spikes depending on its amplitude. (**g**) Number of spikes depending on its width. (**h**) Number of spikes depending on its distance between them. The interspike intervals were distributed into time slots with a resolution of 1 s.

The results obtained for the asynchronous analysis reveal that during the first part of the experiment, which corresponds with this asynchronous behaviour, the amount of spikes detected is much lower (around 10 times lower) than during the synchronous analysis. Comparing the synchronous and asynchronous analysis we conclude that the amount of spikes detected during the asynchronous phase is considerably lower than the amount of spikes detected during the quasi-periodic phase. The spikes are larger and wider during the quasi-periodic activity, as expected for cooperative signals [31,32]. The signal recorded using our large electrode area is the sum of all individual cell contributions. Individual cell signals cannot be resolved with sufficient spatial information. Uncorrelated cell activity appears as noise and low magnitude asynchronous spikes. Thus, we argue that the asynchronous activity regime of Figure 2b is mostly due to uncorrelated single cell activity. The origin is likely to relate with the known expression of K^+ channels of the Kv1.3 family as shown recently in prostate cancer cell lines via patch clamp experiments [42–45].

3.3. Calcium Channel Inhibition

We note that the quasi-periodic nature of signals is slow and routinely occurs during prostate cancer proliferation. Additionally, the quasi-periodicity and form of the current signal resonates well with an extracellular traveling wave across the large area electrode. Once the wave reaches the sensing electrode it raises its potential relative to the counter electrode forcing a large displacement current through the double-layer capacitance, giving rise to upward and downward current spikes corresponding to the wave entrance and exiting on the recording electrode. [31,32,41]. We recorded onward and downward spike differences between 0.7 to 2 s using 1 mm^2 electrodes. This means that we can actually record a wave speed of a few hundreds of micrometres per second, which is in fact supported by reported Ca^{2+} waves propagation speeds [46,47]. Hence, we hypothesize that Ca^{2+} channels could be involved due to their reported periodicity, slower nature and involvement to PC-3 proliferation. Hence, in order to demonstrate a possible role of Calcium channels (Ca^{2+}) in the recorded electrical activity, we decided to block the electrical spikes using a well-known Ca^{2+} inhibitor, Gadolinium (Gd^{3+}) [48].

A Ca^{2+} inhibitor (Gd^{3+}) has been added during the experiment. The inhibitor has been added during 20 min and washed after that time. Gd^{3+} has been diluted with DI water, in concentrations between 10 and 40 μM as in previous works [40]. The medium at the beginning of the experiment was 280 μL, and we used 3 μL of Gd^{3+} in a concentration of 1 mM, together with the medium remained in the culture. A final concentration of Gd^{3+} between 10 and 20 μM was achieved. The electrical activity of PC-3 cells before adding Gd^{3+} is depicted in Figure 3a. Fresh PC-3 cells typically exhibiting fluctuations around 100 pA as explained in detail in Figure 2. Figure 3b demonstrates that the signal of adherent PC-3 cells could be inhibited with the addition of 20 μM of Gd^{3+}. The inhibitor effect is fast and in less than one minute the current fluctuations lower to less than 5 pA of magnitude as given by the red trace in Figure 3a. After about 1 h the cells were washed three times with phosphate buffer saline (PBS) to remove the Gd^{3+} inhibitor and fresh medium was provided. After washing out, the PC-3 cells regain the original electrical activity, yielding spike magnitudes of about 100 pA as illustrated in the final black trace of Figure 3a. Additionally, gadolinium chloride MTT assays are shown in Figure 3c,d to exclude cell death after adding the inhibitor. The error reported was the standard error of the mean and shown as ±S.E.M (Figure 3c,d).

As can be seen in Figure 3, the Ca^{2+} channels are clearly involved in the electrical activity of PC-3 cells. Electrical activity of PC-3 cells together with Gd^{3+} has been recorded during about 20 min (Figure 3a red colour), reducing considerably the previous electrical activity of PC-3 cells (represented in Figure 3a in black colour in the left side of the graph). 20 min after the deposition of the inhibitor, the medium with Gd^{3+} was washed three times to assure the complete elimination of the inhibitor. After the washing, new medium was added and the electrical activity started firing normally (black colour in the right side of the graph) with a quasi-periodic activity. It has been demonstrated that inhibiting Ca^{2+} channels make the electrical activity of PC-3 cells almost disappear,

confirming that these channels have a high influence in the electrical activity of this type of cells. In Figure 3b, the number of spikes detected before, during and after the use of Gd^{3+} are shown. As can be seen in Figure 3b, the number of spikes detected before and after the use of the inhibitor are close, in comparison with the number of spikes detected during the use of the inhibitor, which is almost zero.

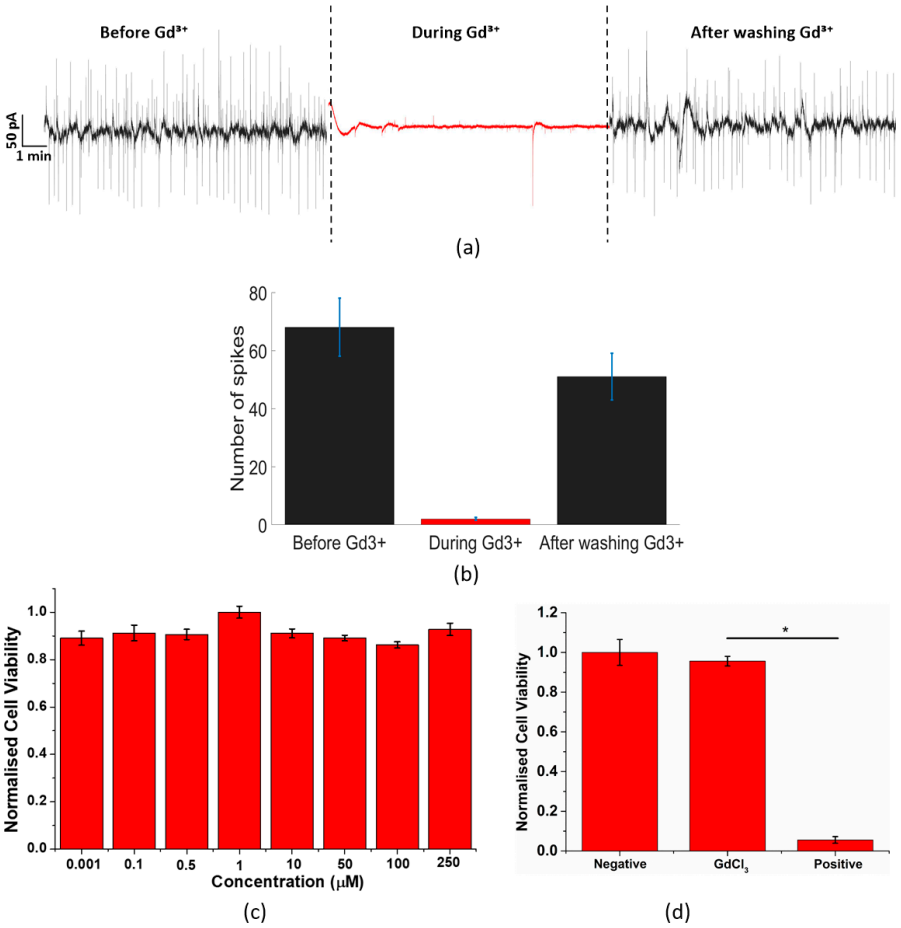

Figure 3. (**a**) Electrical activity of PC-3 cells culture before, during and after using Gd^{3+} has been used as a Ca^{2+} inhibitor. Before and after the use of Gd^{3+}, the electrical activity shows quasi-periodic current oscillations. (**b**) Number of spikes detected in three different moments: before, during and after the use of the Ca^{2+} inhibitor. (**c**) Gadolinium chloride MTT assays. The result shows that there is no significant toxicity of $GdCl^3$ in 20 min of incubation. The results of (**c**) are reported as means ±SEM. The data were analysed by one way ANOVA, $p < 0.05$, which means there is a significant difference between results of different concentrations ($n = 3$). Error bars represent standard error with respect to the repeated six measurements of the same concentration. (**d**) Positive and negative control test of gadolinium chloride. The result shows that there is no significant toxicity of 250 μM $GdCl^3$ in 20 min of incubation compared with negative control (water) and positive control (250 μM triton). The results are reported as means ±SEM. (* $p < 0.05$, Student's *t*-test). There is a significant difference between results of $GdCl^3$ and positive control at 250 μM concentration ($n = 3$). Error bars represent standard error with respect to the three independent experiments.

In Figure 3c,d, an acute $GdCl^3$ viability experiment was conducted. The results show that the cell viability of all concentrations are above 90%. Thus, it proves that $GdCl^3$ will not cause the cytotoxic effect to tested cells and that the reduction of the spikes is due to the inhibition of the calcium channel instead of cell death. In Figure 3d, a positive and negative control results were compared with the $GdCl^3$ results. The $GdCl^3$ has a very close cell viability to the negative control, which is non-cytotoxic. While in the positive control, a cytotoxic reagent at the same concentration of the $GdCl^3$ is introduced and leads to a significant reduction in the cell viability. This proves that $GdCl^3$ is non-toxic to PC-3 cells during our experiments.

4. Conclusions

In this paper we have characterized the electrical activity of a prostate cancer cell line (PC-3) using circular gold electrodes on a silicon oxide substrate chip. PC-3 cells demonstrate a low frequency electrical activity between 0.1 Hz and 10 Hz and two distinct patterns; an asynchronous and sporadic pattern and a synchronous quasi-periodic pattern. The sporadic phase shows weak and fast spikes typically below 100 ms. Yet, the quasi-periodic phase shows spikes having an amplitude of $\pm$150 pA, a width between 50 and 300 ms and an inter-spike interval around 0.5 Hz. The use of the well-known calcium inhibitor Gd^{3+} together with the slowly varying nature of the signal suggests that Ca^{2+} channels are involved in the electrical signalling among a population of PC-3 cells. We therefore demonstrated for the first time the feasibility of a real time and highly sensitive system to understand the signalling pathways among prostate cancer cells.

Author Contributions: Data curation, M.C. and H.G.; Formal analysis, M.C. and H.G.; Investigation, M.C. and P.R.F.R.; Project administration, P.R.F.R.; Resources, C.A., J.M.Q., S.I.P. and P.R.F.R.; Writing—original draft, M.C. and P.R.F.R.; Writing—review & editing, C.A., D.M., P.E., J.M.Q., S.I.P. and P.R.F.R.

Funding: This research was funded by the Spanish Ministry of Science and Innovation S.I.P grant number [TEC2014-54449-C3-2-R, BIOLOP] and ERC-CG O2Sense grant number [617107].

Conflicts of Interest: The authors declare no conflict of interest.

References

1. National Cancer Institute. SEER Cancer Statistics Review, 1975–2015. Available online: https://seer.cancer.gov/csr/1975_2015/ (accessed on 18 April 2018).
2. Weiner, A.B.; Matulewicz, R.S.; Eggener, S.E.; Schaeffer, E.M. Increasing incidence of metastatic prostate cancer in the United States (2004–2013). *Prostate Cancer Prostatic Dis.* **2016**, *19*, 395. [CrossRef] [PubMed]
3. Buzzoni, C.; Auvinen, A.; Roobol, M.J.; Carlsson, S.; Moss, S.M.; Puliti, D.; Lujan, M. Metastatic prostate cancer incidence and prostate-specific antigen testing: New insights from the European Randomized Study of Screening for Prostate Cancer. *Eur. Urol.* **2015**, *68*, 885–890. [CrossRef] [PubMed]
4. Office of National Statistic. Cancer Registration Statistics, England: 2018. 2016. Available online: https://www.ons.gov.uk/peoplepopulationandcommunity/healthandsocialcare/conditionsanddiseases/bulletins/cancerregistrationstatisticsengland/final2016 (accessed on 18 April 2018).
5. Dozmorov, M.G.; Hurst, R.E.; Culkin, D.J.; Kropp, B.P.; Frank, M.B.; Osban, J.; Lin, H.K. Unique patterns of molecular profiling between human prostate cancer LNCaP and PC-3 cells. *Prostate* **2009**, *69*, 1077–1090. [CrossRef] [PubMed]
6. Cell L. BC Cancer Agency. 2014 Nov 21; Cell L. 2001. Available online: http://capcelllines.ca (accessed on 18 April 2018).
7. Stone, K.R.; Mickey, D.D.; Wunderli, H.; Mickey, G.H.; Paulson, D.F. Isolation of a human prostate carcinoma cell line (DU 145). *Int. J. Cancer* **1978**, *21*, 274–281. [CrossRef] [PubMed]
8. Cunningham, D.; You, Z. In vitro and in vivo model systems used in prostate cancer research. *J. Biol. Methods* **2015**, *2*, e17. [CrossRef] [PubMed]
9. Wu, X.; Gong, S.; Roy-Burman, P.; Lee, P.; Culig, Z. Current mouse and cell models in prostate cancer research. *Endocr. Relat. Cancer* **2013**, *20*, R155–R170. [CrossRef] [PubMed]

10. Rea, D.; Del Vecchio, V.; Palma, G.; Barbieri, A.; Falco, M.; Luciano, A.; de Biase, D.; Perdonà, S.; Facchini, G.; Arra, C. Mouse models in prostate cancer translational research: From xenograft to PDX. *BioMed Res. Int.* **2016**, *2016*, 9750795. [CrossRef]
11. Pulukuri, S.M.; Gondi, C.S.; Lakka, S.S.; Jutla, A.; Estes, N.; Gujrati, M.; Rao, J.S. RNA interference-directed knockdown of urokinase plasminogen activator and urokinase plasminogen activator receptor inhibits prostate cancer cell invasion, survival, and tumorigenicity in vivo. *J. Biol. Chem.* **2005**, *280*, 36529–36540. [CrossRef]
12. Harrison, I.P.; Selemidis, S. Understanding the biology of reactive oxygen species and their link to cancer: NADPH oxidases as novel pharmacological targets. *Clin. Exp. Pharmacol. Physiol.* **2014**, *41*, 533–542. [CrossRef]
13. Yang, Y.; Karakhanova, S.; Werner, J.; Bazhin, A.V. Reactive oxygen species in cancer biology and anticancer therapy. *Curr. Med. Chem.* **2013**, *20*, 3677–3692. [CrossRef]
14. Eimon, P.M.; Ghannad-Rezaie, M.; De Rienzo, G.; Allalou, A.; Wu, Y.; Gao, M.; Roy, A.; Skolnick, J.; Yanik, M.F. Brain activity patterns in high-throughput electrophysiology screen predict both drug efficacies and side effects. *Nat. Commun.* **2018**, *9*, 219. [CrossRef] [PubMed]
15. Salvarani, N.; Maguy, A.; De Simone, S.A.; Miragoli, M.; Jousset, F.; Rohr, S. TGF-β1 (Transforming Growth Factor-β1) Plays a Pivotal Role in Cardiac Myofibroblast Arrhythmogenicity. *Circulation* **2017**, *10*, e004567. [PubMed]
16. Kunzelmann, K. Ion channels and cancer. *J. Membr. Biol.* **2005**, *205*, 159. [CrossRef] [PubMed]
17. Fraser, S.P.; Pardo, L.A. Ion channels: Functional expression and therapeutic potential in cancer: Colloquium on Ion Channels and Cancer. *EMBO Rep.* **2008**, *9*, 512–515. [CrossRef] [PubMed]
18. Cuddapah, V.A.; Sontheimer, H. Ion channels and tranporters in cancer. 2. Ion channels and the control of cancer cell migration. *Am. J. Physiol. Cell Physiol.* **2011**, *301*, C541–C549. [CrossRef] [PubMed]
19. Prevarskaya, N.; Skryma, R.; Shuba, Y. Ion channels and the hallmarks of cancer. *Trends Mol. Med.* **2010**, *16*, 107–121. [CrossRef] [PubMed]
20. Prevarskaya, N.; Skryma, R.; Bidaux, G.; Flourakis, M.; Shuba, Y. Ion channels in death and differentiation of prostate cancer cells. *Cell Death Differ.* **2007**, *14*, 1295. [CrossRef]
21. Arcangeli, A.; Becchetti, A. Novel perspectives in cancer therapy: Targeting ion channels. *Drug Resist. Updates* **2015**, *21*, 11–19. [CrossRef]
22. Abdul, M.; Hoosein, N. Expression and activity of potassium ion channels in human prostate cancer. *Cancer Lett.* **2002**, *186*, 99–105. [CrossRef]
23. Yildirim, S.; Altun, S.; Gumushan, H.; Patel, A.; Djamgoz, M.B. Voltage-gated sodium channel activity promotes prostate cancer metastasis in vivo. *Cancer Lett.* **2012**, *323*, 58–61. [CrossRef]
24. Zhang, L.; Barritt, G.J. Evidence that TRPM8 is an androgen-dependent Ca^{2+} channel required for the survival of prostate cancer cells. *Cancer Res.* **2004**, *64*, 8365–8373. [CrossRef] [PubMed]
25. Gkika, D.; Flourakis, M.; Lemonnier, L.; Prevarskaya, N. PSA reduces prostate cancer cell motility by stimulating TRPM8 activity and plasma membrane expression. *Oncogene* **2010**, *29*, 4611. [CrossRef] [PubMed]
26. Wang, Y.; Yue, D.; Li, K.; Liu, Y.L.; Ren, C.S.; Wang, P. The role of TRPC6 in HGF-induced cell proliferation of human prostate cancer DU145 and PC-3 cells. *Asian J. Androl.* **2010**, *12*, 841. [CrossRef] [PubMed]
27. Holzmann, C.; Kilch, T.; Kappel, S.; Dörr, K.; Jung, V.; Stöckle, M.; Peinelt, C. Differential redox regulation of Ca2+ signaling and viability in normal and malignant prostate cells. *Biophys. J.* **2015**, *109*, 1410–1419. [CrossRef]
28. Buzsáki, G.; Anastassiou, C.A.; Koch, C. The origin of extracellular fields and currents—EEG, ECoG, LFP and spikes. *Nat. Rev. Neurosci.* **2012**, *13*, 407. [CrossRef] [PubMed]
29. Szatkowski, M.; Mycielska, M.; Knowles, R.; Kho, A.L.; Djamgoz, M.B.A. Electrophysiological recordings from the rat prostate gland in vitro: Identified single-cell and transepithelial (lumen) potentials. *BJU Int.* **2000**, *86*, 1068–1075. [CrossRef] [PubMed]
30. Rocha, P.R.; Schlett, P.; Schneider, L.; Dröge, M.; Mailänder, V.; Gomes, H.L.; Blom, P.W.M.; De Leeuw, D.M. Low frequency electric current noise in glioma cell populations. *J. Mater. Chem. B* **2015**, *3*, 5035–5039. [CrossRef]
31. Rocha, P.R.; Schlett, P.; Kintzel, U.; Mailänder, V.; Vandamme, L.K.; Zeck, G.; Gomes, H.L.; Biscarini, F.; De Leeuw, D.M. Electrochemical noise and impedance of Au electrode/electrolyte interfaces enabling extracellular detection of glioma cell populations. *Sci. Rep.* **2016**, *6*, 34843. [CrossRef]

32. Rocha, P.R.; Medeiros, M.C.; Kintzel, U.; Vogt, J.; Araújo, I.M.; Mestre, A.L.; Biscarini, F. Extracellular electrical recording of pH-triggered bursts in C6 glioma cell populations. *Sci. Adv.* **2016**, *2*, e1600516. [CrossRef]
33. Thomas, C.A., Jr.; Springer, P.A.; Loeb, G.E.; Berwald-Netter, Y.; Okun, L.M. A miniature microelectrode array to monitor the bioelectric activity of cultured cells. *Exp. Cell Res.* **1972**, *74*, 61–66. [CrossRef]
34. Hoogerwerf, A.C.; Wise, K.D. A three-dimensional microelectrode array for chronic neural recording. *IEEE Trans. Biomed. Eng.* **1994**, *41*, 1136–1146. [CrossRef] [PubMed]
35. Nordhausen, C.T.; Maynard, E.M.; Normann, R.A. Single unit recording capabilities of a 100 microelectrode array. *Brain Res.* **1996**, *726*, 129–140. [CrossRef]
36. Berdondini, L.; Overstolz, T.; De Rooij, N.F.; Koudelka-Hep, M.; Wany, M.; Seitz, P. High-density microelectrode arrays for electrophysiological activity imaging of neuronal networks. In Proceedings of the ICECS 2001, 8th IEEE International Conference on Electronics, Circuits and Systems (Cat. No.01EX483), Malta, Malta, 2–5 September 2001; Volume 3, pp. 1239–1242.
37. Wang, K.; Fishman, H.A.; Dai, H.; Harris, J.S. Neural stimulation with a carbon nanotube microelectrode array. *Nano Lett.* **2006**, *6*, 2043–2048. [CrossRef] [PubMed]
38. Spira, M.E.; Hai, A. Multi-electrode array technologies for neuroscience and cardiology. *Nat. Nanotechnol.* **2013**, *8*, 83. [CrossRef] [PubMed]
39. Obien, M.E.J.; Deligkaris, K.; Bullmann, T.; Bakkum, D.J.; Frey, U. Revealing neuronal function through microelectrode array recordings. *Front. Neurosci.* **2015**, *8*, 423. [CrossRef] [PubMed]
40. Eversmann, B.; Jenkner, M.; Hofmann, F.; Paulus, C.; Brederlow, R.; Holzapfl, B.; Gabl, R. A 128/spl times/128 CMOS biosensor array for extracellular recording of neural activity. *IEEE J. Solid-State Circuits* **2003**, *38*, 2306–2317. [CrossRef]
41. Medeiros, M.C.; Mestre, A.; Inácio, P.; Asgarif, S.; Araújo, I.M.; Hubbard, P.C.; Biscarini, F. An electrical method to measure low-frequency collective and synchronized cell activity using extracellular electrodes. *Sens. Bio-Sens. Res.* **2016**, *10*, 1–8. [CrossRef]
42. Teulon, J.; Ronco, P.M.; Geniteau-Legendre, M.; Baudouin, B.; Estrade, S.; Cassingena, R.; Vandewalle, A. Transformation of renal tubule epithelial cells by simian virus-40 is associated with emergence of Ca^{2+}-insensitive K^+ channels and altered mitogenic sensitivity to K^+ channel blockers. *J. Cell. Physiol.* **1992**, *151*, 113–125. [CrossRef]
43. Sohma, Y.; Harris, A.; Wardle, C.J.C.; Gray, M.A.; Argent, B.E. Maxi K^+ channels on human vas deferens epithelial cells. *J. Membr. Biol.* **1994**, *141*, 69–82. [CrossRef]
44. Logsdon, N.J.; Kang, J.; Togo, J.A.; Christian, E.P.; Aiyar, J. A novel gene, hKCa4, encodes the calcium-activated potassium channel in human T lymphocytes. *J. Biol. Chem.* **1997**, *272*, 32723–32726. [CrossRef]
45. Ouadid-Ahidouch, H.; Van Coppenolle, F.; Le Bourhis, X.; Belhaj, A.; Prevarskaya, N. Potassium channels in rat prostate epithelial cells. *FEBS Lett.* **1999**, *459*, 15–21. [CrossRef]
46. Leybaert, L.; Sanderson, M.J. Intercellular Ca^{2+} waves: Mechanisms and function. *Physiol. Rev.* **2012**, *92*, 1359–1392. [CrossRef] [PubMed]
47. Kuga, N.; Sasaki, T.; Takahara, Y.; Matsuki, N.; Ikegaya, Y. Large-scale calcium waves traveling through astrocytic networks in vivo. *J. Neurosci.* **2011**, *31*, 2607–2614. [CrossRef] [PubMed]
48. Guilak, F.; Zell, R.A.; Erickson, G.R.; Grande, D.A.; Rubin, C.T.; McLeod, K.J.; Donahue, H.J. Mechanically induced calcium waves in articular chondrocytes are inhibited by gadolinium and amiloride. *J. Orthop. Res.* **1999**, *17*, 421–429. [CrossRef] [PubMed]

Sensors & Actuators: B. Chemical 288 (2019) 337–346

Contents lists available at ScienceDirect

Sensors and Actuators B: Chemical

journal homepage: www.elsevier.com/locate/snb

Electrostimulation in an autonomous culture lab-on-chip provides neuroprotection of a retinal explant from a retinitis pigmentosa mouse-model

Miguel Cabello[a,1], Marta Mozo[a,1], Berta De la Cerda[b,*], Carmen Aracil[a], Francisco J. Diaz-Corrales[b], Francisco Perdigones[a], Lourdes Valdes-Sanchez[b], Isabel Relimpio[c], Shom S. Bhattacharya[b], Jose Manuel Quero[a,*]

[a] Department of Electronic Engineering, University of Seville, Seville, Spain
[b] Department of Regeneration and Cell Therapy, Andalusian Molecular Biology and Regenerative Medicine Centre (CABIMER), Seville, Spain
[c] University Hospital Virgen Macarena, Seville, Spain; RETICS Oftared, Carlos III Institute of Health (Spain), Ministry of Health RD16/0008/0010

ARTICLE INFO

Keywords:
Lab-on-chip
Electrostimulation
Retinitis-Pigmentosa
Micro-incubator
Organotypic-culture
Neuroprotection

ABSTRACT

In this paper an autonomous culture system with the capability to electrostimulate organotypic cultures is described, and its utility is demonstrated by the neuroprotection achieved in retinal explants. The system is composed of a lab-on-chip (LOC), an electronic circuit and a data acquisition device. The LOC, in which the culture takes place, includes a microelectrode array (MEA), consisting of a PCB with a group of gold microelectrodes embedded in polydimethylsiloxane (PDMS), a microheater, a thermistor and a microfluidic circuit made of thermoplastic for feeding with culture medium. A plug made of PDMS has been included to facilitate the assembly of the culture LOC, the placement of the mouse retinas inside the MEA and the flow of culture medium. The transparency of the PDMS permits optical applications and a real time monitoring. An electronic circuit allows for a close monitoring of the experiment using a LabVIEW software specifically developed for this setting, including temperature control, heating and electrostimulation. In the experimental conditions, the retinal explants from retinitis pigmentosa mouse-models are dissected the day before neurodegeneration starts, when photoreceptor cell death is expected to progress along the following days, and cultured inside the LOC, using a fluorophore as a live-dead marker. The stimulation is a biphasic square signal of 0.5 V_{pp} and it is applied for five minutes every other day. Unstimulated RP explants and healthy retinas are used as controls. After seven days, a histological study is performed. We have demonstrated the applicability of this system as an organotypic culture LOC to test the effect of electrostimulation in retinal explants from different mouse models, and found a protective effect on photoreceptor cell death in the conditions tested.

1. Introduction

The development of lab on a chips (LOCs) [1–3] started to increase in the past decades and continues nowadays with application in many fields, including biological and medical sciences [4], biomedical and environmental monitoring [5], or diagnosis. Related to diagnosis application, LOC devices have been used, for example, for fast molecular diagnosis of multidrug-resistant tuberculosis [6], or for chronic disease [7]. In biology, LOCs have been used, among other purposes, as microincubators to study the behavior of different tissues or the dynamics of embryonic development, and even to grow the widely used model organism *Caenorhabditis elegans*. Other uses comprise biomedical research [8], bacterial biosensing [9] and cell culture in general [10]. LOCs can also be used as culture plates to keep alive and to analyze biological material.

There are some described examples in the literature of devices designed for *in vitro* studies of biological material being cell or tissue. Some of these devices include perfusion, some electrostimulation, signal acquisition, temperature or CO_2 control. For instance, the full-thickness human skin-on-chip with enhanced epidermal morphogenesis reported on [11] is very representative. This device required perfusion of culture medium to feed the skin, which had to be characterized and

* Co-corresponding authors.
E-mail addresses: mcabellov@gte.esi.us.es (M. Cabello), berta.delacerda@cabimer.es (B.D. la Cerda), quero@us.es (J.M. Quero).
[1] Both authors contributed equally to this work.

https://doi.org/10.1016/j.snb.2019.02.118
Received 20 September 2018; Received in revised form 4 February 2019; Accepted 26 February 2019
Available online 28 February 2019
0925-4005/

quantified. The insertion of the skin required the use of a cap. The perfusion incubator liver chip for 3D cell culture reported on [12] is another interesting and representative device, designed for chronic hepatotoxicity testing. It included a microheater to control the temperature in the biological range. In another example, the portable microfluidic device for the rapid diagnosis of cancer metastatic potential integrates a microincubator with temperature control [13]. None of these systems included microelectrode arrays (MEA) to analyze the samples or as electrostimulation system. Regarding MEA devices, for instance, the incubator-independent cell-culture perfusion platform, or the device used for extracellular recordings of prostate cancer cells, comprise a MEA for signal acquisition, but with no integrated temperature control in the system [14,15]. Among the electrostimulation systems, many MEA devices with electrodes made of different materials have been developed [16–18], but none of them integrates perfusion, heating or temperature control. The 3D-printed devices and electrostimulation chambers for culture reported on [19] proposed an useful approach to include this kind of actuation in a biological culture; however, these stimulation chambers were not integrated as a complete device with temperature control and an acquisition system using MEAs. Another example is the work reported on [20] with a MEA for electrical stimulation of samples and signal detection, but without perfusion.

Most of the devices previously referred demonstrate utility for biomedical or biological applications, which is the research field in which we are mainly interested. Starting from the state of the art, our project was to develop a useful device for biomedical studies in which a complete autonomous organotypic culture may be maintained alive, subjected to controlled electrical estimulation and with the possibility to apply drug administration as well as data acquisition. Our aim was to produce a platform to test different therapeutical interventions on the tissue. Our biological model system to test the utility of the designed device were retinal explants of mouse models for retinal degeneration, specifically, genetic models of retinitis pigmentosa (RP), which is the main cause of hereditary blindness in humans. In RP, the photoreceptors progressively degenerate as a result of different mutations [21]. Several therapeutic and prosthetic approaches are being pursued to help patients, including retinal implants for artificial vision. Among them, Second Sight Inc. developed the Argus II [22]. It has been clinically observed that, once the patient has had the implant working for a given time, a deceleration in the disease course can be empirically detected, even when the implant is not activated. A possible explanation for this observation is a neuroprotective effect of the electrical stimuli on the retinal cells during the implant activation, but experimentation for further confirmation of this theory has not been reported. Several studies have been referred on patients with RP and other retinal diseases [23–25], but as the subjects are patients, no histological data are available. Moreover, estimating stimulation ranges compatible with neuroprotection of the retina is not easy, some authors provide an array of possible strategies for vision restoration through retinal stimulation [26], while others report the damage of the retina due to electrical stimulation [27]. Here we present the testing of the neuroprotective capacity of the electrical stimuli on retinal explants as a proof of concept of the utility of our device for biomedical research.

In summary, the aim of the research work here reported is the development of a novel, autonomous, inexpensive, and electrophysiological useful culture device which works as a microincubator. Therefore, the proposed system includes microelectrodes array to develop the electrical stimuli, the heating and temperature control, that is, a microheater and a temperature sensor, to keep alive the biological material. In addition, the system is compatible with inverted microscopes and therefore transparency in some areas was a requirement, such as the area in which the microelectrodes are embedded in PDMS or the plug, also made of PDMS. In order to check the biocompatibility, viability and reliability of this system, proof of concept experiments have been performed with retinal explants from retinitis pigmentosa mouse-model as biological material and neuroprotection achieved *via* electrostimulation as the read-out for utility of the device. The proposed LOC allowed the culture and electrostimulation of retinal explants of mouse models of RP, but it is not limited to this purpose. The device is intended to be used to study the effect of combination of electrostimulation, controlled drug administration or metabolic conditions on different types of biological materials such as cells or organotypic cultures.

2. Design

The autonomous culture system described in this paper ensures the perfect conditions for long term organotypic cultures. It also supplies the electrostimulation to the tissue, as well as the connection to a computer which monitors the whole device. The design includes microfluidic and electronic components. The integration is an outstanding feature of this system. Moreover, the transparency of the effective working area of the MEA, in which the microelectrodes are embedded in PDMS and where the culture takes place, makes possible the use of a microscope, as it was explained in [20]. An external syringe pump is needed to feed the tissues with culture medium through an inlet port, while an outlet port is connected to a flask to discard the waste. The general assembly is shown in Fig. 1.

The autonomous culture system is divided into two different parts, each one with a different function (Fig. 2). Firstly, the LOC, which is the most important part of the system, because it contains the biological material culture. It allows the supply of nutrients and establishes a direct interface with the retinas. All the materials which are directly in contact with the biological material are biocompatible, making this device suitable for its biomedical and biological application. Secondly, an external electronic module, based on a printed circuit board, is necessary to incorporate the electronic components, both to control the system and to stimulate the culture. The design has been divided in these two modules, to make the LOC more portable. In this way, the electronic module can be reusable for different systems. Both modules are connected by electrical connectors.

Focusing in the LOC, the substrate is a printed circuit board made of fire retardant glass fiber epoxy laminate (FR4) and copper, that includes a MEA with gold microelectrodes to stimulate and acquire the signals from the culture. The MEA also includes a microheater and a Negative Temperature Coefficient (NTC) thermistor to measure and control temperature. Then, the microfluidic circuit, which allows the flow of culture media, made of PMMA, is glued to this substrate. This microfluidic circuit is designed to assure a homogeneous distribution of the culture media. A plug made of PDMS facilitates the insertion and extraction of the retinas in the LOC. A scheme (top view) of this module is shown in Fig. 3.

The external electronic module includes power and acquisition electronic components, connectors to the LOC device and a computer. It

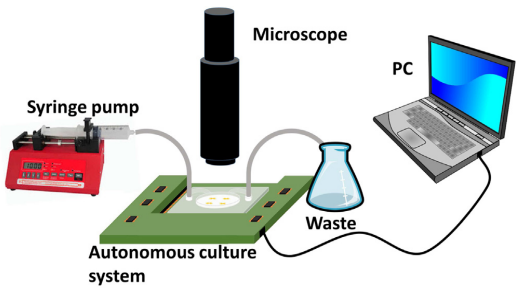

Fig. 1. Scheme of the system assembled with the rest of instruments and equipment. The culture medium is pumped by an external pump, and the waste is stored in a flask. The culture system is connected to a data acquisition device and then to the PC.

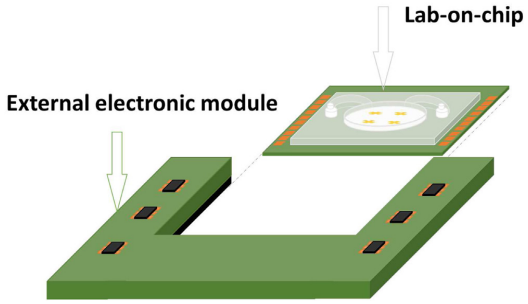

Fig. 2. The autonomous culture system is composed of the lab-on-chip and an external electronic module. Both parts are aligned and connected by means of a connector, and fixed with plastic screws.

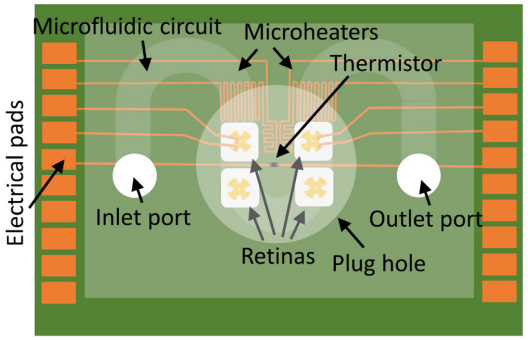

Fig. 3. Simplified scheme of the lab-on-chip. The PDMS plug facilitates the insertion and extraction of retinas. The gold electrodes are embedded in PDMS reservoirs where the retinal explants are placed. Actually, there are twenty electrodes, but only two have been drawn to simplify the scheme. In the same way, the image only includes two microheaters, instead of four. The thermistor is located at the center of the design to measure the temperature adequately. The inlet and outlet ports are connected to the syringe pump and the flask respectively.

incorporates the whole electronic components to achieve the temperature control, the stimulation and the acquisition of the signal from the culture. This electronic module is connected to a data acquisition device, from National Instruments, for monitoring of the whole process. The data acquisition device is controlled through a LabVIEW software program. Different parameters of the signals can be selected in the stimulation.

3. Fabrication process

The most notable aspect of the fabrication process of the presented system is related to the LOC, which integrates a MEA, a microfluidic structure made of PMMA and a plug made of PDMS. The correct assembly between each part of the system determines the proper functioning of the LOC. The fabrication process of the MEA has been carried out following the same process described in Cabello et al. [20]

The step by step fabrication process of the microfluidic structure and its bonding to the MEA is shown Fig. 4. This microfluidic structure is made of PMMA (step (a)). The fabrication process consists in micromilling the piece of PMMA according to a previously designed microfluidic circuit. The diameter of the milling tool is 2 mm, and the channel dimensions are 1 mm of depth and 5 mm of width. A circular hole, with the dimensions of the plug, is located in the center of the microfluidic structure (step (b)). A thick wall of 2 mm of width

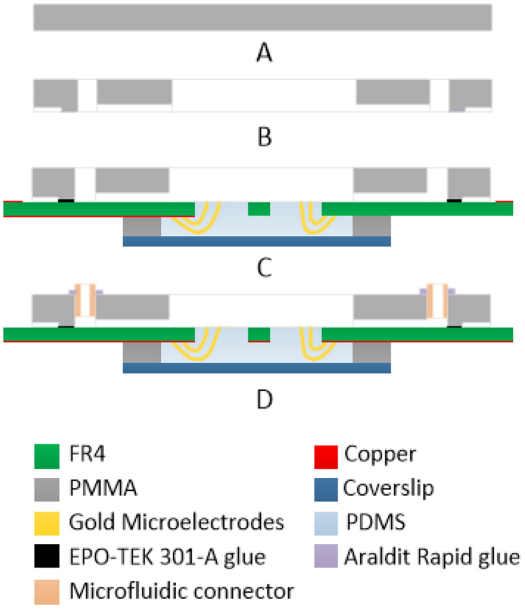

Fig. 4. Steps of the fabrication process and bonding of the microfluidic structure: (A) Piece of PMMA of 5 mm thick; (B) Micromilling of the piece of PMMA; (C) Bonding of the microfluidic structure to the MEA; (D) Bonding of the microfluidic connector to the microfluidic structure.

surrounds the fluidic channels and the hole, in order to facilitate the subsequent bonding; the microfluidic structure is directly bonded to the MEA using a biocompatible, two component, room temperature curing epoxy (EPO-TEK 301, Epoxy Technology). The epoxy glue is deposited in a planar surface using a roller to assure that the glue layer has 86 μm of thickness. Then, a stamping method has been carried out to adhere the epoxy to the microfluidic structure. 24 hours at room temperature are necessary to assure a correct bonding between the MEA and the piece of PMMA (Step (c)). Once the PMMA structure is bonded to the MEA, the microfluidic luer connectors are located in their holes and bonded with a two component epoxy (Araldit Rapid) for one hour (step (d)).

Fig. 5 shows the fabrication process of the plug, step by step. This fabrication process can be carried out separately from the other part of the system. Due to its transparency and biocompatability, the plug is made of PDMS. Other important reason to choose PDMS as the fabrication material of the plug is related to its flexibility and workability. PDMS is deposited in a liquid state and, after a curing time, it becomes a silicone-like solid. The substrate of the mold is an aluminum sheet of 5 mm thick (step (a)). The next step consists in micromilling this aluminum sheet with a 2 mm mill tool, to create the desired microfluidic structure (step (b)). Once the mold is fabricated, a 3D structure made of plastic is located inside the cast (step (c)). This 3D structure allows for the control of PDMS deposition, and it also assures the desired height of the plug. Once PDMS is deposited, the mold is covered with a plastic sheet, to avoid the leakage of the PDMS (step (d)). Finally, the mold with the deposited PDMS is introduced into an oven at 70 °C for 90 min. When the PDMS is cured, it is possible to release it from the mold, resulting in the final plug which is ready to be used together with the rest of the LOC (step (e)).

Fig. 6 a) shows the result of the fabrication process and bonding of the microfluidic structure. It can be observed how the wall surrounding the channels facilitates the adhesion, and how the luer connectors are

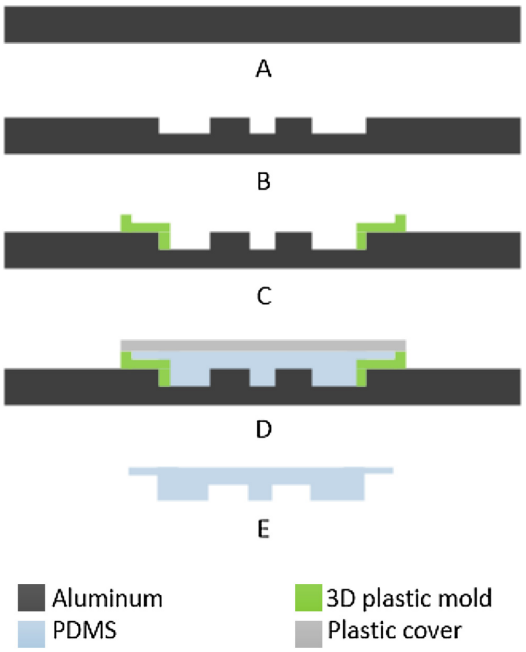

Fig. 5. Steps of the fabrication process of the plug: (A) Aluminum sheet; (B) Micromilling of the mold made of aluminum; (C) 3D structure to control the deposition of PDMS; (D) Deposition of PDMS inside the mold; (E) De-molding of the plug.

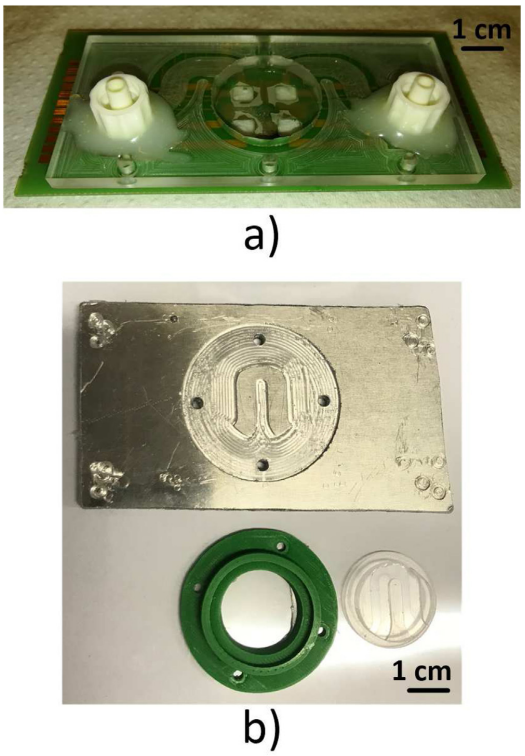

Fig. 6. Final results of the fabrication process: (A) Microfluidic structure bonded to the MEA; (B) Mold, 3D structure and plug made of PDMS after temperature curing.

bonded with glue to assure the water-tightness, which was indispensable to maintain the sterility inside the tissue culture setting. Fig. 6 b) shows the fabricated plug, the mold made of aluminum and the 3D structure which controls the deposition of PDMS. In the complete LOC, with the plug inserted in place, the adherence of the PDMS makes a seal around the plug tight enough to hold the inner pressure from the culture media flow.

4. Materials and methods

4.1. Fluidic connections and culture medium feeding

A combination of male Luer to 10-23 threads screwed inside the PMMA and female Luer to 1/16" ID tubing (45505-84 and 45508-01 respectively, Cole-Parmer Instrument) have been used, assuring the proper connection with the culture device. Tubing is Tygon 2375, with an internal diameter of 1.6 mm (RS). The media reservoir used is a sterilized 60 mL syringe, in which the total volume of media needed for the whole culture experiment is stored. If the media contains any photosensitive substance, the syringe and tubing are completely covered in black insulating. A 0.22 μm-pass filter (Millex-FG, Merck Millipore) is inserted between the tube and the syringe to keep the sterility of the culture medium. A syringe pump (New Era Pump Systems, Inc.) is the impulsion method used for the continuous media flow.

4.2. Biological material

Four biocompatibility tests were performed with adult WT C57BL/6J mice and models of degenerating retina such as albino CD1 and the retinitis pigmentosa models *Pde6b*^{rd10} (rd10) and *Pde6b*^{rd1} (rd1). One retina of each type was used for each test, with a total of 16 animals used and 16 retinas analyzed. Four electrostimulation assays were performed with 7 day-old WT and rd1 mice, In each experiment two retinas of each type were used, with a total of 8 animals used and 16 retinas analyzed. Two electrostimulation experiments were also performed with 14 day-old WT and rd10 mice providing similar results to the rd1 (data not shown), using 8 retinas from 4 animals. The complete set of experiments used 40 retinas from 28 animals. All mice were provided by Jackson Laboratory, and were maintained in-house in cyclic 12:12 hour light cycles in a pathogen-free animal facility and sacrificed using CO_2 inhalation. All experimental procedures have been previously approved by the local "Animal Care and Use" ethical committee.

4.3. Explant culture

Aseptic technique has been used to dissect the neuroretinas. Once the eyes are enucleated, the procedure is performed in a sterile cell culture hood. Regular retinal dissection is performed. Eyes are rinsed in 1% penicillin-streptomycin before dissection. Anterior segment is removed and neuro-retinas peeled from retinal pigmented epithelium. Deposition for culture in the wells of the device in their final position is helped with the support of a PVDF membrane (Amersham Hybond-P, GE Healthcare) as scaffold and explants are covered with 0.4 μM Millicell membrane (Millipore) with the ganglion cell layer downwards for electrostimulation. The culture medium used is Neurobasal A supplemented with 2% B27, 1% N2, 1% penicillin-streptomycin solution and 0.4% glutamax (All media components from Gibco). The

Table 1
Electrical stimulation of the culture

Repetition	Frequency (Hz)	Voltage (V_{pp})
1	30	0.5
2	15	0.5
3	20	0.5
4	40	0.5
5	10	0.5

transparency of the device allows the visualization of the cell viability using FITC-conjugated Cholera toxin subunit B (FITC-CTB; C-1655, Sigma-Aldrich) used according to the manufacturer's instructions.

4.4. Electrostimulation

The starting model for the retinal stimulation in humans is the Argus II retinal prosthesis [28]. The impedance of the electrodes has been calculated, the current values has been converted to voltage values and the pattern of the stimulation frequency has been adapted from the bibliography [24]. The electrical stimulation consists of a biphasic square signal of 0.5 V_{pp}, with frequency ranges between 10 Hz and 40 Hz. Work from Zrenner lab [25] reports stimulation for 30 minutes one day per week during a total of six weeks. According to these calculations, the retinal explant culture for seven days gives an estimation of 3 stimulation periods of 5 minutes distributed along the week of culture. Thus, the electrical stimulation has been applied in 3 alternative days, starting the second day of culture and consisting of 5 stimulations per day, 1 minute per cycle. Between every repetition, the stimulation frequency has been changed in order to achieve different response thresholds (Table 1). The voltage is fixed to 0.5 V_{pp}, and the output current to 2 mA, due to the specification of the NI DAQ 6211 used to control the system and stimulate the culture.

4.5. Histological studies

After the finalization of the culture, tissues are fixed in paraformaldehyde, washed in phosphate buffered saline (PBS), embedded in 4% agarose and cryopreserved by sequentially equilibrating in a solution with increasing sucrose concentration [29]. Blocks for cryostat sectioning are prepared in molds with OCT (Tissue Tech) and 18 μm sections are used for subsequent staining with hematoxylin-eosin or specific antibodies. In both cases, standard staining and immunostaining protocols have been used. For immunofluorescent staining, anti-opsin (AB 5407 Millipore) and anti-rhodopsin (ab190307 Abcam) have been used as primary antibodies; anti-rabbit (emission 488 nm, A-21206 Life technologies) and anti-mouse (emission 633 nm, A-21052 Life technologies) have been used as secondary antibodies, and DAPI for nuclei staining.

4.6. TUNEL staining

Retinal sections obtained from electrostimulated and non-electrostimulated explants are subjected to TUNEL staining following manufacturer's instructions (In Situ Cell Death Detection kit, Fluorescein; Roche). As a positive control of cell death, DNase I treatment is provided to a WT retinal section. DAPI has been used for nuclei staining.

4.7. Imaging and image treatment

Optic microscopy is used for the imaging of hematoxylin-eosin stained sections using a Leica DM 2500 apparatus with 10x magnification. Microscopy in a confocal Leica TCS SP5 apparatus is used for the imaging of immunostained and TUNEL-stained sections with 40x magnification. ImageJ (FIJI version) software is used for the image treatment and for the calculation of signal intensities. For the counting of nuclei per layer, 12 rows of nuclei are counted in five consecutive sections for each of the retinal layers. For the calculation of TUNEL vs. DAPI fluorescence ratio, intensities from 10 sections are measured for each condition. Mean and standard deviation are calculated and represented using Excel.

5. Results and discussion

5.1. Conditions for organotypic culture and biocompatibility

After the fabrication of the LOC with biocompatible materials, the survival of retinal explants inside the LOC has been tested, as well as the conditions of tissue placement and organotypic culture. WT mice retinas have been used as biological material to test the culture conditions. The ganglion cell layer has been deposited facing the PDMS substrate with the gold microelectrodes. The specific deposition method used is described in [30]. To keep the cells alive, nutrients, O_2, CO_2 and a balanced pH are supplied by a continuous flow of culture media (Neurobasal-A, Gibco) [31–33]. The initial flow of culture media has been decided according to data from the bibliography [34,35], which means a constant flow of 3.6 μL/min for the correct maintenance of four retinal explants in our device.

The biological material has been checked along the 7-day explant culture thanks to the transparency of PDMS, used to fabricate the plug and the effective working area with the gold microelectrodes embedded, allowing microscopy and live-fluorescence staining. FITC-conjugated cholera toxin subunit B (CTB) provides specific staining of ganglion cells due to its affinity for the ganglioside GM1. Fluorescence emission requires active transport of the product inside the cell [32], thus labeling only living cells. In this setting, the fluorophore is added to the culture medium every two days, because fluorescence peaks after 24 hours of incubation and decays after 48 h. The viability of CTB as a live-cell marker has been validated by damaging the cells with temperature or with different concentrations of hydrogen peroxide and we have found a good correlation between CTB fluorescence and live-dead status of the retinal tissue (Fig. 7).

Once the conditions for retinal explant culture in the device were set, several biocompatibility tests have been performed, maintaining the retinal explants for seven days inside the LOC without electrical stimulation. As source of biological material, WT mice and animal models of degenerating retina such as albino CD1, and the RP models rd10 and rd1, have been used.

In Fig. 8 the result of the biocompatibility test for WT and CD1 retinas is shown. After seven days of organotypic culture, retinas are taken off the device, fixed and prepared for histological analysis, making sections and immunostaining. It has been checked that, after one week of culture, WT and CD1 retinas both maintain their respective natural structure in layers. Like in the human tissue, mouse retina is a tightly structured tissue in which any distortion of the cell layers can be related to disease. From the outer to the inner side of a retinal section, a structure conformed by cell layers can be found; first, the outer nuclear layer (ONL) constituted by photoreceptors (rods and cones), which sense the light and transmit the neural signal to the processing neurons in the second layer, formed by bipolar, amacrine and horizontal cells, named altogether as inner nuclear layer (INL). The last layer is the ganglion cell layer (GCL), whose axons transport the visual information to the brain. In Fig. 8A and 8 E, DAPI staining of nuclei shows from top to bottom the integrity of the three retinal layers. To further visualize tissue preservation, the immunostaining of sections has been performed with specific antibodies for cones (opsin, in green, in Fig. 8B and 8 F) and for rods (rhodopsin, in red, in 8 C and 8 G) to verify the correct localization of photoreceptor pigments in the retina. Visual pigments of rods and cones in the healthy retina are located in the outer segments of the photoreceptor cells, on top of the ONL (8 B–D) as can be seen for WT retinas. Localization of the pigment signals in the bodies of the photoreceptor layer is shown for CD1 retina (8 F-H) compatible with

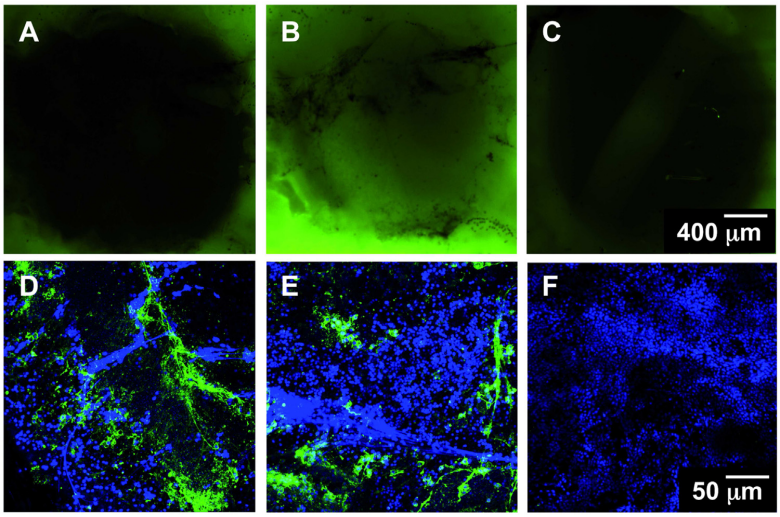

Fig. 7. Viability of CTB as a marker of living ganglion cells in the device. Upper row: Direct microscopy visualization of CTB staining of retinal explants in the LOC system; (A) Retinal explant without CTB; (B) Retinal explant after 24h of CTB incubation in the culture medium; (C) Retinal explant with added CTB and cell death induced by heating of the sample. Bottom row: Confocal microscopy images of ganglion cell fibers stained with CTB (in green) and DAPI for nuclear staining (in blue). CTB signal depends on live-dead status of cells: (D) Healthy tissue; (E) Tissue treated with 600 μM H_2O_2 for 15 min inducing mild cellular damage; (F) Tissue treated with 600 mM H_2O_2 for 15 min inducing complete cell death.

the mild degenerative state naturally found in the albino retina. These results suggest that culturing retinal explant in the proposed LOC keeps the natural features of the retinal tissue for at least one week, both for healthy and dystrophic retinas. Similar results have been obtained for retinas of rd1 and rd10 mouse models (data not shown).

5.2. Electrostimulation results

Along the experiments, CTB live-staining provides a follow-up of the health of the retinal explants. After each 7-day experiment, tissue is collected from the culture system, prepared for histological examination, sectioned and stained using different approaches to check for the preservation of the retinal structure, the correct localization of photoreceptor markers and the quantification of cell death. In every case, all these parameters have been compared between treated and non-treated rd1 retinas and a healthy WT retina has been used as control for normal tissue. The results presented are representative of four independent experimental replicates.

Firstly, the histological structure of the retinal layers is checked using the classic eosin-hematoxylin staining, which stains all cells and nuclei. In Fig. 9, it can be seen that retinal structure is completely distorted in the untreated rd1 sample (Fig. 9C) compared to the healthy control (Fig. 9A), cultured simultaneously in an adjacent well of the device. The electrostimulated rd1 retinal explant presents an intermediate state, with mild degenerative changes only in the ONL. Rd1 degeneration is specific for photoreceptors, so it is expected to see changes mainly in the ONL. A typical measurement for retinal degeneration is the quantification of the number of nuclei per row in the retinal layers. We have calculated the mean number of nuclei from 12 rows per layer, counted in five different retinal sections for each

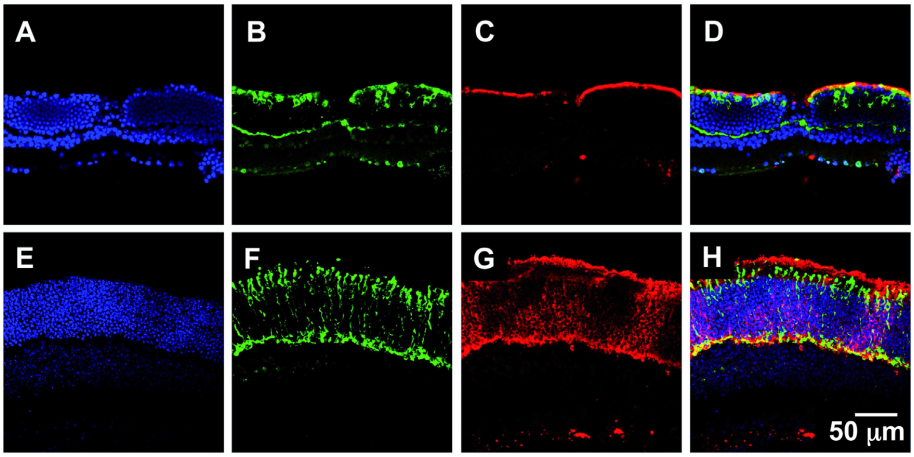

Fig. 8. Biocompaibility of the autonomous device with retinal explant culture from different mouse models. (A-D) Upper row shows pigmented-mouse WT retina sections depicting normal morphology and photoreceptor immunostaining; (E-H) bottom row corresponds to albino CD1 retina showing abnormal localization of rhodopsin and opsin. (A, E) DAPI staining for nuclei in blue; (B, F) immunostaining for opsin (cones) in green; (C, G) immunostaining for rhodopsin (rods) in red; (D, H) composite images.

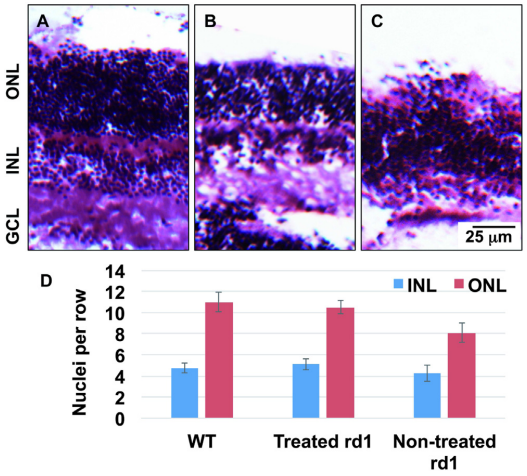

Fig. 9. Effect of electrostimulation in the histology of the tissue. Eosin-hematoxylin staining of retinal explant sections. (A) WT control; (B) Rd1 treated with electrostimulation; (C) Rd1 non-treated control; (D) Quantification of nuclei per row in the ONL and INL of (A), (B) and (C) experimental conditions. ONL: Outer nuclear layer; INL: Inner nuclear layer; GCL: Ganglion cell layer.

experimental condition, and we have observed that the electrostimulation in the device protects the ONL of the rd1 treated retina from loosing cells, as the number of nuclei in this layer is not significantly different from healthy control, while there is a notable difference with the untreated rd1 tissue (Fig. 9D).

Secondly, retinal sections have been used to localize the visual pigments of rods and cones. Delocalization of these pigments is one of the hallmarks of retinal degeneration indicating cell dysfunction preceding cell death.

In the experimental design presented, retinas are dissected the day before the degenerative process starts, and after the 7-day organotypic culture the disease progress is compared in treated and non-treated rd1 retinas, having always a healthy control WT retina cultured at the same time. In Fig. 10, confocal microscopy images of retinal sections stained for nuclei and immunostained for opsin and rhodopsin are shown. These images are organized in three rows, from top to bottom: WT (Fig. 10A-D), treated rd1 (Fig. 10E-H) and non-treated rd1 (Fig. 10I-L). Last picture of each row is a composite image. The main differences between the treated and untreated retinal explants can be seen in the opsin staining pattern, which shows a slight delocalization in Fig. 10F, corresponding to treated rd1 retina, compared to WT (Fig. 10B), but the staining pattern is really distorted in the amount of labeling and the localization of the signal in Fig. 10J, corresponding to non-treated rd1. For rhodopsin, a decrease in the signal can also be seen, as expected, in non-treated rd1 (Fig. 10K), while treated rd1 retina (Fig. 10G) shows the same staining and localization pattern as in WT control (Fig. 10C). In summary, composite images (Fig. 10D, H, L) depict a normal immunostaining for visual pigments in both WT and treated-rd1 retinas cultured for one week in the device, while a dystrophic staining pattern and morphology is shown for non-treated rd1 cultured in the same conditions, as expected for a diseased and degenerating tissue.

From these images, it is possible to confirm that the electrical stimulation to the rd1 RP model retina in the autonomous LOC culture system has a protective effect from the delocalization of visual pigments that occurs during the natural degenerative course of the RP disease.

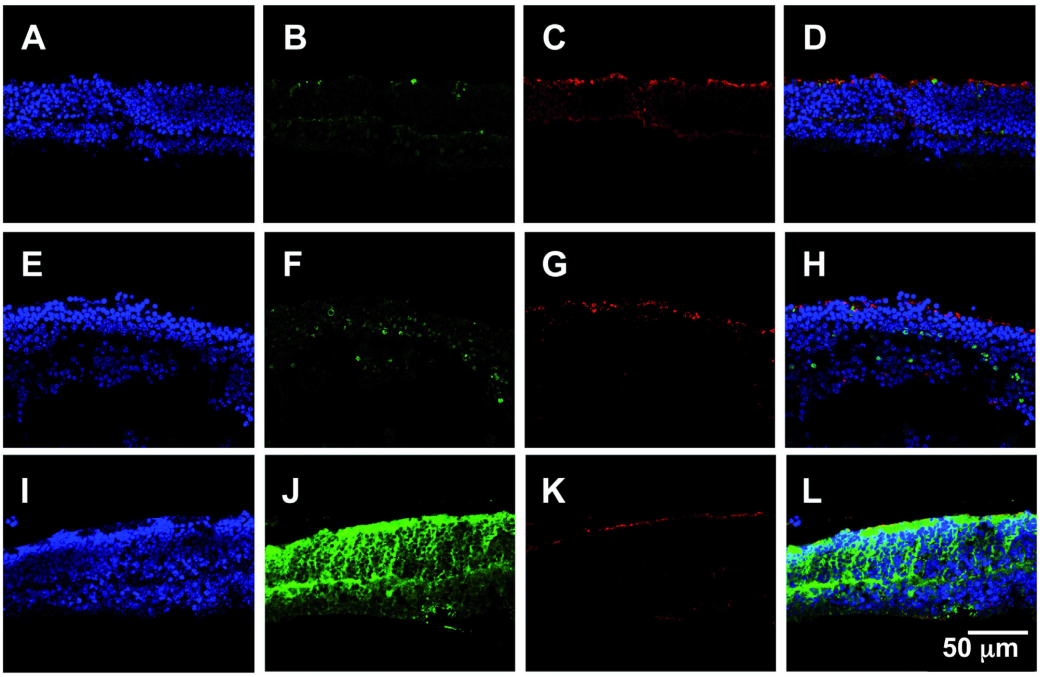

Fig. 10. Effect of electrostimulation in the disorganization of photoreceptor cells in the retinal explants. (A-D) Upper row is WT retina; (E-H) middle row is rd1 electrostimulated retina; (I-L) lower row is rd1 non-treated retina. (A, E, I) DAPI staining for nuclei in blue; (B, F, J) immunostaining for opsin (cones) in green; (C, G, K) immunostaining for rhodopsin (rods) in red; (D, H, L) composite images.

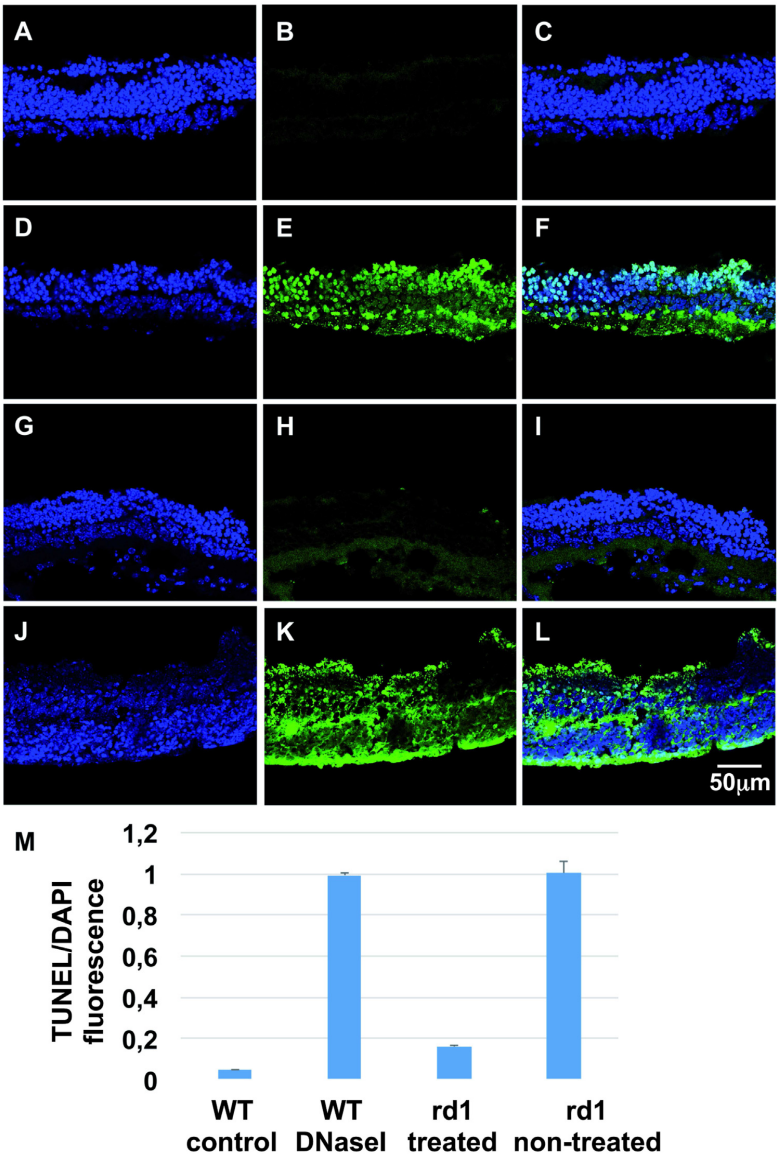

Fig. 11. Effect of electrostimulation in programmed cell death. (A-C) Upper row is WT sample used as negative control; (D-F) second row is WT sample with induced DNA damage used as positive control for TUNEL labeling; (G-I) third row is rd1 retina treated with electrostimulation; (J-L) lower row is non-treated rd1. For all the samples: left column is nuclear DAPI staining; central column is TUNEL fluorescence reflecting DNA damage associated to cell death; and composite images are shown at the right column. (M) Quantification of mean intensity for TUNEL fluorescence relative to DAPI staining.

To gain some insight on the biological effect of the electrical stimuli provided to the retinas cultured in this device, we have performed a TUNEL staining for the visualization and quantification of apoptosis (programmed cell death) at the single cell level [36,37]. The assay has been performed to sections of rd1 retinal tissue subjected or not to electrical stimulation along the organotypic explant culture. WT retina was used as a negative control and a positive control had DNA damage pre-treatment before staining. In Fig. 11 data is presented in columns in which, from left to right it is shown: firstly, the DAPI staining of cell nuclei; in the middle, the FITC labeling of DNA strand breaks due to TUNEL reaction and, at the right, a composite image to visualize co-localization, marking individual apoptotic cells. WT negative control (Fig. 11A-C) depicts absence of cell death, showing just background fluorescence (Fig. 11B). Fig. 11D-F displays the positive control, with a clear co-localization of FITC with the cell nuclei. Fig. 11G-I corresponds to rd1 retina treated with electrostimulation, in which only a few disperse nuclei showed some apoptotic-related fluorescence compared to images of the non-treated rd1 retina in Fig. 11J-L that exhibit the

natural course of retinal degeneration with a very high intensity of fluorescence in Fig. 11K and the co-localization of apoptotic signal with nuclei in Fig. 11L.

In Fig. 11M quantification of relative fluorescence shows approximately the same values for the positive control (WT with induced DNA damage) and for non-treated rd1 retina. Both WT control and electrostimulated rd1 retina present a very low level of relative intensity, indicating that the number of cells undergoing programmed cell death in treated rd1 retinas is similar to the healthy control.

From this last set of data it can be concluded that the stimuli provided to the retinal explants in the autonomous device has protected the photoreceptors from their normal course of apoptotic cell death in an organotypic model of RP.

6. Conclusions

In this paper, an autonomous novel LOC useful for organotypic tissue culture and electrophysiology is presented. The integration of different actuators, such as a microheater or gold microelectrodes, and sensors, such as a NTC thermistor, and their behavior, have been characterized successfully. The development of a plug to provide the sterility and watertightness of the culture module, and to facilitate the insertion and extraction of the biological material, completes the system, which works as a microincubator. In comparison with other devices reported in the literature presenting LOCs or microfluidic culture platforms, our system clusters all the components needed to carry out an autonomous organotypic culture, with perfusion, heating, temperature control and electrostimulation, conjointly controlled through a user-friendly program. Correct and integrated functioning of each part has been tested with mouse retinal explants with satisfactory results, demonstrating the biocompatibility and capability of the system to function as an autonomous tissue culture setting for retinal explants independent of standard CO_2 cell incubator. In addition, we have observed that retinas provided with periodic electrical stimuli along the whole-tissue culture in the autonomous LOC display a better preservation of the tissue structural features and lesser apoptotic cell death in the photoreceptor cell layer compared with non-treated RP retinal explants. This system will be useful to further study the effect of electrical stimuli directly applied on the retinal cells, mimicking what happens with the retinal implants in patients. A more profound understanding of neuroprotection mechanisms elicited by electrical stimuli is of outmost importance for a future use of direct electrical stimulation in the retina as a therapeutic intervention for RP.

The presented LOC may enable laboratories not specialized in biology to perform some studies using biological material without the need of an expensive cell culture incubators, but the fundamental benefit of this device is its flexibility: the design is compatible with different types of cells and tissues that can be exposed to controlled electrical stimulation and/or concomitant metabolic modifications, drug administration, and even light stimulation. In addition to end point histology, monitoring of the biological material along any experiment is feasible by optical microscopy with live staining methods and by analysis of the molecules and metabolites released by the biological material, which may be collected from the wasted culture media. Altogether, the system provides a quite complete set of variable parameters to treat cells or tissue as well as different methods to obtain information about the effect of the treatment/s on the biological material.

Acknowledgements

This work was supported by the Spanish Ministry of Science and Innovation (project TEC2014-54449-C3-2-R, BIOLOP), by ISCIII (Miguel Servet-I, 2015) cofinanced by the European Regional Development Fund (ERDF) (CP15/00071) and the Andalusian Health Ministry (Fundacion Publica Andaluza Progreso y Salud).

References

[1] D. Mark, S. Haeberle, G. Roth, F. von Stetten, R. Zengerle, Microfluidic lab-on-a-chip platforms: requirements, characteristics and applications, Chemical Society Reviews 39(3)(2010)1153-1182.
[2] P. Abgrall, A. Gue, Lab-on-chip technologies: making a microfluidic network and coupling it into a complete microsystem-a review, J. Micromech. Microeng. 17 (5) (2007) R15.
[3] V.C. Romao, S.A. Martins, J. Germano, F.A. Cardoso, S. Cardoso, P.P. Freitas, Lab-on-chip devices: Gaining ground losing size, ACS Nano 11 (11) (2017) 10659–10664.
[4] D. Figeys, D. Pinto, Lab-on-a-chip: a revolution in biological and medical sciences, Anal. Chem. 72 (9) (2000) 330–A.
[5] J. Gardeniers, A. Van den Berg, Lab-on-a-chip systems for biomedical and environmental monitoring, Anal. Bioanal. Chem. 378 (7) (2004) 1700–1703.
[6] A.M. Cabibbe, P. Miotto, R. Moure, F. Alcaide, S. Feuerriegel, G. Pozzi, V. Nikolayevskyy, F. Drobniewski, S. Niemann, K. Reither, et al., Lab-on-chip-based platform for fast molecular diagnosis of multidrug-resistant tuberculosis, J. Clin. Microbiol. 53 (12) (2015) 3876–3880.
[7] J. Wu, M. Dong, C. Rigatto, Y. Liu, F. Lin, Lab-on-chip technology for chronic disease diagnosis, NPJ Digital Med. 1 (1) (2018) 7.
[8] M. Cornaglia, L. Mouchiroud, A. Marette, S. Narasimhan, T. Lehnert, V. Jovaisaite, J. Auwerx, M.A. Gijs, An automated microfluidic platform for C. elegans embryo arraying, phenotyping, and long-term live imaging, Scientific reports 5 (2015) 10192.
[9] E. Clasen, K. Land, T.-H. Joubert, Micro-incubator for bacterial biosensing applications, in: Fourth Conference on Sensors, MEMS, and Electro-Optic Systems, Vol. 10036, International Society for Optics and Photonics, 2017, p. 100360G.
[10] S. Halldorsson, E. Lucumi, R. Gómez-Sjöberg, R.M. Fleming, Advantages and challenges of microfluidic cell culture in polydimethylsiloxane devices, Biosens. Bioelectron. 63 (2015) 218–231.
[11] G. Sriram, M. Alberti, Y. Dancik, B. Wu, R. Wu, Z. Feng, S. Ramasamy, P.L. Bigliardi, M. Bigliardi-Qi, Z. Wang, Full-thickness human skin-on-chip with enhanced epidermal morphogenesis and barrier function, Mater. Today 21 (4) (2017) 326–340.
[12] F. Yu, R. Deng, W.H. Tong, L. Huan, N.C. Way, A. IslamBadhan, C. Iliescu, H. Yu, A perfusion incubator liver chip for 3d cell culture with application on chronic hepatotoxicity testing, Scientific Reports 7 (1) (2017) 14528.
[13] I. Yu, Y. Yu, L. Chen, S. Fan, H. Chou, J. Yang, A portable microfluidic device for the rapid diagnosis of cancer metastatic potential which is programmable for temperature and co2, Lab on a Chip 14 (2014) 3621–3628.
[14] D. Saalfrank, A. Konduri, S. Latifi, R. Habibey, A. Golabchi, A. Martiniuc, A. Knoll, S. Ingebrandt, A. Blau, Incubator-independent cell-culture perfusion platform for continuous long-term microelectrode array electrophysiology and time-lapse imaging, Royal Society Open Sci. 2 (2015) 150031.
[15] M. Cabello, H. Ge, C. Aracil, D. Moschou, P. Estela, J. Quero, S.I. Pascu, P.R.F. Rocha, Extracellular electrophysiology in the prostate cancer cell model pc-3, Sensors 19 (2019) 139.
[16] D. Braeken, R. Huys, J. Loo, C. Bartic, G. Borghs, G. Callewaert, W. Eberle, Localized electrical stimulation of in vitro neurons using an array of sub-cellular sized electrodes, Biosens. Bioelectron. 26 (4) (2010) 1474–1477.
[17] J. Chłopek, B. Czajkowska, B. Szaraniec, E. Frackowiak, K. Szostak, F. Beguin, In vitro studies of carbon nanotubes biocompatibility, Carbon 44 (6) (2006) 1106–1111.
[18] Y.H. Kim, G.H. Kim, A.Y. Kim, Y.H. Han, M.-A. Chung, S.-D. Jung, In vitro extracellular recording and stimulation performance of nanoporous gold-modified multielectrode arrays, J. Neural Eng. 12 (6) (2015) 066029.
[19] J.D. Wardyn, C. Sanderson, L.E. Swan, M. Stagi, Low cost production of 3d-printed devices and electrostimulation chambers for the culture of primary neurons, J. Neurosci. Methods 251 (2015) 17–23.
[20] M. Cabello, C. Aracil, F. Perdigones, M. Mozo, B. de la Cerda, J.M. Quero, Gold microelectrodes array embedded in pdms for electrical stimulation and signal detection, Sens. Actuators B Chem. 257 (2018) 954–962.
[21] D.T. Hartong, E.L. Berson, T.P. Dryja, Retinitis pigmentosa, The Lancet 368 (9549) (2006) 1795–1809.
[22] A.K. Ahuja, J. Dorn, A. Caspi, M. McMahon, G. Dagnelie, P. Stanga, M. Humayun, R. Greenberg, A.I.S. Group, et al., Blind subjects implanted with the argus ii retinal prosthesis are able to improve performance in a spatial-motor task, Br. J. Ophthalmol. 95 (4) (2011) 539–543.
[23] M.S. Humayun, E. de Juan Jr., J.D. Weiland, G. Dagnelie, S. Katona, R. Greenberg, S. Suzuki, Pattern electrical stimulation of the human retina, Vision Res. 39 (15) (1999) 2569–2576.
[24] L. Naycheva, A. Schatz, T. Röck, G. Willmann, A. Messias, K. U. Bartz-Schmidt, E. Zrenner, F. Gekeler, Phosphene thresholds elicited by transcorneal electrical stimulation in healthy subjects and patients with retinal diseases, Investigative ophthalmology & visual science 53(12)(2012)7440-7448.
[25] A. Schatz, T. Röck, L. Naycheva, G. Willmann, B. Wilhelm, T. Peters, K. U. Bartz-Schmidt, E. Zrenner, A. Messias, F. Gekeler, Transcorneal electrical stimulation for patients with retinitis pigmentosa: a prospective, randomized, sham-controlled exploratory study, Investigative ophthalmology & visual science 52(7)(2011)4485-4496.
[26] L. Yue, J.D. Weiland, B. Roska, M.S. Humayun, Retinal stimulation strategies to restore vision: Fundamentals and systems, Prog. Retin. Eye Res. 53 (2016) 21–47.
[27] A. Butterwick, A. Vankov, P. Huie, Y. Freyvert, D. Palanker, Tissue damage by pulsed electrical stimulation, IEEE Trans. Biomed. Eng. 54 (12) (2007) 2261–2267.
[28] J.D. Dorn, A.K. Ahuja, A. Caspi, L. Da Cruz, G. Dagnelie, J.-A. Sahel, R.J. Greenberg,

M.J. McMahon, A.I.S. Group, et al., The detection of motion by blind subjects with the epiretinal 60-electrode (argus ii) retinal prosthesis, JAMA Ophthalmol. 131 (2) (2013) 183–189.

[29] D.J. Hare, J.L. George, L. Bray, I. Volitakis, A. Vais, T.M. Ryan, R.A. Cherny, A.I. Bush, C.L. Masters, P.A. Adlard, et al., The effect of paraformaldehyde fixation and sucrose cryoprotection on metal concentration in murine neurological tissue, J. Anal. At. Spectrom. 29 (3) (2014) 565–570.

[30] K. Reinhard, A. Tikidji-Hamburyan, H. Seitter, S. Idrees, M. Mutter, B. Benkner, T.A. Münch, Step-by-step instructions for retina recordings with perforated multi electrode arrays, PLoS One 9 (8) (2014) e106148.

[31] R. M. Sappington, T. Sidorova, D. J. Long, D. J. Calkins, Trpv1: contribution to retinal ganglion cell apoptosis and increased intracellular ca2+ with exposure to hydrostatic pressure, Investigative ophthalmology & visual science 50(2)(2009) 717-728.

[32] K.H. Dodson, F.D. Echevarria, D. Li, R.M. Sappington, J.F. Edd, Retina-on-a-chip: a microfluidic platform for point access signaling studies, Biomed. Microdevices 17 (6) (2015) 114.

[33] A. Takano, T. Ogawa, M. Tanaka, N. Futai, On-chip incubation system for long-term microfluidic cell culture, in: Engineering in Medicine and Biology Society, EMBC, 2011 Annual International Conference of the IEEE, IEEE, 2011, pp. 8404-8407.

[34] K. Kooragayala, N. Gotoh, T. Cogliati, J. Nellissery, T. R. Kaden, S. French, R. Balaban, W. Li, R. Covian, A. Swaroop, Quantification of oxygen consumption in retina ex vivo demonstrates limited reserve capacity of photoreceptor mitochondria, Investigative ophthalmology & visual science 56(13)(2015)8428-8436.

[35] F. Vendruscolo, M.J. Rossi, W. Schmidell, J.L. Ninow, Determination of oxygen solubility in liquid media, ISRN Chem. Eng. 2012 (2012) 1–5.

[36] Y. Gavrieli, Y. Sherman, S.A. Ben-Sasson, Identification of programmed cell death in situ via specific labeling of nuclear dna fragmentation, J. Cell Biol. 119 (3) (1992) 493–501.

[37] W. Gorczyca, J. Gong, B. Ardelt, F. Traganos, Z. Darzynkiewicz, The cell cycle related differences in susceptibility of hl-60 cells to apoptosis induced by various antitumor agents, Cancer Res. 53 (13) (1993) 3186–3192.

Conditioning Lab on PCB to Control Temperature and Mix Fluids at the Microscale for Biomedical Applications.

Miguel Cabello, Carmen Aracil, Francisco Perdigones and José M. Quero, *Senior Member, IEEE,*

***Abstract*—In this paper, a Lab on PCB (LOP) for conditioning the medium of cell culture is presented. The target is to control its temperature at 37 °C ± 0.1 °C, to assure the appropriate temperature conditions around the cells. The Lab on PCB is also able to mix other fluids into the medium, if it is necessary. The integration of a PDMS microfluidic circuit over a Printed Circuit Board (PCB) results in a smart platform with a low-cost fabrication process. The microfluidic platform of the system includes three inlet ports, microchannels, a micromixer and one outlet port. The correct operation of the LOP assures that the medium is within the adequate conditions in the outlet port. The PCB incorporates a NTC thermistor to measure the temperature, and microheaters that are activated if the medium temperature is under 36.9 °C. The microheater fabrication process consists of patterning the copper layer of the PCB. The NTC thermistor is welded into copper pads and embedded in PDMS to avoid the contact with the fluid. The system is designed to allow the mixing and heating of fluids and it is connected to a cell culture Lab on PCB, and to an electronic control module, which include the electronic adapting circuit of the NTC and the control of the microheaters. The results of this study concerning the heating and mixing of fluids and the monitoring of temperature are successful.**

I. Introduction

Lab-on-chip (LOC) technology gives the possibilities to create powerful platforms suitable for its biological and medical application in order to study life sciences in the best conditions [1], [2]. Particularly, cells' behavior can be controlled through a Lab-on-chip platform that permits even the control of the complete cellular microenviroment. [3]. Moreover, the small scale of Microfluidics is advantageous because it is characterized with a large surface-area-to-volume ratio [4]. This is reflected in the supply of nutrients and oxygen to cells in a more efficiently way, a decrease of their time of response and the reduction of the amount of waste, among others. Thus, long-term cell culture can be performed in microfluidic platforms in which cells should be conditioning to survive [5]. In the last years many microincubators or bioreactors have been designed to create the appropriate conditions for cell culture [6]. Nevertheless, their complexity and the external connections make some of them not really practical.

Regarding the fabrication, the most popular technology for manufacturing microfluidic devices aimed at biomedical applications is currently based on a soft-lithography of polydimethylsiloxane (PDMS) [7], [8]. The reasons why PDMS is the most commonly material used for biomedical applications are its transparency, biocompatibility, and gas permeability [9],

The integration with electronic components can add intelligence to the system. However, this is a hard issue to develop in a PDMS structure. On the contrary, the use of Printed Circuits Board (PCB), is the best option for the incorporation of electronics components [10], [11]. Our proposal is to design a Lab on PCB (LOP) for conditioning the medium, which fed the cell culture. This paper presents an integration of PDMS with PCB, giving rise to a smart system with low-cost and biocompatible technology.

II. Design

The system outlined in this paper is divided into three different parts, each of which has a specific function. Firstly, a microfluidic circuit module, with three inlet ports, one outlet port, and microchannels, which enables the flow and mixing of fluids. Secondly, a Printed Circuit Board (PCB) with a microheater made of copper and a Negative Temperature Coefficient (NTC) thermistor to measure the temperature. This PCB is covered with a thick layer of PDMS to protect the electrical connection from liquids. Finally, an electronic circuit for signal conditioning and control. It measures temperature through the NTC thermistor and controls the external power supply that provides 5V/1A to the microheater. The system is controlled via LabView software, from National Instruments.The connections between the LOP and the Labview software are possible thanks to a National Instruments Data Acquisition (NI-DAQ), Fig. 1. All the materials which are in contact with fluids are biocompatible.

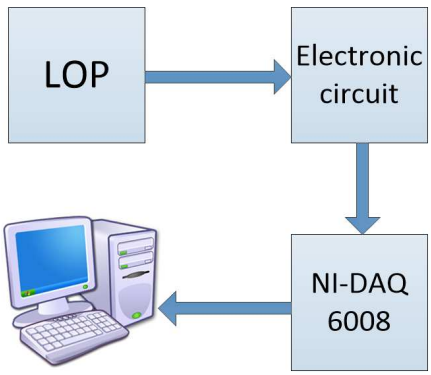

Fig. 1. Parts of the system and how they are connected between them

978-1-5090-5072-7/17/$31.00 ©2017 IEEE

A. Microfluidic Circuit

Due to its biocompatible properties, PDMS has been the material chosen for the fabrication of the microfluidic structure. Consequently, this microfluidic circuit is suitable for preparing a medium for cell culture.

The microfluidic circuit makes possible the distribution and mixing (if necessary) of the medium. In order to manufacture the microfluidic circuit, a mold made of aluminum has been designed. The microfluidic circuit includes more than one inlet port, when the mixing of different fluids is required.

The microfluidic circuit is closely related to the PCB module since it has to be aligned to the microheater to optimized the control of temperature. Hence, the microfluidic circuit is located over the PCB module that contains the microheater and the NTC thermistor embedded in PDMS, facilitating the adhesion between the PCB and the microfluidic circuit. The design of the microfluidic circuit assures the optimal conditions and mixing (if necessary) of the fluid when it passes through the outlet port.

B. PCB module

The Printed Circuit Board (PCB) used in this module contents the NTC thermistor, EPCOS B572xxV5, and the microheater patterned in its copper layer. it also includes the pads to weld the components and the electrical connection where the electronic circuit and the Labview hardware are connected, so that some parameters, such as temperature or power, can be monitored.

The microheater is implemented by a copper serpentine on the PCB. It has to be aligned just below the microchannel of the microfluidic circuit to allow the correct heating of the fluid, Fig. 2. In order to improve the accuracy of the temperature measurement, the NTC thermistor is placed near the outlet port, and it, consequently, assures the established conditions of the medium. The microheater and the NTC thermistor are completely covered by a thick layer of PDMS which avoids the contact with the medium.

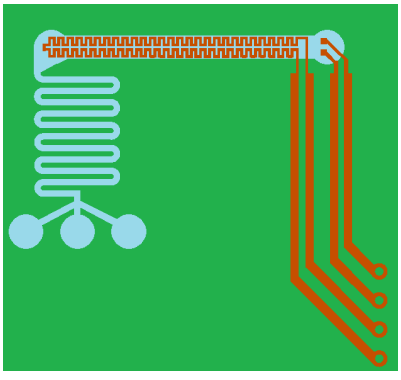

Fig. 2. Top view of the mask utilized in the LOP: in blue color the microfluidic circuit, the red color represents the copper paths and the green one the FR4 from the PCB substrate

C. Electronic circuit

Apart from the conditioning LOP developed in this paper, an external module, including some electronic circuits, is necessary to ensure the proper functioning of the system components. There are several conditioning circuits included in this module, as described below.

The first one is necessary for the correct operation of the NTC thermistor. It consists of a voltage divider. It has been characterized in such a way that the output voltage (captured by the DAQ card) is converted, via LabView software from National Instruments, into the real temperature. The NI-DAQ 6008 also supplies the 5V the NTC thermistor needs to operate.

The microheater contained in the LOP requires a 5V/1A external power source. The activation of this external source is also controlled via LabView software, from National Instruments. The conditioning circuit needed in this case consists of a transistor that control the pass of current from the external power supply to the microheater. The transistor is activated, allowing the pass of current, when the temperature is under 36.9 °C, and it will be off when the temperature is over 37.1 °C, operating as a Pulse Width Modulation (PWM).

III. Fabrication process

The description outlined below refers to the fabrication process of each part of the developed system. It includes the manufacturing process of the microfluidic circuit made of PDMS. It is also described how the PCB module, together with its NTC thermistor and the microheater, has been fabricated.

Due to its biocompatibility properties, polydimethylsiloxane (PDMS) has been chosen as the material to made the microfluidic circuit. Firstly, a mold made of aluminum has been designed and fabricated, Fig. 3. A Computer Numerical Control (CNC) milling machine has been utilized to accomplish the construction of the mold. The microchannels are 1mm wide. The milling tool used has a diameter of 1 mm. The final depth of the mold is also 1mm. Once the milling process is finished, PDMS is deposited inside the mold and introduced in a belt vacuum chamber for 30 minutes in order to remove the possible bubbles that may appear during the deposition. When there are no bubbles, PDMS is cured with temperature, so the mold with PDMS is introduced in a oven at 65 °C for 1 hour and 30 minutes. Once PDMS deposited in the mold is completely cured, it may be released from the aluminum mold, resulting in the final structure of the microfluidic circuit. The last step consists of drilling the holes of the inlet and outlet ports with a punch.

The typical photo-lithographic process is performed to fabricate the PCB module, that includes the copper paths and the NTC thermistor. A standard Printed Circuit Board (PCB) with a FR4 standard thickness of 1,6 mm and a copper standard thickness of 35 μm has been chosen. The NTC thermistor is welded into the copper pads and it is located close to the outlet port to assure that the temperature of the medium is accurate, since it is measured when leaves the microfluidic circuit. Once the copper is patterned, the NTC thermistor is

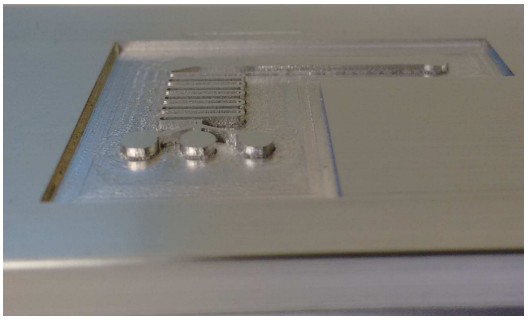

Fig. 3. Mold made of aluminum utilized to create the microfluidic circuit with PDMS

welded. Then a layer of PDMS of 500 μm, enough to cover the NTC thermistor, is deposited over the whole PCB, included the microheater and the NTC thermistor, apart from connections to the external electronic circuit. Thanks to this layer of PDMS, the medium will never be directly in contact with the electrical part of the system.

The complete fabrication process of both parts previously described is shown in Fig. 4. A top view of the LOP already fabricated (Microfluidic circuit and PCB module) is presented, Fig. 5.

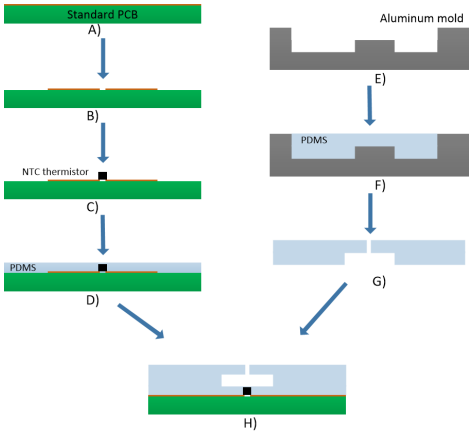

Fig. 4. Fabrication process of the PCB module: A) Standard PCB of FR4 and copper; B) Photolithographic process; C) NTC thermistor welded to the copper; D) PDMS layer over the copper and the NTC thermistor. Microfluidic circuit: E) Aluminum mold; F) Deposition of PDMS; G) PDMS fabricated after its cured. H) Complete structure (LOP) after bonding the microfluidic circuit to the PCB module

IV. Experimental results and discussion

The whole system is tested to show its behavior. The first objective is to demonstrate the correct distribution of the fluids and its mixing once they are introduced into the microfluidic platform made of PDMS. Finally, these tests evaluate the adequate operation of the microheater with the NTC thermistor that measures the temperature. It is also necessary to test the

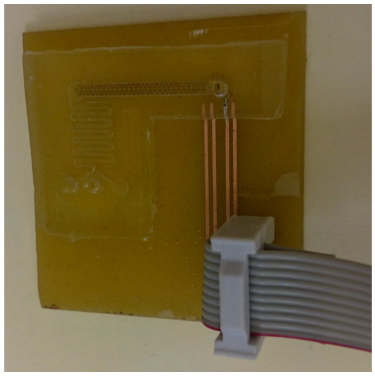

Fig. 5. Top view of the LOP after its fabrication

system control with the Labview software using the NI-DAQ 6008, from National Instruments.

The first experiment carried out tests the correct operation of the microfluidic circuit. It is crucial that the fluids are correctly mixed inside the microchannel. In order to achieve this goal, three different inlet ports are included in the microfluidic platform. The appropriate behavior of the microfluidic circuit has been demonstrated. The microchannel presents a serpentine distribution to facilitate the mixing of the different fluids. Moreover, PDMS allows the vision of liquids due to its transparency, Fig. 6. One of the most important aspects of this first proof is the verification of a complete isolation between the electronic and the microfluidic circuits for security reasons. Therefore, it is demonstrated the correct isolation of the electronic part of the system, when the fluids are introduced inside the microfluidic circuit.

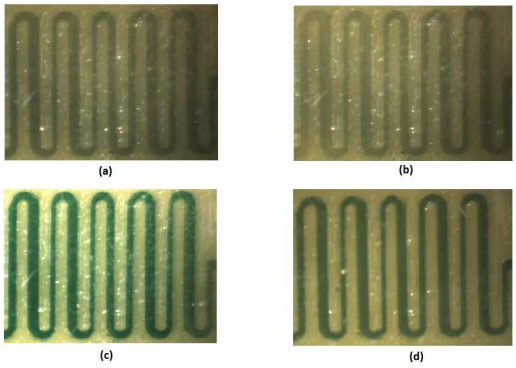

Fig. 6. Mixing of fluids inside the microchannel: (a) Blue ink; (b) Blue ink mixed with water; (c) Green ink; (d) Green ink mixed with water and blue ink

Once the microfluidic circuit is operating correctly, the next step is the evaluation of the microheater operation and the NTC thermistor that measure the temperature of the fluids. A external power supply (5V/1A) is utilized to feed the microheater. A program that implement a PWM model is developed with

the Labview software, from National Instruments, Fig. 7. This program also measures the system's temperature through the NTC thermistor. The objective is to assure 37 °C in order to conditioning the medium for the purpose of using this system in many bio-medical applications, such as cell culture. The NTC thermistor is located as close as possible to the outlet port with the purpose of favoring a more accurate measurement of the temperature of the fluid. The program in charge of the temperature measured through the NTC thermistor operates in such a way that, if it is over 37.1 °C the power supply is disconnected, and, if it is under 36.9 °C the microheater made of copper is fed. It is demonstrated that the temperature is correctly controlled and it is possible to keep it on 37 °C ± 0.1 °C, Fig. 8.

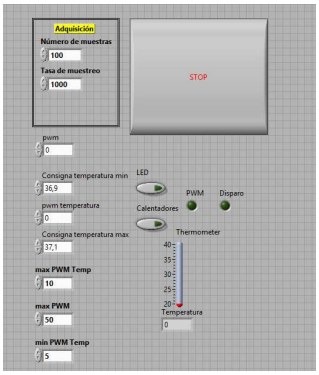

Fig. 7. Labview software panel by mean which it is possible to control the temperature of the LOP

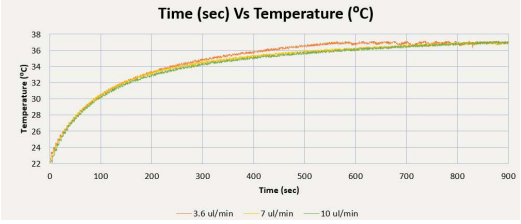

Fig. 8. Heating process for different inlet flows

V. Conclusions

A Lab on PCB for conditioning the medium of cell culture has been successfully developed. The system has been proved and tested with satisfactory results. The microfluidic structure permits the mixing of fluids, if necessary, thanks to three inlet ports and a serpentine microchannel. The use of a PCB as a substrate has some important advantages, such as its low cost and the possibility of including electronic components and copper paths. The operation of the microheater allows the maintenance of a specific temperature that is measured with a NTC thermistor, being able to ensure the 37 °C ± 0.1 needed for cell culture. The temperature control is carried out through the NI-DAQ 6008, from National Instruments, and the Labview software, where a program based on a PWM has been implemented. The use of PDMS to cover the welded NTC thermistor and the microheater, avoids the contact between the electronic part and the fluids and guarantees that the medium is only in direct contact with PDMS, being perfectly bio-compatible.

This conditioning system is designed to prepare the medium and, subsequently, introduce it in the best conditions into a cell culture. The temperature could be directly modified in the Labview software, but it is important not to exceed the maximum temperature that the materials used could bear or at which the medium could be evaporated. The operation of this conditioning system accomplishes the goal of this paper and can ensure the temperature needed for cell culture.

Acknowledgment

This work was supported by the Spanish Ministry of Economy and Competitiveness under grant TEC2014-54449-C3-2-R, BIOLOP.

References

[1] P. Abgrall and A. Gue, "Lab-on-chip technologies: making a microfluidic network and coupling it into a complete microsystemâa review," *Journal of Micromechanics and Microengineering*, vol. 17, no. 5, p. R15, 2007.

[2] S. Schumacher, J. Nestler, T. Otto, M. Wegener, E. Ehrentreich-Förster, D. Michel, K. Wunderlich, S. Palzer, K. Sohn, A. Weber *et al.*, "Highly-integrated lab-on-chip system for point-of-care multiparameter analysis," *Lab on a Chip*, vol. 12, no. 3, pp. 464–473, 2012.

[3] L. Y. Yeo, H.-C. Chang, P. P. Chan, and J. R. Friend, "Microfluidic devices for bioapplications," *small*, vol. 7, no. 1, pp. 12–48, 2011.

[4] T. M. Squires and S. R. Quake, "Microfluidics: Fluid physics at the nanoliter scale," *Reviews of modern physics*, vol. 77, no. 3, p. 977, 2005.

[5] M. Mehling and S. Tay, "Microfluidic cell culture," *Current opinion in Biotechnology*, vol. 25, pp. 95–102, 2014.

[6] K. S. Elvira, X. C. i Solvas, R. C. R. Wootton, and A. J. deMello, "The past, present and potential for microfluidic reactor technology in chemical synthesis," *Nat Chem*, vol. 5, pp. 905 – 915, 2013.

[7] G. M. Whitesides, E. Ostuni, S. Takayama, X. Jiang, and D. E. Ingber, "Soft lithography in biology and biochemistry," *Annual review of biomedical engineering*, vol. 3, no. 1, pp. 335–373, 2001.

[8] Y. Xia and G. M. Whitesides, "Soft lithography," *Annual review of materials science*, vol. 28, no. 1, pp. 153–184, 1998.

[9] V. Faustino, S. O. Catarino, R. Lima, and G. Minas, "Biomedical microfluidic devices by using low-cost fabrication techniques: A review," *Journal of Biomechanics*, vol. 49, no. 11, 2280 - 2292, selected Articles from the International Conference on {CFD} in Medicine and Biology (Albufeira, Portugal â August 30th - September 4th, 2015). [Online]. Available: http://www.sciencedirect.com/science/article/pii/S0021929015006739

[10] C. Aracil, F. Perdigones, J. M. Moreno, A. Luque, and J. M. Quero, "Portable lab-on-pcb platform for autonomous micromixing," *Microelectronic Engineering*, vol. 131, pp. 13–18, 2015.

[11] T. Merkel, M. Graeber, and L. Pagel, "A new technology for fluidic microsystems based on pcb technology," *Sensors and Actuators A: Physical*, vol. 77, no. 2, pp. 98–105, 1999.

Lab-on-PCB: low cost 3D Microelectrode array device for extracellular recordings

Miguel Cabello, Carmen Aracil, Francisco Perdigones and José M. Quero, Senior Member, IEEE.
Universidad de Sevilla
Seville, Spain
mcabellov@gte.esi.us.es

Paulo R.F. Rocha
Centre for Biosensors, Bioelectronics and Biodevices (C3Bio) and Department of Electronic and Electrical Engineering
University of Bath
Bath, United Kingdom

***Abstract*— Lab on a Chip (LOC) technologies are emerging candidates for highly sensitive and real time disease diagnostics and treatments. Yet, the high manufacturing costs of LOC devices has been a downfall. Microelectrode arrays (MEA), as a subclass of LOC technologies, record extracellular field potentials of cells or tissues adhered to the electrodes. The electrical reaction of cells to different pharmacological compounds allows in this way better and real time diagnostics. A current disadvantage is the limited signal-to-noise ratio (SNR) due to (1) the weak coupling between cells and sensing electrodes and (2) the high electrode impedance of current MEAs. In this paper, we present a low cost fabrication process to develop new LOC devices using Printed Circuit Board Technologies (Lab-on-PCB), coupled with 3D microelectrode arrays to improve SNR by optimizing cell-electrode coupling, decreasing the electrode impedance and improving the contact in organotypic cultures. Apart of the fabrication process, the characterization of 3D gold microelectrodes by measuring its impedance and baseline noise under different electrolytes conductivities is presented. Impedance measurements show similar values to state-of-the-art MEAs, e.g, 1KΩ at high frequencies, as well as a baseline noise in the order of the 10 μV_{pp} for a 100 µm diameter microelectrode. Hence, we show that Lab on PCB devices are a valid low cost solution for the new generation of electrophysiological LOC applications.**

Keywords—Impedance, MEA, Micro-fabrication, Lab-on-PCB

I. Introduction

Lab-on-chip (LOC) technologies make possible the creation of devices with multiple applications [1]. From all of these technologies, those that are based on Printed Circuit Board (PCB) technologies, Lab-on-PCB, give the possibility of develop low cost devices with multiple applications, as well as permit the integration of electronic circuit together with microfluidic structures [2,3]. Microelectrodes arrays (MEAs) are very close related to LOC technologies. The fabrication of this kind of devices requires the combination of different techniques, not only to decrease their cost, but also to improve their functionality. Previous research works have demonstrated the huge applications of MEA devices [4]. Out of all of them, those applications related with the detection of electrical signals from cells or tissues have a special importance in biomedical research and diagnostic. In this field, MEAs play and important role in basic in vitro research to provide extracellular electrophysiological information [5]. MEAs are also used for long term recordings of cell and neuron electrical activity [6,7], or stimulation of different cultures by applying potential on the electrodes [8,9].

The impedance of the microelectrodes affects the acquirement of the electrophysiological information. This impedance depends on the frequency, being higher at low frequencies than at high frequencies [10-12]. Normally, extracellular voltages range between 10 µV and 1 mV. For such small voltages, the background noise should be minimized to allow the correct detection of the electrical signal. This background noise is close related to the impedance of the electrodes. For that reason, minimizing the impedance is indispensable to improve the signal acquirement, and reduce the signal-noise ratio. State of the art about MEAs shows that an acceptable background noise is close to 10 μV_{pp} [7]. Nevertheless, recent studies exhibit a lower background noise, closer to 1 μV_{pp} for a few mm² area electrodes [13].

Hence, in this paper the fabrication process of a 3D MEA on PCB substrate is presented, as well as the impedance measurement of it and its comparison with a previously developed MEA with gold wires embedded in Polydimethylsiloxane (PDMS).

II. Design and Fabrication Process

In this paper, a MEA device consisting of a group of microelectrodes grown through gold electroplating on PCB is presented, which gives the possibility of integrating electronic circuits together with microfluidic structures. Due to its lack of biocompatibility, in order to minimize the amount of copper used, a PCB with a layer of 5 µm of copper has been chosen. The electrodes have been designed as micro-pillars, using the copper layer of the PCB as the base. The diameter of the pillars is 100 microns, and the height ranges between 25 and 40 microns. Gold is grown through electroplating deposition (Spa Plating, Bath, UK). The minimum width of the copper tracks is around 50 µm, with a length of 3 mm. As it has been said previously, the biocompatibility is an important goal to achieve to make this MEA suitable for biological applications. For that reason, all the materials which could be in contact with a biological sample inside the MEA are biocompatible, such as the electrodes which are made of copper covered with gold, or the passive layer which is made of SU-8.

978-1-5386-5779-9/18/$31.00 ©2018 IEEE

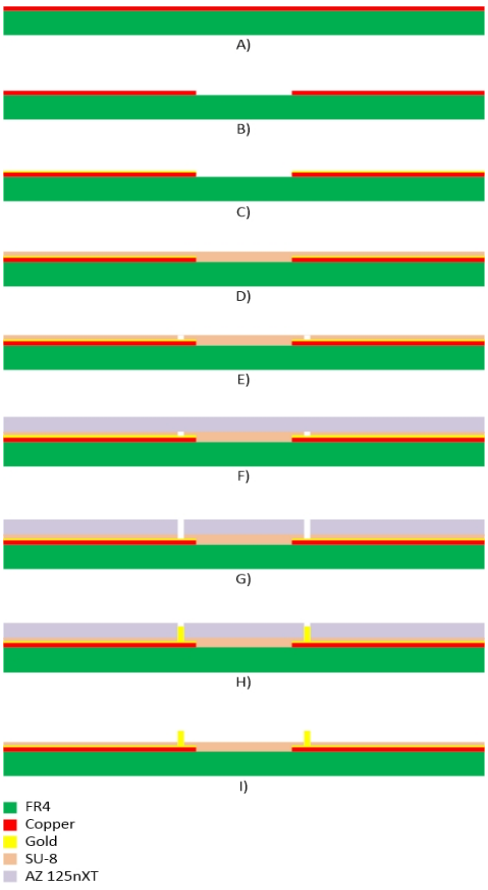

Fig. 1. Fabrication process of the 3D gold pillars MEA. A) PCB of FR4 and copper; B) Photo-lithographic process; c) First gold coating; D) SU-8 deposition; E) SU-8 UV light exposition and developing; F) AZ 125nXT deposition; G) AZ 125nXT UV light exposition and developing; H) Second gold coating to obtain the 3D pillars; I) Elimination of AZ 125nXT layer.

The fabrication process of the 3D pillars MEA can be seen in Fig 1. The fabrication process starts using a standard PCB of 1.5 mm of FR4 and 5 µm of copper as substrate (Fig 1A). Firstly, the copper tracks are obtained through the typical photolithographic process (Fig 1B). Then, a first layer of gold is grown through gold electroplating (Fig 1C). This layer avoids a possible contact between the biological sample and a non-biocompatible material as copper. The next step consists in the deposition of 15 microns of SU-8 as a passive layer, enough to cover the metal tracks (Fig 1D). Later on, through the photolithographic process of the SU-8, the holes for the growth of the 3D pillars are fabricated (Fig 1E). Then another layer of 50 microns of AZ 125nXT, which is used as a sacrificial layer, is deposited over the SU-8 (Fig 1F). By repeating the same photolithographic process that was done for the SU-8, the holes for growing the 3D pillars are released (Fig 1G). The next step consists in the growth of gold to fabricate the 3D pillars (Fig 1H). The company that provides the electroplating kit (Spa plating, Bath, UK), facilitates the use of a calculator to know the exact current needed depending on the area. For the fabrication of these gold 3D pillars, to grow around 40 µm of gold on a surface of around 0.01 cm^2, it is needed 5 hours and 40 minutes with a current of 0.1 mA. After that time inside the electroplating solution, the sacrificial layer of AZ 125nXT is removed, leaving the end of the gold microelectrode around 25 microns over the SU-8 layer (Fig 1I). Finally, a squared piece of PMMA is bonded, surrounding the 3D microelectrodes.

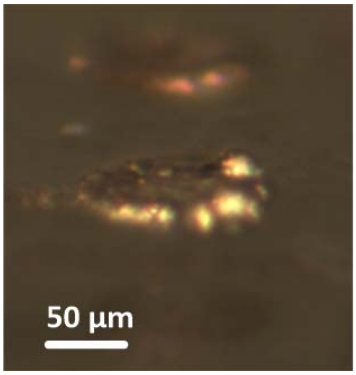

Fig. 2. Amplified view of a 3D gold pillar. The gold is around 25 microns over the SU-8 layer.

Figure 2 shows and enlarged image of a 3D gold pillar once the fabrication process is completed. As can be seen, the way the gold grows over the copper is not exactly as a pillar, but as a "mushroom". This is due to how the gold is deposited through the electroplating technique. The height of the electrode is around 40 µm, 25 µm over the SU-8 layer, and the diamater is 100 µm. The main advantage of this fabrication process is the use of low cost material. The total amount of gold used on each MEA is less than 30 mg, which implies a cost of about 1.5 euros of gold. The other important advantage of this MEA is the possibility of its used with organotypic culture, because the 3D pillars assure the contact between the tissue cultured and the electrodes.

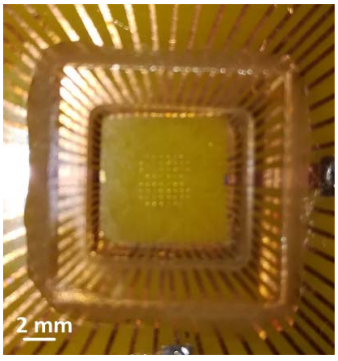

Fig. 3. Fabricated 3D Gold pillars MEA.

Figure 3 shows the whole MEA, with all the microelectrodes surrounded by a piece of PMMA. There are a total of 60 microelectrodes in an area of about 16 mm^2.

III. Experimental Results and Discussion

A 3D pillars MEA has been fabricated and characterized. This type of microelectrodes can improve the contact with a tissue in an organotypic culture, in comparison with planar MEA. This better contact improves the acquirement of electrical signal in that kind of cultures.

As it has been explained previously, the presented MEA has been characterized and compared with another MEA used for culturing mice retinas [9], fabricated with gold microelectrodes embedded in PDMS using the wire bonding technique (in advance it will be called wire bonding MEA).

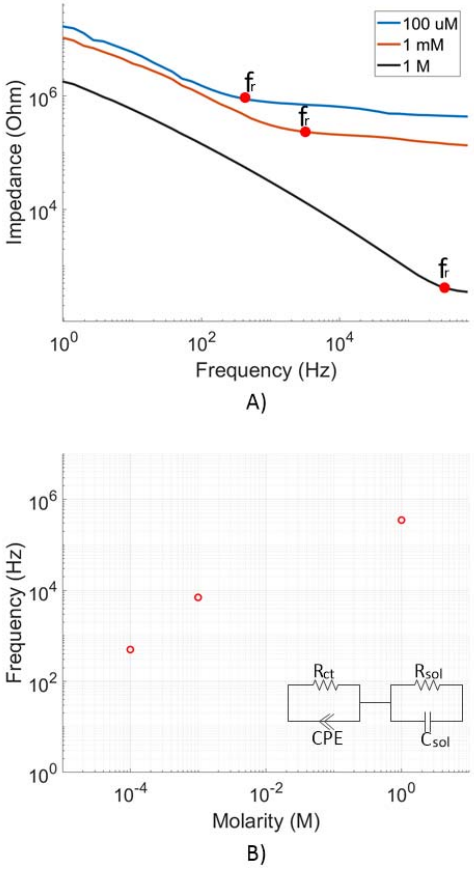

Fig. 4. A) Impedance as a function of molarity of the KCl solution. Impedance decrease over the frequency, and depends on the concentration of the solution, as it was expected. Red circles represent the relaxation frequencies in each case; B) Relaxation frecuency as a function of molarity obtained from the experimental results. The higher the molarity is the higher the relaxation frequency is. The measurments were taken in the 3D pillars MEA.

In order to characterize the MEA with the 3D pillars, the impedance was measured using a solution of potassium-chloride (KCl) with different concentrations (100 µM, 1mM and 1M). As can be observed in figure 4A, the impedance decreases over the frequency, as it was expected, exhibiting an impedance of about 10^6 Ω to 10^7 Ω at very low frequencies, and a value close to 10^2 Ω with the 1M of KCl. Values of impedance obtained with the spectroscopy equipment following the previous research work of Rocha et. al [13].

For low concentrations of KCl, the relaxation frequency appears around 10^3 Hz, but that does not occur for high concentrations of KCl. The Maxwell-Wagner relaxation effect occurs when current pass an interface between two dielectrics. This effect can be simplified by using the Randles equivalent circuit, consisting in a two RC circuit in series (figure 4B), recreating the electrode interface (R_{ct} and CPE) and the solution (R_{sol} and C_{sol}), as it is shown in equation (1).

$$F_r = 1/2\pi(QR_{ct}R_{sol}/(R_{ct}+R_{sol}))^{-1/n}, \quad (1)$$

where Q is a frequency independent, phenomenological parameter. R_{ct} is the charge transfer resistance of the gold electrode. R_{sol} is the resistance solution due to the spreading of current from the localized electrode to a distant counter electrode in the solution, and depends on the conductivity of the solution and the radius of the electrode. The solution capacitance (C_{sol}) is negligible.

The relaxation frequency obtained from the experimental results as a function of the molarity is shown in figure 4B. In which the relaxation frequency strongly depends on the molarity, in such a way that, the higher the molarity is, the lower the relaxation frequency is. The results obtained for the relaxation frequency fit with the theoretical calculations carried out using the Randles' equivalent circuit, in which, R_{ct} is equal to 0.4 Ω for the wire bonding MEA and 0.07 Ω for the 3D MEA, as well as R_{sol} varies with the radius of the electrode, which differs from 12.5 µm in the wire bonding MEA to 50 µm in the 3D MEA. The conclusions agree with what Rocha et al. described [13]. That is to say, the main influence of the electrode occurs at low frequencies, while at high frequency the impedance depends on the KCl solution.

Once the 3D MEA impedance was measured, this result was compared to the impedance measurements of the MEA with gold microelectrodes embedded in PDMS. (Figure 5)

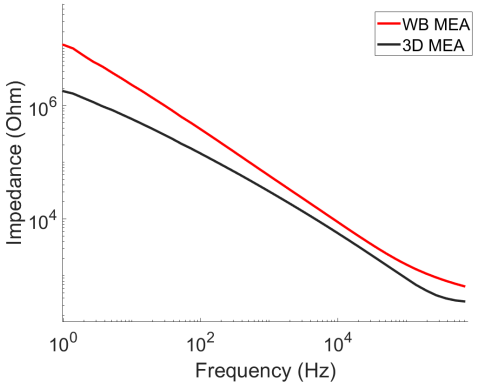

Fig. 5. Impedance measurement of the microelectrodes in a solution of 1M of KCl. Comparison between the impedance in the wire bonding MEA and the 3D pillars MEA for a frequency between 10^0 to 10^6 Hz.

Figure 5 shows the difference between the 3D MEA impedance and the wire bonding MEA impedance. As can be observed, at low frequencies, around 10^0 Hz, the 3D MEA impedance is around one order of magnitude smaller than the wire bonding MEA impedance. This is due to, at low frequencies, the electrode has more influence than the KCl solution. However, when the frequency increases, the difference between both MEAs decreases, being that difference smaller than one order of magnitude.

The presented results of the 3D MEA impedance improve the suitability of the wire bonding MEA for its use as an electrophysiological device for extracellular recordings. Moreover, these results are close to the MEAs, with similar applications, found in the state of the art.

To enforce the results obtained through the impedance measurements, the baseline noise of both MEAs were measured and compared between them and with the state of the art MEAs (Figure 6).

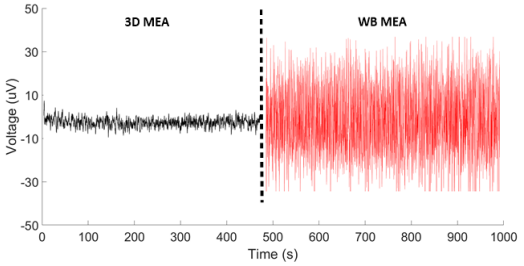

Fig. 6. Basline noise of both, 3D MEA and wire bonding MEA, measured using a KCl solution of 1 M.

As it is shown in figure 6, the 3D MEA baseline noise is clearly smaller than that of the wire bonding MEA, which is what was expected from the results obtained from the impedance measurements. The 3D MEA baseline noise is 10 μV_{pp}, while that of the wire bonding MEA is over 50 μV_{pp}. Results obtained for the 3D MEA are according to the state of the art [7], but are higher that the values given by Rocha et al. [13]. The main reason is that the area of the electrode have a huge influence, increasing the baseline noise for smaller areas.

IV. Conclusions

In this paper, a non-expensive fabrication method of a MEA with 3D gold pillars is presented. The use of biocompatible materials, such as SU-8 and gold, makes this device suitable for its use with biological samples. The 3D gold pillars are over the passive layer, assuring a good contact between the electrodes and the culture. The main advantages of the presented MEA are its low manufacturing cost (about 1.5 € each MEA), and its integration capabilities to other materials, electronics and microfluidics. In order to demonstrate that this device is comparable with other MEAs, its characterization has been done. The obtained impedance decreases over frequency and the baseline noise depends on the area of the electrode. These results were compared with other MEA, which were developed by our research group using the wire bonding technique to fabricate the microelectrodes. The results of the impedance measurements and the baseline noise of the microelectrodes suggest that the 3D MEA improve the electrical behavior of the wire bonding MEA. The present MEA presents similar values to the state of the art MEAs, but with a lower cost and higher integration capabilities.

Acknowledgments

This work was supported by the Spanish Ministry of Science andnnovation (project TEC2014-54449-C3-2-R, BIOLOP),

References

[1] Mark D., Haeberle S., Roth G., Von Stetten F., Zengerle R. (2010) Microfluidic Lab-on-a-Chip Platforms: Requirements, Characteristics and Applications. In: Kakaç S., Kosoy B., Li D., Pramuanjaroenkij A. (eds) Microfluidics Based Microsystems. NATO Science for Peace and Security Series A: Chemistry and Biology. Springer, Dordrecht

[2] Aracil, C., Perdigones, F., Moreno, J. M., Luque, A., & Quero, J. M. (2015). Portable Lab-on-PCB platform for autonomous micromixing. *Microelectronic Engineering*, *131*, 13-18.

[3] Moschou, D., & Tserepi, A. (2017). The lab-on-PCB approach: tackling the μTAS commercial upscaling bottleneck. *Lab on a Chip*, *17*(8), 1388-1405.

[4] Jones, I.L., Livi, P., Lewandowska, M.K., Fiscella, M., Roscic, B., & Hierlemann, A. (2011). The potential of microelectrode arrays and microelectronics for biomedical research and diagnostics. Analytical and bioanalytical chemistry, 399 7, 2313-29.

[5] Hai, A., Shappir, J., & Spira, M. E. (2010). Long-term, multisite, parallel, in-cell recording and stimulation by an array of extracellular microelectrodes. *Journal of neurophysiology*, *104*(1), 559-568.

[6] Rocha, P. R., Schlett, P., Schneider, L., Dröge, M., Mailänder, V., Gomes, H. L., ... & De Leeuw, D. M. (2015). Low frequency electric current noise in glioma cell populations. Journal of Materials Chemistry B, 3(25), 5035-5039.

[7] Obien, M. E. J., Deligkaris, K., Bullmann, T., Bakkum, D. J., & Frey, U. (2015). Revealing neuronal function through microelectrode array recordings. Frontiers in neuroscience, 8, 423.

[8] Hosseini, V., Gantenbein, S., Avalos Vizcarra, I., Schoen, I., & Vogel, V. (2016). Stretchable silver nanowire microelectrodes for combined mechanical and electrical stimulation of cells. Advanced healthcare materials, 5(16), 2045-2054.

[9] Cabello, M., Aracil, C., Perdigones, F., Mozo, M., de la Cerda, B., & Quero, J. M. (2018). Gold microelectrodes array embedded in PDMS for electrical stimulation and signal detection. Sensors and Actuators B: Chemical, 257, 954-962.

[10] Paredes, J., Becerro, S., Arizti, F., Aguinaga, A., Del Pozo, J. L., & Arana, S. (2013). Interdigitated microelectrode biosensor for bacterial biofilm growth monitoring by impedance spectroscopy technique in 96-well microtiter plates. Sensors and Actuators B: Chemical, 178, 663-670.

[11] Prasad, A., & Sanchez, J. C. (2012). Quantifying long-term microelectrode array functionality using chronic in vivo impedance testing. Journal of neural engineering, 9(2), 026028.

[12] Maria C.R. Medeiros, Ana Mestre, Pedro Inácio, Sanaz Asgarif, Inês M. Araújo, Peter C. Hubbard, Zélia Velez, M. Leonor Cancela, Paulo R.F. Rocha, Dago M. de Leeuw, Fabio Biscarini, Henrique L. Gomes, An electrical method to measure low-frequency collective and synchronized cell activity using extracellular electrodes, Sensing and Bio-Sensing Research, Volume 10, 2016, Pages 1-8,ISSN 2214-1804.

[13] Rocha, P. R., Schlett, P., Kintzel, U., Mailänder, V., Vandamme, L. K., Zeck, G., ... & De Leeuw, D. M. (2016). Electrochemical noise and impedance of Au electrode/electrolyte interfaces enabling extracellular detection of glioma cell populations. Scientific reports, 6, 34843.

Annex B

Other contributions

In this appendix, other contributions not directly related with this thesis work are presented. These merits have been gained during the development of this thesis and add value to this PhD. Among these contributions, it is included: two international journal publication, one congress contribution, one patent and the foundation of a spin-off company.

International journal publications

Franco, E., Salvador, B., Perdigones, F., Cabello, M., & Quero, J. M. (2018). Fabrication method of lab-on-PCB devices using a microheater with a thermo-mechanical barrier. Microelectronic Engineering, 194, 31-39.

Perdigones, F., Cabello, M., & Quero, J. M. (2019). Single-use impulsion system for displacement of liquids on thermoplastic-based lab on chip. Sensors and Actuators A: Physical, 298, 111568.

Congress contributions

Flores, G., Perdigones, F., Aracil, C., Cabello, M., & Quero, J. M. (2015, February). Microfluidic platform with absorbance sensor for glucose detection. In 2015 10th Spanish Conference on Electron Devices (CDE) (pp. 1-4). IEEE.

Patents

Perdigones Sanchez, Francisco Antonio, Quero, José M., Cabello, Miguel: Método de unión de sustratos y plásticos mediante zona de adhesión térmica controlada. Patente de invención, Propiedad industrial. Solicitud: 2016-09-28.

Know-how transfer

CEO and co-founder of the spin-off company named Biodevices Technologies S.L. and created on July 2018.

Microelectronic Engineering 194 (2018) 31–39

Contents lists available at ScienceDirect

Microelectronic Engineering

journal homepage: www.elsevier.com/locate/mee

Research paper

Fabrication method of lab-on-PCB devices using a microheater with a thermo-mechanical barrier

Emilio Franco*, Blas Salvador, Francisco Perdigones, Miguel Cabello, José Manuel Quero

University of Seville, Avda de los Descubrimientos s/n, 41092, Spain

ARTICLE INFO

Article history:
Received 4 November 2017
Received in revised form 27 December 2017
Accepted 17 February 2018
Available online 23 February 2018

Keywords:
Lab-on-PCB
Thermal bonding
Microfluidics
Thermoplastics
Thermo-mechanical barrier

ABSTRACT

A thermal method for bonding thermoplastics with a printed circuit board has been developed for its use in Lab on Chip applications. In order to define and control the bonded zones of the device, a thermo-mechanical barrier is included. The thermoplastic used is polymethylmethacrylate (PMMA), and the substrate is a double-side PCB. The copper layer is used to fabricate simultaneously a microheater and the thermo-mechanical barrier by wet etching, and the piece of PMMA used is micromilled before its bonding to the PCB. Once the PCB and the piece of PMMA are processed, a good alignment of both parts is important. After that, a controlled current is applied by a power supply in order to increase the temperature of the microheater. Time needed for bonding is predicted by numerical simulations of the whole system. As an example of a possible application of this procedure, the proposed method is applied to fabricate a two-dimensional hydrodynamic focusing device. This device has been tested showing an appropriate behaviour. The dimensions of the generated streams lie between 81 and 224 µm showing a good correspondence with the theory. In addition, the device presents a correct functioning, without leakages demonstrating that the bonding is good. The presented method has been studied in order to characterize the maximum pressure the whole device is able to withstand. In this case, the materials used withstand 481 kPa. This method can be easily extended to industrial production of microfluidic devices, such as lab on chips and µTAS.

1. Introduction

The microfluidic field was born several decades ago, and, nowadays, it continues being an important source of research. Currently, microfluidics has an interesting potential of development. This field, together with different areas, has provided important and successful solutions for many problems. For instance, the development of Lab on Chip (LOC) devices [1, 2]. These devices mean the miniaturization of conventional laboratories and processes in small platforms with the size of a credit card, for example in drug discovery [3]. In case of using PCB as substrate, those devices are called Lab-on-PCB (LOP) devices [4]. The generation of droplets and microcapsules [5, 6] are other examples in which microfluidics contributes with its characteristics. In addition, biology has taken advantage of this important field to improve several applications [7], in particular microfluidics for assisted reproduction [8, 9]. These are only a few examples among a huge field of applications.

Microfluidic devices have been developed by many research groups. The first steps of the development of a device are the fabrication and evaluation of it as a proof of concept. Thus, rapid prototyping has been used. This technique involves the use of low cost materials and facilities in order to fabricate the device. In general, the fabrication process used for carrying out microfluidic LOC's can not be extended for industrial production. For example, many rapid prototyping microfluidic systems are fabricated using the photoresist SU-8 [10]. The typical process for this material requires, among others, the steps of deposition and spin coating. These steps are a good choice for rapid prototyping but are difficult to extent for industrial production due to dimensions of microfluidic devices. Soft lithography technique of polydimethylsiloxane (PDMS) is also used in the fabrication process of this type of devices [11, 12]. Two components have to be mixed to obtain the PDMS material. Then the mixture has to be degassed. In addition, controlled baking steps are necessary for the cure of this kind of silicone. Both materials, SU-8 and PDMS, are supplied in liquid state and then have to be solidified, the first one by UV light exposure and temperature, and the second one by temperature. Furthermore, this typical process implies a big amount of waste of material during the spin coating step for SU-8, and the pouring of PDMS on the mold. All these issues can be solved by using a polymeric solid material to be processed by hot

* Corresponding author.
E-mail address: efranco@us.es (E. Franco).

https://doi.org/10.1016/j.mee.2018.02.019
0167-9317/

embossing or micromilling. The most commonly used materials are: polymethylmethacrylate (PMMA), polycarbonate (PC), polyethylene terephthalate (PET) and cyclic olefin copolymer (COC) [13].

Hot embossing technique and micromilling processes provide open structures, that is, open microchannels or microchambers which have to be closed with a cover. This problem is the same for the most of the microfluidic devices, independently of the material used [14]. For instance, SU-8 and PDMS need a cover to fabricate the microchannels [15, 16]. Microfluidic structures made of silicon, glass or a combination of them, also need to be bonded in order to fabricate buried microchannels and microchambers [17, 18, 19]. In this respect, materials like PMMA, PC or COC need to be bonded or glued to a substrate. Typically, the bonding is performed using the material itself, that is, PMMA to PMMA [20], PC to PC [21], or COC to COC [22]. However, there are several works which use different types of substrates to bond the polymeric materials.

It is important to highlight that printed circuit boards (PCB) have driven the use of this material as substrate due to the possibility of including an electronic circuit, for example, the multilayer PCB which includes both the passive and active fluid elements, and the electronics for performing the control and evaluation reported on [23, 24]. Apart from the circuitry, the PCB technology allows to include sensors and actuators, for example, the PCB-based *Ag/AgCl* reference electrodes, an important component of biosensors for microfluidic platforms [25]. In addition, silicon sensors can be integrated on PCB [26]. Regarding the actuators, the microfluidic platform based on PCB reported on [27] includes integrated micropumps. Moreover, microvalves have been integrated for PCB microfluidic platforms [28]. The methods used for joining a PCB substrate with a polymer structure are based on the use of glues [29] and/or adhesive tapes [25, 30, 31].

In this paper, a thermal method to assembly a polymer structure and a PCB is proposed. The procedure is intended to develop an automatic manufacturing process for microfluidic platform in mass production. The process consists of using the copper lines of a PCB as microheaters, in order to bond the polymer structure between copper lines and FR4 without leakages. Using this method, the copper layer is suitable for bonding the polymer structure to the FR4. It is also possible to include an electronic circuit, sensors and actuators in the same substrate. The method includes a thermo-mechanical barrier to control the bonded area. This bonding procedure is used for fabricating a device based on the two-dimensional hydrodynamic focusing effect [32] in order to demonstrate the validity of the method.

The rest of the paper is structured as follows. Section 2 describes the proposed method in detail. The characterization of the process is commented in Section 3. Then, in Section 4, the process is performed for a hydrodynamic focusing device. Finally, in Section 5, the main conclusion of the work will be summarized.

2. Bonding technique

The objective of the proposed technique consists in the bonding between thermoplastics and a PCB as substrate. This PCB is composed by an FR4 layer and two copper layers on both sides of the FR4. The bonding technique is based on the controlled melting of the thermoplastic part of the device over one side of the PCB, in order to bond them both when the melted part of the thermoplastic return to its solid state. For a good bonding between both parts, the most homogeneous as possible distribution of temperature in the contact area is necessary. A microheater is fabricated by wet etching of one of the copper layers in order to achieve the melting temperature of the piece of thermoplastic and the correct distribution of heat. A zigzagged geometry of the microheater is chosen to assure a high ratio between the length and the occupied area of the microheater, Fig. 1. Here, the dimensional parameters and their names can be seen too. Using this geometry, the resistance of the microheater is maximized in that area, and therefore the Joule effect is also maximized. The top surface of the microheater has to be directly in contact with the bottom surface of the thermoplastic part to be bonded.

When the thermoplastic is melted it flows in all directions. This is a problem when fabricating microchannels or microchambers because the design dimensions has to be kept. Otherwise, the microchannels and microchambers would reduce their width and area, respectively. In order to avoid this problem, a copper track, which is fabricated at the same time that the microheater was added to the design and located between the microheater and the microchannels, Fig. 1. That track acts as a thermal barrier dissipating the heat and reducing the temperature below the glass transition point of the thermoplastic in that zone, stopping the melting. In addition, the copper track acts as a mechanical barrier because the melted zone reaches the barrier reducing the flow of thermoplastic [33]. For both previously commented reasons, the copper track is called thermo-mechanical barrier. This part is defined as basic cell and it is important in the bonding method to keep the dimensions of the microfluidic systems.

Once the geometry is chosen, their dimensions have to be defined. For that purpose, a parametric optimization study is performed using COMSOL Multiphysics [34]. These simulations find the combination of dimensions which provides the minimum difference between the maximum temperature of the heater and its average. Therefore, an homogeneous distribution of temperature is achieved. Simulation results show how the thermo-mechanical barrier affects the temperature. The closer to the microheater the barrier is, the higher the temperature of the barrier is. In addition, the temperature of the barrier is greater. When the microheater reaches about 130 °C (temperature below the boiling point of the thermoplastic), the distance between the barrier and the microheater must ensure a temperature lower than the glass transition temperature (Tg) in the thermo-mechanical barrier. The Tg of the thermoplastic (PMMA) used in this work is 95 °C, provided by the manufacturer (Plazit Polygal). The temperature is studied in a "line under study" placed below the microheater and centered in the geometry, in the position shown in Fig. 1. It is important to highlight that the simulations take into account that the thermoplastic is placed over the PCB.

The effect of the parameters values in the final results are studied separately. In order to do so, the temperature is plotted along the "line under study" for several values of the separation of the zigzag tracks ω_{sep}, keeping constant the rest of parameters. The result is shown in Fig. 2a). As can be seen, the lower ω_{sep} is, the higher the heater temperature is. However, the influence of this parameter in the barrier's temperature is not really significant. The lowest limit of ω_{sep} is 150 μm, that is, the minimum dimension possible to reach in the fabrication process. For the same reason, the value of the microheater cooper line width ω_m is also limited to 200 μm. Once ω_{sep} and ω_m are fixed, a parametric study of the barrier separation ω_b is performed, in Fig. 2b). If the barrier is close to the microheater, the temperature of both parts is similar. Then, there is a small difference of temperature between the bonding areas and those areas where the bonding must finish. This fact reduces the effect of the barrier. However, if the barrier is far enough from the heater, its thermal relaxation effect will be negligible. Therefore, a compromise solution approach has to be chosen. This solution corresponds to the situation in which the microheater temperature is below the boiling point of the thermoplastic 130 °C, and the barrier temperature remains below the glass transition temperature of PMMA, which is 95 °C. These requirements are fulfilled for a ω_b of 250 μm.

Complex geometries can be configured by repetition of the previously commented basic cell. This assures the same thermal behaviour than the basic cell. Therefore, this basic geometry makes possible the bonding of a huge amount of different microfluidic circuits with different geometries to a PCB. A concentration of temperature may occur in complex geometries with corners. This effect can

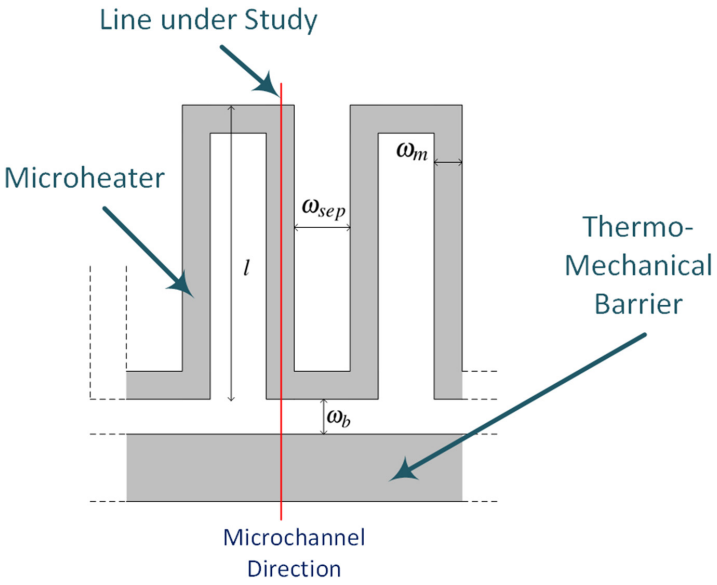

Fig. 1. Basic cell with dimensions.

be taken into account by optimizing the geometry of the microheater copper lines.

A particular case takes place when isolated areas, for example, two concentric circumferences, have to be bonded. This fact makes impossible the access of the copper pads to the inner region of the microheater using an one-side PCB. For those cases, a double-side PCB is needed. Thus, some vias between the two sides of the PCB are needed to access the inner area to be bonded, crossing the outer area to be bonded in the opposite side of the place where the microheater and the barrier are. Following this method, the vias could be used to integrate electronic devices into the microchambers and microchannels.

Once parameters have been defined it is necessary to ensure that the design works properly. For that purpose, a simple microchannel have been fabricated in a piece of PMMA and a microheater made of a concatenation of the basic geometries have been used to bond the microfluidic part and the PCB. The initial state of the bonding process and the end of it, can be seen in Fig. 3.

3. Characterization

The bonding method requires several parameters to be defined. Some of them have been previously fixed by simulation in Section 2. The microheater is composed of copper lines with a width of $\omega_m = 200$ μm and a length of $l = 2000$ μm, providing the gap between the tracks of the microheater ω_{sep} of 150 μm, as it was commented in Section 2. The width of the barrier $\omega_{barrier}$ is 400 μm and the gap between the barrier and the microheater ω_b is 250 μm. The microheater is fabricated using a commercial double-side PCB with a thickness of FR4 of 1.5 mm and two copper layers with a thickness of 35 μm. Finally, the thermoplastic used for the characterization is polymethylmethacrylate (PMMA).

PMMA and the PCB are put together and aligned. Then, the microheater is connected to a power supply to provide a constant current which causes an increase of temperature. At the same time, a pressure of 6.3 kPa is applied on top of the thermoplastic to assure a homogeneous flow of the melted thermoplastic through the microheater geometry. Using the dimensions previously commented, the bonding method requires about 95 °C. When that temperature is achieved, the thermoplastic placed over the microheater reaches a temperature above the glass transition point, and, thus, it starts to flow between the copper lines which compose the microheater. The temperature continues rising until it is close to 130 °C, when the material achieves the boiling point and stars to bubble. This effect is not desirable due to the imperfections caused in the bonding surface, which decrease the effective bonding area and, consequently, make the bonding softer.

A criterion to stop the bonding process has to be defined. For that purpose, some simulations have been performed, using COMSOL Multiphysics software, in order to obtain the time where the bonding is completed. This time depends on the total area to be bonded, the resistance of the microheater, and the characteristics of the FR4 and the PMMA. Two time values have been extracted from the simulations. The first value corresponds to the moment when the glass transition temperature is reached, and the second one coincides with a temperature below the boiling point of the material, but close to it, in this case 130 °C.

Some tensile tests have been performed in order to obtain the ultimate debonding pressure for several areas, 10 mm^2, 25 mm^2 and 90 mm^2. The obtained value is considered to be the average of all the values obtained in the test, which corresponds to 481 kPa with a standard deviation of 45 kPa. This value is similar to the debonding pressure of double-side tapes (3M-VHB 4991) with a value of 415 kPa, and much lower than the value for glue (Loctite 401) with a value of 7 MPa.

As can be seen, the ultimate pressure admissible in the proposed bonding method is much smaller than the one which Loctite provides. However, this is a very large value compared to the range of typical pressures that can be found in microfluidic circuits. Those pressures are about a few atmospheres, at most. Moreover, Loctite 401 (cyanoacrylate) is not a biocompatible glue. In addition, the curing time is very low. Therefore the alignment is very critical because

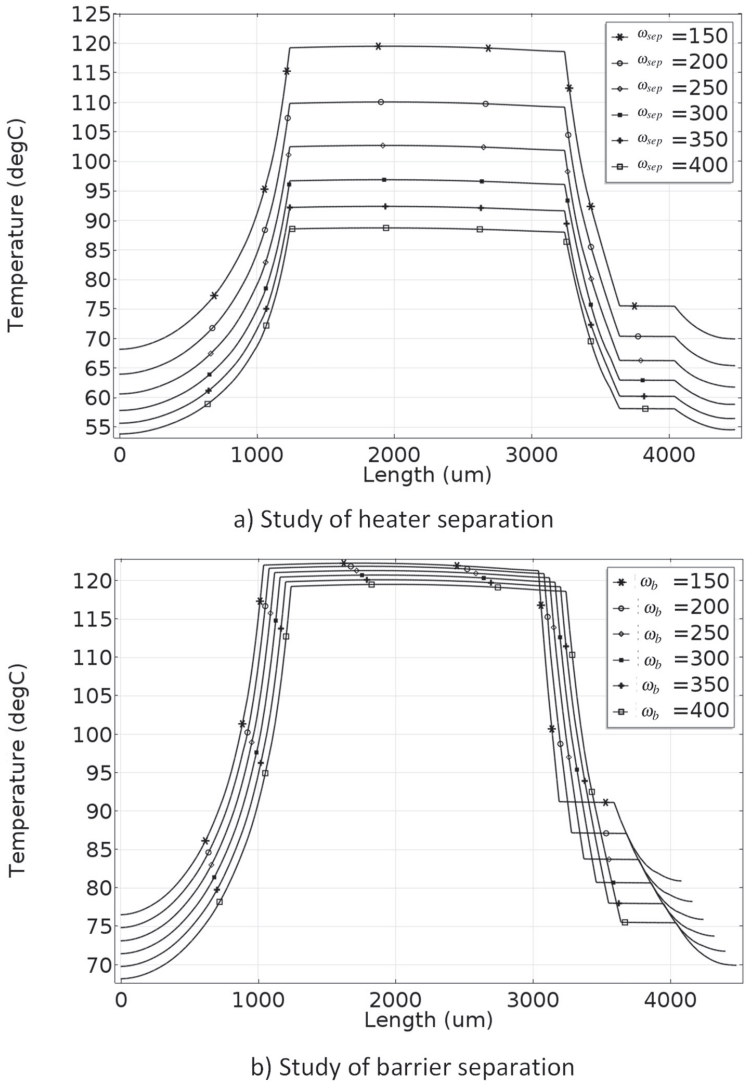

Fig. 2. Parametric study of ω_{sep} and ω_b.

the glue could be cured before completing the alignment. The same problem takes place when using UV cyanoacrylate because the UV behaviour is not dominant for thin layers of about 50 μm. Finally, the use of glues with anaerobic behaviour are not recommendable because uncured glue could remain in parts of the circuit. From our point of view, epoxy glues are the best choice for gluing microfluidic circuits for rapid prototyping. However, the use of glue is not as industrial as the method proposed in this paper.

The characteristic parameter values are summarized in Table 1. The bonding method can work with different microheater dimensions, but the rest of the parameters would need to be recalculated in each case. All these values depend on the substrate and the plastic material, in this case, PCB and PMMA respectively. The method has to be reconfigured for different PCB substrates or thermoplastic.

4. Application to a hydrodynamic focusing device

The bonding method described in Section 2 and characterized in Section 3 has been applied to fabricate a PCB-based 2D hydrodynamic focusing device in order to demonstrate the viability of the method. The operation of the hydrodynamic focusing is well-known [35]. It consists in the focusing of a fluid due to the action of other fluid surrounding it. If the interfacial pressure is not high enough to break the inner fluid, the device works into the hydrodynamic focusing regime.

The bonding of isolated areas is a hard issue, our solution is outlined below. Once the device is fabricated using the bonding method proposed in this paper, the device operation is tested by experimentation, varying the flow rate ratios.

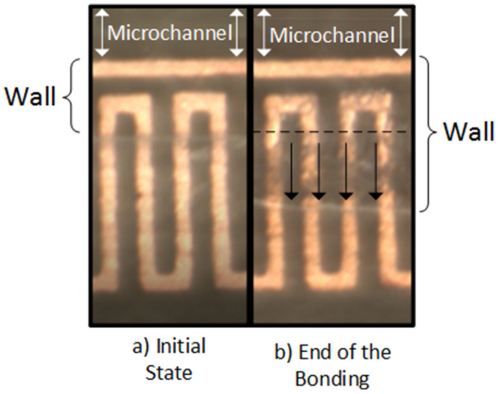

Fig. 3. Bonding process of a simple microchannel.

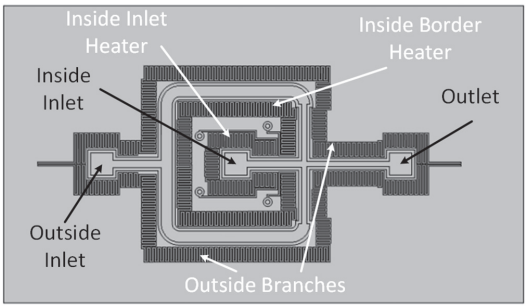

Fig. 4. Plan view of the geometry used in the simulation.

4.1. Design and simulation

The microfluidic circuit of the hydrodynamic focusing is similar to the configuration reported in Ref. [36]. The circuit is designed using the basic geometries previously studied to define the whole copper structure, Fig. 4. As can be seen, the dimensions of the microchannels are defined by the thermo-mechanical barrier. In addition, the microheaters are placed beside the thermo-mechanical barrier. This fact assures that the expansion of the melted PMMA will stop before reaching the barrier.

The configuration of the whole microheater implies regions with different generated heat if the complete microheater is actuated. These regions are the corners or the center of large linear parts. Thus, the heating speed is different in each part of the device, being really hard to control the bonding time. For example, the heating rate is lower in the microheater surrounding the "inside inlet" than "outside inlet" due to the fact that the "outside inlet" is longer than the "inside inlet". This effect leads to the onset of zones where the desired temperature is not reached, but others where it is highly overpassed. In order to avoid these problems, the microheater is divided into four different parts, namely, two symmetrical ones outside the device, the "outside branches", and two in the inside closed region: one around the inside inlet, "inside inlet microheater", and the other in the inside border, "inside border microheater". All these microheaters are independent and they are actuated separately, Fig. 4.

The hydrodynamic circuit configuration requires an isolated microheater region. Therefore, the device has to be fabricated using a double-side PCB to allow the electrical connections between both parts of the board.

Table 1
Characteristic parameters of the thermal bonding method.

Parameter	Value
Heater lines length	2 mm
Heater lines width	200 μm
Heater lines separation	150 μm
Barrier-Heater separation	250 μm
Barrier lines width	400 μm
Copper lines thickness	35 μm
FR4 thickness	1.5 mm
PMMA type	Extruded sheet
PMMA thickness	2 mm
PMMA wall width	2 mm
Debonded pressure	481 kPa
Applied pressure	6.3 kPa

Once the device is designed, a thermal-electric COMSOL simulation is performed to study the behaviour of the bonding method. In this study the four microheaters are analysed separately. The temperature field of the model is shown in Fig. 5, in which one of the outside branch is heated during $t = 120$ s. The materials used are copper for the electrical tracks, FR4 for the substrate, PMMA as a surface material over the copper tracks, and air on the rest of the boundaries. The previously mentioned materials are into the COMSOL materials library. Existing boundary conditions in the model, are all of them, convection conditions with air. To model this convection, correlations included in COMSOL which compute the heat transfer coefficient in horizontal and vertical walls are used.

The temperature losses by convection with air and conduction with PMMA and glass are taken into account. The glass is used to exert pressure in order to have an homogeneous bonding. When solved, the simulations provides the temperature as a function of the time in each microheater. This means an estimation of the time needed to assure a temperature above the glass transition temperature of the PMMA in the desired bonding area.

Simulation results show that outside branches reach the desired temperature in a shorter time than those in the inside. Two limited time values are calculated for each microheater. The first value (t_i) is fixed when the average temperature along the microheater is about 95 °C, which corresponds to the start of the bonding. The second value (t_f) is fixed when the temperature is about 130 °C, which corresponds to the ultimate stopping point of the method. The time values reached by simulations, together with those obtained by experimentation, are shown in Table 2. The time values for outside branches are the same due to the symmetry.

Transient simulation for all branches in the hydrodynamic focusing circuit, have been done in order to obtain the characteristic time values of the process. Results are shown in Fig. 6. A comparison of these time values and the experimental ones are shown in Table 2.

4.2. Device fabrication

Once the design and the simulations are verified, the next step is the fabrication of the device. The microchannels are micromachined in a piece of PMMA using a CNC milling machine, and PCB is done using a typical chemical wet etching technique. In Fig. 4, the designed geometry is presented. Top view of the fabricated PCB is shown in Fig. 7a), the piece of PMMA part in Fig. 7b), bottom view of the PCB part in c) and the whole device in Fig. 7d).

Several vias have been drilled to the PCB or to the piece of PMMA. These vias allow the air flow from the internal region to the outside, when the piece of PMMA is placed over the PCB. The vias in the internal region of the whole device are shown in Fig. 7a). Three holes are drilled to the PCB in order to make the inputs and the output of the

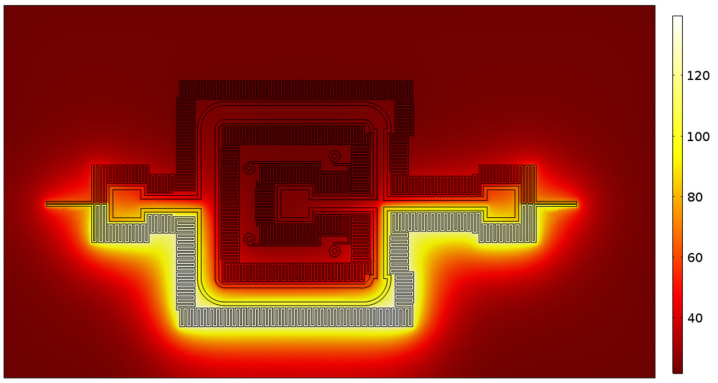

Fig. 5. Temperature field in $t = 120$ s for one branch heating.

liquids. Finally, both parts are aligned using a microscope, and the microheaters are connected to a power supply to provide a constant value of current. At the same time, a pressure of 6.3 kPa is applied on top of thermoplastic part. The experimental heating times for the bonding of the different microheaters are show in Table 2.

The fabricated device is not biocompatible due to the use copper. However, this problem can be solved using a gold electroplating of the copper lines.

4.3. Experimental results

As previously mentioned, a 2D hydrodynamic focusing device fabricated using the proposed bonding method has been tested in the laboratory. The experiment demonstrates the viability of the proposed bonding method. The absence of liquid leakages has been proved during the test with satisfactory results.

Two liquids are used for the experiments, one of them as focused liquid, namely coloured deionized water (the green one), and the other one used as focusing fluid is deionized water (the transparent one). In Fig. 7d), the device full of the greenish liquid can be seen. The focused liquid is injected in the device through the inside inlet and the focusing one is inserted through the outside inlet. The total flow rate of the focusing fluid is fixed to 0.4 mL/min and several flow rates of the focused fluid are chosen to generate streams with different dimensions. These values can be seen in Table 3 together with the dimension of the streams.

Theoretical values (w_{st}) are calculated using the expression Eq. (1) reported in Ref. [37] assuming $\gamma = 1$, where γ is the ratio between average velocity of the focused stream and average velocity of the outlet channel, as commented in Ref. [37].

$$w_{st} = W\frac{Q_d}{\gamma(Q_d + Q_{s1} + Q_{s2})} \tag{1}$$

where Q_{s1} and Q_{s2} are the flow rates of the side channels and Q_d is the flow rate of the focused fluid. In this particular fabricated device, the side channels have been designed in order to have the same flow rate, that is, $Q_{s1} = Q_{s2} = Q_s$.

Table 2
Starting and ending time in s of the bonding for simulation and experimental cases.

	Simulation		Experiments	
Branch	t_i	t_f	t_i	t_f
Outside	34	81	36	76
Inside inlet	60	124	53	117
Inside border	61	121	51	114

The experimental results of the hydrodynamic focusing device operation are shown in Fig. 8.

As can be seen, the hydrodynamic focusing experiments fit the theoretical results being the Reynolds numbers (Re_{Dh}) about 10 for all the cases studied in this paper. Therefore, the laminar regime is assured [36]. The good behaviour of the device confirms that its design and fabrication have been successfully carried out. Moreover, a robust bonding between the fabricated PCB and the piece of PMMA without leakages is demonstrated. Finally, the proposed bonding method supports the microfluidic requirements of the device. Furthermore, the bonding method reported in this paper is not limited to be used for fabricating hydrodynamic focusing devices. The method of thermal bonding using the thermo-mechanical barrier can be used for developing lab on chips for different applications.

5. Conclusions

A thermal method for bonding thermoplastics and printed circuit board has been developed. The procedure includes a thermo-mechanical barrier which defines and controls the bonded areas of the device. The thermoplastic used for the fabrication of the microfluidic circuit is PMMA, and the substrate is a double-side PCB. Time values of bonding are predicted by numerical simulations of

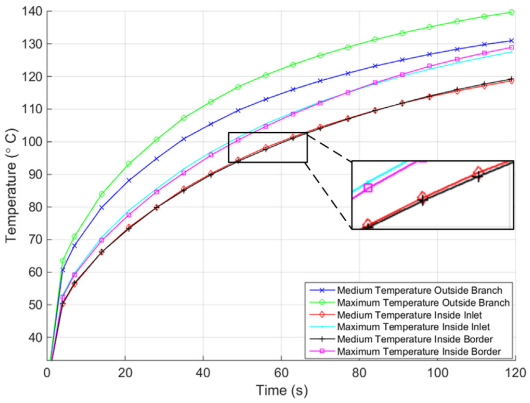

Fig. 6. Transient simulation results of the heating of the branches.

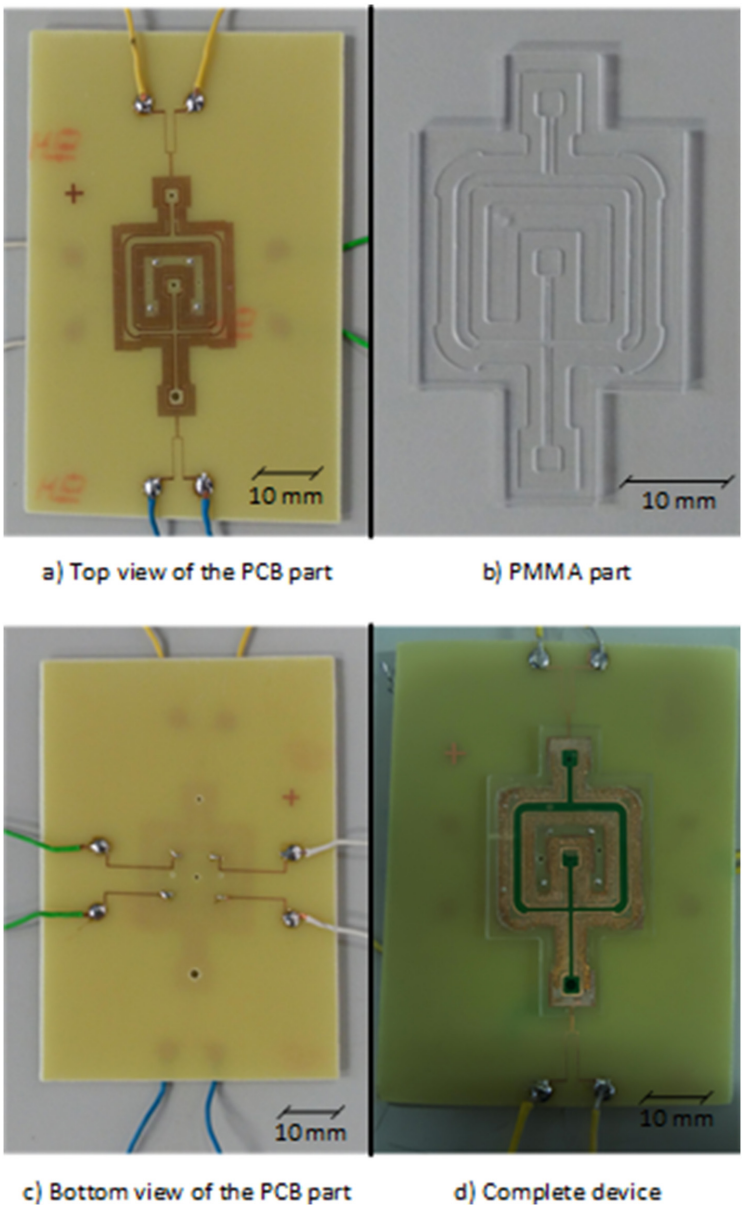

Fig. 7. Fabricated parts of the device: a) top view of the PCB, b) PMMA part, c) bottom view of the PCB and d) final fabricated device.

Table 3
Flow rates and stream dimensions.

Experiment|	Q_s (mL/min)|	Q_d (mL/min)|	w_s (μm)|	w_{st}
1	0.2	0.05	81	78
2	0.2	0.1	135	140
3	0.2	0.15	188	190
4	0.2	0.2	224	223

the whole system. In order to demonstrate its good behaviour, the proposed method is applied to fabricate a two-dimensional hydrodynamic focusing device. The dimensions of the streams lie between 81 and 224 μm showing a good correspondence with the theory. In addition, the device presents a correct operation without leakages demonstrating a good bonding, being the ultimate pressure that the method can support 481 kPa.

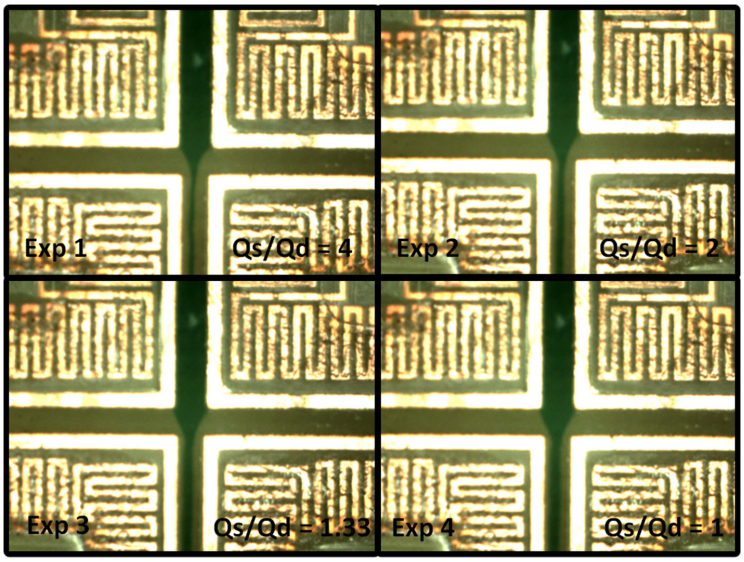

Fig. 8. Experimental results of the fabricated device operation. a) Experiment 1: $Q_s = 0.2$ mL/min, $Q_d = 0.05$ mL/min. b) Experiment 2: $Q_s = 0.2$ mL/min, $Q_d = 0.1$ mL/min. c) Experiment 3: $Q_s = 0.2$ mL/min, $Q_d = 0.15$ mL/min. d)Experiment 4: $Q_s = 0.2$ mL/min, $Q_d = 0.2$ mL/min.

The proposed method allows the integration of PCB-based sensors such as electrodes, and actuators such as microvalves, together with the microheater and the thermo-mechanical barrier of the proposed process. All of them can be fabricated at the same time. It is also important to highlight that the materials are not limited to be the used ones. The PMMA could be replace by other thermoplastic, and the PCB could be a multilayer configuration of a non conductive and conductive materials, for instance, the FR4 can be replace by a glass substrate and the copper layers by titanium or gold, providing a biocompatible device for lab on chip applications. It should be noted that the melting temperature of the thermoplastic has to be lower than the temperature the substrate supports. Once the materials are chosen, the time values and characteristic temperatures have to be known in order to define the parameters of the bonding process. Moreover, the proposed method allows the fabrication of several devices at the same time. Therefore, it is useful for industrial production of microfluidic devices.

Acknowledgments

This work was supported in part by the Spanish Ministry of Science and Innovation (projectTEC2014-54449-C3-2-R, BIOLOP) and the Proyectos de Excelencia de la Junta de Andalucia (projectP12-TIC-2296, Microrad).

References

[1] P. Abgrall, A. Gue, Lab-on-chip technologies: making a microfluidic network and coupling it into a complete microsystem — a review, J. Micromech. Microeng. 17 (5) (2007) R15.
[2] C.D. Chin, V. Linder, S.K. Sia, Lab-on-a-chip devices for global health: past studies and future opportunities, Lab Chip 7 (1) (2007) 41–57.
[3] P.S. Dittrich, A. Manz, Lab-on-a-chip: microfluidics in drug discovery, Nat. Rev. Drug Discovery 5 (3) (2006) 210–218.
[4] D. Moschou, A. Tserepi, The lab-on-PCB approach: tackling the μTAS commercial upscaling bottleneck, Lab Chip 17 (8) (2017) 1388–1405.
[5] Z.Z. Chong, S.H. Tan, A.M. Gañán-Calvo, S.B. Tor, N.H. Loh, N.-T. Nguyen, Active droplet generation in microfluidics, Lab Chip 16 (1) (2016) 35–58.
[6] C. Kim, S. Chung, Y.E. Kim, K.S. Lee, S.H. Lee, K.W. Oh, J.Y. Kang, Generation of core-shell microcapsules with three-dimensional focusing device for efficient formation of cell spheroid, Lab Chip 11 (2) (2011) 246–252.
[7] J.P. Wikswo, E.L. Curtis, Z.E. Eagleton, B.C. Evans, A. Kole, L.H. Hofmeister, W.J. Matloff, Scaling and systems biology for integrating multiple organs-on-a-chip, Lab Chip 13 (18) (2013) 3496–3511.
[8] D. Beebe, M. Wheeler, H. Zeringue, E. Walters, S. Raty, Microfluidic technology for assisted reproduction, Theriogenology 57 (1) (2002) 125–135.
[9] D. Lai, S. Takayama, G.D. Smith, Recent microfluidic devices for studying gamete and embryo biomechanics, J. Biomech. 48 (9) (2015) 1671–1678.
[10] P. Abgrall, V. Conedera, H. Camon, A.-M. Gue, N.-T. Nguyen, SU-8 as a structural material for labs-on-chips and microelectromechanical systems, Electrophoresis 28 (24) (2007) 4539–4551.
[11] S.K. Sia, G.M. Whitesides, Microfluidic devices fabricated in poly (dimethylsiloxane) for biological studies, Electrophoresis 24 (21) (2003) 3563–3576.
[12] J.C. McDonald, G.M. Whitesides, Poly (dimethylsiloxane) as a material for fabricating microfluidic devices, Acc. Chem. Res. 35 (7) (2002) 491–499.
[13] C.-W. Tsao, D.L. DeVoe, Bonding of thermoplastic polymer microfluidics, Microfluid. Nanofluid. 6 (1) (2009) 1–16.
[14] Y. Temiz, R.D. Lovchik, G.V. Kaigala, E. Delamarche, Lab-on-a-chip devices: how to close and plug the lab? Microelectron. Eng. 132 (2015) 156–175.
[15] M.A. Eddings, M.A. Johnson, B.K. Gale, Determining the optimal PDMS-PDMS bonding technique for microfluidic devices, J. Micromech. Microeng. 18 (6) (2008) 067001.
[16] C. Aracil, F. Perdigones, J.M. Moreno, J.M. Quero, BETTS: Bonding, exposing and transferring technique in SU-8 for microsystems fabrication, J. Micromech. Microeng. 20 (3) (2010) 035008.
[17] E.H. Klaassen, K. Petersen, J.M. Noworolski, J. Logan, N.I. Maluf, J. Brown, C. Storment, W. McCulley, G.T. Kovacs, Silicon fusion bonding and deep reactive ion etching: a new technology for microstructures, Sensors Actuators A Phys. 52 (1) (1996) 132–139.
[18] S. Queste, R. Salut, S. Clatot, J.-Y. Rauch, C.G.K. Malek, Manufacture of microfluidic glass chips by deep plasma etching, femtosecond laser ablation, and anodic bonding, Microsyst. Technol. 16 (8-9) (2010) 1485–1493.
[19] R. Wolffenbuttel, K. Wise, Low-temperature silicon wafer-to-wafer bonding using gold at eutectic temperature, Sensors Actuators A Phys. 43 (1-3) (1994) 223–229.
[20] A. Toossi, H. Moghadas, M. Daneshmand, D. Sameoto, Bonding PMMA microfluidics using commercial microwave ovens, J. Micromech. Microeng. 25 (8) (2015) 085008.
[21] D. Ogończyk, J. Węgrzyn, P. Jankowski, B. Dąbrowski, P. Garstecki, Bonding of microfluidic devices fabricated in polycarbonate, Lab Chip 10 (10) (2010) 1324–1327.
[22] J. Steigert, S. Haeberle, T. Brenner, C. Müller, C. Steinert, P. Koltay, N. Gottschlich, H. Reinecke, J. Rühe, R. Zengerle, Rapid prototyping of microfluidic chips in COC, J. Micromech. Microeng. 17 (2) (2007) 333.
[23] A. Wego, S. Richter, L. Pagel, Fluidic microsystems based on printed circuit board technology, J. Micromech. Microeng. 11 (5) (2001) 528.

[24] S. Gaßmann, I. Ibendorf, L. Pagel, Realization of a flow injection analysis in PCB technology, Sensors Actuators A Phys. 133 (1) (2007) 231–235.
[25] D. Moschou, T. Trantidou, A. Regoutz, D. Carta, H. Morgan, T. Prodromakis, Surface and electrical characterization of Ag/AgCl pseudo-reference electrodes manufactured with commercially available PCB technologies, Sensors 15 (8) (2015) 18102–18113.
[26] F. Perdigones, C. Aracil, J.M. Quero, M. Gutiérrez, C. Jiménez, P. Giménez, Integration method of silicon sensors on SU-8-based microfluidic platforms, Microsyst. Technol. 21 (1) (2015) 155–161.
[27] S. Schumacher, J. Nestler, T. Otto, M. Wegener, E. Ehrentreich-Förster, D. Michel, K. Wunderlich, S. Palzer, K. Sohn, A. Weber, et al. Highly-integrated lab-on-chip system for point-of-care multiparameter analysis, Lab Chip 12 (3) (2012) 464–473.
[28] C. Aracil, F. Perdigones, J.M. Moreno, A. Luque, J.M. Quero, Portable lab-on-PCB platform for autonomous micromixing, Microelectron. Eng. 131 (2015) 13–18.
[29] I. Burdallo, C. Jimenez-Jorquera, C. Fernández-Sánchez, A. Baldi, Integration of microelectronic chips in microfluidic systems on printed circuit board, J. Micromech. Microeng. 22 (10) (2012) 105022.
[30] A. Petropoulos, G. Kaltsas, D. Goustouridis, E. Gogolides, A flexible capacitive device for pressure and tactile sensing, Procedia Chem. 1 (1) (2009) 867–870.
[31] S. Gassmann, A. Trozjuk, J. Singhal, H. Schuette, M.L. Miranda, O. Zielinski, PCB Based Micro Fluidic System for Thermal Cycling of Seawater Samples, Industrial Technology (ICIT), 2015 IEEE International Conference On, IEEE. 2015, pp. 3365–3369.
[32] C. Simonnet, A. Groisman, Two-dimensional hydrodynamic focusing in a simple microfluidic device, Appl. Phys. Lett. 87 (11) (2005) 114104.
[33] B. Salvador, E. Franco, F. Perdigones, J.M. Quero, Método de unión de sustratos y plásticos mediante zona de adhesión térmica controlada, 2016, Spain Patent P201600809.
[34] A. Comsol, COMSOL Multiphysics User's Guide, Version: September 10, 2005, 333.
[35] A. Ga nan-Cálvo, Device and method for creating spherical particles of uniform size, 2001, US Patent 6,197,835.
[36] S.L. Anna, N. Bontoux, H.A. Stone, Formation of dispersions using flow focusing in microchannels, Appl. Phys. Lett. 82 (3) (2003) 364–366.
[37] G.-B. Lee, C.-C. Chang, S.-B. Huang, R.-J. Yang, The hydrodynamic focusing effect inside rectangular microchannels, J. Micromech. Microeng. 16 (5) (2006) 1024.

Sensors and Actuators A 298 (2019) 111568

Contents lists available at ScienceDirect

Sensors and Actuators A: Physical

journal homepage: www.elsevier.com/locate/sna

Single-use impulsion system for displacement of liquids on thermoplastic-based lab on chip

Francisco Perdigones, Miguel Cabello*, Jose Manuel Quero

Department of Electronic Engineering, University of Seville, Seville, Spain

ARTICLE INFO

Article history:
Received 7 June 2019
Received in revised form 12 August 2019
Accepted 20 August 2019
Available online 10 September 2019

Keywords:
Impulsion-system
Thermoplastics
Lab-on-chip
Microfluidics

ABSTRACT

In this paper, an impulsion system of liquids for thermoplastic microfluidic circuits is described. The presented device is composed of a membrane made of polymethylmethacrylate (PMMA) which separates two microchambers (top and bottom microchamber). The bottom microchamber is pressurized to a fixed pressure, while the top microchamber remains at atmospheric pressure. The actuation consists on increasing the temperature of the membrane by Joule effect using an aluminum microheater which is fabricated over the membrane. Once the temperature of the membrane is close to the glass transition temperature of the thermoplastic, the membrane deforms due to the different pressure of the bottom microchamber, blocking the top microchamber. The trapped air fits the volume of liquid which will be impulsed inside the microchannel. Unlike other membranes used in microfluidics, the presented membrane keeps deformed when the actuation is removed. The fabricated impulsion system is designed to move a volume of 30 μL. The experimental results correspond to a theoretical design with an average error of about 6.32%. The proposed impulsion system is easily integrable on thermoplastic lab on chips for liquid management.

1. Introduction

The control of small volumes of fluid is an important issue in microelectromechanical systems (MEMS), in particular on lab on chip (LOC) and lab on printed circuit board, also named lab on PCB (LOP) [1]. The development of LOCs dates back to the end of the 20th century, growing exponentially during the 21st century. In the present days, the amount of application of LOCs in many different fields make possible to keep this growth, especially on biomedicine and environment [2–6]. One of the most important part of LOC devices is the microfluidic circuit. The different applications of LOCs have helped to improve the reliability and performance of the microfluidic circuits integrated within LOC devices. Focusing on the management of small volumes of fluids, microvalves and impulsion systems become the most significant components in many LOCs. These kinds of devices are intended for several functions, such as performing the regulation of flow rates, and blocking or opening the fluid flow inside the microfluidic circuit.

There are several methods to impulse liquids inside a lab on chip device, which can be integrated or not together with the LOC. Among the non-integrated impulsion systems, one of the most typical one used for obtaining a controlled continuous flow in LOC devices is through external syringe pumps [7,8]. Regarding the integrated impulsion systems, digital microfluidics, also named electrowetting and optoelectrowetting, is a technology that controls droplets on an array of electrodes [9,10]. Another technique based on surface acoustic waves has been used for fluids handling. The working principle of this technique consists on using the piezoelectric behavior of certain materials, such as zinc oxide (ZnO) or crystal lithium niobate ($LiNbO_3$), to convert the electric energy into mechanical energy making surface acoustic waves [11,12]. Other method is based on using pressurized microchambers for storing the energy needed to impulse liquid samples in a discrete manner. In this case, the working principle consists on opening small microchannels to release the pressurized gas stored inside the microchamber. Once the gas is released, the liquid samples are displaced all along the microchannel [13–15]. Peristaltic micropumps are another type of devices to achieve a continuous movement of fluids. These impulsion systems are based on blocking microchambers through the deformation of membranes [16,17]. These membranes recover the initial state after the actuation. Normally, the method used to deform the membrane consists on the expansion of a gas by increasing the temperature, following the basis of the Joule effect. In order to achieve a precise control of liq-

* Corresponding author.
E-mail addresses: perdi@zipi.us.es (F. Perdigones), mcabellov@gte.esi.us.es (M. Cabello).

https://doi.org/10.1016/j.sna.2019.111568
0924-4247/

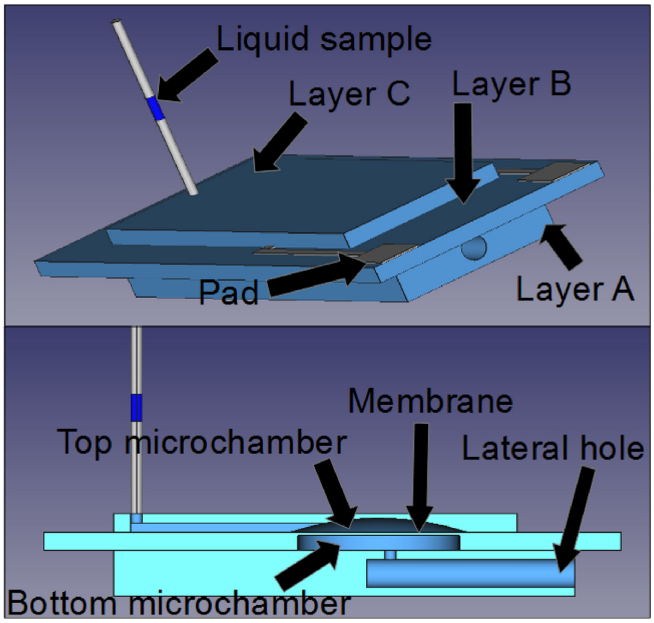

Fig. 1. Top: assembly of the three layers and the tube with the sample. Bottom: cross sectional view of the system; the bottom microchamber and the thermoplastic membrane are shown.

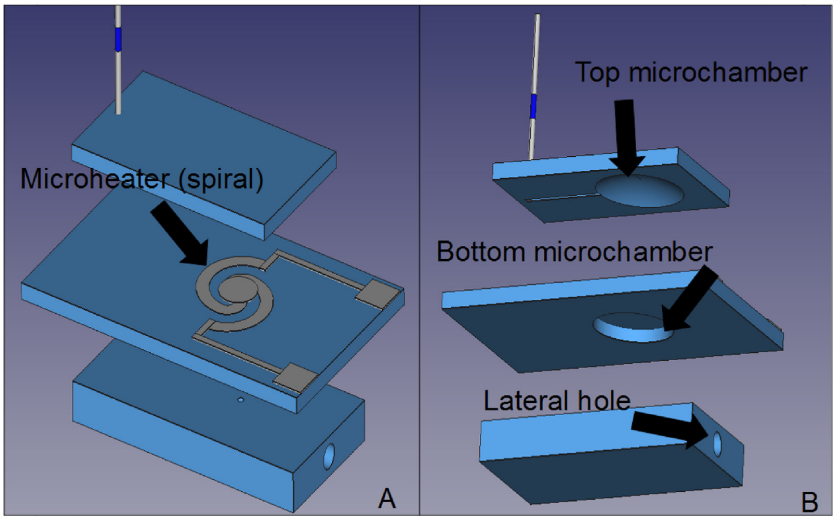

Fig. 2. Different parts of the system before the assembly. (A) The microheater and the pads can be seen as part of layer B. (B) Different components of each layer are shown: the lateral hole in layer A, the bottom microchamber and the thermoplastic membrane in layer B and the top microchamber in layer C.

uids, the deformation of the membrane could be either performed by piezoelectric effect [18] or by using electrolytic gas generation. A power source, a liquid solution and electrodes are necessary to carry out the electrolytic gas method [19]. Another technique to achieve the transport of liquid samples is based on the use of centrifugal forces. These kinds of devices are known as lab on disk [20]. One last discrete impulsion system is based on the use of azobis-isobutyronitrile (AIBN) as the solid chemical propellant. This technique consists on increasing the temperature of the AIBN up to 70 °C to generate nitrogen and impulse the liquid sample thanks to the volume expansion [21]. The methods previously described are only a few examples of the reported impulsion systems.

In this paper, a PMMA/aluminum discrete impulsion system is developed. This device is composed of a membrane which deforms and blocks a top microchamber in the same way than peristaltic micropumps, but with one important difference: the membrane

keeps the deformation when the actuation is removed. Therefore, the impulsed liquid does not return to the initial position. The main advantages that justified the development of this microvalve are its ease of fabrication and its integration on thermoplastic LOCs. In addition, a low cost fabrication process, such as the one described in this paper, is required to create disposable LOC devices, which are widely used for biological and medical applications. In this respect, the proposed impulsion system fulfills an inexpensive manufacturing procedure by using low cost materials and facilities. Moreover, the materials chosen to perform the fabrication are PMMA, aluminum and glue, being replaceable for biocompatible materials to make this impulsion system suitable for life sciences applications. Thus, in this paper we present an impulsion system which could not be found on literature, that is, an impulsion system in which the membrane keeps the deformation without the actuation.

The rest of the paper is structured as follows. Section 2 describes the proposed method in detail. In Section 2, the design is detailed. The fabrication process is presented in Section 3. Then, in Section 4, the device is experimentally tested. Finally, in Section 5, the main conclusions of this research work are summarized.

2. Impulsion system description

The system is composed of a pressurized microchamber (bottom microchamber), a thermoplastic membrane, a top microchamber and a microheater, as can be seen in Figs. 1 and 2 .

The working principle consists on the deformation of the membrane which blocks the top microchamber. The liquids are impulsed a certain volume corresponding to those of the top microchamber. The actuation method is based on both the Joule effect, to increase the temperature of the membrane near the glass transition temperature, and a difference of pressure, to deform the membrane when it is heated up. In order to minimize the consumption of energy of the actuation, the microheater is placed over the membrane, allowing the free deformation of the membrane. Because of that, the microheater is a metallic Fermat spiral with a disk in the center. The reason why this disk is placed in the center of the spiral is to avoid a high increase of temperature. The shape of the spiral is shown in Fig. 2.

The actuation is explained step by step in Fig. 3. In the initial step (step 1), the bottom microchamber is not pressurized. Then, in step 2 a plunger is inserted in the lateral hole, making the thermoplastic membrane to withstand the pressure with no deformation. After that (step 3), in order to reach a temperature close to the glass transition temperature of the material, an electrical current is supplied to the spiral microheater through the pads. In step 4, the membrane starts to deform due to both the pressure stored in the bottom microchamber, and the decreasing of the Young modulus, due to the increase of temperature. In the last step (step 5), the membrane finally blocks the top microchamber. During steps 4 and 5, the volume of gas of the top microchamber (V_1) is impulsed to the outside. If this volume of gas is connected to a microchannel with a liquid inside, this liquid will be displaced the same amount of volume that is storage in the top microchamber (V_1). Finally, in step 6, the current is removed, the membrane recovers the room temperature, and therefore its initial stiffness, keeping the deformation.

It is important to highlight that the increase of temperature leads an increase of volume that has to be added to the one created by the deformation of the membrane. However, it is a transient state because the liquid reaches the desired position when the system recovers the room temperature. This effect depends on the thermoplastic material and its glass transition temperature. It can be minimized by locating the impulsion system as far away as possible to the liquids.

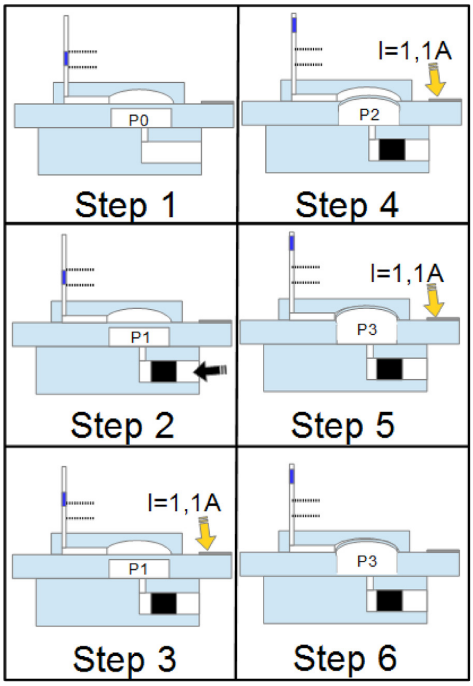

Fig. 3. Cross-sectional view of the system for explaining the actuation.

Unlike membrane-based impulsion systems, the membrane of the proposed system does not recover the initial state when the actuation is removed. Therefore, the liquid remains in the final position. The working principle is intended to be single-use for disposable lab on chips.

There are many different methods to control fluids in LOCs. For example, those systems based on membranes pneumatically actuated by vacuum or pressure. This method allows the opening and close of microchannels through the regulation of the flow rate of the working fluid. These microvalves are very useful for constant flow regulation. However, they are not the best choice to place a liquid sample in a designed location because, in order to actuate, the position of the liquid sample as a function of the time is required. In this respect, the impulsion system proposed in this paper only needs the initial and final location of the sample, that is, the volume to be impulsed. Therefore, the microfluidic design is easier than the pneumatic membranes systems. Another device used to stop a liquid sample in a specific location of the LOC is the stop valve. These kinds of systems are based on capillarity forces and hydrophobicity. These microvalves are especially used on centrifugal microfluidic systems (lab-on-a-disc) because their nature of passive microvalve is interesting. Lab-on-a-disc devices mean a good solution to place liquid samples in a microfluidic circuit. Nevertheless, stop valves have an indispensable requirement: a motor and a precise control of the angular acceleration is needed to stop the samples. In this respect, the proposed impulsion system does not need an external actuator (the motor) and its control. It only requires a constant current to move the liquid sample with precision. Finally, the impulsion systems based on either AIBN or electrolytic gas have been reported. These methods require the integration of an additional material in the LOC, which adds complexity to the fabrication process. The proposed impulsion system

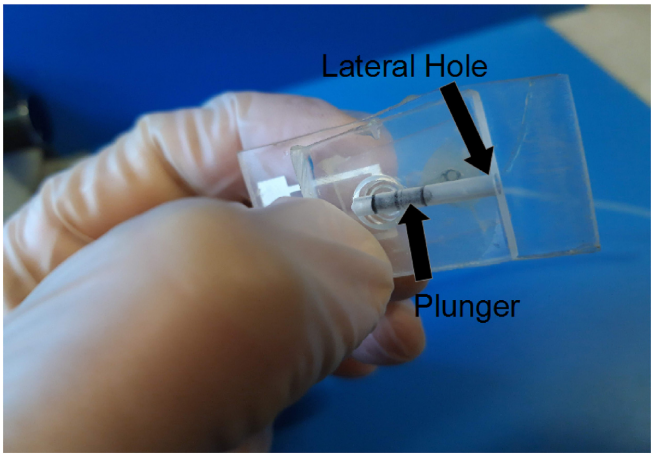

Fig. 4. The plunger is inserted inside the lateral hole for achieving the increase of pressure in the bottom microchamber.

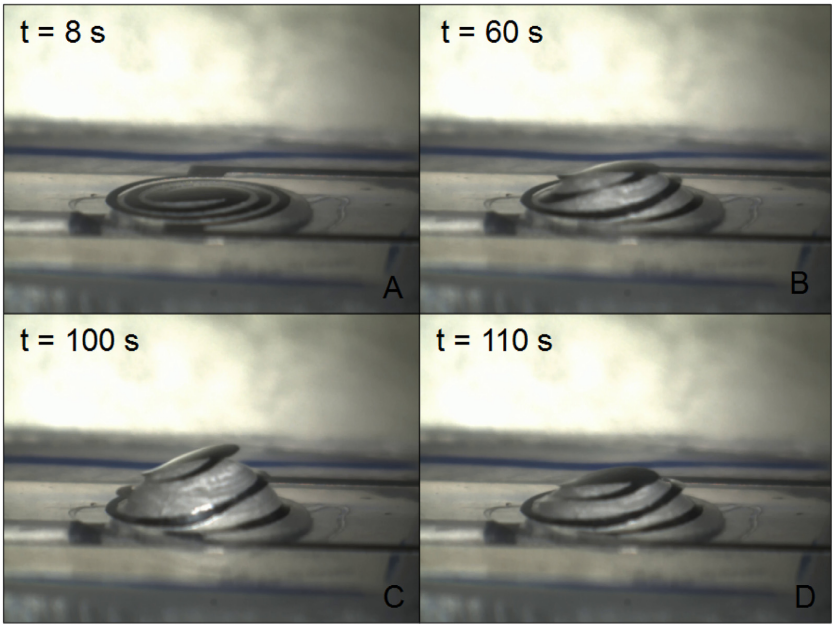

Fig. 5. (A) Initial state of the membrane before the activation. (B) Intermediate state. (C) Maximum deformation of the membrane. (D) The membrane just after breaking.

is highly integrable, and no additional material are used, merely the metal and the thermoplastic.

3. Fabrication, materials and dimensions

The system is composed of three layers (layer A, layer B and layer C), as can be seen in Figs. 1 and 2 . The layer A is a piece of PMMA of 5 mm of thickness with two drilled holes. One of the holes has a diameter *D* of 3.7 mm and a length of 18 mm, from the edge to the center of the piece. The other one has a diameter *d* of 1 mm and it connects the end of lateral hole with the bottom microchamber.

The function of the holes is explained in Section 4. The layer B is a PMMA piece with a thickness of 2 mm. This layer is milled with a CNC machine to fabricate the membrane and the bottom microchamber. This membrane has a diameter of 7.2 mm and a thickness of 350 μm. After that, an aluminum layer is placed over the PMMA following the procedure reported on [22], and subsequently etched to fabricated the spiral microheater and the pads. The layer C is a PMMA piece of 2 mm where the top microchamber with a quasi-spherical shape is milled with a spherical milling tool (radius = 2.4 mm). The height of the top microchamber is 1 mm and the diameter is 7.2 mm. The reason why this shape has been chosen is to minimize the dead volume when the membrane blocks

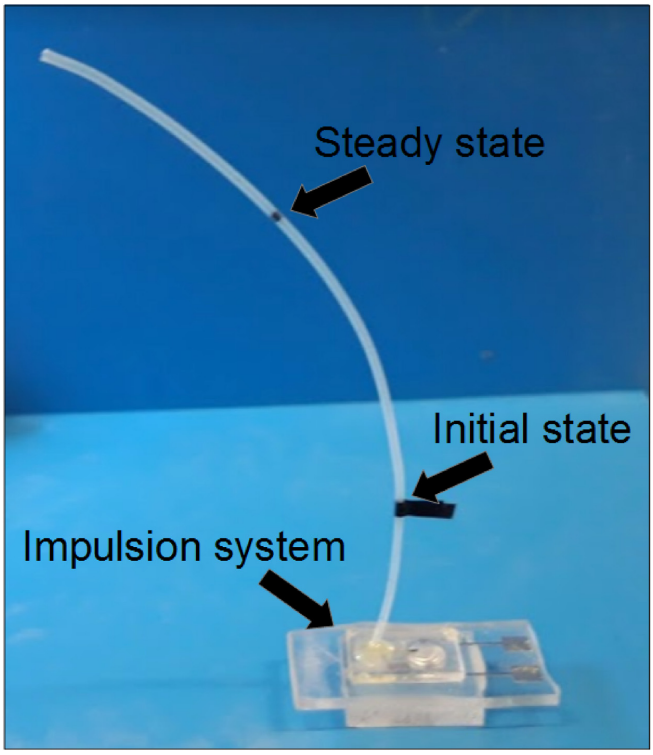

Fig. 6. The initial state of the impulsion before actuation and the steady state of the impulsion after actuation are marked.

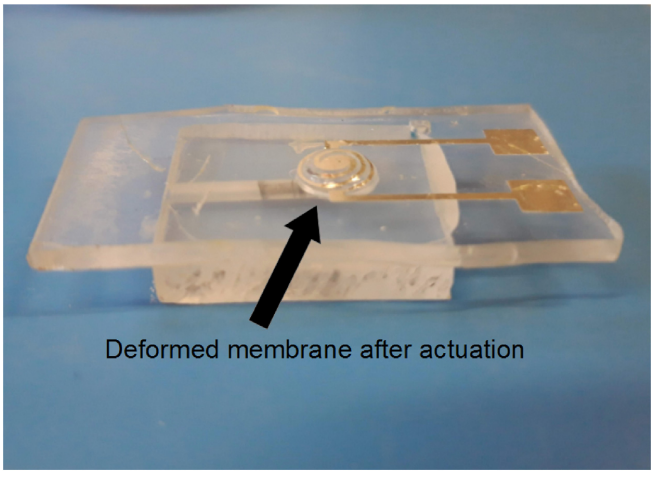

Fig. 7. The deformed membrane after actuation in the disassembled system.

the microchamber. The volume of the top microchamber is 30 μL. In addition, a small microchannel which links the top microchamber with the outlet port is milled. A tube (D_{tube} = 0.864 mm) is inserted in the outlet port. Finally, the three layer are glued.

4. Experimental setup and results

The experiments consist on impulsing a small volume of blue ink along a tube. The first step to perform the experiments is the

Table 1
Experimental results of the impulsions and error.

Experiment	Experimental impulsed volume (μL)	Error (%)
1	32.24	7.5
2	31.42	4.7
3	32.83	9.4
4	31.36	4.5
5	31.66	5.5
Average	31.9	6.32

pressurization of the bottom microchamber by inserting a plunger inside the lateral hole of the layer A, Fig. 4. The final pressure of the bottom microchamber is $P1 = 0.162$ MPa over the atmospheric pressure ($P0$).

This pressure is calculated using the Boyle law and the dimensions of the bottom microchamber and the lateral hole. The expression is described as follow:

$$P1 = P0 \cdot \frac{V_{lateral\text{-}hole} + V_{bottom\text{-}chamber}}{V_x + V_{bottom\text{-}chamber}} \quad (1)$$

where $P1$ and $P0$ are the final and initial pressure, respectively. $V_{lateral\text{-}hole} = 193.53$ μL is the volume of the whole lateral hole, $V_{bottom\text{-}chamber} = 67.17$ μL is the volume of the bottom chamber and $V_x = 32.25$ μL is the remaining volume of the lateral hole after the insertion of the plunger.

Then, the tube is filled with 1 μL of blue ink through a hole which will be blocked with a black tape. After that, the system is ready to be used. Both the initial and steady states of the fluid sample are shown in Fig. 5. The actuation occurs when a current of $I = 1.1$ A is applied to the spiral microheater through the pads. This current is experimentally fixed to avoid the melting of the membrane during the impulsion, which last for about 26 s.

The deformation of the membrane without the top microchamber is shown in Fig. 5. This deformation starts when the current is applied, as can be seen Fig. 5A. Fig. 5B presents the membrane with an intermediate deformation. The maximum deformation reached is shown in Fig. 5C, just before its breaking. Finally, the membrane breaks and deflates, as can be seen in Fig. 5D. In Fig. 5 it is possible to observe how the microheater delaminates during the deformation of the membrane. However, the membrane blocks the top microheater before the delamination of the microheater and before the breaking of the own membrane (Fig. 6).

In order to see the deformation of the membrane, a disassembled system after the actuation is shown in Fig. 7. In this case, the current has been removed and the membrane remains deformed. However, as it was previously commented, the spiral microheater is still glued to the membrane, so delamination does not occur.

The experimental results are shown in Table 1.

Despite the theoretical impulsion volume of our design was 30 μL, there is an average error in the impulsion of $\epsilon = 6.32\%$. The maximum difference in the volume impulsion is $\Delta V_{max} = 2.83$ μL, and the minimum is $\Delta V_{min} = 1.36$ μL. Nevertheless, this deviation is perfectly assumable for most of the microfluidic applications.

The liquids placement inside a LOC is an important issue when designing the protocol to be developed [23]. This placement has an error that depends on the error of the impulsed volume and on the cross-sectional area of the microchannel. Therefore, for the same error in the impulsed volume, the lower the cross-sectional area is, the higher the error of the placement will be. For that reason, precision during the fabrication process becomes crucial, as well as the minimization of tolerances.

5. Conclusions

A proof of concept of an impulsion system for single-use lab on chip has been designed, fabricated and tested. The proposed working principle of this device allows the placement of liquids with no backward movement when the actuation is removed. This behavior is possible thanks to the thermal and mechanical properties of the thermoplastic materials. Therefore, the device is intended to be used integrated within thermoplastic-based microfluidic platforms. In its current form, the device is not biocompatible due to the aluminum. A biocompatible metal could be chosen as long as it is compatible with the fabrication process. The experiments carried out show the good behavior of the impulsion system, with an average error of 6.32% respect to the designed impulsed volume. Despite the designed device is intended to pressurize a previously fixed volume of 30 μL, this value is easily adjustable just modifying the dimensions of the membrane and the microchambers.

Acknowledgements

This work was supported by the Spanish Ministry of Science and Innovation (project TEC2014-54449-C3-2-R, BIOLOP).

References

[1] D. Moschou, A. Tserepi, The lab-on-PCB approach: tackling the μTAS commercial upscaling bottleneck, Lab Chip 17 (8) (2017) 1388–1405.
[2] D. Mark, S. Haeberle, G. Roth, F. von Stetten, R. Zengerle, Microfluidic lab-on-a-chip platforms: requirements, characteristics and applications, Chem. Soc. Rev. 39 (3) (2010) 1153–1182.
[3] P. Abgrall, A. Gue, Lab-on-chip technologies: making a microfluidic network and coupling it into a complete microsystem – a review, J. Micromech. Microeng. 17 (5) (2007) R15.
[4] D. Figeys, D. Pinto, Lab-on-a-chip: a revolution in biological and medical sciences, Anal. Chem. 72 (9) (2000) 330–A.
[5] J. Gardeniers, A. Van den Berg, Lab-on-a-chip systems for biomedical and environmental monitoring, Anal. Bioanal. Chem. 378 (7) (2004) 1700–1703.
[6] A.M. Cabibbe, P. Miotto, R. Moure, F. Alcaide, S. Feuerriegel, G. Pozzi, V. Nikolayevskyy, F. Drobniewski, S. Niemann, K. Reither, et al., Lab-on-chip-based platform for fast molecular diagnosis of multidrug-resistant tuberculosis, J. Clin. Microbiol. 53 (12) (2015) 3876–3880.
[7] M. Cabello, M. Mozo, B. De la Cerda, C. Aracil, F.J. Diaz-Corrales, F. Perdigones, L. Valdes-Sanchez, I. Relimpio, S.S. Bhattacharya, J.M. Quero, Electrostimulation in an autonomous culture lab-on-chip provides neuroprotection of a retinal explant from a retinitis pigmentosa mouse-model, Sens. Actuators B: Chem. 288 (2019) 337–346.
[8] G.D. Kaprou, V. Papadopoulos, D.P. Papageorgiou, I. Kefala, G. Papadakis, E. Gizeli, S. Chatzandroulis, G. Kokkoris, A. Tserepi, Ultrafast, low-power, PCB manufacturable, continuous-flow microdevice for DNA amplification, Anal. Bioanal. Chem. (2019).
[9] C. Dong, T. Chen, J. Gao, Y. Jia, P.-I. Mak, M.-I. Vai, R.P. Martins, On the droplet velocity and electrode lifetime of digital microfluidics: voltage actuation techniques and comparison, Microfl. Nanofl. 18 (4) (2015) 673–683.
[10] S.N. Pei, J.K. Valley, Y.-L. Wang, M.C. Wu, Distributed circuit model for multi-color light-actuated opto-electrowetting microfluidic device, J. Lightwave Technol. 33 (16) (2015) 3486–3493.
[11] U. Farooq, Z. Haider, X.M. Liang, K. Memon, S.C. Hossain, Y. Zheng, H. Xu, A. Qadir, F. Panhwar, S. Dong, et al., Surface-acoustic-wave-based lab-on-chip for rapid transport of cryoprotectants across cell membrane for cryopreservation with significantly improved cell viability, Small (2019).
[12] L.Y. Yeo, J.R. Friend, Surface acoustic wave microfluidics, Annu. Rev. Fluid Mech. 46 (2014) 379–406.
[13] G. Flores, C. Aracil, F. Perdigones, J. Quero, Low consumption single-use microvalve for microfluidic PCB-based platforms, J. Micromech. Microeng. 24 (6) (2014) 065013.
[14] F. Perdigones, E. Franco, B. Salvador, G. Flores, J.M. Quero, Highly integrable microfluidic impulsion system for precise displacement of liquids on lab on PCBs, J. Microelectromech. Syst. 27 (3) (2018) 479–486.
[15] C. Aracil, F. Perdigones, J.M. Moreno, A. Luque, J.M. Quero, Portable lab-on-PCB platform for autonomous micromixing, Microelectron. Eng. 131 (2015) 13–18.
[16] O.C. Jeong, S.W. Park, S.S. Yang, J.J. Pak, Fabrication of a peristaltic PDMS micropump, Sens. Actuators A: Phys. 123 (2005) 453–458.
[17] O.C. Jeong, S. Konishi, Fabrication of a peristaltic micro pump with novel cascaded actuators, J. Micromech. Microeng. 18 (2) (2008) 025022.
[18] L.-S. Jang, W.-H. Kan, Peristaltic piezoelectric micropump system for biomedical applications, Biomed. Microdev. 9 (4) (2007) 619–626.
[19] C.R. Neagu, J.G. Gardeniers, M. Elwenspoek, J.J. Kelly, An electrochemical microactuator: principle and first results, J. Microelectromech. Syst. 5 (1) (1996) 2–9.
[20] M.M. Aeinehvand, F. Ibrahim, S.W. Harun, A. Kazemzadeh, H.A. Rothan, R. Yusof, M. Madou, Reversible thermo-pneumatic valves on centrifugal microfluidic platforms, Lab Chip 15 (16) (2015) 3358–3369.

[21] C.-C. Hong, S. Murugesan, S. Kim, G. Beaucage, J.-W. Choi, C.H. Ahn, A functional on-chip pressure generator using solid chemical propellant for disposable lab-on-a-chip, Lab Chip 3 (4) (2003) 281–286.
[22] B. Salvador, E. Franco, F. Perdigones, J.M. Quero, Fabrication process for inexpensive, biocompatible and transparent PCBs. application to a flow meter, Microelectron. Eng. 173 (2017) 6–12.
[23] G. Flores, C. Aracil, F. Perdigones, J.M. Quero, Lab-protocol-on-PCB: prototype of a laboratory protocol on printed circuit board using MEMS technologies, Microelectron. Eng. 200 (2018) 26–31.

Biographies

Francisco Perdigones was born in Huelva, Spain, in 1979. He received the M.Sc. and Ph.D. degrees in electronics engineering from the University of Seville, Seville, Spain, in 2006 and 2010, respectively. He joined the Aerospace Engineering and Fluid Mechanics Department in 2006. In 2009, he joined the Electronic Engineering Department, where he is currently working. His research interests include polymer microstructures, sensors, actuators, and lab-on-chip devices.

Miguel Cabello was born in Córdoba, Spain, in 1988. He received M.Sc. degree in Telecommunication Engineering from University of Seville, Seville, in 2014, where he is currently pursuing the Ph.D. degree with the Electronic Engineering Department. His research interests include PCB-MEMS, microelectrode arrays for biomedical and biological application, microfabrication, and lab-on-chip technologies.

José Manuel Quero received the M.Sc. and Ph.D. degrees in electrical engineering from the University of Seville, Spain, in 1988 and 1991, respectively. He has been a Full Professor with the Department of Electronic Engineering, Universidad de Sevilla, since 2000. He is also a Senior Researcher within AICIA, a non-profit research organization. He has been an Evaluator and Reviewer for the European Commission in the Information Society Technology program since 2002. He is currently the CEO of Solar MEMS Technologies, a spin-off company, specialized in MEMS applications for space. His research interests include MEMS sensors and actuators and their application in microfluidics, BioMEMS, RF, and space.

Microfluidic Platform with Absorbance Sensor for Glucose Detection

G. Flores, F. Perdigones, C. Aracil, M. Cabello and J.M. Quero
University of Seville
Seville, Spain
Email: gflores@gte.esi.us.es

***Abstract*—In this paper, a microfluidic Lab on Chip (LOC) platform for clinical diagnosis of glucose is proposed. The method is based on measuring the amount of glucose in a sample using a colorimetric enzyme-kinetic method. The colorimetric changes are detecting using an absorbance system consisting of a light emitting diode and a phototransistor working on the wave length of 505 nm. The proposed platform is intended to be integrated with microfluidic PCB-based platforms for portable use. The experiments have shown good stability of the measure due to the use of a differential measurement circuit.**

I. Introduction

The glucose detection in human physiological fluids is an important issue in the biomedical field. Diabetes is the most common metabolic disorder world-wide, with more than 300 million affected people. In recent years, a number of approaches have been raised toward the development of glucose sensors. This employs different transduction mechanisms as well as recognition elements. The glucose biosensors reported in the bibliography mainly utilize electrochemical signal transduction [1]–[3], fluorescence [4], [5] and absorbance [6].

Lab on Chip (LOC) devices are an alternative method towards the glucose detection. They offer many advantages over macroscopic systems, including low volume of samples and low reagents consumption, low waste production, high levels of throughput, automation and portability. The target of microfluidic lab-on-a-chip (LOC) systems is focused on integrating a complete analytical process into a single device capable to perform sampling, sample pre-treatment, analytical separation, bio-chemical reaction, analyze detection and data analysis operations. There have been several approaches [7], [8] in glucose assay. However, these are not easily integrable in a multifunction microfluidic circuits due to the complexity in the fabrication process.

In this paper, an absorbance MEMS platform is developed and characterized. This is an approach toward a LOC glucose detection system which is thought to be a component of a microfluidic circuit for impulsion, mixing, heating and sensing. The proposed platform is highly portable and integrable with other microfluidic components due to the fabrication materials, that is, SU-8, PCB and glass. Moreover, its optical detection electronic circuit is robust since it uses the differential measure mode, and the stability of an assembly system, avoiding any mechanical disturbance.

II. Glucose Detection

The method of glucose detection in our system is based on the colorimetric enzyme-kinectic principle. A glucose Trinder GOD-POD (Spinreact, S.A) [9] is used. In this reaction, the glucose oxidase catalyzes the oxidation of glucose to gluconic acid (1). The hydrogen peroxide generated is detected by a chromogenic oxygen acceptor, phenol-aminophenazone in the presence of peroxidase (2). The preparation method consists of a working reagent and a glucose cal, Glucose aqueous primary standard 100 mg/dL. A working reagent is prepared dissolving the context of enzymes, which will react with the glucose, and with a buffer (phenol). The reagent is mixed with the glucose sample in different volumen ratios, depending on the dilution factors (DF) (3). The reaction of glucose with the working reagent generates a red colored quinoneimine, which has an absorbance peak at 505 nm. The intensity of that color is proportional to the glucose concentration in the sample, Fig. 1.

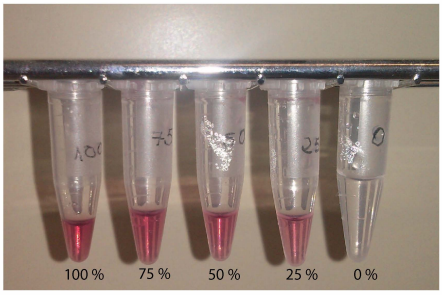

Fig. 1. Different concentration of the reaction products.

$$\beta - D - Glucose + H_2O \rightarrow GluconicAcid + H_2O \quad (1)$$

$$H_2O_2 + Phenol + Aminophenazone \rightarrow Quinone + H_2O \quad (2)$$

$$DF = \frac{V solution}{V solute} \quad (3)$$

III. Microfluidic system for glucose reaction

The purpose of this paper is to develop a microfluidic platform for glucose detection. The fabrication process is designed to integrate different microfluidics components in that platform. In the paper, the mixure of reagents and sample is going to be done manually. However, several active and passive components have been already developed for PCB-based platforms [10], [11].

978-1-4799-8108-3/151$31.00 ©2015 IEEE

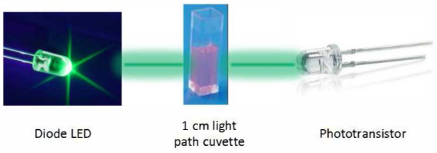

Fig. 2. Schematic system of the optoelectronic system detection.

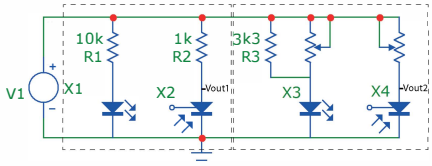

Fig. 3. Schematic circuit for the optoelectronic system detection.

IV. Optoelectronic System for Detection

The optical detection system consists of a green light emitting diode (Nichia NEPE510JS), which generates light that goes through a detection chamber, and reachs a phototransistor (Vishay TEPT4400), as can be seen in Fig. 2.

The absorbance for the reaction products reduces the amount of light intensity detected by the phototransistor. According to the polarization of the phototransistor Fig. 3, the redder is the glucose assay, the more light is observed by the liquid, and therefore the output voltage (Vout1) will be increased.

The electronic system works in differential mode to avoid any disturbance from ambient noise. In parallel with the reaction chamber, there are a replicated microfluidic and an electronic circuit using X3 and X4 amplified. The output voltage of this system is proportional to the difference Vout1-Vout2. The polarization system will have a signal output (Vout1 and Vout2) between 0 a 370 mV for a range of glucose from 0 mg/dL to 100 mg/dL.

V. Fabrication Process and Setup

The Lab on Chip is manufactured in PCB, glass and SU-8. The schematic of the platform consists of a PCB, as a substrate where the microfluidic circuit is fabricated, and a plastic (PLA) structure where the electronic system is assembled. The PCB with the microfluidic circuits contains two chambers with 5 mm of diameter where the different concentrations are located, Fig. 4 A) schematic top view, and B) schematic bottom view.

The fabrication process can be observed in Fig. 4 C). In the step (a), the process begins with 1 mm thick glass and a single PCB. Then, in the step (b), the FR4 is milled with the same dimensions of the glass. In order to do so, a automatic CNC milling machine is used. After milling, in the step (c), two holes of 5 mm are drilled. The chambers will be located over these two holes. After that, in the step (d), the glass is placed into the milled area of the PCB, and glued to ensure the permeability and stability. The typical SU-8 process is performed above the glass and the FR4 to fabricate

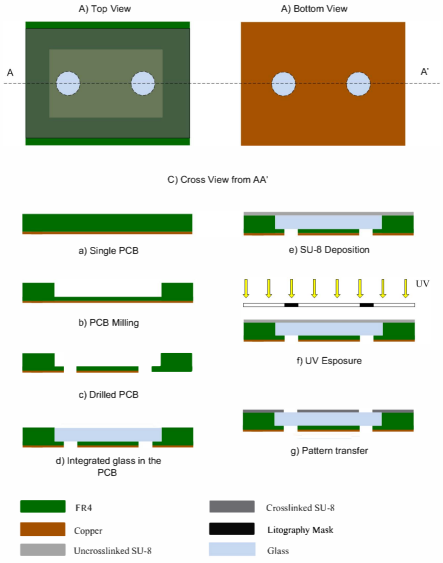

Fig. 4. A) Top view and B) Bottom view of the microfluidic PCB. C) Fabrication process from cross view AA'.

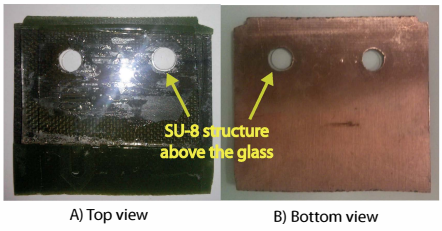

Fig. 5. A) Top view and B) Bottom view of the fabricated microfluidic PCB.

the microfluidic circuit. Also, the SU-8 polymer avoids any leakage between the glass and the PCB. In step (e), a layer of 300 μm of SU-8 2050 (MicroChem Corp.) is deposited over the FR4 and the glass in order to fabricate the two chambers. To do this task, a deposition of 150 μm -thick SU-8 layer is carried out at 700 rpm during 60 s and a softbake of 5 min at 65°C and then at 95°C during 15 min. Then, an adittional deposition of a layer of 150 μm is performed, with the same spin speed but with a softbake of 5 min at 65°C and 2 h at 95°C is carried out to achieve the desired thickness of 300 μm. Subsequently, in step (f), the photoresist is exposed to UV light for 2 min using a mask to define the chambers. Later on, in step (g), the uncrosslinked SU-8 is developed by immersion and agitation in Mr600 Developer (MicroChem Corp.) during 7 min. Finally, the whole structure is cleaned with IPA. In this way, the entire structure is defined, Fig. 5. In this process, the main concern is the cleaning of the structure, because if there is any uncrosslinked SU-8 in the chambers, it will affect significantly the measure of glucose.

Afterward, the complete Lab on Chip is inserted in a

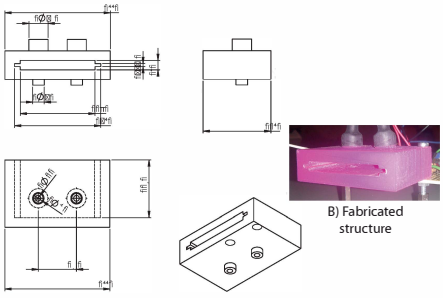

Fig. 6. Plastic structure for the optical reader detection electronic system.

plastic reader which was manufactured using a 3D printer, Fig. 6. The plastic structure of the reader contains two LEDs and photodetectors completely aligned and faced with one another, and an aperture. The microfluidic circuit will be introduced in that aperture, and it is found between the LEDs and phototransistor. Finally, this plastic structure is fixed to a new PCB where the detection electronic system is assembled.

VI. Experimental Results

A. Optical detection

In a first bunch of experiments, the focus is on the validation of the calibration of the optical circuit. A calibration with a standard cuvette of 1 cm light path is done to prove the validation and linearity of the system, as previously presented in Fig. 2. The dilution factor used to prove the system is 100. This has been chosen for being the most typical for 1 cm light path. A electronic circuit adapted to this volume of liquid is assembled in a protoboard with the same LEDs and phototransistors.

The glucose assay is performed filling five cuvettes with 1 mL of reagent. Different concentration of glucose are manually pipette in each cuvette. Then, they are mixed for 10 min at 37 ºC. These cuvettes are always placed in the protoboard between the LED and the phototransistor in the same position and orientation. It is important to highlight that any change in the relative position of the detection chamber, respect to the LEDs, signicantly modifies the measure. All experiments were performed at room temperature and data were acquired 30 s after the reagent and glucose are mixed. The result shows six different experiments for five glucose concentrations, Fig. 7. The experiments show a good repetitiveness and linearity.

The data dispersion in the measurement for one glucose concentration are justified for the use of a manual set up, which does not guarantee a reproducible optical geometry.

As will be explained in the next section, the proposed device will increase the stability of the signal by using a mechanical structure, which determines an accuracy geometric between LED, phototransistor and chamber.

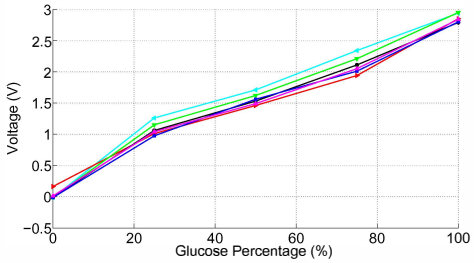

Fig. 7. Output voltage for 1 cm light path cuvette as a function of glucose concentration.

B. Experimental procedure

In the second bunch of experiments, the complete set up have been carried out. One of the chambers is filled with reagent liquid and the other is filled with glucose assay. The two chambers have a volume of 5.89 μL. One small glass is put above the chamber, acting like a cover to ensure that the chamber is completely filled, and to avoid a curved interface liquid-air which can affect the measure. Five different glucose concentration assays have been done with a dilution factor (DF) of 5, which is smaller than those used in typical colorimetric sensors (DF = 100). The reason for not using DF = 100 is for improving the absorbance and avoid any external noise. The experiments consist in measuring the different voltage in the phototransistor for different solutions. Special care should be taken in the cleanness of the LOC, since any disturbance will have an impact on the measurement. Moreover, the microfluidic PCB is introduced in the reader structure manually, any deviation in the led position will change the output voltage. In order to avoid these problems, after cleaning the PCB and before filling the chambers, it is inserted and measured to validate the zero output. In addition, the diameter of the chambers (5 mm) was chosen smaller than the phototransistors diameter (3mm) to solve the problem of the manually PCB insertion.

The same volume of sample and reagent are mixed in 5 cuvettes with different concentrations of glucose (0%, 25%, 50%, 75%, 100%) and pippeted to the chambers. The output for 4 experiments is shown in Fig. 8. The results show very similar behavior for the four different experiments. Moreover, it can be observed the non linearity in the slope of these curves in comparison with Fig. 7. It is caused by the differential in the dilution factor, from 100 to 5. However, the similarity between the experiments has improved significantly.

VII. Conclusion

An integrable microfluidic platform for photometric glucose sensor has been reported. The reported device is steady due to the differential mode of measurement and the plastic structure used to integrate the whole system. The values for a glucose assay concentrations have an average variation of only 13 mV from an output of 350 mV, which means an error of 3.7%. In addition, the decive is highly integrable in a more complex microfluidic circuit due to his fabrication process. The future work will be to include a detection system in a

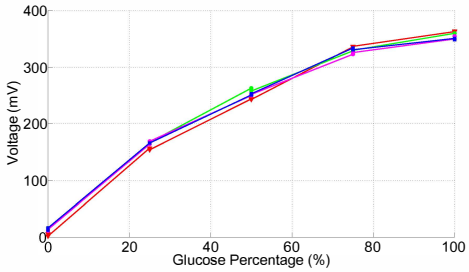

Fig. 8. Output voltage of the proposed device for four different experiment as a function of glucose concentration.

general multipurpose microfluidic platform using microvalves, impulsion system, mixers and heaters. It will be managed automatically and sensed with the electronic reader.

ACKNOWLEDGMENT

This work was supported by the Spanish Ministry of Science and Innovation under grants TEC2011-29045-C04-02, ISILAB.

REFERENCES

[1] Joseph Wang. Electrochemical glucose biosensors. *Chemical reviews*, 108(2):814–825, 2008.

[2] Sejin Park, Taek Dong Chung, and Hee Chan Kim. Nonenzymatic glucose detection using mesoporous platinum. *Analytical chemistry*, 75(13):3046–3049, 2003.

[3] Xiangjie Bo, Jean Chrysostome Ndamanisha, Jing Bai, and Liping Guo. Nonenzymatic amperometric sensor of hydrogen peroxide and glucose based on pt nanoparticles/ordered mesoporous carbon nanocomposite. *Talanta*, 82(1):85–91, 2010.

[4] Elizabeth A Moschou, Bethel V Sharma, Sapna K Deo, and Sylvia Daunert. Fluorescence glucose detection: advances toward the ideal in vivo biosensor. *Journal of fluorescence*, 14(5):535–547, 2004.

[5] Ryan J Russell, Michael V Pishko, Christopher C Gefrides, Michael J McShane, and Gerard L Cote. A fluorescence-based glucose biosensor using concanavalin a and dextran encapsulated in a poly (ethylene glycol) hydrogel. *Analytical Chemistry*, 71(15):3126–3132, 1999.

[6] Wenbing Shi, Qinlong Wang, Yijuan Long, Zhiliang Cheng, Shihong Chen, Huzhi Zheng, and Yuming Huang. Carbon nanodots as peroxidase mimetics and their applications to glucose detection. *Chemical Communications*, 47(23):6695–6697, 2011.

[7] Saeedeh Lotfi Mohammad Abad and Keivan Maghooli. Different approaches for detecting glucose. In *Bioinformatics and Biomedical Engineering, 2008. ICBBE 2008. The 2nd International Conference on*, pages 1535–1538. IEEE, 2008.

[8] Joseph Wang, Alfredo Ibáñez, and Madhu Prakash Chatrathi. On-chip integration of enzyme and immunoassays: simultaneous measurements of insulin and glucose. *Journal of the American Chemical Society*, 125(28):8444–8445, 2003.

[9] Glucosa-TR: Trinder. GOD-POD *SPINREACT, www.spinreact.com*

[10] Carmen Aracil, Francisco Perdigones, José Miguel Moreno, Antonio Luque, and José Manuel Quero. Portable lab-on-PCB platform for autonomous micromixing. *Microelectronic Engineering*, 2014.

[11] G Flores, C Aracil, F Perdigones, and JM Quero. Low consumption single-use microvalve for microfluidic PCB-based platforms. *Journal of Micromechanics and Microengineering*, 24(6):065013, 2014.

Annex C

Media impact

The development of this thesis work has led us to some publications which have had a media impact. Thus, during this PhD I have been involved in two media activities. The first one was a written article on canalciencia.us.es about our research work, particularly about the investigations carried out at the University of Bath with the prostate cancer cells. The other one was an interview in a TV program on channel 7tvandalucia, about the microsystem group and the influence and impact of the research work presented on this thesis.

Interview on canalciencia.us.es

Expertos de la Universidad de Bath, en Reino Unido, y la Universidad de Sevilla han llevado a cabo una serie de experimentos con los que han logrado caracterizar por vez primera en tiempo real la actividad eléctrica normal de las células del cáncer de próstata PC-3, obteniendo un patrón eléctrico a baja frecuencia, esto es, entre 0.1 y 10 Hertzios.

"Hemos observado que esta actividad eléctrica evoluciona desde un comportamiento asíncrono y esporádico a un comportamiento síncrono y quasi-periódico. Una vez conocido el patrón eléctrico normal de este tipo de células, empleamos un inhibidor de los canales iónicos de calcio, en concreto tricloruro de gadolinio, ya que estos canales están directamente relacionados con la actividad eléctrica de las células del cáncer de próstata (PC-3)", explica el ingeniero de telecomunicaciones de la Universidad de Sevilla Miguel Cabello.

Para realizar el cultivo de las células PC-3 los expertos utilizaron chips de silicio con electrodos de oro. Este chip, que estaba conectado a un equipo que permite la adquisición de las señales eléctricas de las células cultivadas, permitió analizar el comportamiento

eléctrico de grandes poblaciones de células cultivadas en esos chips con electrodos de oro, para obtener su actividad extracelular y encontrar un patrón de comportamiento para una monitorización en tiempo real y con gran precisión.

"Una posible aplicación de estos estudios consistiría en realizar experimentos de liberación de medicamentos en el cultivo, midiendo las variaciones en la actividad eléctrica de las células tras el uso de dichos medicamentos", destaca el profesor Cabello.

Actualmente, los tratamientos de este tipo de enfermedad dependen de la etapa en la que se encuentre el cáncer. De esta manera, los tratamientos pueden ser locales, mediante cirugía o radioterapia, así como ensayos clínicos para estadios iniciales; mientras que para etapas más avanzadas podrían ser necesarios, además de los métodos citados anteriormente, cirugías más complejas que lleguen a extirpar los ganglios afectados.

"Nuestra línea de investigación con las células del cáncer de próstata está más orientada a su uso, no en pacientes, sino en cultivos celulares de células cancerígenas, como las PC-3, para estudiar y encontrar una relación entre los patrones eléctricos y la proliferación de las células cancerígenas y, también, encontrar una relación entre las variaciones en los niveles de PH del cultivo durante el experimento, su actividad eléctrica y la proliferación de las mismas. Es decir, nuestros estudios están orientados a las primeras fases de investigación, antes de ser apropiados para su uso en pacientes", aclara este investigador.

El siguiente paso en esta investigación será realizar estudios biológicos de la proliferación de las células en función de los medicamentos empleados, para ver si se puede encontrar una relación entre la actividad eléctrica de las células PC-3 con una menor proliferación de éstas. Todo esto realizado en tiempo real, gracias a la adquisición continua de la actividad eléctrica del cultivo.

Interview on 7tvandalucia

https://7tvandalucia.es/andalucia/nuevos-talentos/2-1-27092019-impulsos-electricos-e-historia-piragismo/49517/

Annex D

Acronyms and abbreviations. Symbols

D.1 Acronyms and abbreviations

PCB	Printed circuit board
MEMS	Microelectromechanical systems
μTAS	micro-total analysis systems
LOC	Lab on chip
LOP	Lab on PCB
MEA	Microelectrode Array
PMMA	Poly methyl methacrylate
PDMS	Polydimethylsiloxane
$3D$	Three dimensional
$PC-3$	Prostate cancer cell line
CO_2	Carbon dioxide
CNM	National Center of Microelectronics
MST	Mycrosystem technology
RGT	Resonant gate transistor
TIJ	Thermal inkjet technology
LIGA	Lithographie, galvanoformung, adformung
MCNC	Microelectronic Center of North Carolina
MUMPs	Multiuser MEMS processes
IC	Integrated circuit
*FR*4	Flame retardant fiberglass

UV	Ultraviolet
HARM	High-aspect-ratio micromachining
RIE	Reactive ion etching
DRIE	Deep reactive ion etching
SOI	Silicon-on-insulators
NS	Navier-Stokes
PCR	polymerase chain reactions
DNA	Deoxyribonucleic acid
MOSFET	Metal-oxide-semiconductor Field-effect transistor
PEB	Post-exposure bake
IPA	Isopropyl alcohol
PS	Polystyrene
PC	Polycarbonate
COC	Cycloolefine copolymer
PET	polyethylene terephthalate
SEM	Scanning electron microscopy
CNC	Computer numerical control
CMOS	Complementary metal-oxide-semiconductor
EO	Electroosmotic
SPE	Solid-phase extraction
LED	Light emitting diode
SPR	Surface plasmon resonance
ECTCs	Engineered 3D cardiac tissue constructs
RP	Retinitis pigmentosa
ROs	Retina organoids
CVD	Chemical vapor deposition
NTC	Negative temperature coefficient
EMI	Electromagnetic interferences
PLA	Polylactic acid
PWM	Pulse width modulation
CDE	Spanish Conference on Electron Devices
PBS	Phosphate buffered saline
PVDF	Polyvinylidene difluoride
WT	Wild type
CTB	Cholera toxin subunit B
ONL	Outer nuclear layer
INL	Inner nuclear layer
GCL	Ganglion cell layer
FITC	Fluorescein Isotiocyanate
PH	Potential Hydrogen
Ca^{2+}	Calcium channel
Gd^{3+}	Gadolinium
K^{+}	Potasium channel
Na^{+}	Sodium channel
FBS	Fetal bovine serum

FCS	Fetal calf serum
SK − N − SH	Human neuroblastoma cell line
DI	Deionized
DMEM	Dulbecco's Modified Eagle Medium
MTT	3-(4.5-Dimethylthiazol-2-yl)-2.5-Diphenyltetrazolium Bromide

D.2 Symbols

ρ	Fluid density
u	Flow velocity
∇	Vector differential operator
p	Pressure
μ	Fluid dynamic viscosity
v	Fluid velocity
L	Characteristic length
ν	Fluid viscosity
σ	Surface tension
D	Diffusion coefficient
Re	Reynolds number
We	Weber number
Ca	Capillary number
Pe	Péclet number
T_g	Glass transition temperature
G	Amplifier gain
R	Resistor
v	Voltage
i	Current
F	Frequency
V	Volume
Z	Impedance
τ	Time constant
C	Capacitor

Bibliography

[1] P. F. Partnership, "An introduction to mems (micro-electromechanical systems)," *Prime Faraday Partnership*, 2002.

[2] J. Bryzek, "Impact of mems technology on society," *Sensors and Actuators A: Physical*, vol. 56, no. 1-2, pp. 1–9, 1996.

[3] B. Vigna, "More than moore: micro-machined products enable new applications and open new markets," in *IEEE InternationalElectron Devices Meeting, 2005. IEDM Technical Digest.* IEEE, 2005, pp. 8–pp.

[4] L. G. Villanueva, J. Bausells, and J. Brugger, "Grand challenge in n/mems," *Frontiers in Mechanical Engineering*, vol. 1, p. 15, 2016.

[5] V. Autores, "Yoledevelopment," urlhttp://www.yole.fr/, 2019, accedido 29-10-2019.

[6] C. S. Smith, "Piezoresistance effect in germanium and silicon," *Physical review*, vol. 94, no. 1, p. 42, 1954.

[7] R. Feynman, "There's plenty of room at the bottom," in *Feynman and computation*. CRC Press, 2018, pp. 63–76.

[8] G. E. Moore *et al.*, "Cramming more components onto integrated circuits," 1965.

[9] H. C. Nathanson, W. E. Newell, R. A. Wickstrom, and J. R. Davis, "The resonant gate transistor," *IEEE Transactions on Electron Devices*, vol. 14, no. 3, pp. 117–133, 1967.

[10] F. Faggin, M. E. Hoff, S. Mazor, and M. Shima, "The history of the 4004," *IEEE Micro*, vol. 16, no. 6, pp. 10–20, 1996.

[11] J. L. Vaught, F. L. Cloutier, D. K. Donald, J. D. Meyer, C. A. Tacklind, and H. H. Taub, "Thermal ink jet printer," Dec. 25 1984, uS Patent 4,490,728.

[12] K. E. Petersen, "Silicon as a mechanical material," *Proceedings of the IEEE*, vol. 70, no. 5, pp. 420–457, 1982.

[13] E. Becker, W. Ehrfeld, P. Hagmann, A. Maner, and D. Münchmeyer, "Fabrication of microstructures with high aspect ratios and great structural heights by synchrotron radiation lithography, galvanoforming, and plastic moulding (liga process)," *Microelectronic engineering*, vol. 4, no. 1, pp. 35–56, 1986.

[14] L. M. Roylance and J. B. Angell, "A batch-fabricated silicon accelerometer," *IEEE Transactions on Electron Devices*, vol. 26, no. 12, pp. 1911–1917, 1979.

[15] B. Boxenhorn, "Planar inertial sensor," Jul. 8 1986, uS Patent 4,598,585.

[16] P. J. Bohrer and R. G. Johnson, "Flow sensor," Oct. 23 1984, uS Patent 4,478,077.

[17] K. A. Shaw, Z. L. Zhang, and N. C. MacDonald, "Scream i: a single mask, single-crystal silicon, reactive ion etching process for microelectromechanical structures," *Sensors and Actuators A: Physical*, vol. 40, no. 1, pp. 63–70, 1994.

[18] M. J. Madou, *Manufacturing techniques for microfabrication and nanotechnology*. CRC press, 2011, vol. 2.

[19] H. Miyajima and M. Mehregany, "High-aspect-ratio photolithography for mems applications," *Journal of microelectromechanical systems*, vol. 4, no. 4, pp. 220–229, 1995.

[20] M. J. Madou, *Fundamentals of microfabrication: the science of miniaturization*. CRC press, 2002.

[21] P. Rai-Choudhury, *Handbook of microlithography, micromachining, and microfabrication: microlithography*. Iet, 1997, vol. 1.

[22] R. Ghodssi and P. Lin, *MEMS materials and processes handbook*. Springer Science & Business Media, 2011, vol. 1.

[23] R. Lawes, "Manufacturing costs for microsystems/mems using high aspect ratio microfabrication techniques," *Microsystem technologies*, vol. 13, no. 1, pp. 85–95, 2007.

[24] K. E. Bean, "Anisotropic etching of silicon," *IEEE Transactions on electron devices*, vol. 25, no. 10, pp. 1185–1193, 1978.

[25] H. Seidel, L. Csepregi, A. Heuberger, and H. Baumgärtel, "Anisotropic etching of crystalline silicon in alkaline solutions i. orientation dependence and behavior of passivation layers," *Journal of the electrochemical society*, vol. 137, no. 11, pp. 3612–3626, 1990.

[26] J. Park, H. Park, Y. Hahn, G.-C. Yi, and A. Yoshikawa, "Dry etching of zno films and plasma-induced damage to optical properties," *Journal of Vacuum Science & Technology B: Microelectronics and Nanometer Structures Processing, Measurement, and Phenomena*, vol. 21, no. 2, pp. 800–803, 2003.

[27] C. L. Cheung, R. Nikolić, C. Reinhardt, and T. Wang, "Fabrication of nanopillars by nanosphere lithography," *Nanotechnology*, vol. 17, no. 5, p. 1339, 2006.

[28] J. M. Bustillo, R. T. Howe, and R. S. Muller, "Surface micromachining for microelectromechanical systems," *Proceedings of the IEEE*, vol. 86, no. 8, pp. 1552–1574, 1998.

[29] A. Cohen, G. Zhang, F.-G. Tseng, U. Frodis, F. Mansfeld, and P. Will, "Efab: rapid, low-cost desktop micromachining of high aspect ratio true 3-d mems," in *Technical Digest. IEEE International MEMS 99 Conference. Twelfth IEEE International Conference on Micro Electro Mechanical Systems (Cat. No. 99CH36291)*. IEEE, 1999, pp. 244–251.

[30] F. Ayazi and K. Najafi, "High aspect-ratio combined poly and single-crystal silicon (harpss) mems technology," *Journal of Microelectromechanical Systems*, vol. 9, no. 3, pp. 288–294, 2000.

[31] M. K. Hooda, M. Wadhwa, S. Verma, M. Nayak, P. George, and A. Paul, "A systematic study of drie process for high aspect ratio microstructuring," *Vacuum*, vol. 84, no. 9, pp. 1142–1148, 2010.

[32] H.-K. Chang and Y.-K. Kim, "Uv-liga process for high aspect ratio structure using stress barrier and c-shaped etch hole," *Sensors and Actuators A: Physical*, vol. 84, no. 3, pp. 342–350, 2000.

[33] C. K. Malek and V. Saile, "Applications of liga technology to precision manufacturing of high-aspect-ratio micro-components and-systems: a review," *Microelectronics journal*, vol. 35, no. 2, pp. 131–143, 2004.

[34] J. Hruby, "Liga technologies and applications," *MRS bulletin*, vol. 26, no. 4, pp. 337–340, 2001.

[35] M. Heckele, W. Bacher, and K. Müller, "Hot embossing-the molding technique for plastic microstructures," *Microsystem technologies*, vol. 4, no. 3, pp. 122–124, 1998.

[36] H. Becker and U. Heim, "Hot embossing as a method for the fabrication of polymer high aspect ratio structures," *Sensors and Actuators A: Physical*, vol. 83, no. 1-3, pp. 130–135, 2000.

[37] M. Alexe and U. Gösele, *Wafer bonding: applications and technology*. Springer Science & Business Media, 2013, vol. 75.

[38] M. A. Schmidt, "Wafer-to-wafer bonding for microstructure formation," *Proceedings of the IEEE*, vol. 86, no. 8, pp. 1575–1585, 1998.

[39] X. X. Zhang and J.-P. Raskin, "Low-temperature wafer bonding: A study of void formation and influence on bonding strength," *Journal of microelectromechanical systems*, vol. 14, no. 2, pp. 368–382, 2005.

[40] M. Shimbo, K. Furukawa, K. Fukuda, and K. Tanzawa, "Silicon-to-silicon direct bonding method," *Journal of Applied Physics*, vol. 60, no. 8, pp. 2987–2989, 1986.

[41] N. Miki, X. Zhang, R. Khanna, A. Ayon, D. Ward, and S. Spearing, "Multi-stack silicon-direct wafer bonding for 3d mems manufacturing," *Sensors and Actuators A: Physical*, vol. 103, no. 1-2, pp. 194–201, 2003.

[42] D. Liang and J. Bowers, "Highly efficient vertical outgassing channels for low-temperature inp-to-silicon direct wafer bonding on the silicon-on-insulator substrate," *Journal of Vacuum Science & Technology B: Microelectronics and Nanometer Structures Processing, Measurement, and Phenomena*, vol. 26, no. 4, pp. 1560–1568, 2008.

[43] T. Corman, P. Enoksson, and G. Stemme, "Deep wet etching of borosilicate glass using an anodically bonded silicon substrate as mask," *Journal of micromechanics and microengineering*, vol. 8, no. 2, p. 84, 1998.

[44] J. Wei, H. Xie, M. Nai, C. Wong, and L. Lee, "Low temperature wafer anodic bonding," *Journal of Micromechanics and Microengineering*, vol. 13, no. 2, p. 217, 2003.

[45] F. Niklaus, G. Stemme, J.-Q. Lu, and R. Gutmann, "Adhesive wafer bonding," *Journal of applied physics*, vol. 99, no. 3, p. 2, 2006.

[46] G. Flores Salado, "Self-contained microfluidic platform for general purpose lab-on-chip using pcb-mems technology." 2017.

[47] J. S. L. Philpot, "The use of thin layers in electrophoretic separation," *Transactions of the Faraday Society*, vol. 35, pp. 38–46, 1940.

[48] S. C. Terry, J. H. Jerman, and J. B. Angell, "A gas chromatographic air analyzer fabricated on a silicon wafer," *IEEE transactions on electron devices*, vol. 26, no. 12, pp. 1880–1886, 1979.

[49] D. R. Reyes, D. Iossifidis, P.-A. Auroux, and A. Manz, "Micro total analysis systems. 1. introduction, theory, and technology," *Analytical chemistry*, vol. 74, no. 12, pp. 2623–2636, 2002.

[50] D. B. Weibel and G. M. Whitesides, "Applications of microfluidics in chemical biology," *Current opinion in chemical biology*, vol. 10, no. 6, pp. 584–591, 2006.

[51] S.-W. Cho, D.-K. Kang, J.-B. Choo, A. J. Demllo, and S.-I. Chang, "Recent advances in microfluidic technologies for biochemistry and molecular biology," *BMB reports*, vol. 44, no. 11, pp. 705–712, 2011.

[52] M. A. Qasaimeh, S. G. Ricoult, and D. Juncker, "Microfluidic probes for use in life sciences and medicine," *Lab on a Chip*, vol. 13, no. 1, pp. 40–50, 2013.

[53] H. A. Stone, A. D. Stroock, and A. Ajdari, "Engineering flows in small devices: microfluidics toward a lab-on-a-chip," *Annu. Rev. Fluid Mech.*, vol. 36, pp. 381–411, 2004.

[54] H. Bruus, *Theoretical microfluidics*. Oxford university press Oxford, 2008, vol. 18.

[55] B. R. Munson, T. H. Okiishi, W. W. Huebsch, and A. P. Rothmayer, *Fluid mechanics*. Wiley Singapore, 2013.

[56] K. V. Sharp and R. J. Adrian, "Transition from laminar to turbulent flow in liquid filled microtubes," *Experiments in fluids*, vol. 36, no. 5, pp. 741–747, 2004.

[57] T. M. Squires and S. R. Quake, "Microfluidics: Fluid physics at the nanoliter scale," *Reviews of modern physics*, vol. 77, no. 3, p. 977, 2005.

[58] A. Frohn and N. Roth, *Dynamics of droplets*. Springer Science & Business Media, 2013.

[59] A. Utada, L.-Y. Chu, A. Fernandez-Nieves, D. Link, C. Holtze, and D. Weitz, "Dripping, jetting, drops, and wetting: The magic of microfluidics," *Mrs Bulletin*, vol. 32, no. 9, pp. 702–708, 2007.

[60] P. Tabeling, *Introduction to microfluidics*. Oxford University Press on Demand, 2005.

[61] N. Fries and M. Dreyer, "The transition from inertial to viscous flow in capillary rise," *Journal of colloid and interface science*, vol. 327, no. 1, pp. 125–128, 2008.

[62] J. Atencia and D. J. Beebe, "Controlled microfluidic interfaces," *Nature*, vol. 437, no. 7059, p. 648, 2004.

[63] L. D. Landau, J. Bell, M. Kearsley, L. Pitaevskii, E. Lifshitz, and J. Sykes, *Electrodynamics of continuous media*. elsevier, 2013, vol. 8.

[64] M. A. Ansari and K.-Y. Kim, "Mixing performance of unbalanced split and recombine micomixers with circular and rhombic sub-channels," *Chemical Engineering Journal*, vol. 162, no. 2, pp. 760–767, 2010.

[65] P. N. Nge, C. I. Rogers, and A. T. Woolley, "Advances in microfluidic materials, functions, integration, and applications," *Chemical reviews*, vol. 113, no. 4, pp. 2550–2583, 2013.

[66] K. Ren, J. Zhou, and H. Wu, "Materials for microfluidic chip fabrication," *Accounts of chemical research*, vol. 46, no. 11, pp. 2396–2406, 2013.

[67] S. C. Terry, J. H. Jerman, and J. B. Angell, "A gas chromatographic air analyzer fabricated on a silicon wafer," *IEEE transactions on electron devices*, vol. 26, no. 12, pp. 1880–1886, 1979.

[68] A. Manz, D. J. Harrison, E. M. Verpoorte, J. C. Fettinger, A. Paulus, H. Lüdi, and H. M. Widmer, "Planar chips technology for miniaturization and integration of separation techniques into monitoring systems: capillary electrophoresis on a chip," *Journal of Chromatography A*, vol. 593, no. 1-2, pp. 253–258, 1992.

[69] C. Iliescu, H. Taylor, M. Avram, J. Miao, and S. Franssila, "A practical guide for the fabrication of microfluidic devices using glass and silicon," *Biomicrofluidics*, vol. 6, no. 1, p. 016505, 2012.

[70] S. Marre and K. F. Jensen, "Synthesis of micro and nanostructures in microfluidic systems," *Chemical Society Reviews*, vol. 39, no. 3, pp. 1183–1202, 2010.

[71] J. Liu, J. Shang, J. Tang, and Q.-A. Huang, "Micromachining of pyrex 7740 glass by silicon molding and vacuum anodic bonding," *Journal of microelectromechanical systems*, vol. 20, no. 4, pp. 909–915, 2011.

[72] D. J. Laser and J. G. Santiago, "A review of micropumps," *Journal of micromechanics and microengineering*, vol. 14, no. 6, p. R35, 2004.

[73] K. W. Oh and C. H. Ahn, "A review of microvalves," *Journal of micromechanics and microengineering*, vol. 16, no. 5, p. R13, 2006.

[74] S. Franssila, S. Marttila, K. Kolari, P. Ostman, T. Kotiaho, R. Kostiainen, R. Lehtiniemi, C.-M. Fager, and J. Manninen, "A microfabricated nebulizer for liquid vaporization in chemical analysis," *Journal of microelectromechanical systems*, vol. 15, no. 5, pp. 1251–1259, 2006.

[75] Y. Nakashima and T. Yasuda, "Cell differentiation guidance using chemical stimulation controlled by a microfluidic device," *Sensors and Actuators A: Physical*, vol. 139, no. 1-2, pp. 252–258, 2007.

[76] A. Luque, J. M. Quero, C. Hibert, P. Flückiger, and A. M. Gañán-Calvo, "Integrable silicon microfluidic valve with pneumatic actuation," *Sensors and Actuators A: Physical*, vol. 118, no. 1, pp. 144–151, 2005.

[77] P. Mao and J. Han, "Fabrication and characterization of 20 nm planar nanofluidic channels by glass–glass and glass–silicon bonding," *Lab on a Chip*, vol. 5, no. 8, pp. 837–844, 2005.

[78] C. Iliescu, K. L. Tan, F. E. Tay, and J. Miao, "Deep wet and dry etching of pyrex glass: A review," in *Proceedings of the ICMAT (Symposium F), Singapore*, 2005, pp. 75–78.

[79] K. Seiler, Z. H. Fan, K. Fluri, and D. J. Harrison, "Electroosmotic pumping and valveless control of fluid flow within a manifold of capillaries on a glass chip," *Analytical Chemistry*, vol. 66, no. 20, pp. 3485–3491, 1994.

[80] A. C. Lewis, J. F. Hamilton, C. N. Rhodes, J. Halliday, K. D. Bartle, P. Homewood, R. J. Grenfell, B. Goody, A. M. Harling, P. Brewer *et al.*, "Microfabricated planar glass gas chromatography with photoionization detection," *Journal of Chromatography A*, vol. 1217, no. 5, pp. 768–774, 2010.

[81] C. J. Easley, J. A. Humphrey, and J. P. Landers, "Thermal isolation of microchip reaction chambers for rapid non-contact dna amplification," *Journal of Micromechanics and Microengineering*, vol. 17, no. 9, p. 1758, 2007.

[82] P. A. Jenkins, S. Boland, P. Kavanagh, and D. Leech, "Evaluation of performance and stability of biocatalytic redox films constructed with different copper oxygenases and osmium-based redox polymers," *Bioelectrochemistry*, vol. 76, no. 1-2, pp. 162–168, 2009.

[83] M. Castano-Alvarez, D. F. P. Ayuso, M. G. Granda, M. T. Fernández-Abedul, J. R. García, and A. Costa-García, "Critical points in the fabrication of microfluidic devices on glass substrates," *Sensors and Actuators B: Chemical*, vol. 130, no. 1, pp. 436–448, 2008.

[84] J. H. Chua, R.-E. Chee, A. Agarwal, S. M. Wong, and G.-J. Zhang, "Label-free electrical detection of cardiac biomarker with complementary metal-oxide semiconductor-compatible silicon nanowire sensor arrays," *Analytical chemistry*, vol. 81, no. 15, pp. 6266–6271, 2009.

[85] G. Flores, F. Perdigones, C. Aracil, M. Cabello, and J. Quero, "Microfluidic platform with absorbance sensor for glucose detection," in *2015 10th Spanish Conference on Electron Devices (CDE)*. IEEE, 2015, pp. 1–4.

[86] V. Faustino, S. O. Catarino, R. Lima, and G. Minas, "Biomedical microfluidic devices by using low-cost fabrication techniques: A review," *Journal of biomechanics*, vol. 49, no. 11, pp. 2280–2292, 2016.

[87] V. Autores, "Microchem," urlhttp://www.microchem.com/ash, 2019, accedido 28-05-2019.

[88] K. Lee, N. LaBianca, S. Rishton, S. Zolgharnain, J. Gelorme, J. Shaw, and T.-P. Chang, "Micromachining applications of a high resolution ultrathick photoresist," *Journal of Vacuum Science & Technology B: Microelectronics and Nanometer Structures Processing, Measurement, and Phenomena*, vol. 13, no. 6, pp. 3012–3016, 1995.

[89] H. Lorenz, M. Despont, N. Fahrni, N. LaBianca, P. Renaud, and P. Vettiger, "Su-8: a low-cost negative resist for mems," *Journal of Micromechanics and Microengineering*, vol. 7, no. 3, p. 121, 1997.

[90] K. V. Nemani, K. L. Moodie, J. B. Brennick, A. Su, and B. Gimi, "In vitro and in vivo evaluation of su-8 biocompatibility," *Materials Science and Engineering: C*, vol. 33, no. 7, pp. 4453–4459, 2013.

[91] V. Kumar and N. Sharma, "Su-8 as hydrophobic and dielectric thin film in electrowetting-on-dielectric based microfluidics device," *Journal of Nanotechnology*, vol. 2012, 2012.

[92] E. H. Conradie and D. F. Moore, "Su-8 thick photoresist processing as a functional material for mems applications," *Journal of Micromechanics and Microengineering*, vol. 12, no. 4, p. 368, 2002.

[93] J. C. McDonald, D. C. Duffy, J. R. Anderson, D. T. Chiu, H. Wu, O. J. Schueller, and G. M. Whitesides, "Fabrication of microfluidic systems in poly (dimethylsiloxane)," *ELECTROPHORESIS: An International Journal*, vol. 21, no. 1, pp. 27–40, 2000.

[94] J. C. McDonald and G. M. Whitesides, "Poly (dimethylsiloxane) as a material for fabricating microfluidic devices," *Accounts of chemical research*, vol. 35, no. 7, pp. 491–499, 2002.

[95] D. Qin, Y. Xia, and G. M. Whitesides, "Soft lithography for micro-and nanoscale patterning," *Nature protocols*, vol. 5, no. 3, p. 491, 2010.

[96] A. Bubendorfer, X. Liu, and A. V. Ellis, "Microfabrication of pdms microchannels using su-8/pmma moldings and their sealing to polystyrene substrates," *Smart Materials and Structures*, vol. 16, no. 2, p. 367, 2007.

[97] S. Natarajan, D. Chang-Yen, and B. Gale, "Large-area, high-aspect-ratio su-8 molds for the fabrication of pdms microfluidic devices," *Journal of Micromechanics and Microengineering*, vol. 18, no. 4, p. 045021, 2008.

[98] Y. Hwang, O. H. Paydar, and R. N. Candler, "3d printed molds for non-planar pdms microfluidic channels," *Sensors and Actuators A: Physical*, vol. 226, pp. 137–142, 2015.

[99] H. Wu, T. W. Odom, D. T. Chiu, and G. M. Whitesides, "Fabrication of complex three-dimensional microchannel systems in pdms," *Journal of the American Chemical Society*, vol. 125, no. 2, pp. 554–559, 2003.

[100] M. A. Eddings, M. A. Johnson, and B. K. Gale, "Determining the optimal pdms–pdms bonding technique for microfluidic devices," *Journal of Micromechanics and Microengineering*, vol. 18, no. 6, p. 067001, 2008.

[101] W. W. Y. Chow, K. F. Lei, G. Shi, W. J. Li, and Q. Huang, "Microfluidic channel fabrication by pdms-interface bonding," *Smart materials and structures*, vol. 15, no. 1, p. S112, 2005.

[102] D. Bodas and C. Khan-Malek, "Formation of more stable hydrophilic surfaces of pdms by plasma and chemical treatments," *Microelectronic engineering*, vol. 83, no. 4-9, pp. 1277–1279, 2006.

[103] G. Firpo, E. Angeli, L. Repetto, and U. Valbusa, "Permeability thickness dependence of polydimethylsiloxane (pdms) membranes," *Journal of Membrane Science*, vol. 481, pp. 1–8, 2015.

[104] M. Mehling and S. Tay, "Microfluidic cell culture," *Current opinion in Biotechnology*, vol. 25, pp. 95–102, 2014.

[105] M. Figurová, D. Pudis, P. Gaso, and I. Cimrak, "Pdms microfluidic structures for loc applications," in *2016 ELEKTRO*. IEEE, 2016, pp. 608–611.

[106] R. Mukhopadhyay, "When pdms isn't the best," 2007.

[107] E. Berthier, E. W. Young, and D. Beebe, "Engineers are from pdms-land, biologists are from polystyrenia," *Lab on a Chip*, vol. 12, no. 7, pp. 1224–1237, 2012.

[108] I. M. Ward and J. Sweeney, *Mechanical properties of solid polymers*. John Wiley & Sons, 2012.

[109] H. Becker and C. Gärtner, "Polymer microfabrication technologies for microfluidic systems," *Analytical and bioanalytical chemistry*, vol. 390, no. 1, pp. 89–111, 2008.

[110] M. Biron, *Thermoplastics and thermoplastic composites*. William Andrew, 2018.

[111] D. Voicu, G. Lestari, Y. Wang, M. DeBono, M. Seo, S. Cho, and E. Kumacheva, "Thermoplastic microfluidic devices for targeted chemical and biological applications," *RSC Advances*, vol. 7, no. 5, pp. 2884–2889, 2017.

[112] E. W. Young, E. Berthier, D. J. Guckenberger, E. Sackmann, C. Lamers, I. Meyvantsson, A. Huttenlocher, and D. J. Beebe, "Rapid prototyping of arrayed microfluidic systems in polystyrene for cell-based assays," *Analytical chemistry*, vol. 83, no. 4, pp. 1408–1417, 2011.

[113] Y. Fan, H. Li, Y. Yi, and I. G. Foulds, "Pmma to polystyrene bonding for polymer based microfluidic systems," *Microsystem technologies*, vol. 20, no. 1, pp. 59–64, 2014.

[114] C. Tsao, L. Hromada, J. Liu, P. Kumar, and D. DeVoe, "Low temperature bonding of pmma and coc microfluidic substrates using uv/ozone surface treatment," *Lab on a Chip*, vol. 7, no. 4, pp. 499–505, 2007.

[115] C.-H. Yuan and J. Shiea, "Sequential electrospray analysis using sharp-tip channels fabricated on a plastic chip," *Analytical chemistry*, vol. 73, no. 6, pp. 1080–1083, 2001.

[116] J. Liu, J. Wang, Z. Chen, Y. Yu, X. Yang, X. Zhang, Z. Xu, and C. Liu, "A three-layer pmma electrophoresis microchip with pt microelectrodes insulated by a thin film for contactless conductivity detection," *Lab on a Chip*, vol. 11, no. 5, pp. 969–973, 2011.

[117] C. L. Chagas, L. Costa Duarte, E. O. Lobo-Júnior, E. Piccin, N. Dossi, and W. K. Coltro, "Hand drawing of pencil electrodes on paper platforms for contactless conductivity detection of inorganic cations in human tear samples using electrophoresis chips," *Electrophoresis*, vol. 36, no. 16, pp. 1837–1844, 2015.

[118] Z. J. A. Amer, J. K. Ahmed, and S. F. Abbas, "Chitosan/pmma bioblend for drug release applications," *Int J Eng and Tech*, vol. 4, no. 5, pp. 1–6, 2014.

[119] J. M. Łopacińska, J. Emnéus, and M. Dufva, "Poly (dimethylsiloxane)(pdms) affects gene expression in pc12 cells differentiating into neuronal-like cells," *PLoS One*, vol. 8, no. 1, p. e53107, 2013.

[120] K. F. Lei, C.-H. Chang, and M.-J. Chen, "Paper/pmma hybrid 3d cell culture microfluidic platform for the study of cellular crosstalk," *ACS applied materials & interfaces*, vol. 9, no. 15, pp. 13 092–13 101, 2017.

[121] J. Chang, X. Zhang, T. Ge, and J. Zhou, "Fully printed electronics on flexible substrates: High gain amplifiers and dac," *Organic Electronics*, vol. 15, no. 3, pp. 701–710, 2014.

[122] D. Ogończyk, J. Węgrzyn, P. Jankowski, B. Dąbrowski, and P. Garstecki, "Bonding of microfluidic devices fabricated in polycarbonate," *Lab on a Chip*, vol. 10, no. 10, pp. 1324–1327, 2010.

[123] S. K. Sia and G. M. Whitesides, "Microfluidic devices fabricated in poly (dimethylsiloxane) for biological studies," *Electrophoresis*, vol. 24, no. 21, pp. 3563–3576, 2003.

[124] C. Wang, X. Gao, K. Mawatari, and T. Kitamori, "Clogging-free irreversible bonding of polycarbonate membranes to glass microfluidic devices," *Journal of The Electrochemical Society*, vol. 164, no. 5, pp. B3087–B3090, 2017.

[125] J. Y. Wong and A. C. Pfahnl, "3d printing of surgical instruments for long-duration space missions," *Aviation, space, and environmental medicine*, vol. 85, no. 7, pp. 758–763, 2014.

[126] Y. Wang, Q. He, Y. Dong, and H. Chen, "In-channel modification of biosensor electrodes integrated on a polycarbonate microfluidic chip for micro flow-injection amperometric determination of glucose," *Sensors and Actuators B: Chemical*, vol. 145, no. 1, pp. 553–560, 2010.

[127] C.-W. Chang, Y.-J. Cheng, M. Tu, Y.-H. Chen, C.-C. Peng, W.-H. Liao, and Y.-C. Tung, "A polydimethylsiloxane–polycarbonate hybrid microfluidic device capable of generating perpendicular chemical and oxygen gradients for cell culture studies," *Lab on a Chip*, vol. 14, no. 19, pp. 3762–3772, 2014.

[128] V. R. Sastri, *Plastics in medical devices: properties, requirements, and applications*. William Andrew, 2013.

[129] H.-K. Rhee, I.-S. Nam, and J. M. Park, *New Developments and Application in Chemical Reaction Engineering: Proceedings of the 4th Asia-Pacific Chemical Reaction Engineering Symposium (APCRE'05), Gyeongju, Korea, June 12-15 2005*. Elsevier, 2006, vol. 159.

[130] J. Zhang, C. Das, and Z. H. Fan, "Dynamic coating for protein separation in cyclic olefin copolymer microfluidic devices," *Microfluidics and Nanofluidics*, vol. 5, no. 3, pp. 327–335, 2008.

[131] J. Liu, C.-F. Chen, C.-W. Tsao, C.-C. Chang, C.-C. Chu, and D. L. DeVoe, "Polymer microchips integrating solid-phase extraction and high-performance liquid chromatography using reversed-phase polymethacrylate monoliths," *Analytical chemistry*, vol. 81, no. 7, pp. 2545–2554, 2009.

[132] J. Steigert, S. Haeberle, T. Brenner, C. Müller, C. Steinert, P. Koltay, N. Gottschlich, H. Reinecke, J. Rühe, R. Zengerle *et al.*, "Rapid prototyping of microfluidic chips in coc," *Journal of Micromechanics and Microengineering*, vol. 17, no. 2, p. 333, 2007.

[133] S. A. Aghvami, A. Opathalage, Z. Zhang, M. Ludwig, M. Heymann, M. Norton, N. Wilkins, and S. Fraden, "Rapid prototyping of cyclic olefin copolymer (coc) microfluidic devices," *Sensors and Actuators B: Chemical*, vol. 247, pp. 940–949, 2017.

[134] Q. Pu, O. Oyesanya, B. Thompson, S. Liu, and J. C. Alvarez, "On-chip micropatterning of plastic (cylic olefin copolymer, coc) microfluidic channels for the fabrication of biomolecule microarrays using photografting methods," *Langmuir*, vol. 23, no. 3, pp. 1577–1583, 2007.

[135] C. Tsao, L. Hromada, J. Liu, P. Kumar, and D. DeVoe, "Low temperature bonding of pmma and coc microfluidic substrates using uv/ozone surface treatment," *Lab on a Chip*, vol. 7, no. 4, pp. 499–505, 2007.

[136] S. S. Bale, A. Manoppo, R. Thompson, A. Markoski, J. Coppeta, H. Azizgolshani, M. Lu, J. Gosset, P. Keegan, and J. Charest, "A thermoplastic microfluidic microphysiological system to recapitulate hepatic function and multi-cellular interactions," *Biotechnology and bioengineering*, 2019.

[137] J. S. Jeon, S. Chung, R. D. Kamm, and J. L. Charest, "Hot embossing for fabrication of a microfluidic 3d cell culture platform," *Biomedical microdevices*, vol. 13, no. 2, pp. 325–333, 2011.

[138] D. S. Kim, S. H. Lee, C. H. Ahn, J. Y. Lee, and T. H. Kwon, "Disposable integrated microfluidic biochip for blood typing by plastic microinjection moulding," *Lab on a Chip*, vol. 6, no. 6, pp. 794–802, 2006.

[139] A. L. Andrady and M. A. Neal, "Applications and societal benefits of plastics," *Philosophical Transactions of the Royal Society B: Biological Sciences*, vol. 364, no. 1526, pp. 1977–1984, 2009.

[140] Z. Hu and X. Chen, "Fabrication of polyethylene terephthalate microfluidic chip using co2 laser system," *International Polymer Processing*, vol. 33, no. 1, pp. 106–109, 2018.

[141] J.-C. Chou, Y.-L. Tsai, T.-Y. Cheng, Y.-H. Liao, G.-C. Ye, and S.-Y. Yang, "Fabrication of arrayed flexible screen-printed glucose biosensor based on microfluidic framework," *IEEE Sensors Journal*, vol. 14, no. 1, pp. 178–183, 2013.

[142] J. Derix, G. Gerlach, S. Wetzel, S. Perike, and R. Funk, "Porous polyethylene terephthalate membranes in microfluidic applications," *physica status solidi (a)*, vol. 206, no. 3, pp. 442–448, 2009.

[143] N. Recek, M. Resnik, R. Zaplotnik, M. Mozetic, H. Motaln, T. Lah-Turnsek, A. Vesel *et al.*, "Cell proliferation on polyethylene terephthalate treated in plasma created in so2/o2 mixtures," *Polymers*, vol. 9, no. 3, p. 82, 2017.

[144] W. Khan, E. Muntimadugu, M. Jaffe, and A. J. Domb, "Implantable medical devices," in *Focal controlled drug delivery*. Springer, 2014, pp. 33–59.

[145] V. Piotter, K. Mueller, K. Plewa, R. Ruprecht, and J. Hausselt, "Performance and simulation of thermoplastic micro injection molding," *Microsystem Technologies*, vol. 8, no. 6, pp. 387–390, 2002.

[146] J. Giboz, T. Copponnex, and P. Mélé, "Microinjection molding of thermoplastic polymers: a review," *Journal of micromechanics and microengineering*, vol. 17, no. 6, p. R96, 2007.

[147] L. Martynova, L. E. Locascio, M. Gaitan, G. W. Kramer, R. G. Christensen, and W. A. MacCrehan, "Fabrication of plastic microfluid channels by imprinting methods," *Analytical chemistry*, vol. 69, no. 23, pp. 4783–4789, 1997.

[148] E. Vereshchagina, E. Andreassen, R. Gaarder, and M. Mielnik, "Synergy of 3d printing and injection molding: A new prototyping method for rapid design optimization and manufacturing of microfluidic devices," in *Proceedings of 21st International Conference on Miniaturized Systems and Life Sciences*, 2017, pp. 315–316.

[149] T.-Y. Lin, T. Do, P. Kwon, and P. B. Lillehoj, "3d printed metal molds for hot embossing plastic microfluidic devices," *Lab on a Chip*, vol. 17, no. 2, pp. 241–247, 2017.

[150] S. Wiedemeier, R. Römer, S. Wächter, U. Staps, C. Kolbe, and G. Gastrock, "Precision moulding of biomimetic disposable chips for droplet-based applications," *Microfluidics and Nanofluidics*, vol. 21, no. 11, p. 167, 2017.

[151] L. Peng, Y. Deng, P. Yi, and X. Lai, "Micro hot embossing of thermoplastic polymers: a review," *Journal of Micromechanics and Microengineering*, vol. 24, no. 1, p. 013001, 2013.

[152] X. Chen and L. Zhang, "Review in manufacturing methods of nanochannels of

bio-nanofluidic chips," *Sensors and Actuators B: Chemical*, vol. 254, pp. 648–659, 2018.

[153] K. M. Weerakoon-Ratnayake, C. E. OÑeil, F. I. Uba, and S. A. Soper, "Thermoplastic nanofluidic devices for biomedical applications," *Lab on a Chip*, vol. 17, no. 3, pp. 362–381, 2017.

[154] D. Konstantinou, A. Shirazi, A. Sadri, and E. W. Young, "Combined hot embossing and milling for medium volume production of thermoplastic microfluidic devices," *Sensors and Actuators B: Chemical*, vol. 234, pp. 209–221, 2016.

[155] B. Gale, A. Jafek, C. Lambert, B. Goenner, H. Moghimifam, U. Nze, and S. Kamarapu, "A review of current methods in microfluidic device fabrication and future commercialization prospects," *Inventions*, vol. 3, no. 3, p. 60, 2018.

[156] M. E. Wilson, N. Kota, Y. Kim, Y. Wang, D. B. Stolz, P. R. LeDuc, and O. B. Ozdoganlar, "Fabrication of circular microfluidic channels by combining mechanical micromilling and soft lithography," *Lab on a Chip*, vol. 11, no. 8, pp. 1550–1555, 2011.

[157] D. P. Yen, Y. Ando, and K. Shen, "A cost-effective micromilling platform for rapid prototyping of microdevices," *Technology*, vol. 4, no. 04, pp. 234–239, 2016.

[158] D. J. Guckenberger, T. E. de Groot, A. M. Wan, D. J. Beebe, and E. W. Young, "Micromilling: a method for ultra-rapid prototyping of plastic microfluidic devices," *Lab on a Chip*, vol. 15, no. 11, pp. 2364–2378, 2015.

[159] P.-C. Chen, C.-W. Pan, W.-C. Lee, and K.-M. Li, "Optimization of micromilling microchannels on a polycarbonate substrate," *International journal of precision engineering and manufacturing*, vol. 15, no. 1, pp. 149–154, 2014.

[160] ——, "An experimental study of micromilling parameters to manufacture microchannels on a pmma substrate," *The International Journal of Advanced Manufacturing Technology*, vol. 71, no. 9-12, pp. 1623–1630, 2014.

[161] A. Lashkaripour, R. Silva, and D. Densmore, "Desktop micromilled microfluidics," *Microfluidics and Nanofluidics*, vol. 22, no. 3, p. 31, 2018.

[162] D. Teixidor, T. Thepsonthi, J. Ciurana, and T. Özel, "Nanosecond pulsed laser micromachining of pmma-based microfluidic channels," *Journal of Manufacturing Processes*, vol. 14, no. 4, pp. 435–442, 2012.

[163] Y.-K. Hsieh, S.-C. Chen, W.-L. Huang, K.-P. Hsu, K. Gorday, T. Wang, and J. Wang, "Direct micromachining of microfluidic channels on biodegradable materials using laser ablation," *Polymers*, vol. 9, no. 7, p. 242, 2017.

[164] R. Suriano, A. Kuznetsov, S. M. Eaton, R. Kiyan, G. Cerullo, R. Osellame, B. N. Chichkov, M. Levi, and S. Turri, "Femtosecond laser ablation of polymeric substrates for the fabrication of microfluidic channels," *Applied Surface Science*, vol. 257, no. 14, pp. 6243–6250, 2011.

[165] S. Prakash and S. Kumar, "Fabrication of microchannels on transparent pmma using co 2 laser (10.6 μm) for microfluidic applications: An experimental investigation," *International Journal of Precision Engineering and Manufacturing*, vol. 16, no. 2, pp. 361–366, 2015.

[166] S. S. Zakariyah, P. P. Conway, D. A. Hutt, K. Wang, and D. R. Selviah, "Co2 laser micromachining of optical waveguides for interconnection on circuit boards," *Optics and Lasers in Engineering*, vol. 50, no. 12, pp. 1752–1756, 2012.

[167] N. Vasilakis, D. Moschou, D. Carta, H. Morgan, and T. Prodromakis, "Long-lasting fr-4 surface hydrophilisation towards commercial pcb passive microfluidics," *Applied Surface Science*, vol. 368, pp. 69–75, 2016.

[168] T. Merkel, M. Graeber, and L. Pagel, "A new technology for fluidic microsystems based on pcb technology," *Sensors and Actuators A: Physical*, vol. 77, no. 2, pp. 98–105, 1999.

[169] L. L. Wu, S. Babikian, G.-P. Li, and M. Bachman, "Microfluidic printed circuit boards," in *2011 IEEE 61st electronic components and technology conference (ECTC)*. IEEE, 2011, pp. 1576–1581.

[170] G. Flores, C. Aracil, F. Perdigones, and J. M. Quero, "Lab-protocol-on-pcb: Prototype of a laboratory protocol on printed circuit board using mems technologies," *Microelectronic Engineering*, vol. 200, pp. 26–31, 2018.

[171] E. Franco, B. Salvador, F. Perdigones, M. Cabello, and J. M. Quero, "Fabrication method of lab-on-pcb devices using a microheater with a thermo-mechanical barrier," *Microelectronic Engineering*, vol. 194, pp. 31–39, 2018.

[172] M. Souilah, A. Chaabi, F. Perdigones, J. M. Quero, G. Flores, and M. R. Lain, "Fabrication process for pcbmems capacitive pressure sensors using the cu layer to define the gap," *IEEE Sensors Journal*, vol. 16, no. 5, pp. 1151–1157, 2015.

[173] B. Salvador, E. Franco, F. Perdigones, and J. M. Quero, "Fabrication process for inexpensive, biocompatible and transparent pcbs. application to a flow meter," *Microelectronic Engineering*, vol. 173, pp. 6–12, 2017.

[174] M. Cabello, C. Aracil, F. Perdigones, M. Mozo, B. de la Cerda, and J. M. Quero, "Gold microelectrodes array embedded in pdms for electrical stimulation and signal detection," *Sensors and Actuators B: Chemical*, vol. 257, pp. 954–962, 2018.

[175] F. Perdigones, C. Aracil, J. M. Moreno, A. Luque, and J. M. Quero, "Highly integrable pressurized microvalve for portable su-8 microfluidic platforms," *Journal of Microelectromechanical Systems*, vol. 23, no. 2, pp. 398–405, 2013.

[176] A. Wego, S. Richter, and L. Pagel, "Fluidic microsystems based on printed circuit board technology," *Journal of Micromechanics and Microengineering*, vol. 11, no. 5, p. 528, 2001.

[177] D. Moschou and A. Tserepi, "The lab-on-pcb approach: tackling the μtas commercial upscaling bottleneck," *Lab on a Chip*, vol. 17, no. 8, pp. 1388–1405, 2017.

[178] Y.-X. Guan, Z.-R. Xu, J. Dai, and Z.-L. Fang, "The use of a micropump based on capillary and evaporation effects in a microfluidic flow injection chemiluminescence system," *Talanta*, vol. 68, no. 4, pp. 1384–1389, 2006.

[179] M. K. Dehghan Manshadi, D. Khojasteh, M. Mohammadi, and R. Kamali, "Electroosmotic micropump for lab-on-a-chip biomedical applications," *International Journal of Numerical Modelling: Electronic Networks, Devices and Fields*, vol. 29, no. 5, pp. 845–858, 2016.

[180] T. Satoh, G. Narazaki, R. Sugita, H. Kobayashi, S. Sugiura, and T. Kanamori, "A pneumatic pressure-driven multi-throughput microfluidic circulation culture system," *Lab on a Chip*, vol. 16, no. 12, pp. 2339–2348, 2016.

[181] A. K. Au, H. Lai, B. R. Utela, and A. Folch, "Microvalves and micropumps for biomems," *Micromachines*, vol. 2, no. 2, pp. 179–220, 2011.

[182] G. Flores, C. Aracil, F. Perdigones, and J. Quero, "Low consumption single-use microvalve for microfluidic pcb-based platforms," *Journal of Micromechanics and Microengineering*, vol. 24, no. 6, p. 065013, 2014.

[183] C.-Y. Lee, W.-T. Wang, C.-C. Liu, and L.-M. Fu, "Passive mixers in microfluidic systems: A review," *Chemical Engineering Journal*, vol. 288, pp. 146–160, 2016.

[184] V. Hessel, H. Löwe, and F. Schönfeld, "Micromixers—a review on passive and active mixing principles," *Chemical Engineering Science*, vol. 60, no. 8-9, pp. 2479–2501, 2005.

[185] Q.-S. Kang, Y. Li, J.-Q. Xu, L.-J. Su, Y.-T. Li, and W.-H. Huang, "Polymer monolith-integrated multilayer poly (dimethylsiloxane) microchip for online microextraction and capillary electrophoresis," *Electrophoresis*, vol. 31, no. 18, pp. 3028–3034, 2010.

[186] C. R. Reedy, C. W. Price, J. Sniegowski, J. P. Ferrance, M. Begley, and J. P. Landers, "Solid phase extraction of dna from biological samples in a post-based, high surface

area poly (methyl methacrylate)(pmma) microdevice," *Lab on a Chip*, vol. 11, no. 9, pp. 1603–1611, 2011.

[187] B. C. Giordano, D. S. Burgi, S. J. Hart, and A. Terray, "On-line sample preconcentration in microfluidic devices: A review," *Analytica Chimica Acta*, vol. 718, pp. 11–24, 2012.

[188] P. N. Nge, W. Yang, J. V. Pagaduan, and A. T. Woolley, "Ion-permeable membrane for on-chip preconcentration and separation of cancer marker proteins," *Electrophoresis*, vol. 32, no. 10, pp. 1133–1140, 2011.

[189] M. Yu, Q. Wang, J. E. Patterson, and A. T. Woolley, "Multilayer polymer microchip capillary array electrophoresis devices with integrated on-chip labeling for high-throughput protein analysis," *Analytical chemistry*, vol. 83, no. 9, pp. 3541–3547, 2011.

[190] J. L. Felhofer, L. Blanes, and C. D. Garcia, "Recent developments in instrumentation for capillary electrophoresis and microchip-capillary electrophoresis," *Electrophoresis*, vol. 31, no. 15, pp. 2469–2486, 2010.

[191] I. Mitra, Z. Zhuang, Y. Zhang, C.-Y. Yu, Z. T. Hammoud, H. Tang, Y. Mechref, and S. C. Jacobson, "N-glycan profiling by microchip electrophoresis to differentiate disease states related to esophageal adenocarcinoma," *Analytical chemistry*, vol. 84, no. 8, pp. 3621–3627, 2012.

[192] P. A. Levkin, S. Eeltink, T. R. Stratton, R. Brennen, K. Robotti, H. Yin, K. Killeen, F. Svec, and J. M. Fréchet, "Monolithic porous polymer stationary phases in polyimide chips for the fast high-performance liquid chromatography separation of proteins and peptides," *Journal of Chromatography A*, vol. 1200, no. 1, pp. 55–61, 2008.

[193] W. B. Zimmerman, "Electrochemical microfluidics," *Chemical Engineering Science*, vol. 66, no. 7, pp. 1412–1425, 2011.

[194] D. B. Gunasekara, M. K. Hulvey, and S. M. Lunte, "In-channel amperometric detection for microchip electrophoresis using a wireless isolated potentiostat," *Electrophoresis*, vol. 32, no. 8, pp. 832–837, 2011.

[195] M. Vázquez, C. Frankenfeld, W. K. T. Coltro, E. Carrilho, D. Diamond, and S. M. Lunte, "Dual contactless conductivity and amperometric detection on hybrid pdms/glass electrophoresis microchips," *Analyst*, vol. 135, no. 1, pp. 96–103, 2010.

[196] D. E. Angelescu, *Highly integrated microfluidics design*. Artech House, 2011.

[197] F. B. Myers and L. P. Lee, "Innovations in optical microfluidic technologies for point-of-care diagnostics," *Lab on a Chip*, vol. 8, no. 12, pp. 2015–2031, 2008.

[198] A. Pais, A. Banerjee, D. Klotzkin, and I. Papautsky, "High-sensitivity, disposable lab-on-a-chip with thin-film organic electronics for fluorescence detection," *Lab on a Chip*, vol. 8, no. 5, pp. 794–800, 2008.

[199] P. Singh, "Spr biosensors: historical perspectives and current challenges," *Sensors and actuators B: Chemical*, vol. 229, pp. 110–130, 2016.

[200] S. Firdous, S. Anwar, and R. Rafya, "Development of surface plasmon resonance (spr) biosensors for use in the diagnostics of malignant and infectious diseases," *Laser Physics Letters*, vol. 15, no. 6, p. 065602, 2018.

[201] A. Manz, N. Graber, and H. á. Widmer, "Miniaturized total chemical analysis systems: a novel concept for chemical sensing," *Sensors and actuators B: Chemical*, vol. 1, no. 1-6, pp. 244–248, 1990.

[202] P. Abgrall and A. Gue, "Lab-on-chip technologies: making a microfluidic network and coupling it into a complete microsystem—a review," *Journal of micromechanics and microengineering*, vol. 17, no. 5, p. R15, 2007.

[203] Y. Temiz, R. D. Lovchik, G. V. Kaigala, and E. Delamarche, "Lab-on-a-chip devices: How to close and plug the lab?" *Microelectronic Engineering*, vol. 132, pp. 156–175, 2015.

[204] D. Mark, S. Haeberle, G. Roth, F. Von Stetten, and R. Zengerle, "Microfluidic lab-on-a-chip platforms: requirements, characteristics and applications," in *Microfluidics based microsystems*. Springer, 2010, pp. 305–376.

[205] W. Jung, J. Han, J.-W. Choi, and C. H. Ahn, "Point-of-care testing (poct) diagnostic systems using microfluidic lab-on-a-chip technologies," *Microelectronic Engineering*, vol. 132, pp. 46–57, 2015.

[206] Y. Lu, L. Yang, W. Wei, and Q. Shi, "Microchip-based single-cell functional proteomics for biomedical applications," *Lab on a Chip*, vol. 17, no. 7, pp. 1250–1263, 2017.

[207] Y. Zhang, S. Ge, and J. Yu, "Chemical and biochemical analysis on lab-on-a-chip devices fabricated using three-dimensional printing," *TrAC Trends in Analytical Chemistry*, vol. 85, pp. 166–180, 2016.

[208] A. Jang, Z. Zou, K. K. Lee, C. H. Ahn, and P. L. Bishop, "State-of-the-art lab chip sensors for environmental water monitoring," *Measurement Science and Technology*, vol. 22, no. 3, p. 032001, 2011.

[209] G. M. Walker, H. C. Zeringue, and D. J. Beebe, "Microenvironment design considerations for cellular scale studies," *Lab on a Chip*, vol. 4, no. 2, pp. 91–97, 2004.

[210] M. Huang, S. Fan, W. Xing, and C. Liu, "Microfluidic cell culture system studies and computational fluid dynamics," *Mathematical and Computer Modelling*, vol. 52, no. 11-12, pp. 2036–2042, 2010.

[211] J. H. Yeon and J.-K. Park, "Microfluidic cell culture systems for cellular analysis," *Biochip J*, vol. 1, no. 1, pp. 17–27, 2007.

[212] I. Meyvantsson and D. J. Beebe, "Cell culture models in microfluidic systems," *Annu. Rev. Anal. Chem.*, vol. 1, pp. 423–449, 2008.

[213] S. Halldorsson, E. Lucumi, R. Gómez-Sjöberg, and R. M. Fleming, "Advantages and challenges of microfluidic cell culture in polydimethylsiloxane devices," *Biosensors and Bioelectronics*, vol. 63, pp. 218–231, 2015.

[214] P. M. van Midwoud, A. Janse, M. T. Merema, G. M. Groothuis, and E. Verpoorte, "Comparison of biocompatibility and adsorption properties of different plastics for advanced microfluidic cell and tissue culture models," *Analytical chemistry*, vol. 84, no. 9, pp. 3938–3944, 2012.

[215] S. Lindström and H. Andersson-Svahn, "Overview of single-cell analyses: microdevices and applications," *Lab on a Chip*, vol. 10, no. 24, pp. 3363–3372, 2010.

[216] A. Super, N. Jaccard, M. P. C. Marques, R. J. Macown, L. D. Griffin, F. S. Veraitch, and N. Szita, "Real-time monitoring of specific oxygen uptake rates of embryonic stem cells in a microfluidic cell culture device," *Biotechnology journal*, vol. 11, no. 9, pp. 1179–1189, 2016.

[217] R. Gomez-Sjoeberg, A. A. Leyrat, D. M. Pirone, C. S. Chen, and S. R. Quake, "Versatile, fully automated, microfluidic cell culture system," *Analytical chemistry*, vol. 79, no. 22, pp. 8557–8563, 2007.

[218] M. Rothbauer, J. M. Rosser, H. Zirath, and P. Ertl, "Tomorrow today: organ-on-a-chip advances towards clinically relevant pharmaceutical and medical in vitro models," *Current opinion in biotechnology*, vol. 55, pp. 81–86, 2019.

[219] A. Junaid, A. Mashaghi, T. Hankemeier, and P. Vulto, "An end-user perspective on organ-on-a-chip: assays and usability aspects," *Current Opinion in Biomedical Engineering*, vol. 1, pp. 15–22, 2017.

[220] C. Probst, S. Schneider, and P. Loskill, "High-throughput organ-on-a-chip systems: Current status and remaining challenges," *Current Opinion in Biomedical*

Engineering, vol. 6, pp. 33–41, 2018.

[221] B. Zhang, A. Korolj, B. F. L. Lai, and M. Radisic, "Advances in organ-on-a-chip engineering," *Nature Reviews Materials*, vol. 3, no. 8, p. 257, 2018.

[222] D. Huh, B. D. Matthews, A. Mammoto, M. Montoya-Zavala, H. Y. Hsin, and D. E. Ingber, "Reconstituting organ-level lung functions on a chip," *Science*, vol. 328, no. 5986, pp. 1662–1668, 2010.

[223] B. Zhang, M. Montgomery, M. D. Chamberlain, S. Ogawa, A. Korolj, A. Pahnke, L. A. Wells, S. Massé, J. Kim, L. Reis *et al.*, "Biodegradable scaffold with built-in vasculature for organ-on-a-chip engineering and direct surgical anastomosis," *Nature materials*, vol. 15, no. 6, p. 669, 2016.

[224] G. Ligresti, R. J. Nagao, J. Xue, Y. J. Choi, J. Xu, S. Ren, T. Aburatani, S. K. Anderson, J. W. MacDonald, T. K. Bammler *et al.*, "A novel three–dimensional human peritubular microvascular system," *Journal of the American Society of Nephrology*, vol. 27, no. 8, pp. 2370–2381, 2016.

[225] S. Wei, C. Yu-Qing, L. Guo-An, M. ZHANG, H.-Y. ZHANG, W. Yue-Rong, and H. Ping, "Organs-on-chips and its applications," *Chinese Journal of Analytical Chemistry*, vol. 44, no. 4, pp. 533–541, 2016.

[226] X. Yang, K. Li, X. Zhang, C. Liu, B. Guo, W. Wen, and X. Gao, "Nanofiber membrane supported lung-on-a-chip microdevice for anti-cancer drug testing," *Lab on a Chip*, vol. 18, no. 3, pp. 486–495, 2018.

[227] H. Kimura, Y. Sakai, and T. Fujii, "Organ/body-on-a-chip based on microfluidic technology for drug discovery," *Drug metabolism and pharmacokinetics*, vol. 33, no. 1, pp. 43–48, 2018.

[228] H. AVCI, F. D. GÜZEL, S. Erol, and A. Akpek, "Recent advances in organ-on-a-chip technologies and future challenges: a review," *Turkish Journal of Chemistry*, vol. 42, no. 3, pp. 587–610, 2018.

[229] K.-J. Jang and K.-Y. Suh, "A multi-layer microfluidic device for efficient culture and analysis of renal tubular cells," *Lab on a Chip*, vol. 10, no. 1, pp. 36–42, 2010.

[230] K.-J. Jang, A. P. Mehr, G. A. Hamilton, L. A. McPartlin, S. Chung, K.-Y. Suh, and D. E. Ingber, "Human kidney proximal tubule-on-a-chip for drug transport and nephrotoxicity assessment," *Integrative Biology*, vol. 5, no. 9, pp. 1119–1129, 2013.

[231] M. J. Powers, K. Domansky, M. R. Kaazempur-Mofrad, A. Kalezi, A. Capitano, A. Upadhyaya, P. Kurzawski, K. E. Wack, D. B. Stolz, R. Kamm *et al.*, "A microfabricated array bioreactor for perfused 3d liver culture," *Biotechnology and*

bioengineering, vol. 78, no. 3, pp. 257–269, 2002.

[232] B. Vinci, C. Duret, S. Klieber, S. Gerbal-Chaloin, A. Sa-Cunha, S. Laporte, B. Suc, P. Maurel, A. Ahluwalia, and M. Daujat-Chavanieu, "Modular bioreactor for primary human hepatocyte culture: medium flow stimulates expression and activity of detoxification genes," *Biotechnology journal*, vol. 6, no. 5, pp. 554–564, 2011.

[233] K. Domansky, W. Inman, J. Serdy, A. Dash, M. H. Lim, and L. G. Griffith, "Perfused multiwell plate for 3d liver tissue engineering," *Lab on a chip*, vol. 10, no. 1, pp. 51–58, 2010.

[234] S.-A. Lee, E. Kang, J. Ju, D.-S. Kim, S.-H. Lee *et al.*, "Spheroid-based three-dimensional liver-on-a-chip to investigate hepatocyte–hepatic stellate cell interactions and flow effects," *Lab on a Chip*, vol. 13, no. 18, pp. 3529–3537, 2013.

[235] V. Autores, "Ihme," urlhttp://www.healthdata.org, 2019, accedido 16-09-2019.

[236] A. A. Werdich, E. A. Lima, B. Ivanov, I. Ges, M. E. Anderson, J. P. Wikswo, and F. J. Baudenbacher, "A microfluidic device to confine a single cardiac myocyte in a sub-nanoliter volume on planar microelectrodes for extracellular potential recordings," *Lab on a Chip*, vol. 4, no. 4, pp. 357–362, 2004.

[237] X. Jin, L. Xia, L.-S. Wang, J.-Z. Shi, Y. Zheng, W.-L. Chen, L. Zhang, Z.-G. Liu, G.-Q. Chen, and N.-Y. Fang, "Differential protein expression in hypertrophic heart with and without hypertension in spontaneously hypertensive rats," *Proteomics*, vol. 6, no. 6, pp. 1948–1956, 2006.

[238] A. Grosberg, P. W. Alford, M. L. McCain, and K. K. Parker, "Ensembles of engineered cardiac tissues for physiological and pharmacological study: heart on a chip," *Lab on a chip*, vol. 11, no. 24, pp. 4165–4173, 2011.

[239] Y. S. Zhang, A. Arneri, S. Bersini, S.-R. Shin, K. Zhu, Z. Goli-Malekabadi, J. Aleman, C. Colosi, F. Busignani, V. DellÉrba *et al.*, "Bioprinting 3d microfibrous scaffolds for engineering endothelialized myocardium and heart-on-a-chip," *Biomaterials*, vol. 110, pp. 45–59, 2016.

[240] V. Y. Sidorov, P. C. Samson, T. N. Sidorova, J. M. Davidson, C. C. Lim, and J. P. Wikswo, "I-wire heart-on-a-chip i: Three-dimensional cardiac tissue constructs for physiology and pharmacology," *Acta biomaterialia*, vol. 48, pp. 68–78, 2017.

[241] N. Wu, "Neuromorphic vision chips," *Science China Information Sciences*, vol. 61, no. 6, p. 060421, 2018.

[242] K. Achberger, C. Probst, J. Haderspeck, S. Bolz, J. Rogal, J. Chuchuy, M. Nikolova, V. Cora, L. Antkowiak, W. Haq *et al.*, "Human retina-on-a-chip: Merging organoid

and organ-on-a-chip technology to generate complex multi-layer tissue models," *bioRxiv*, p. 552158, 2019.

[243] J. N. Mazerik, S. Becker, and P. A. Sieving, "3-d retina organoids: Building platforms for therapies of the future," *Cell Medicine*, vol. 10, p. 2155179018773758, 2018.

[244] X. Zhong, C. Gutierrez, T. Xue, C. Hampton, M. N. Vergara, L.-H. Cao, A. Peters, T. S. Park, E. T. Zambidis, J. S. Meyer *et al.*, "Generation of three-dimensional retinal tissue with functional photoreceptors from human ipscs," *Nature communications*, vol. 5, p. 4047, 2014.

[245] K. J. Wahlin, J. A. Maruotti, S. R. Sripathi, J. Ball, J. M. Angueyra, C. Kim, R. Grebe, W. Li, B. W. Jones, and D. J. Zack, "Photoreceptor outer segment-like structures in long-term 3d retinas from human pluripotent stem cells," *Scientific reports*, vol. 7, no. 1, p. 766, 2017.

[246] K. H. Dodson, F. D. Echevarria, D. Li, R. M. Sappington, and J. F. Edd, "Retina-on-a-chip: a microfluidic platform for point access signaling studies," *Biomedical microdevices*, vol. 17, no. 6, p. 114, 2015.

[247] S. Mishra, A. Thakur, S. Redenti, and M. Vazquez, "A model microfluidics-based system for the human and mouse retina," *Biomedical microdevices*, vol. 17, no. 6, p. 107, 2015.

[248] B. Zhang and M. Radisic, "Organ-on-a-chip devices advance to market," *Lab on a Chip*, vol. 17, no. 14, pp. 2395–2420, 2017.

[249] C. Thomas Jr, P. Springer, G. Loeb, Y. Berwald-Netter, and L. Okun, "A miniature microelectrode array to monitor the bioelectric activity of cultured cells," *Experimental cell research*, vol. 74, no. 1, pp. 61–66, 1972.

[250] R. Kim, S. Joo, H. Jung, N. Hong, and Y. Nam, "Recent trends in microelectrode array technology for in vitro neural interface platform," *Biomedical Engineering Letters*, vol. 4, no. 2, pp. 129–141, 2014.

[251] R. Kim, N. Hong, and Y. Nam, "Gold nanograin microelectrodes for neuroelectronic interfaces," *Biotechnology journal*, vol. 8, no. 2, pp. 206–214, 2013.

[252] J.-H. Kim, G. Kang, Y. Nam, and Y.-K. Choi, "Surface-modified microelectrode array with flake nanostructure for neural recording and stimulation," *Nanotechnology*, vol. 21, no. 8, p. 085303, 2010.

[253] V. Autores, "Multichannelsystems," urlhttps://www.multichannelsystems.com/, 2019, accedido 17-10-2019.

[254] D. Tsai, E. John, T. Chari, R. Yuste, and K. Shepard, "High-channel-count, high-density microelectrode array for closed-loop investigation of neuronal networks," in *2015 37th Annual International Conference of the IEEE Engineering in Medicine and Biology Society (EMBC)*. IEEE, 2015, pp. 7510–7513.

[255] L. Guo, G. S. Guvanasen, X. Liu, C. Tuthill, T. R. Nichols, and S. P. DeWeerth, "A pdms-based integrated stretchable microelectrode array (ismea) for neural and muscular surface interfacing," *IEEE transactions on biomedical circuits and systems*, vol. 7, no. 1, pp. 1–10, 2012.

[256] E. Seker, Y. Berdichevsky, M. R. Begley, M. L. Reed, K. J. Staley, and M. L. Yarmush, "The fabrication of low-impedance nanoporous gold multiple-electrode arrays for neural electrophysiology studies," *Nanotechnology*, vol. 21, no. 12, p. 125504, 2010.

[257] M. Heim, B. Yvert, and A. Kuhn, "Nanostructuration strategies to enhance microelectrode array (mea) performance for neuronal recording and stimulation," *Journal of Physiology-Paris*, vol. 106, no. 3-4, pp. 137–145, 2012.

[258] M. E. J. Obien, K. Deligkaris, T. Bullmann, D. J. Bakkum, and U. Frey, "Revealing neuronal function through microelectrode array recordings," *Frontiers in neuroscience*, vol. 8, p. 423, 2015.

[259] E. Moutaux, B. Charlot, F. Bardin, F. Saudou, and M. Cazorla, "An integrated microelectrode array and microfluidic platform for stimulating and recording reconstructed neuronal networks," 2017.

[260] E. Moutaux, B. Charlot, A. Genoux, F. Saudou, and M. Cazorla, "An integrated microfluidic/microelectrode array for the study of activity-dependent intracellular dynamics in neuronal networks," *Lab on a Chip*, vol. 18, no. 22, pp. 3425–3435, 2018.

[261] M. Cabello, H. Ge, C. Aracil, D. Moschou, P. Estela, J. Quero, S. I. Pascu, and P. RF Rocha, "Extracellular electrophysiology in the prostate cancer cell model pc-3," *Sensors*, vol. 19, p. 139, 2019.

[262] P. R. Rocha, P. Schlett, U. Kintzel, V. Mailänder, L. K. Vandamme, G. Zeck, H. L. Gomes, F. Biscarini, and D. M. De Leeuw, "Electrochemical noise and impedance of au electrode/electrolyte interfaces enabling extracellular detection of glioma cell populations," *Scientific reports*, vol. 6, p. 34843, 2016.

[263] C. Sekirnjak, P. Hottowy, A. Sher, W. Dabrowski, A. M. Litke, and E. Chichilnisky, "High-resolution electrical stimulation of primate retina for epiretinal implant design," *Journal of Neuroscience*, vol. 28, no. 17, pp. 4446–4456, 2008.

[264] V. Gautam, D. Rand, Y. Hanein, and K. Narayan, "A polymer optoelectronic interface provides visual cues to a blind retina," *Advanced Materials*, vol. 26, no. 11, pp. 1751–1756, 2014.

[265] M. Cabello, M. Mozo, B. De la Cerda, C. Aracil, F. J. Diaz-Corrales, F. Perdigones, L. Valdes-Sanchez, I. Relimpio, S. S. Bhattacharya, and J. M. Quero, "Electrostimulation in an autonomous culture lab-on-chip provides neuroprotection of a retinal explant from a retinitis pigmentosa mouse-model," *Sensors and Actuators B: Chemical*, vol. 288, pp. 337–346, 2019.

[266] D. T. Hartong, E. L. Berson, and T. P. Dryja, "Retinitis pigmentosa," *The Lancet*, vol. 368, no. 9549, pp. 1795–1809, 2006.

[267] B. M. Nash, D. C. Wright, J. R. Grigg, B. Bennetts, and R. V. Jamieson, "Retinal dystrophies, genomic applications in diagnosis and prospects for therapy," *Translational pediatrics*, vol. 4, no. 2, p. 139, 2015.

[268] A. K. Ahuja, J. Dorn, A. Caspi, M. McMahon, G. Dagnelie, P. Stanga, M. Humayun, R. Greenberg, A. I. S. Group *et al.*, "Blind subjects implanted with the argus ii retinal prosthesis are able to improve performance in a spatial-motor task," *British Journal of Ophthalmology*, vol. 95, no. 4, pp. 539–543, 2011.

[269] L. Naycheva, A. Schatz, T. Röck, G. Willmann, A. Messias, K. U. Bartz-Schmidt, E. Zrenner, and F. Gekeler, "Phosphene thresholds elicited by transcorneal electrical stimulation in healthy subjects and patients with retinal diseases," *Investigative ophthalmology & visual science*, vol. 53, no. 12, pp. 7440–7448, 2012.

[270] M. E. Pennesi, K. V. Michaels, S. S. Magee, A. Maricle, S. P. Davin, A. K. Garg, M. J. Gale, D. C. Tu, Y. Wen, L. R. Erker *et al.*, "Long-term characterization of retinal degeneration in rd1 and rd10 mice using spectral domain optical coherence tomography," *Investigative ophthalmology & visual science*, vol. 53, no. 8, pp. 4644–4656, 2012.

[271] L. Zhao, M. K. Zabel, X. Wang, W. Ma, P. Shah, R. N. Fariss, H. Qian, C. N. Parkhurst, W.-B. Gan, and W. T. Wong, "Microglial phagocytosis of living photoreceptors contributes to inherited retinal degeneration," *EMBO molecular medicine*, vol. 7, no. 9, pp. 1179–1197, 2015.

[272] A. Takano, T. Ogawa, M. Tanaka, and N. Futai, "On-chip incubation system for long-term microfluidic cell culture," in *Engineering in Medicine and Biology Society, EMBC, 2011 Annual International Conference of the IEEE*. IEEE, 2011, pp. 8404–8407.

[273] J. D. Dorn, A. K. Ahuja, A. Caspi, L. Da Cruz, G. Dagnelie, J.-A. Sahel, R. J. Greenberg, M. J. McMahon, A. I. S. Group *et al.*, "The detection of motion by

blind subjects with the epiretinal 60-electrode (argus ii) retinal prosthesis," *JAMA ophthalmology*, vol. 131, no. 2, pp. 183–189, 2013.

[274] A. Schatz, T. Röck, L. Naycheva, G. Willmann, B. Wilhelm, T. Peters, K. U. Bartz-Schmidt, E. Zrenner, A. Messias, and F. Gekeler, "Transcorneal electrical stimulation for patients with retinitis pigmentosa: a prospective, randomized, sham-controlled exploratory study," *Investigative ophthalmology & visual science*, vol. 52, no. 7, pp. 4485–4496, 2011.

[275] D. J. Hare, J. L. George, L. Bray, I. Volitakis, A. Vais, T. M. Ryan, R. A. Cherny, A. I. Bush, C. L. Masters, P. A. Adlard *et al.*, "The effect of paraformaldehyde fixation and sucrose cryoprotection on metal concentration in murine neurological tissue," *Journal of Analytical Atomic Spectrometry*, vol. 29, no. 3, pp. 565–570, 2014.

[276] K. Reinhard, A. Tikidji-Hamburyan, H. Seitter, S. Idrees, M. Mutter, B. Benkner, and T. A. Münch, "Step-by-step instructions for retina recordings with perforated multi electrode arrays," *PLoS One*, vol. 9, no. 8, p. e106148, 2014.

[277] R. M. Sappington, T. Sidorova, D. J. Long, and D. J. Calkins, "Trpv1: contribution to retinal ganglion cell apoptosis and increased intracellular ca2+ with exposure to hydrostatic pressure," *Investigative ophthalmology & visual science*, vol. 50, no. 2, pp. 717–728, 2009.

[278] K. Kooragayala, N. Gotoh, T. Cogliati, J. Nellissery, T. R. Kaden, S. French, R. Balaban, W. Li, R. Covian, and A. Swaroop, "Quantification of oxygen consumption in retina ex vivo demonstrates limited reserve capacity of photoreceptor mitochondria," *Investigative ophthalmology & visual science*, vol. 56, no. 13, pp. 8428–8436, 2015.

[279] F. Vendruscolo, M. J. Rossi, W. Schmidell, and J. L. Ninow, "Determination of oxygen solubility in liquid media," *ISRN Chemical Engineering*, vol. 2012, pp. 1–5, 2012.

[280] Y. Gavrieli, Y. Sherman, and S. A. Ben-Sasson, "Identification of programmed cell death in situ via specific labeling of nuclear dna fragmentation." *The Journal of cell biology*, vol. 119, no. 3, pp. 493–501, 1992.

[281] W. Gorczyca, J. Gong, B. Ardelt, F. Traganos, and Z. Darzynkiewicz, "The cell cycle related differences in susceptibility of hl-60 cells to apoptosis induced by various antitumor agents," *Cancer research*, vol. 53, no. 13, pp. 3186–3192, 1993.

[282] M. Cabello, C. Aracil, F. Perdigones, and J. M. Quero, "Conditioning lab on pcb to control temperature and mix fluids at the microscale for biomedical applications," in *2017 Spanish Conference on Electron Devices (CDE)*. IEEE, 2017, pp. 1–4.

[283] M. C. Medeiros, A. Mestre, P. Inácio, S. Asgarif, I. M. Araújo, P. C. Hubbard, Z. Velez, M. L. Cancela, P. R. Rocha, D. M. de Leeuw *et al.*, "An electrical method to measure low-frequency collective and synchronized cell activity using extracellular electrodes," *Sensing and Bio-Sensing Research*, vol. 10, pp. 1–8, 2016.

[284] P. R. Rocha, M. C. Medeiros, U. Kintzel, J. Vogt, I. M. Araújo, A. L. Mestre, V. Mailänder, P. Schlett, M. Dröge, L. Schneider *et al.*, "Extracellular electrical recording of ph-triggered bursts in c6 glioma cell populations," *Science advances*, vol. 2, no. 12, p. e1600516, 2016.

[285] P. R. Rocha, P. Schlett, L. Schneider, M. Dröge, V. Mailänder, H. L. Gomes, P. W. Blom, and D. M. De Leeuw, "Low frequency electric current noise in glioma cell populations," *Journal of Materials Chemistry B*, vol. 3, no. 25, pp. 5035–5039, 2015.

[286] V. autores, "Seer cancer statistics review," url:https://seer.cancer.gov/, 2020, accedido 12-01-2020.

[287] A. Weiner, R. Matulewicz, S. Eggener, and E. M. Schaeffer, "Increasing incidence of metastatic prostate cancer in the united states (2004–2013)," *Prostate cancer and prostatic diseases*, vol. 19, no. 4, p. 395, 2016.

[288] C. Buzzoni, A. Auvinen, M. J. Roobol, S. Carlsson, S. M. Moss, D. Puliti, H. J. de Koning, C. H. Bangma, L. J. Denis, M. Kwiatkowski *et al.*, "Metastatic prostate cancer incidence and prostate-specific antigen testing: new insights from the european randomized study of screening for prostate cancer," *European urology*, vol. 68, no. 5, pp. 885–890, 2015.

[289] K. Kolostova, M. Broul, J. Schraml, M. Cegan, R. Matkowski, M. Fiutowski, and V. Bobek, "Circulating tumor cells in localized prostate cancer: isolation, cultivation in vitro and relationship to t-stage and gleason score," *Anticancer research*, vol. 34, no. 7, pp. 3641–3646, 2014.

[290] K. R. Stone, D. D. Mickey, H. Wunderli, G. H. Mickey, and D. F. Paulson, "Isolation of a human prostate carcinoma cell line (du 145)," *International journal of cancer*, vol. 21, no. 3, pp. 274–281, 1978.

[291] D. Cunningham and Z. You, "In vitro and in vivo model systems used in prostate cancer research," *Journal of biological methods*, vol. 2, no. 1, 2015.

[292] X. Wu, S. Gong, P. Roy-Burman, P. Lee, and Z. Culig, "Current mouse and cell models in prostate cancer research," *Endocrine-related cancer*, vol. 20, no. 4, pp. R155–R170, 2013.

[293] D. Rea, V. Del Vecchio, G. Palma, A. Barbieri, M. Falco, A. Luciano, D. De Biase,

S. Perdonà, G. Facchini, and C. Arra, "Mouse models in prostate cancer translational research: from xenograft to pdx," *BioMed research international*, vol. 2016, 2016.

[294] S. M. Pulukuri, C. S. Gondi, S. S. Lakka, A. Jutla, N. Estes, M. Gujrati, and J. S. Rao, "Rna interference-directed knockdown of urokinase plasminogen activator and urokinase plasminogen activator receptor inhibits prostate cancer cell invasion, survival, and tumorigenicity in vivo," *Journal of biological chemistry*, vol. 280, no. 43, pp. 36 529–36 540, 2005.

[295] I. P. Harrison and S. Selemidis, "Understanding the biology of reactive oxygen species and their link to cancer: Nadph oxidases as novel pharmacological targets," *Clinical and Experimental Pharmacology and Physiology*, vol. 41, no. 8, pp. 533–542, 2014.

[296] Y. Yang, S. Karakhanova, J. Werner, and A. V Bazhin, "Reactive oxygen species in cancer biology and anticancer therapy," *Current medicinal chemistry*, vol. 20, no. 30, pp. 3677–3692, 2013.

[297] B. Hille, "Ionic channels in excitable membranes. current problems and biophysical approaches," *Biophysical Journal*, vol. 22, no. 2, pp. 283–294, 1978.

[298] P. M. Eimon, M. Ghannad-Rezaie, G. De Rienzo, A. Allalou, Y. Wu, M. Gao, A. Roy, J. Skolnick, and M. F. Yanik, "Brain activity patterns in high-throughput electrophysiology screen predict both drug efficacies and side effects," *Nature communications*, vol. 9, no. 1, p. 219, 2018.

[299] N. Salvarani, A. Maguy, S. A. De Simone, M. Miragoli, F. Jousset, and S. Rohr, "Tgf-β1 (transforming growth factor-β1) plays a pivotal role in cardiac myofibroblast arrhythmogenicity," *Circulation: Arrhythmia and Electrophysiology*, vol. 10, no. 5, p. e004567, 2017.

[300] K. Kunzelmann, "Ion channels and cancer," *The Journal of membrane biology*, vol. 205, no. 3, p. 159, 2005.

[301] V. A. Cuddapah and H. Sontheimer, "Ion channels and tranporters in cancer. 2. ion channels and the control of cancer cell migration," *American Journal of Physiology-Cell Physiology*, vol. 301, no. 3, pp. C541–C549, 2011.

[302] A. Arcangeli and A. Becchetti, "Novel perspectives in cancer therapy: Targeting ion channels," *Drug resistance updates*, vol. 21, pp. 11–19, 2015.

[303] M. Abdul and N. Hoosein, "Expression and activity of potassium ion channels in human prostate cancer," *Cancer letters*, vol. 186, no. 1, pp. 99–105, 2002.

[304] S. Yildirim, S. Altun, H. Gumushan, A. Patel, and M. B. Djamgoz, "Voltage-gated

sodium channel activity promotes prostate cancer metastasis in vivo," *Cancer letters*, vol. 323, no. 1, pp. 58–61, 2012.

[305] L. Zhang and G. J. Barritt, "Evidence that trpm8 is an androgen-dependent ca2+ channel required for the survival of prostate cancer cells," *Cancer research*, vol. 64, no. 22, pp. 8365–8373, 2004.

[306] D. Gkika, M. Flourakis, L. Lemonnier, and N. Prevarskaya, "Psa reduces prostate cancer cell motility by stimulating trpm8 activity and plasma membrane expression," *Oncogene*, vol. 29, no. 32, p. 4611, 2010.

[307] Y. Wang, D. Yue, K. Li, Y.-L. Liu, C.-S. Ren, and P. Wang, "The role of trpc6 in hgf-induced cell proliferation of human prostate cancer du145 and pc3 cells," *Asian journal of andrology*, vol. 12, no. 6, p. 841, 2010.

[308] C. Holzmann, T. Kilch, S. Kappel, K. Dörr, V. Jung, M. Stöckle, I. Bogeski, and C. Peinelt, "Differential redox regulation of ca2+ signaling and viability in normal and malignant prostate cells," *Biophysical journal*, vol. 109, no. 7, pp. 1410–1419, 2015.

[309] G. Buzsáki, C. A. Anastassiou, and C. Koch, "The origin of extracellular fields and currents—eeg, ecog, lfp and spikes," *Nature reviews neuroscience*, vol. 13, no. 6, p. 407, 2012.

[310] B. Eversmann, M. Jenkner, F. Hofmann, C. Paulus, R. Brederlow, B. Holzapfl, P. Fromherz, M. Merz, M. Brenner, M. Schreiter *et al.*, "A 128/spl times/128 cmos biosensor array for extracellular recording of neural activity," *IEEE Journal of Solid-State Circuits*, vol. 38, no. 12, pp. 2306–2317, 2003.

[311] M. C. Medeiros, A. Mestre, P. Inácio, S. Asgarif, I. M. Araújo, P. C. Hubbard, Z. Velez, M. L. Cancela, P. R. Rocha, D. M. de Leeuw *et al.*, "An electrical method to measure low-frequency collective and synchronized cell activity using extracellular electrodes," *Sensing and Bio-Sensing Research*, vol. 10, pp. 1–8, 2016.

[312] J. Teulon, P. M. Ronco, M. Geniteau-Legendre, B. Baudouin, S. Estrade, R. Cassingena, and A. Vandewalle, "Transformation of renal tubule epithelial cells by simian virus-40 is associated with emergence of ca2+-insensitive k+ channels and altered mitogenic sensitivity to k+ channel blockers," *Journal of cellular physiology*, vol. 151, no. 1, pp. 113–125, 1992.

[313] Y. Sohma, A. Harris, C. Wardle, M. Gray, and B. Argent, "Maxi k+ channels on human vas deferens epithelial cells," *The Journal of membrane biology*, vol. 141, no. 1, pp. 69–82, 1994.

[314] N. J. Logsdon, J. Kang, J. A. Togo, E. P. Christian, and J. Aiyar, "A novel gene,

hkca4, encodes the calcium-activated potassium channel in human t lymphocytes," *Journal of Biological Chemistry*, vol. 272, no. 52, pp. 32 723–32 726, 1997.

[315] L. Leybaert and M. J. Sanderson, "Intercellular ca2+ waves: mechanisms and function," *Physiological reviews*, vol. 92, no. 3, pp. 1359–1392, 2012.

[316] N. Kuga, T. Sasaki, Y. Takahara, N. Matsuki, and Y. Ikegaya, "Large-scale calcium waves traveling through astrocytic networks in vivo," *Journal of Neuroscience*, vol. 31, no. 7, pp. 2607–2614, 2011.

[317] F. Guilak, R. A. Zell, G. R. Erickson, D. A. Grande, C. T. Rubin, K. J. McLeod, and H. J. Donahue, "Mechanically induced calcium waves in articular chondrocytes are inhibited by gadolinium and amiloride," *Journal of orthopaedic research*, vol. 17, no. 3, pp. 421–429, 1999.

[318] M. Cabello, C. Aracil, F. Perdigones, J. M. Quero, and P. R. Rocha, "Lab-on-pcb: Low cost 3d microelectrode array device for extracellular recordings," in *2018 Spanish Conference on Electron Devices (CDE)*. IEEE, 2018, pp. 1–4.

[319] F. Halitzchi, L. Jianu, and B. Amuzescu, "Electrophysiology and pharmacology study of a human neuroblastoma cell line," *Romanian Reports in Physics*, vol. 67, no. 2, pp. 439–451, 2015.